NOTE TO USERS

This reproduction is the best copy available.

UMI®

Use of vanes in sharp bends to improve open-channel flow characteristics: Laboratory and numerical experiments

Sang soo HAN

A Thesis

In

The Department

of

Building, Civil and Environmental Engineering

Presented in Partial Fulfilment of the Requirements

for the Degree of Doctor of Philosophy at

Concordia University

Montreal, Quebec, Canada

January 2010

Library and Archives
Canada

Published Heritage
Branch

395 Wellington Street
Ottawa ON K1A 0N4
Canada

Bibliothèque et
Archives Canada

Direction du
Patrimoine de l'édition

395, rue Wellington
Ottawa ON K1A 0N4
Canada

Canada

ABSTRACT

Use of vanes in sharp bends to improve open-channel flow characteristics:
Laboratory and numerical experiments

Sang soo Han, Ph.D.

Concordia University, 2010

Sharp open-channel bends are commonly encountered in hydraulic engineering design. The flow around these bends is highly three-dimensional (3D) due to combined effects of secondary flow cells, large variation of free surface in the bend, and flow separation along the inner bend wall. Disturbances such as secondary flows and flow separation caused by the bend may persist for considerable distances in the downstream channel. A simple way of reducing these disturbances is through the insertion of continuous vertical vanes in the bend section. First, a Laser Doppler Anemometry (LDA) unit was used to measure the three-dimensional mean and turbulent velocity components of flow in an experimental rectangular open-channel bend. Flow characteristics of the bend with no vane were compared with those of bends having 1 or 3 vertical vanes. The key bend flow characteristics such as the size of the flow separation zone at the inner wall of the bend, the intensity of secondary flow, the level of turbulence generated, the extent of energy loss and the fluctuation of water surface were determined.

Several 3D numerical simulations were tested using various grid generation methods, different turbulence models and water surface treatment methods to determine the complex flow field in the sharp bend and in the channel downstream of the bend. The simulations revealed that the Reynolds stress turbulence model (RSM) with body-fitted coordinates, combined with the volume of fluid (VOF) method for water surface

representation, gave the best validation when compared to experimental data. Following this, the simulations were extended for the bend with vanes. This allowed a more detailed quantification of the mean and turbulent characteristics of flow between vanes, without experiencing the limitations encountered in experiments.

Results from both experimental and numerical investigations confirm that placing vertical vanes in the bend is a very effective way of reducing the intensity of the secondary flow and the extent of the flow separation zone along the inner wall. Energy loss for bends with vanes is also slightly reduced compared to the no-vane case. The 3-vane configuration is particularly efficient at creating a very uniform flow downstream of the bend.

KEYWORDS

ACKNOWLEDGEMENT

TABLE OF CONTENTS

LIST OF TABLES

NOMENCLATURE

The following symbols are used:

A_i = area for any segment of the cross section (m^2);

B = flume width (m);

B_s = maximum width of separation zone (cm);

c =volume fraction of a phase in the cell volume;

I_s = intensity of secondary flow;

K_a = turbulence energy;

ke = total turbulence kinetic energy (m^2/s^2);

LES = large eddy simulation;

L_s = length of flow separation zone (cm);

$L_{u/s}$ = start location of flow separation zone;

$L_{d/s}$ = reattachment location of flow separation zone;

Q = flow rate (m^3/s);

PISO = Pressure-Implicit with Splitting of Operators;

rms = root mean square;

R= mean radius of the bend (m);

R_1 = inner radius (m);

R_2 = outer radius (m);

R_h = hydraulic radius (m);

RANS = Reynolds averaged Navier Stokes;

RNG = renormalized group;

RSM = Reynolds stress turbulence model;

u_j =average flow velocity(m/s);

u_τ = friction velocity;

U = streamwise velocity (m/s);

U_a = average velocity for sub segment of the cross section (m/s);

U_i = average velocity for sub segment of the cross section (m/s);

U_T = mean velocity vector (m/s);

u', v', and w' = fluctuating velocities in streamwise, lateral, and vertical directions in the measuring volume, respectively (m/s);

u_{rms}, v_{rms}, and w_{rms} = root mean square values of streamwise, lateral, and vertical turbulent velocity components (m/s);

V = lateral velocity (m/s);

W = vertical velocity (m/s);

x_d = downstream distance from 90° of bend (m)

x_u = upstream distance from 90° of bend (m)

z = elevation above bed (m);

z_w = normal distance to the wall;

Z = flow depth (m);

2D = two-dimensional;

3D = three-dimensional;

v = kinematic viscosity (m²/s);

τ_w = bed shear stress.

1. INTRODUCTION

1.4 General background

Flow in open channel bends is commonly encountered in natural and artificial channel systems in hydraulic design practice. Clarifying and controlling flow structure and bed evolution in channel bends has been a major subject of research in river engineering and water resource engineering, because of the complex flow features such as flow separation, secondary flow, and water surface variation. Understanding the development of meanders is key in order to predict the development of river channels. Flow around bends also has an important role in mixing and transport of pollutants, since the mixing phenomenon is highly influenced by the secondary flows and flow turbulence.

Curvature effects in open channel lead to many problems such as water surface superelevation, bank stability, energy loss and secondary flow. Due to the very large number of variables and geometries linked to the three-dimensional (3D) nature of bend flow, it is difficult to arrive at an analytic or empirical solution which is reliable (Steffler 1984; Duan 2004). Yet, considerable amount of analytical and experimental studies have been conducted to investigate the different aspects of flow around bends. Most of the investigations were on closed conduit bends and consideration was mainly given to secondary flow and energy loss due to bend resistance. Intrusive techniques were widely used in previous studies, and they provided good insights in flow mechanics in bend flow. However, the intrusive nature of such techniques limited the data to be used in investigations of bend flow in a qualitative manner which may be important in fully understanding the three dimensional nature of bend flows.

1

One has a choice between experimental, numerical, and analytical methods to solve a physical problem in hydraulic engineering. Some of the disadvantages of the physical modeling are the time requirement to construct a model, the scale effect, and the precise control of the flow parameters. Computational Fluid Dynamics (CFD) techniques have been used extensively in the hydraulic engineering area in the last few decades, and it is not an exception in study of flow around bend. A carefully calibrated numerical model can be a very powerful and precise tool to predict the dynamics of flow in channel bends. However, the lack of reliable experimental data related to the three-dimensional flow field and the turbulence structure in bend flows has been a limitation in understanding the physical mechanisms of such flows (Blanckaert and Graf 2001). The lack of reliable experimental data also limits the verification of numerical simulations.

Efforts to control the flow characteristics of the flow around open channel bends to be beneficial for engineering practices by placing artificial structures such as vanes and weirs to help navigation of ships, economical design of a free board, protection of river bank, and sediment control (Odgaard and Kennedy 1983; Odgaard and Spoljaric 1986; Fukuoka and Watanabe 1989; Odgaard and Wang 1991a, b; Barkdoll et al. 1999; Flokstra 2006). However, not all the applications of the theses studies have produced satisfactory results (Waterway Simulation technology, inc. 1999; Blanckaert and Walter 2001). Continuous vertical vanes, also called guide vanes, are widely used in water and wind tunnels to limit bend energy losses and obtain a more uniform flow in sections downstream of the bend (Sahlin and Johansson 1991; Wetzel and Arndt 1991; Barlow et al. 1999; Luo and Razinski 2009). However, they have not been tested so far in open-channel bends. With an appropriate design of such vanes, it is conceivable that flow

2

separation, secondary flow and energy loss can also be reduced in an open channel bend, besides obtaining a more uniform flow in the channel downstream of the bend.

1.5 Research objectives

The general objective of this study is to determine the main characteristics of the flow around sharp rectangular open-channel bends and to test designs that would reduce secondary flow in open-channel bends. The specific objectives are listed below:

1. To determine the complex three-dimensional bend flow structure in terms of the size of the flow separation zone, the intensity of secondary flows, the intensity of turbulence energy, and the level of energy loss.

2. To assess the effectiveness of placing continuous vertical vanes in the bend to improve the channel performance downstream of the bend.

3. To calibrate and validate a 3D CFD model for sharp open-channel bends and to use this model to quantify the 3D mean and turbulent flow field with and without guiding vanes.

1.6 Layout of the thesis

Chapter 2 provides a detailed literature review on bend flows in open channels. Topics covered include fundamental and applied experimental studies as well as numerical modelling studies.

Chapter 3 presents experimental work which details bend flow characteristics and compares situations with and without vanes. The material presented in this chapter was submitted to *Journal of Irrigation and Drainage Engineering, ASCE* (Han et al., in review a).

Chapter 4 presents results of 3D CFD simulations using various parameters for turbulence model, grid generation, etc. The results from this analysis lead to the choice of the commercial code FLUENT with the Reynolds stress turbulence model that was used in Chapter 5.

Chapter 5 presents a detailed analysis of the 3D numerical simulations of sharp open-channel bends with and without guide vanes to limit the impact of secondary flow. The material presented in this chapter was submitted to *Journal of Hydraulic Research* (Han et al., in review b).

Chapter 6 summarizes the results of the present experimental and numerical bend flow studies and further explores topics that need to be addressed in future research on bend flows.

2. LITERATURE REVIEW

2.1 Analytical studies of bends

Only few analytical solutions for the flow in a bend are readily available even for the very simple 2D circular arc elbow in potential flow (Brizuela 1993). Most of them are for the pipe flows such as predicting the pattern of flow separation in pipe bends (Chu 2003; Mankabadi and Zaki 1986; Lichtarowicz and Markland 1963). Only specific classes of problems and certain aspects of the flow around open channel bends can be solved analytically without using a computer such as the secondary circulation in shallow channels far from side walls, and the channel bottom geometry approximation (Engelund 1974). Leeder and Bridge (1975) suggested an empirical criterion for predicting the onset of separation. The three dimensionality of the flow around open channel bends represented by the secondary circulations and the turbulent nature of the flow makes it difficult to develop analytical solution.

2.2 Experimental studies of bends

A large number of analytical and experimental studies have been conducted to investigate the different aspects of bend flows (Table 2.1). One of the earliest experimental studies was done by Shukry (1949) using a Pitot sphere measuring the secondary flow in rectangular open channel bend flow. Since then, many experimental studies have been carried out using different channel types and measurement techniques to investigate different aspects of the flow around open channel bend. Rozovskii (1957) identified the secondary circulation quantitatively in open-channel bends of rectangular and triangular

channel cross sections. Ippen & Drinker (1962) investigated the bed shear stress and velocity in curved trapezoidal channels using modified a Pitot tube to measure streamwise velocity. Following Rozovskii, Ippen & Drinker, other studies (Bathurst et al. 1977; de Vriend 1979, 1981; Kalkwijk and de Vriend 1980; Dietrich and Smith 1983; Odgaard 1989a, b) added more insight of the curved flow around bend in open channels experimentally. Marriot (1999) investigated the effect of the flow separation near the inner bank on the performance of the open channel bend using an electromagnetic current meter. However, these investigations were relying on intrusive techniques such as Pitot tube and propeller type velocity measurement device. Also, they used one- or two-dimensional mean velocity measurements with a coarse spatial resolution. Furthermore, they were often obtained in the central portion of the flow (Blanckaert and Graf 2001).

Three-dimensional mean and turbulent velocity data were provided by more recent studies (Booij 2003; Blanckaert and De Vriend 2004; Roca et al. 2007; Blanckaert 2009). However, considerable attention was devoted to secondary flow characteristics, without much emphasis on the flow separation.

The development of more advanced techniques such as the laser Doppler anemometry (LDA), acoustic Doppler velocity profiler (ADVP) and Particle Image Velocimetry (PIV) helped to provide more detailed and accurate information about flow mechanisms (Steffler 1984; Hicks et al. 1990; Blanckaert and Graf 2001; Booij 2003; Blanckaert 2009). It allowed researchers to measure 2D or 3D mean and turbulent velocity field without disturbing the flow with great accuracy. Considering the scale of a physical model in the laboratory, the size of the control volume is important. The dimensions

(length and width) of the measuring volume of LDA are of the order of millimetres and the sampling frequency is high compared to traditional intrusive measuring devices. PIV, which is also a nonintrusive measurement technique, provides instantaneous velocity data acquisition for the whole field. PIV has been getting more and more attention in velocity field data acquisition in recent years despite some of the disadvantages such as very high cost and relatively poor temporal resolution (Wernet et al. 2000; Edward et al. 2004; Nezu and Sanjou 2008). For the present study, a 2D LDA unit was used to collect the velocity data.

Other studies were carried out bends with movable bed investigating the sedimentation process in river meander (Hooke 1974; Kalkwijk and de Vriend 1980; Odgaard 1981). They mapped the topography of the channel bed in equilibrium state and the free water surface profile. Only few studies reported measurements of the flow field in mobile bed experiments. Blanckaert and his colleagues investigated the secondary flow induced by the curvature of the open channel bend using sand bed in context of river meander and the enhanced mixing process (Blanckaert and de Vriend 2004, 2005a, b; Blanckaert and Graf 2001, 2004). Three-dimensional flow field data in a chosen cross section were reported. The laboratory channel had transparent rigid vertical walls allowing the use of ADVP. As noted by Steffler (1984), the movable bed experiments with vertical walls may not be free from the criticisms applied to the channels with prismatic cross sections such as not representing the real meander river.

2.3 Numerical studies of bends

The cost and time requirements of physical experiments prompted many investigators to explore the potential of numerical models as a more flexible and inexpensive tool to examine flow behaviour subject to various geometries and boundary conditions. A carefully validated numerical model can be a very powerful and precise tool to obtain the flow behaviour in bends.

Most of the earlier studies on numerical modeling of open-channel bends were using a depth-averaged technique to reduce the channel or river flows to a two-dimensional problem (Table 2.2). Kuipers and Vreugdenhil (1973) developed one of the first mathematical models to solve 2D depth-averaged equations. Kalkwijk and de Vriend (1980)'s depth-averaged model predicted the flow pattern in a shallow bend, in which the flow depth approaches to zero towards the banks gradually. The model of Vreugdenhil and Wijbenga (1982) adopted a Cartesian coordinate system rather than curvilinear coordinates, so the river boundaries were defined with steps. Odgaard (1986a) developed 2D bend flow models for steady flow assuming that the velocity and water depth are constant along the centerline of a channel and their variation in the transverse direction are linear over the central portion of the cross section. Following Odgaard's concept, Yen and Ho (1990) developed a model to predict the bed evolution in channel bends. In steady-flow models, the flow depth at the centerline can be computed by the integration of discharge over the cross section.

The water surface profile in the transverse direction can be linearized with respect to the centerline value following Odgaard (1986a) and Yen and Ho (1990), or computed by the

method of integration as Kalkwijk and de Vriend's model (1980). Jin and Steffler (1993) developed a depth-averaged model to include the vertical variation of the streamwise velocity by using empirical velocity distribution relationship. The depth-averaged model of Molls and Chaudhry (1995) adopted a general coordinate system with an explicit algorithm and constant eddy viscosity. They used Rozovskii's experimental result (1957) of a 180° bend for the validation of the model. The concept of integrated effective stress, consisting of laminar viscosity stress, turbulence stress, and dispersion stress due to depth averaging, was used for the model. Unlike Jin and Steffler's model (1993), the non-uniform distribution of vertical velocity was ignored for simplicity (Lien et al 1999). Nagata et al. (1997) attempted to improve Kalkwijk and de Vriend's model (1980) by considering a secondary flow component that was derived by the vertical distributions of the main and transverse velocities. Zhou and Goodwill (1997) and Klonidis and Soulis (2001) also developed depth-averaged models and validated their models by comparing the model prediction of a water surface profile along a 180° bend and a velocity distribution along a channel contraction and expansion with experimental data, respectively. Kassem and Chaudry (2002) developed a depth-averaged model to predict the time variation of bed deformation in alluvial channel bends using body fitted coordinate.

Accurate representation of the flow requires 3D models (De Vriend 1981; Demuren and Rodi 1986; Cheng and Farokhi 1992; Meselhe and Sotiropoulos 2000; Wu et al. 2000; Wilson et al. 2003).

The large numbers of 2D depth-averaged models that have been proposed is due to two key advantages, namely the simplicity of the numerical computations and the small computational cost compared to 3D numerical models. However, despite the continuous improvements of depth-averaged models, the capability of incorporating the influence of secondary flow and free surface variation into the model is limited (Hsieh and Yang 2003; Lu et al. 2004). In open channel flow, the hydrostatic component of the water pressure is normally larger than the hydrodynamic pressure component, and induces secondary flow in the transverse direction. In order to accurately approximate the actual flow, the flow in open channel should be considered and simulated by three dimensional CFD models (Lu et al. 2004).

One of the earliest investigations of the flow around open channel bend using three dimensional numerical model is Leschziner and Rodi (1979)'s study. The model is based on partially parabolic version of the averaged Navier–Stokes equations and the k-ε turbulence model. Some 3D numerical models for simulating flow around open channels or rivers have been developed and reported following Leschziner and Rodi (1979)'s study, for example Vriend (1981), Galmes et al. (1984), Demuren and Rodi (1986), Shimisu et al. (1990), Cheng and Farokhi (1992), Demuren (1993), Ambrosi et al. (1996), Meselhe (2000), Wu et al. (2000), Morvan et al. (2002), Wilson et al. (2003), Olsen (2003). Some of the open-channel bend studies with 3D models are summarised in Table 2.3. These studies showed that 3D models can be accurate in predicting general characteristics of the flow in curved channels. Most of these proposed models used the Reynolds averaged Navier Stokes equations (RANS) closed by the original or variation of k–ε turbulence models with isotropic eddy viscosity hypothesis.

The variations of the water surface level in the open channel bend are very large, and hence a proper use of a free surface approximation method is essential. The free-surface flow can be treated using a rigid-lid assumption or using the surface tracking or capturing methods available to simulate free water surface, e.g. the marker and cell (MAC) method and the level set method (LSM), and the volume of fluid (VOF) method (Liu and Garcia 2007). The rigid-lid assumption has been widely used to simulate the turbulent flow in open channels with k-ε turbulence models (Demuren and Rodi 1986; Pezzinga 1994; Hodskinson 1996; Wu et al. 2000; Huang et al. 2001, Zeng et al. 2008; van Balen et al. 2009). However, this assumption introduces nonphysical errors for the flow with fluctuating water surface (e.g. super elevation of the water surface in open channel bends, hydraulic jump). Many 3D models used for the investigation of flow dynamics and sediment transport of channel bends still rely on the rigid lid assumption (Demuren and Rodi 1986; Naot and Rodi 1982; Pezzinga 1994; Meselhe 2000; Hodskinson 1996; Ye and McCorquodale 1997; Wu et al. 2000; Huang et al. 2001). Discrepancies between the predicted water surface level and the measured one was reported along the inner bank of region (Ye and McCorquodale 1996).

Some models adopted the free surface kinematic equation to solve non-hydrostatic pressure to overcome drawbacks of the rigid-lid assumption (Morvan et al. 2002; Ferguson et al 2003; Lai et al. 2003; Rameshwaran and Naden 2004; Khosronejad et al. 2007). However, the average water depth should be known prior to constructing grids (Ferguson et al. 2003; Rameshwaran and Naden 2004; Ruether and Olsen 2005).

Hirt and Nichols (1981) proposed the VOF method to trace the free water surface using a donor-acceptor formulation, and the model has been used successfully for the study of variety of flows with fluctuating free water surface (Hieu and Tanimoto 2005; Ramamurthy et al. 2006). However, it is rarely used for the study of the flow around open channel bends.

2.4 Modifying bend flow characteristics

The curvature of the open channel contributes to complex flow characteristics. These characteristics include secondary flow, accelerated flow moving towards the outer bank, super-elevation of the free water surface, and separated flow at the inner bank. The accelerated flow combined with the secondary current has been noticed to push ships toward outer bank causing difficulty of navigating (Jia et al. 2005). Also, the same flow pattern related to secondary flows is responsible for bank scour. The flow near the inner bank, negotiating the curvature of the bend, accelerates when it enters the curved section. Then, the flow decelerates after leaving the bend and creates an adverse pressure gradient. This tends to result in flow separation from the wall boundary. This also affects the performance of the channel by inducing reversed flow and formation of dead zones. These zones of flow separation are very unstable. Most of the models of sedimentation and erosion in curved channels ignore the effects of flow separation (Marriot 1999).

In engineering practice, control of the bend flow characteristics has been achieved by placing various appurtenances in the bend to reduce the free board requirement, to promote river bank protection, and to reduce sedimentation problem. Odgaard and Kennedy (1983) used short, vertical submerged vanes installed in a river bend to

counteract secondary current and reduce traverse bed slope. Przedwojski et al. (1995) and Abad et al. (2008) proposed the use of groynes, or bendway weirs, to redirect the flow toward the center of the channel and promote sedimentation near the bank. These appurtenances deflect the near-bed high velocity flow away from the outer bank and disrupt the main secondary flow (Thornton et al. 2005). Hersbergre (2002) studied the effect of macro roughness elements at vertical outer banks to decrease the flow velocity adjacent to the bank and reduce bend scour. Odgaard and Wang (1991a,b) installed small, slender, airfoil shaped submerged vanes which generate secondary currents that modify near-bed flow patterns, reduce channel erosion, and also redistribute flow and sediment transport. However, studies aiming at reducing the zone of flow separation in open-channel bends have been limited.

Table 2.1. Summary of the experimental studies

	Investigator	Year	Bend angle	Cross-section	Fr	Re (10^4)	Flow features	Velocity measurement
Fixed bed	Shurky	1949	45°, 90°	⊔	0.10~0.90	0.10~0.79	U, V, Superelevation	Pitot sphere
	Rozovskii	1957	29°~180°	⊔, ∨	0.20~0.50	0.03~2.70	U, V, Superelevation	Movable bed
	Ippen & Drinker	1962	60°	∨	0.32'0.50	1.10~7.50	U, Superelevation, Wall shear	Modified Pitot tube
	Yen	1965	90°	∨	0.36~0.82	6.30~13.80	U, V, Superelevation, Bed shear	Pitot tube
	Hooke	1974	sinusoidal		0.27~0.40		Bed pattern, Shear stress, Sediment discharge	Pitot tube
	Choudhary & Narasimhan	1977	180°	⊔	0.20~0.60	4.1	U, V, Z, and Bed shear	
	Steffler	1984	270°	⊔	0.49, 0.46	2.30, 3.60	U, V, u', v'	LDA
	Hicks et al.	1990	270°	∨	0.41~0.55	1.90~4.00	U, V, u', v'	LDA
	Reinauer & Hager	1997	30°	⊔	4.00, 6.00		Wave height	Pitot static tube
	Marriott	1998	sinusoidal	⊔	0.17, 0.46, 0.46	2.68, 1.57, 3.25	U, V,	electromagnetic current meter
	Tominaga et al.	1999	60°	⊔	0.2	4.4	U, V, W	3D electromagnetic velocimeter
	Tominaga & Nagao	2000	60°	∨	0.2~0.24	3.25~5.4	U, V, W	3D electromagnetic velocimeter

14

Table 2.1. Summary of the experimental studies (continued)

	Investigator	Year	Bend angle	Cross-section	Fr	Re (10⁴)	Flow features	Velocity measurement
Fixed bed	Booij, R.	2003	rotating 360°	⊔	0.19	17.4	U, W, u', w'	LDA
Fixed bed			180°	⊔	0.39	1.04	U,V,W, u', v', w' at 1 cross section	LDA
Fixed bed	Blanckaert	2009	193°	⊔	0.39, 0.35, 0.26	4.3, 6.9, 8.1	U,V,W, u', v', w' at the center, Water surface elevation	ADVP
Fixed bed	Present study	2010	90°	⊔	0.25, 0.38	1.6, 2.2	U, V, W, u', v', w', Super elevation, Water surface fluctuation	LDA
Mobile bed	Odgaard	1981					Meandering pattern	
Mobile bed	Da Silva	1999	Lab model				Scour, Meandering pattern	-
Mobile bed	Blanckaert & Graf	2001	120°	⊔	0.36	4.2	U, V, W, u', v', w' at 1 cross section	ADVP
Mobile bed	Roca et al.	2007	186°	⊔	0.37~0.42	6.0~10.3	Scour, Bed pattern	ADVP
Mobile bed	Binns et al.	2009	Laboratory meander		0.29~0.59	0.8~1.7	Scour	-
Mobile bed	Roca et al.	2009	186°	⊔	0.37, 0.39	4.1, 4.3	Scour, Bed pattern, U, V, W, u',v',w'	ADVP
River	Bathurst et al.	1977		Meander			U, V	electromagnetic flow meter
River	Kalkwijk & de Vriend	1980	90°	River bend	0.14 ~ 0.28		Depth averaged velocity, Z	

Table 2.1. Summary of the experimental studies (continued)

	Investigator	Year	Bend angle	Cross-section	Fr	Re (10^4)	Flow features	Velocity measurement
Analytical	de Vriend	1981	180°	⎵			Secondary current	
	Odgaard	1981					Bed pattern	

16

Table 2.2. Summary of depth-averaged model studies

Investigators	Year	Coordinate	Features
Kalkwijk & de Vriend	1980	Curvilinear	
Vreugdenhil & Wijbenga	1982	Cartesian	
Odgaard	1989a	Curvilinear	linearized velocity and flow depth in the lateral direction with respect to their centerline values
Yen & Ho	1990	Curvilinear	steady state bed formation
Jin & Steffler	1993	Curvilinear	vertical variation of U by empirical relationship
Molls & Chaudhry	1995	General	added influence of constant viscosity
Ambrosi et al.	1996	Curvilinear	included tidal effect
Nagata et al.	1997	Curvilinear	calculated secondary flow component
Zhou & Goodwill	1997	Curvilinear	predicted water surface profile
Lien et al.	1999	Curvilinear	calculated secondary flow component
Klonidis & Soulis	2001	Curvilinear	predicted water surface profile
Kassem & Chaudry	2002	Curvilinear	included time variation of bed evolution

17

Table 2.3. Summary of 3D model studies

Investigators	Year	Bend type	Turbulence model	Free surface treatment	Code
Leschziner and Rodi	1979	180°	Standard k-ε		
Demuren and Rodi	1986	Meander channel	Standard k-ε	Rigid-lid assumption	
Shimizu et al.	1990	Meander channel	Standard k-ε	Rigid-lid assumption+ bed deformation	
Cheng and Farokhi	1992	S-bend, 180° duct	Standard k-ε		
Meselhe and Sotiropoulos	2000	Meander channel	Standard k-ε	Mesh deformation	
Wu et al.	2000	180° + movable bed	Standard k-ε	From 2D Poisson equation	
Morvan et al.	2002	Meander channel	Standard k-ε	Rigid-lid assumption	CFX [1]
Wilson et al.	2003	Meander channel	Standard k-ε	Rigid-lid assumption	SSIIM [2]
Olson	2003	Meander channel	Standard k-ε	Rigid-lid assumption	
Naot and Rodi	1982			Rigid-lid	
Pezzinga	1994	Meander channel	Standard k-ε	Rigid-lid	
Hodskinson	1996	River bend	Standard k-ε	Rigid-lid	FLUENT
Ye and McCorquodale	1997	180° + meandering channel	Standard k-ε	Rigid-lid	
Huang et al.	2001	S-shaped open channel bend	Standard k-ω	Rigid-lid	
Ferguson et al.	2003	Meander channel	Rng k-ε	Free surface kinetic equation	Phoenics

18

Table 2.3. Summary of 3D model studies (continued)

Investigators	Year	Bend type	Turbulence model	Free surface treatment	Code
Lai et al.	2003	Meander channel	Standard k-ε	Rigid-lid	
Rameshwaran and Naden	2004	Meander channel	Standard k-ε	Spacial variation	
Ruether and Olsen	2005	90°	Standard k-ε	Rigid-lid+ bed deformation	
Khosronejad et al.	2007	90° and 135°	Standard k-ω	Rigid-lid	
Van Balen et al.	2009	180°	LES	Rigid-lid	
Booij	2003	Rotating 360° and 180°	2d, 3d les	Rigid-lid	
Present	2010	90°	RSM	VOF	FLUENT

[1] CFX is a commercial CFD code from ANSYS.
[2] SSIM is an abbreviation for Sediment Simulation in Intakes with Multiblock option, and developed by Olsen (2002) of the Norwegian University of Science and Technology.

3. CHARACTERISTICS OF FLOW AROUND OPEN CHANNEL 90° BENDS WITH VANES

3.1 Introduction

Flow in open channel bends is commonly encountered in natural and artificial channel systems in hydraulic design practice. It is characterised by flow separation, secondary flows, energy losses and water surface variations caused by the bend curvature. Many earlier bend flow studies (Shurky 1949; Rozovskii 1957; Ippen & Drinker 1962; Kalkwijk and de Vriend 1980; De Vriend 1981; Dietrich and Smith 1983; Odgaard 1989a,b; Blanckaert and Graf 2001) provided only one- or two-dimensional mean velocity measurements with a relatively coarse spatial resolution, and they were often obtained in the central portion of the flow. Flow structures near the zone of flow separation and the secondary flow cell in the bend produce highly complex three-dimensional (3D) flow patterns which would be difficult to describe without the help of 3D velocity measurements. Recent velocity measurement methods such as the acoustic Doppler velocity profiler (ADVP) and laser Doppler anemometry (LDA) yield detailed 3D velocity data on a finer grid to identify flow characteristics like counter rotating secondary flow cells in open channel bends (Reinauer and Hager 1997; Tominaga et al. 1999; Tominaga and Nagao 2000; Blanckaert and Graf 2001; Booij 2003; Blanckaert and Lemmin 2006; Blanckaert 2009). Methods such as particle image velocimetry (PIV) are also increasingly used to get the detailed turbulent flow structure in complex flow fields (Ishigaki et al. 2002; Hyun et al. 2003; Sanjou and Nezu 2009).

In previous open channel bend studies (Shurky 1949; Rozovski 1957; De Vriend 1977; Booij 2003; Blanckaert and De Vriend 2004), considerable attention was devoted to

secondary flow characteristics, without much emphasis on the flow separation that has broad and significant consequences for flows in bends of irrigation channels and natural meandering rivers. Various successful attempts were made in the past to counteract secondary currents using bendway weirs (Przedwojski et al. 1995; Jia et al. 2005; Abad et al. 2008), outer bank footings (Roca et al. 2007), and submerged vanes (Odgaard and Kennedy 1983; Odgaard and Spoljaric 1986, 1989; Odgaard and Wang 1991a,b; Derrick et al. 1994). Bendway weirs, also known as rock vanes, spur dikes, groynes or jetties, have been used for decades to reduce erosion in river bends. These appurtenances deflect the near-bed high velocity flow away from the outer bank and disrupt the main secondary flow (Thornton et al. 2005). For bend flows, Odgaard and Wang (1991a,b) installed submerged vanes which are small, slender, airfoil shaped vanes. These were shown to generate secondary currents that modify near-bed flow patterns, reduce channel erosion, and also redistribute flow and sediment transport. Continuous vertical vanes, also called guide vanes, are widely adopted in water and wind tunnels to limit bend energy losses and obtain a very uniform flow at the straight section downstream of the bend (Barlow et al. 1999; Sahlin & Johansson 1991; Wetzel and Arndt 1991; Luo and Razinski 2009). With an appropriate design of such vanes, it is conceivable that flow separation, secondary flow and energy loss can also be reduced in an open channel bend, besides obtaining a more uniform flow in the channel downstream of the bend.

In engineering design of curved channels of width B and radius R, B/R has to be limited to at least 0.33 to avoid secondary flows and flow separation (US Army Corps of Engineers 1994), although lower B/R values result in higher construction costs. Sharp bends for which B/R exceeds 0.33 are not avoidable in practice in irrigation channels.

However, very few investigators in the past (Blanckaert 2009, Roca et al. 2009) have studied the role of secondary flows and turbulence energy on erosion especially in sharp bend flow.

The objectives of the present study are to advance the understanding of the complex 3D flow structure around a sharp 90° bend and to assess the effectiveness of continuous vertical vanes in reducing flow separation and secondary flows. Specifically, flow characteristics such as secondary flows, water surface fluctuations, flow separation, turbulence energy, and energy loss in sharp bends with and without vanes are examined.

3.2 Experimental apparatus and procedure

The experimental layout is shown schematically in Fig. 3.1a. A 90° sharp bend is connected to upstream (u/s) and downstream (d/s) rectangular channels with a horizontal bed of width $B = 0.61$m. The bend has an inner radius $R_1 = 0.15$ m and an outer radius $R_2 = 0.76$ m. The constant head tank had contractions, screens, and honeycombs that reduced turbulence. The bend and its upstream and downstream channels were made of plexiglas to facilitate the use of LDA and visual observations. To investigate the effects of vertical dividing concentric vanes on the bend flow characteristics, both 1-vane and 3-vane systems were used (Fig. 3.1b,c). The vanes extended 0.3m upstream and downstream of the bend. They were made of 1.6 mm thick plexiglas plates, and the leading edges were bevelled (1:4). Details of flow conditions are presented in Table 3.1. The flow was subcritical and turbulent.

The velocity data were collected using a 2D Dantec LDA unit. The duration of each velocity measurement was 60 seconds with a sampling frequency varying between 20 Hz and 150 Hz depending on the flow zone. The error in velocity measurements is estimated to be 1%. 3D velocity measurements were obtained using two LDA probe orientations. In one probe orientation, the laser beam axis was parallel to the channel wall, and in another, it was parallel to the bed. This yielded the mean velocity components U, V and W as well as the fluctuating velocity components u', v' and w' in the streamwise, lateral and vertical direction, respectively. Because of the vane interference, 3D LDA measurements were restricted to the upstream and downstream cross-sections of the bend for the vane cases.

For the no-vane system, in the region G to H (Fig. 3.2), velocities were measured at 13 cross-sections (Fig. 3.2). At each cross-section, velocity measurements were taken at 21 lateral positions and 6 vertical positions corresponding to dimensionless heights z/Z equal to 0.07, 0.17, 0.28, 0.50, 0.72, and 0.89. At the two cross-sections further downstream (I, x_d = 3.0B and J, x_d = 4.0B), velocity data were collected at 5 vertical (z/Z = 0.11, 0.33, 0.56, 0.78, and 0.89) and 13 lateral positions. For the configurations of bends with vanes, LDA measurements were taken at 5 cross-sections downstream of the bend (Fig. 3.1b,c). At each of these measuring cross-sections, 5 vertical (z/Z = 0.11, 0.33, 0.56, 0.78, and 0.89) and 13 lateral positions were sampled.

Following Sudo et al. (2001), the two following equations are used to calculate the intensity of secondary circulation I_s and the turbulence energy K_a, respectively:

$$I_s = \frac{1}{R_h^2 U_i^2} \int_0^Z \int_0^B (V^2 + W^2) dB \, dZ \qquad (3.1)$$

$$K_a = \frac{1}{R_h^2 U_i^2} \int_0^Z \int_0^B \frac{1}{2}\left(\overline{u'^2} + \overline{v'^2} + \overline{w'^2}\right) dB \, dZ \qquad (3.2)$$

where R_h is hydraulic radius, U_i is the inlet velocity and the overbar indicates a time average.

To determine the dimensions of the flow separation zone, a cotton tuft of diameter 2mm was moved near the inner wall, to locate the flow separation point $L_{u/s}$ and the reattachment point $L_{d/s}$ (Fig. 3.1a) where the sign of U changes. This was followed by gently releasing a dye drop using a hypodermic needle. The dye used was a neutral buoyancy mixture of water-soluble black ink and ethyl alcohol. A digital camera was used to record all observations. Using the dye test data, the length L_s (corresponding to the distance between $L_{u/s}$ and $L_{d/s}$) and the maximum width B_s of the separation zone adjoining the inner wall were obtained. The uncertainty in determining B_s and L_s in dye tests is estimated to be 10 mm. To confirm these estimated values of B_s and L_s, they were compared to streamwise velocity data from LDA measurements for the no-vane configuration. To this end, the values of U along a radial line were measured starting from the inner wall. U changes its sign from negative to positive further away from the wall. The value of B_s was approximated as the distance between the wall and the point where the net flow crossing the radial line is zero, whereas the length of the separation zone was determined by noting its end positions, where U changed signs near the inner wall. A comparison of values of B_s and L_s obtained from dye experiments and LDA computations at different heights above the bed for the no-vane case is presented in Table 3.2. The values are not statistically different (ANOVA p-values of 0.80 and 0.78 for B_s and L_s, respectively) and it was thus concluded that dye experiments could be used to

determine separation zone dimensions for the vane configurations where no LDA

measurements can be obtained in the bend section.

A standard 30° v-notch-tank system was used to measure the flow rate Q. The maximum

error in the discharge measurement is estimated to be 3%. The inlet velocity was

calculated based on Q and the measured flow depth Z upstream of the bed section

(position F, Fig. 3.1a). The upstream specific energy (E_I) at F and the downstream

specific energy (E_2) at I, located 1.81 m (= 3.0B) downstream of the bend exit (Fig. 3.1a)

were computed as:

$$E = Z + \propto \frac{U^2}{2g} \qquad (3.3)$$

where the velocity distribution coefficient, α, is:

$$\alpha = \frac{\sum_{i=1}^{n} U_a{}^3 A_i}{U^3 A}, \qquad (3.4)$$

where U_a is the average velocity for any segment of the cross section, and A_a is the area

for that segment (Strum 2001). As the bed is horizontal, the specific energy loss ($\Delta E = E_I$

$- E_2$) for the bend channel system also denotes the total energy loss.

Mean values of the free water surface levels were collected using a point gauge with an

accuracy of 0.1 mm. During water surface profiling, significant fluctuations of the water

surface level were noticed near the flow separation zone. Temporal fluctuations of the

free water surface were recorded at a frequency of 16 Hz using three ultrasonic sensors,

which sent out cone shaped sound pulses that were reflected by the water surface

(Lundhal DCU 7110). The data logger (Campbell CR5000) recorded the time intervals

between the transmitted and received signals, and converted them into a distance between the water surface and the sensor (ITRC 1998).

3.3 Results

3.3.1 No-vane system

The three velocity components U, V, and W were used to compute the mean velocity vector U_T defined in eq. 3.5.

$$U_T = \sqrt{(U^2 + V^2 + W^2)} \qquad (3.5)$$

For the flow condition described in Table 3.1, Fig. 3.3 shows the contour plots of U_T with superimposed vector plots of V and W at three heights above the bed. In all cases, flow accelerates near the inner wall and decelerates near the outer wall of the bend ($\theta = 45°$) due to the favourable and unfavourable streamwise pressure gradients. As the flow enters the bend, the strength of the secondary flow increases. Planform vectors are generally oriented towards the inner wall near the channel bed (Fig. 3.3a) and towards the outer wall near the water surface (Fig. 3.3c). Secondary flow becomes more intense as the flow reaches the bend exit, and the fast flow near the inner wall is convected towards the outer wall by the secondary flow.

As the flow crosses the central section of the bend ($45°<\theta<50°$), the lateral slope of the water surface starts to recover (Fig. 3.4), and the flow begins to accelerate near the outer wall and to decelerate near the inner wall, leading to the separation of flow at the inner wall (Fig. 3.3). The upstream location of the flow separation zone $L_{u/s}$ is close to $\theta \approx 50$ ° for all heights above the bed (Fig. 3.3), which also corresponds to the onset of the adverse

26

pressure gradient along the inner wall (Fig. 3.4). However, the reattachment point $L_{d/s}$ is located further downstream near the water surface, indicating that L_s reaches its maximum value near the free surface (Fig. 3.3c). The values of L_s and B_s recorded near the free surface are respectively 55 cm and 9 cm, whereas the values of L_s and B_s recorded near the bed are respectively 32 cm and 2 cm (Table 3.2).

The water surface difference between the super-elevation zone at the outer radius and the water surface depression at the inner radius is 0.75 cm (Fig. 3.4). This corresponds to 8.8% of the average flow depth. The maximum water surface elevation is in the bend region along the outer wall ($45° < \theta < 50°$), and the minimum water surface elevation is near the 50° cross-section along the inner wall. The lateral slope of water surface disappears over a short distance ($x_d/B = 1.2$) in the downstream channel.

Near the reattachment point at the inner wall, the flow was observed to be slightly unsteady near the free surface, due to the vertical current moving towards the water surface at the inner wall. Time series of the water surface fluctuations recorded by acoustic sensors reveal larger root mean square (rms) values along the inner wall (rms = 2.5 mm) than along the outer wall (rms = 1.8 mm), confirming that water surface fluctuations are more intense along the inner wall near the flow separation zone than along the outer wall (Fig. 3.5).

The development of secondary flow circulation in the bend is more clearly identified from the lateral and vertical velocity vector plots (Fig. 3.6). There is an upward movement of the flow close to the inner radius and a downward movement near the outer radius associated with a clockwise secondary flow cell (Fig. 3.6a-f). A weaker counter-

27

rotating secondary flow cell near the free surface of the outer wall is also present. The presence of such a weaker counter-rotating secondary flow cell has been observed in previous studies of flow in bends (Blanckaert and Graf 2001; Booij 2003). These two secondary flow cells gain strength as they move further downstream of the bend (Fig. 3.6b-d), as illustrated by the increase in the magnitude of the lateral velocity. Later, these cells weaken as they move into the straight downstream channel (Fig. 3.6f,g).

For the present flow configuration of the bend with no vanes (B/Z = 6.8), V is expected to be much larger than W. Hence, for the secondary flow generated in the downstream channel, V is the dominant component contributing to the intensity of secondary flow I_s (Eq. 3.1). As such, large reduction of V will manifest as a drastic reduction of I_s.

Only limited experimental studies related to the measurement of turbulence quantities for flow around bends exist (Booij 2003; Blanckaert 2009; and Sanjou and Nezu 2009). The total turbulent kinetic energy (ke) is calculated using the variance of the turbulent velocity measurements as:

$$ke = \frac{1}{2}\left(\overline{u'^2} + \overline{v'^2} + \overline{w'^2}\right) \qquad (3.6)$$

An area of high ke exists between the separation zone and the high velocity zone (Fig. 3.7). This can be related to the shear zone between the accelerated fast moving flow just outside the separation bubble and the very slow moving flow in the recirculation zone. In the downstream part of the bend ($50° < \theta < 90°$), ke weakens. For the region close to the free surface where flow separation is the largest, Fig. 3.8 shows the contour plots of rms values of the lateral (v_{rms}) and vertical (w_{rms}) turbulent velocity components normalized

by the streamwise turbulent velocity component (u_{rms}). A marked variation of v_{rms}/u_{rms} (Fig. 3.8a) is apparent in the counter rotating secondary flow cell zone near the top of the outer wall. Furthermore, a significant variation of the ratio w_{rms}/u_{rms} (Fig. 3.8b) is apparent in the flow separation zone near the inner wall. This suggests that the isotropic assumption used in most computational fluid dynamics (CFD) turbulence models might result in significant errors when predicting the flow field around an open channel bend.

3.3.2 Bends with Vanes

The mean velocity fields for the 1-vane and the 3-vane systems are presented in Fig. 3.9. For these vane systems, the distribution of streamwise velocity U is more uniform than in the no-vane case. For the 3-vane system, flow is even more uniform than for the 1-vane system. Lateral and vertical velocity plots reveal the presence of two and four secondary flow cells for the 1-vane and the 3-vane systems, respectively at $x_d/B = 1$ and 2 (Fig. 3.10). Compared to the no vane system (Fig. 3.6c-g), the secondary flow pattern is markedly different and much weaker, especially in the 3-vane system (Fig. 3.10). For the no-vane system, a large shift of accelelated high velocity flow from the inner wall towards the outer wall was observed (Fig. 3.3). However, a less significant shift of flow is noticed for the 1-vane system (Fig. 3.9a,b), and an even less important shift is observed for the 3-vane system (Fig. 3.9c,d). The contour plots of U_T and vectors indicate that flow recovers rapidly to form a nearly uniform flow at $x_d/B = 4.0$, in particular for 3-vane system (Fig. 3.10b).

The dimensions of the separation zone are also markedly reduced in the presence of vanes (Table 3.2). A reduced flow separation zone is noticed only near the inner wall of

the bend with vanes, and no flow separation is discerned in the vicinity of the vanes. Compared to the no-vane system, for the 3-vane system, the length and width reductions of the zone of flow separation are 65% and 62%, respectively.

The magnitude of ke is also noticeably reduced for bends with vanes (Fig. 3.11). Besides the high turbulence zone near the inner wall due to the flow separation, local pockets of high turbulence are observed downstream of each vane for both vane configurations (Fig. 3.11). Highly sheared flows occur just downstream of the vane tips, since all the merging pairs of secondary flow cells rotate clockwise (looking downstream, Fig. 3.10). These result in local high turbulence zones marked as l, m, n, and o in Fig. 3.11, at the cross-section immediately downstream of the vanes. The local high turbulence zone near the inner wall persists further downstream from the bend, but the turbulence pockets associated with the vanes decay rapidly, mainly for the 3-vane system (Fig. 3.11b).

The variations of parameters I_s and K_a along the channel downstream of the bend are shown in Fig. 3.12. Compared to the no-vane system, for the 1-vane system, the value of I_s (= 0.6) is smaller at the exit of the bend. For the 3-vane system, I_s at the end of the bend (= 0.18) is still smaller compared to the 1-vane system. In the 3-vane system, I_s reaches the lowest asymptotic value (I_s = 0.003) over a very short distance at x_d/B = 4.0 downstream of the bend (Fig. 3.12a). In all 3 systems, there is a very large and rapid decay of I_s from the exit of the bend to a downstream location where x_d/B = 2.0. The rate of decay becomes further reduced downstream in the straight channel (Fig. 3.12a). Blanckaert (2009) and Zeng et al. (2008) used circulation strength of the normalized depth-averaged cross-stream to indicate the development of the secondary flow in a 193°

open-channel bend. Their studies showed that the secondary circulation and turbulent kinetic energy intensified as the flow passed the bend section, and peaked at the cross-section at 90°. This strong secondary flow diminished further downstream of the bend, and the reported distance for the strength of secondary flow to reach its asymptotic value in the downstream channel was close to our observations of 2.0B.

The initial value of K_a at the exit of the bend is relatively high for the no-vane system. It is lower for the systems with vanes (Fig. 3.12b). For all three systems, K_a generally decays rapidly as the flow leaves the bend and enters the downstream channel. In the 3-vane system, K_a reaches the lowest asymptotic value ($K_a = 0.04$) in a very short distance at $x_d/B = 4.0$ downstream of the bend (Fig. 3.12b). For the no vane system, the residual turbulence is relatively high ($K_a = 0.089$) at $x_d/B = 4.0$, and has not reached the asymptotic value of $K_a = 0.04$. One notices a slight increase of K_a for the 3-vane system between the bend exit and $x_d/B = 1.0$. This may be directly traced to the local shear generated by the adjacent merging pairs of secondary flow cells that emerge from the subareas of the 3-vane system. As stated earlier, these secondary flow cells are rotating in the same direction, and hence generate a highly sheared flow when they meet at the tip of the vanes. Values of both I_s (insert, Fig. 3.12a) and K_a (Fig. 3.12b) are the lowest for the 3-vane system, indicating that this bend-vane configuration is very effective in reducing intensities of both secondary flow and turbulence.

The specific energy loss ΔE between locations F and I (Fig. 3.1a), which also denotes the total energy loss, is 0.32 cm for the no-vane system (Fig. 3.4). For both bend systems with vanes, ΔE is 0.14cm. Hence, the energy loss is smaller for the systems with vanes.

Although the 3-vane system provides a more uniform flow compared to the 1-vane system, possibly the increased boundary friction losses in the former results in similar energy loss for both systems. As such, in practice, only fewer vanes need be used in the case with vanes, if energy conservation is a primary goal.

3.4 Summary and Conclusions

The study reveals marked differences in the mean and turbulent flow characteristics for flows in bends with and without vanes. The three-dimensional flow characteristics in a rectangular open-channel 90° bend (no-vane system) compare well with the large number of studies that have highlighted the existence of multiple secondary flow cell structures in open-channel bends. The results confirm the existence of a main inner bank cell and a counter-rotating, weaker outer bank cell in the channel downstream of the bend.

The adverse pressure gradient caused by the rapid recovery of the water surface along the inner wall ($\theta = 50°$) induces a large flow separation zone for the bend with no vanes. For bends with vanes, the extent of flow separation zone is drastically reduced along the inner wall, especially for the 3-vane system. Higher degree of flow separation leads to increased energy losses caused by higher turbulence. An anisotropic high turbulence zones exist near the flow separation zone and persists for long distances downstream, especially for the no vane system. Consequently, only advanced turbulence models that can properly resolve all Reynolds stress components can adequately simulate sharp bend flows.

At the exit of the bend, the intensity of secondary flow I_s and turbulence energy K_a are much smaller for flow in a bend with vanes compared to the bend with no vanes. For the former, the low asymptotic values of I_s (= 0.003) and K_a (= 0.005) are quickly reached at $x_d/B=4.0$ in the downstream channel. However, for the no-vane system, the residual values of I_s (= 0.007) and K_a (= 0.089) are still high at $x_d/B = 4$ and they still have not reached their asymptotic values. The improved performance in bend flows when vanes are present can be attributed to the reduced ratio of width to depth in the subsections of the bend. This results in a drastic reduction of the intensity of secondary flow (I_s, Fig. 2.12a). More uniform flow is established both in the bend and in the downstream channel due to the presence of vanes. For instance, the maximum value of U near the inner wall at $\theta = 45°$ is 50% more for the bend with no-vane compared to the maximum value of U for the bend with 3-vanes. Bends with vanes have lower intensity of secondary flow besides having a lower value for the maximum value of U. These features contribute to a decrease in the tendency for channel erosion in unlined channels. Further, results indicate that vanes are effective in slightly reducing energy losses which in turn permits an increase in the area subject to irrigation.

In the case of bends with vanes, differential hydrodynamic forces are present due to the large pressure differences on either side of the curved vane surfaces. As such, they have to be well anchored below the bed. For a field version of these experimental vanes, it may be appropriate to use thin continuous stainless steel plates having 9 segments (10°) rather than a single curved (90°) vane. However, the feasibility of this arrangement should be verified by laboratory experiments or numerical simulations. Considering the difficulties

of obtaining 3D velocity data close to vanes in experimental studies, 3D numerical

models would be required to pursue these investigations.

Table 3.1. Experimental flow conditions

Channel width (B)	Flow depth (Z)	Inner radius (R1)	Outer radius (R2)	Flow rate (Q)	Inlet mean velocity (U)	Reynolds number (Re)	Froude number (Fr)
0.61m	0.091m	0.15m	0.76m	0.013 m3/s	0.238m/s	15870	0.252

Note: U=Q/BZ; $Fr = \dfrac{U}{\sqrt{gZ}}$; and Re=UZ/$v$, where v is kinematic viscosity.

Table 3.2. Dimensions of inner wall flow separation zone for the no-vane, 1-vane, and 3-vane systems.

Location above bed z (cm)	Length (L_s, cm)			Width (B_s, cm)		
	No vane	1 Vane	3 Vanes	No vane	1 Vane	3 Vanes
2.0	32 (30)	13	0	2 (1.5)	1	0
4.0	40 (35)	21	5	5 (4.4)	3	1
6.0	51 (51)	24	15	7 (6.5)	6	2
8.0	55 (54)	28	18	9 (8.2)	5	3

Note: values in brackets are from calculation using LDA velocity measurements.
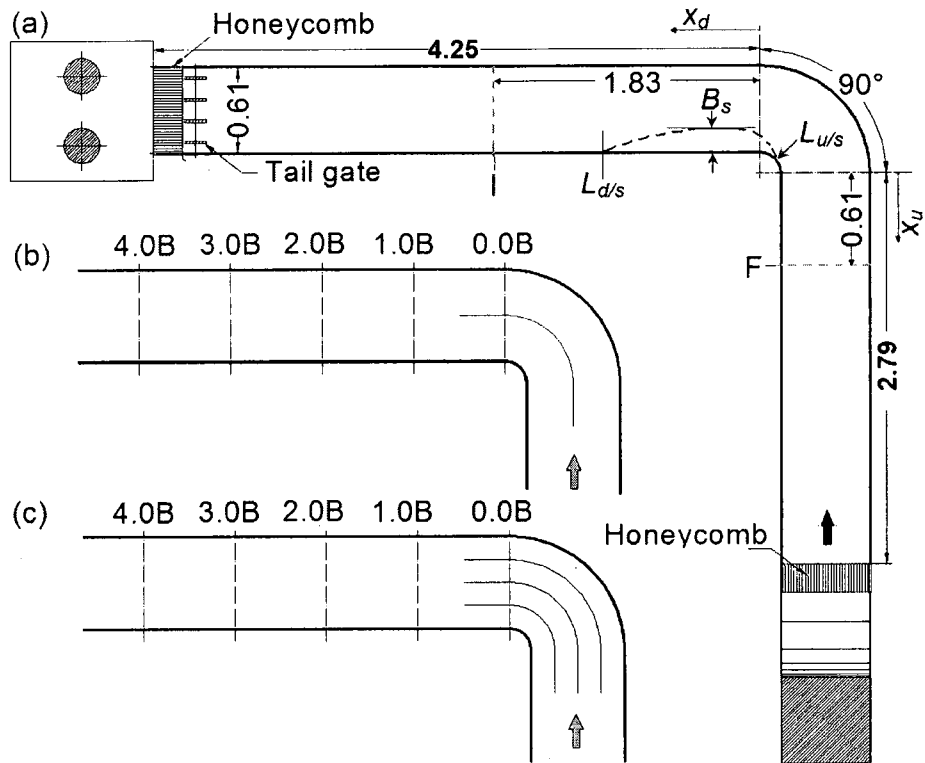
Fig. 3.1. (a) Layout of the flume (dimensions are in meters); zoomed bend and downstream sections with the position of the measured cross sections (distances based on the width (B=0.61 m)) for the configurations using (b) 1 vane; (c) 3 vanes.
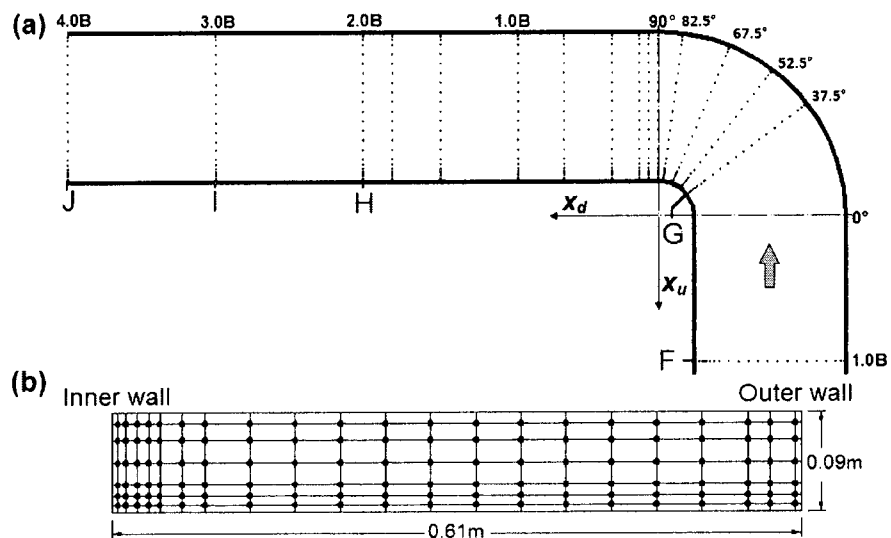
Fig. 3.2. (a) Planform positions for LDA velocity measurements; (b) measuring points for no-vane system.
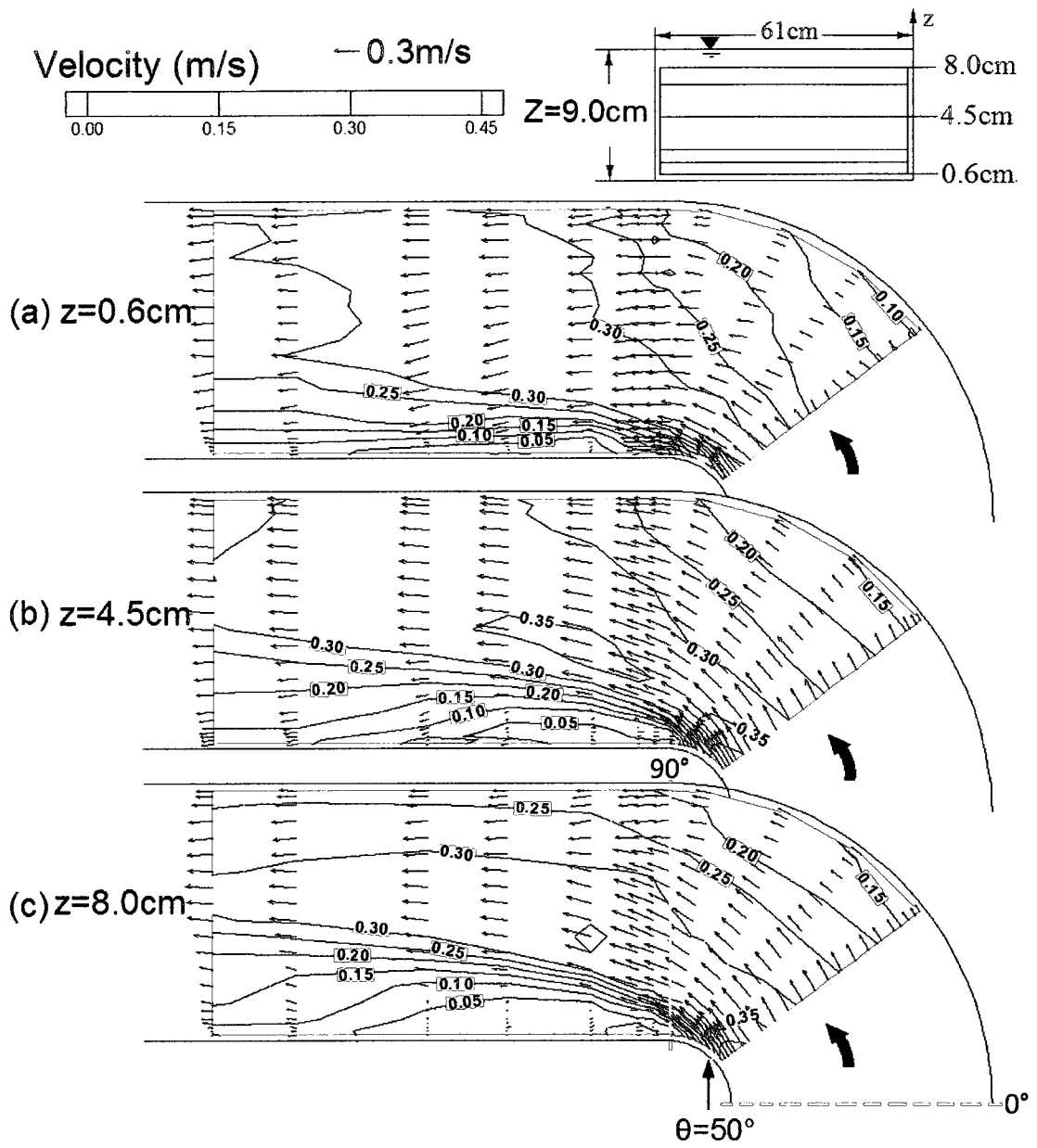
Fig. 3.3. *U-V* vectors overlaid on contour plots of U_T
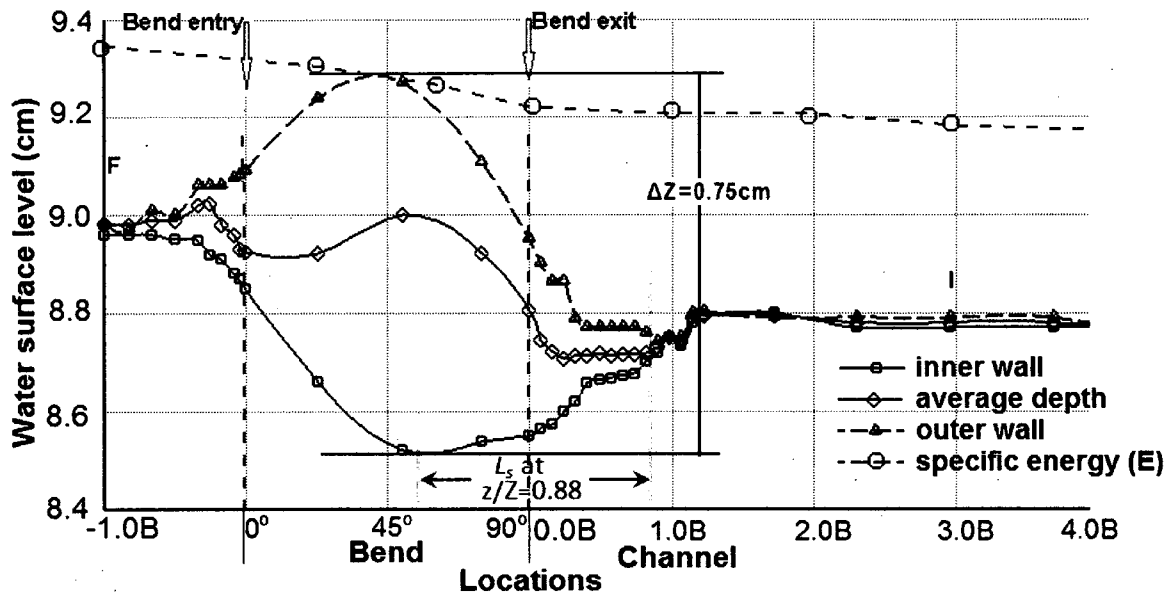
Fig. 3.4. Water surface profiles at inner (blue squares) and outer (black triangles) walls with average water depth (red diamonds) and specific energy (green circles). Bend locations are in terms of θ and channel locations are in terms of B
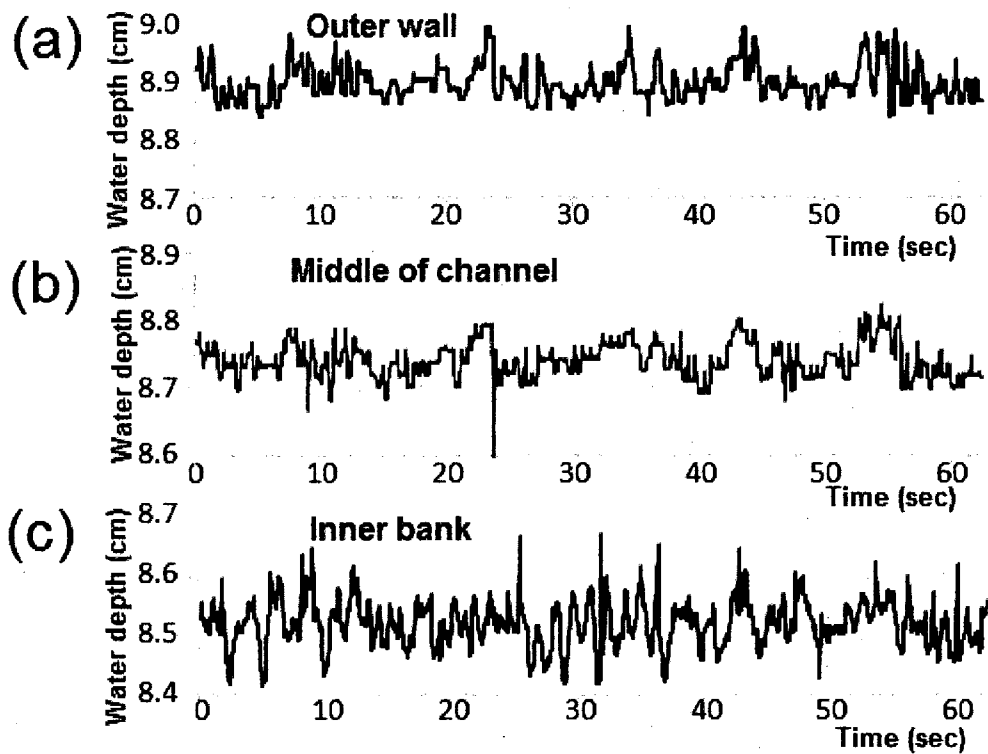
Fig. 3.5. Measured water surface level fluctuations at 0.1 B downstream of the bend: (a) outer wall; (b) middle of channel; (c) inner wall
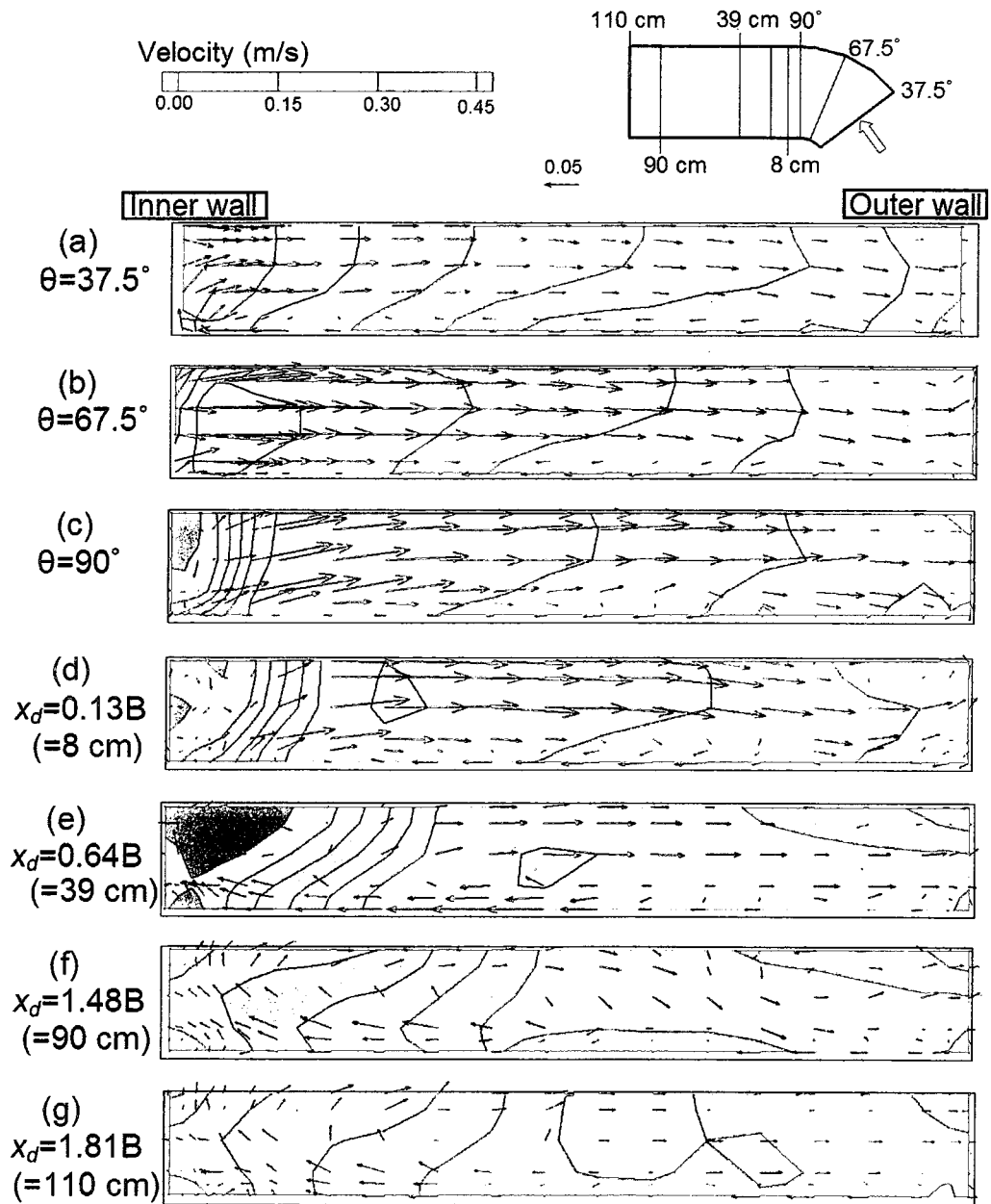
Fig. 3.6. Vector plots of lateral and vertical velocity superimposed on contours of velocity magnitude (looking downstream) in the bend cross-sections at positions: (a) 37.5°; (b) 67.5°; (c) 90°; and in the downstream channel at cross-sections (d) 0.13B (=8 cm); (e) 0.64B (=39 cm); (f) 1.48B (=90 cm) and (g) 1.81B (=110 cm).

39
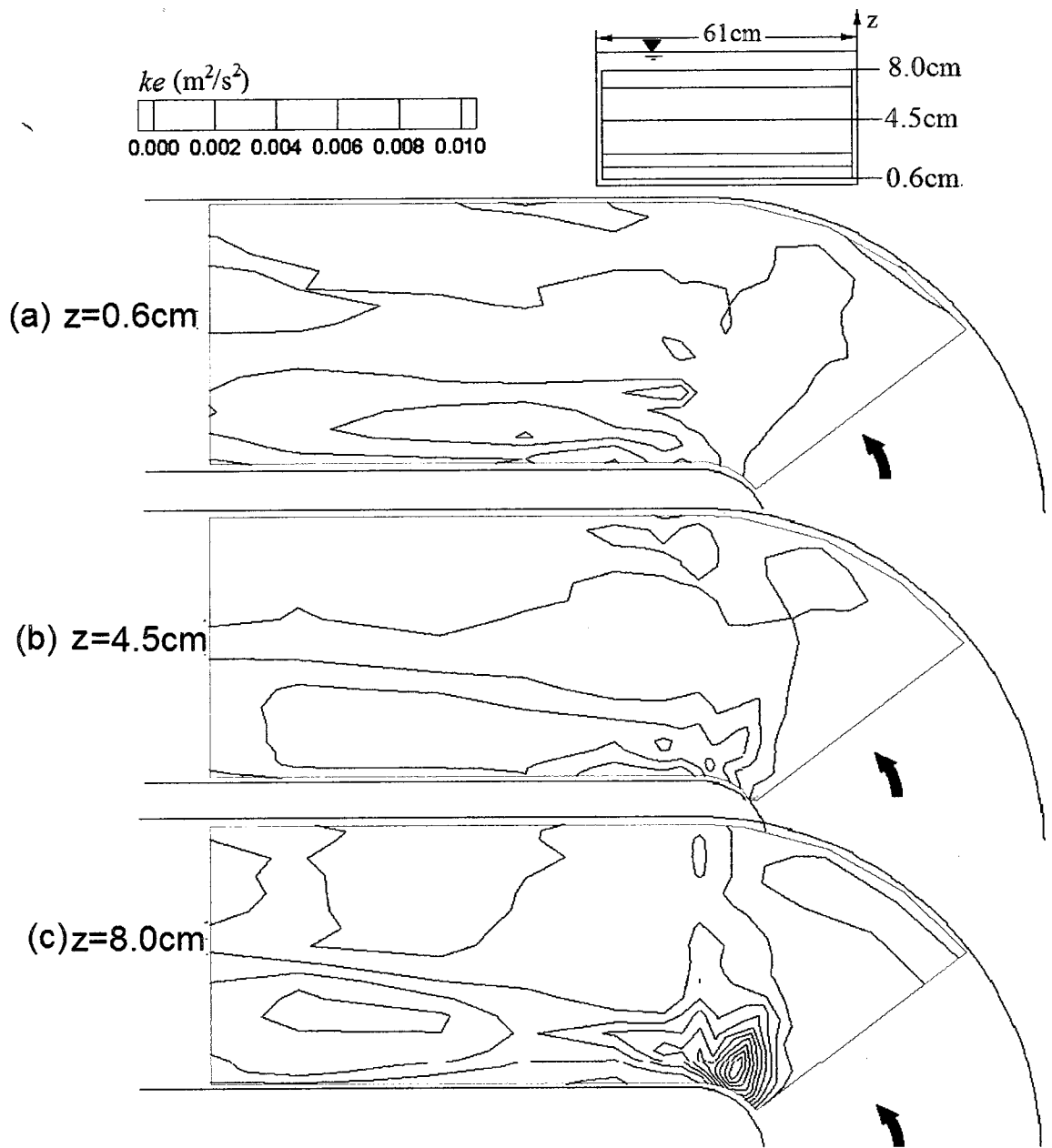
Fig. 3.7. Contour plots of turbulent kinetic energy (*ke*) at non-dimensional heights above bed (z/Z) of a) 0.07, b) 0.50 and c) 0.88.
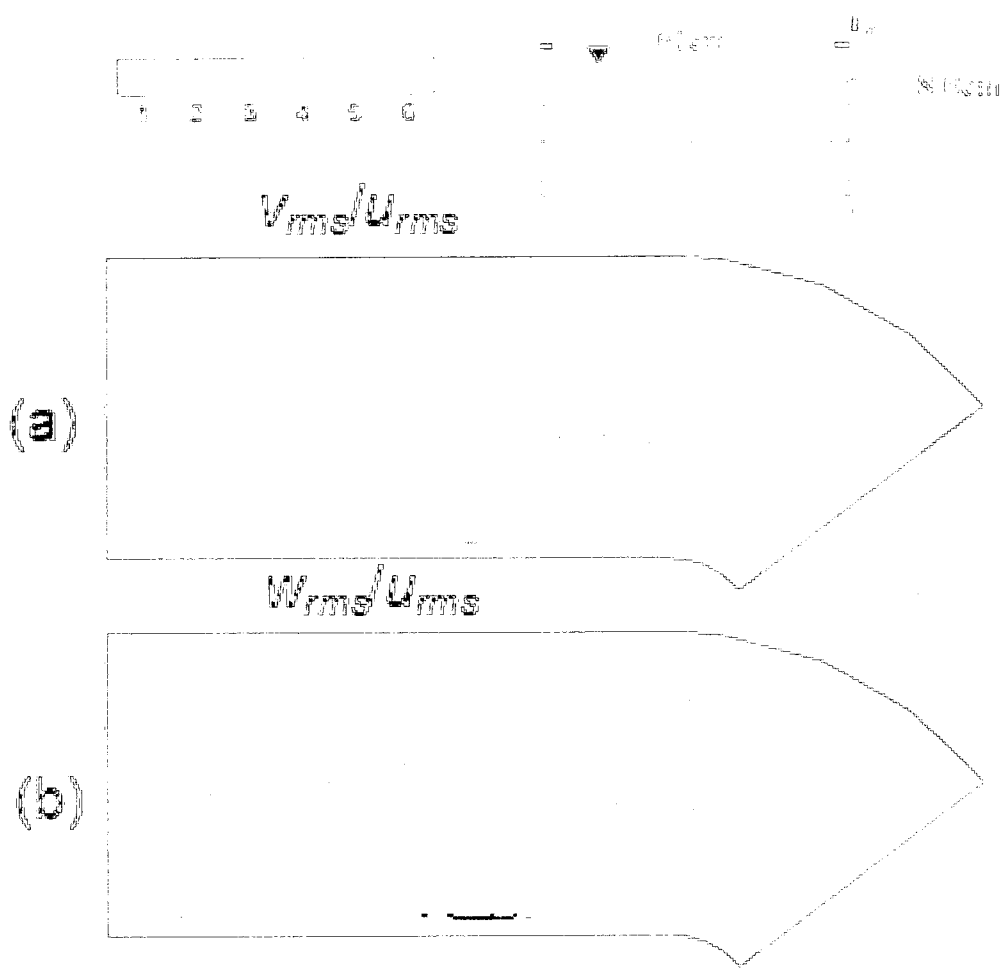
Fig. 3.8. Comparison of the ratio of root-mean square (rms) values of the velocity fluctuations at z/Z = 0.88: (a) v_{rms}/u_{rms}; (b) w_{rms}/u_{rms}
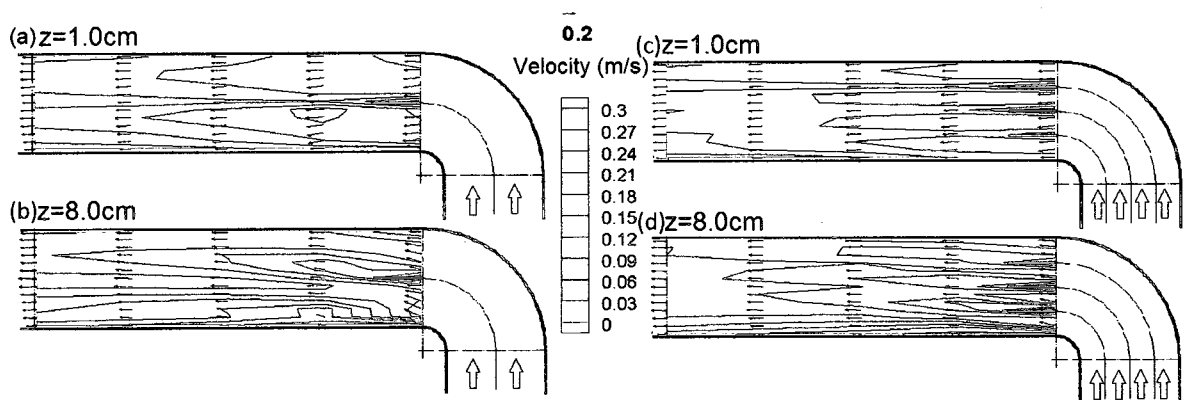
Fig. 3.9. Contours and vector plots of velocity for the downstream cross-sections of the bend with 1 vane at a) z/Z=0.11 and b) z/Z= 0.88, and with 3 vanes at c) z/Z = 0.11 and d) z/Z = 0.88.
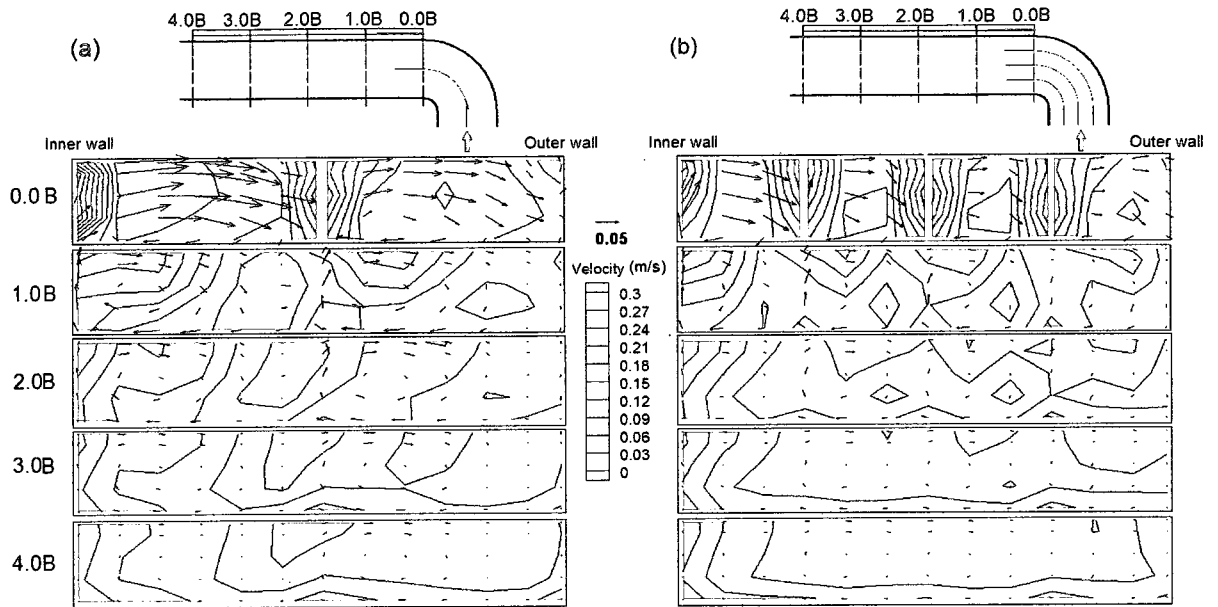
Fig. 3.10. Velocity magnitude with superimposed lateral and vertical velocity vectors at x_d/B = 0.0, 1.0, 2.0, 3.0, 4.0 looking downstream for the configuration with: (a) 1 vane; (b) 3 vanes.
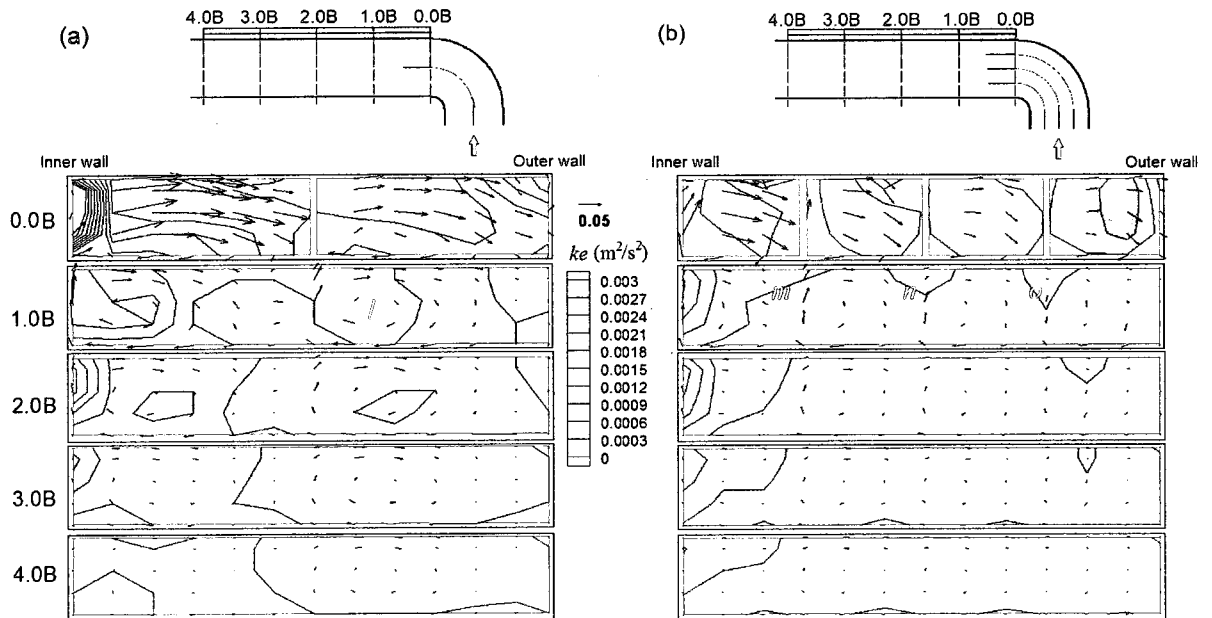
Fig. 3.11. Turbulent kinetic energy (*ke*) with superimposed lateral and vertical velocity vectors at x_d/B = 0.0, 1.0, 2.0, 3.0, 4.0 looking downstream for the configuration with: (a) 1 vane; (b) 3 vanes. Letters l, m, n, o represent pockets of high turbulence associated with each vane.
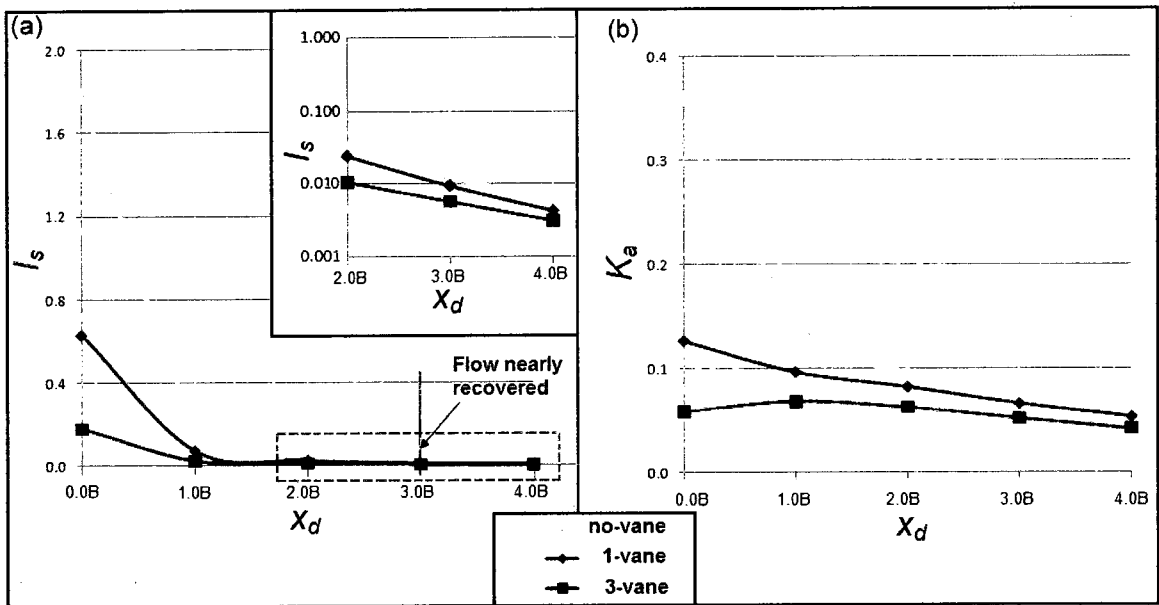
Fig. 3.12. Cross-sectional average values of I_s and K_a along downstream channel for the bend configuration with and without vanes: (a) I_s; (b) K_a. Insert: Details of I_s for range $2.0 \leq x_d/B \leq 4.0$.

4. OPTIMAL 3D NUMERICAL MODEL PARAMETERS FOR BEND FLOWS

4.1 Introduction

Very detailed description of complex flows is possible with the use of traditional non-intrusive velocity measurement techniques such as LDA and PIV. Some of the disadvantages of physical modeling are the time requirements to construct a model and, the scale effects. As mentioned before, CFD applications can solve these problems and they have been used successfully to characterize flows related to a large number of hydraulic structures that also include open-channel bend flows. A carefully validated numerical model can be a very powerful and precise tool to predict the flow behaviour in bends.

Recent studies have increasingly used 3D numerical models to investigate flow around bends (e.g. Morvan et al. 2002, Booij, 2003, Rameshwaran and Nadan 2004, Raisee et al. 2006, Khosronejad et al. 2007, Zeng et al. 2008). Several studies investigated the mechanisms of the secondary flow cell structure in strongly curved bends, and concluded that both the centrifugal force and the anisotropy of the cross-stream turbulence interact and result in a counter-rotating secondary flow cell near the outer bank (Blanckaert and de Vriend 2004; van Balen et al. 2009). Hence, turbulence models that can properly resolve all Reynolds stress components are required for an adequate simulation of bend flows. Using the rigid-lid assumption, Booij (2003) compared the large eddy simulation (LES) with the k-ε model for the flow in a shallow (B/Z = 10) and mildly curved (B/R = 0.12) open channel 180° bend, and concluded that LES models provide a better prediction

of complicated secondary flow patterns compared to Reynolds-Averaged Navier-Stokes (RANS) models. However, LES models require substantially finer grids than those typically used for RANS model.

Although the investigation of open-channel flows occurring around dykes, groynes, bridge piers, and bends generally involves large variation of water surface level, many studies used a rigid-lid assumption for the water surface treatment (Koken and Constantinescu 2008; Zeng et al. 2008; Huang et al. 2009). Large free surface variations along the bend walls are present, in particular near the inner wall. As such, more complex free surface treatment techniques such as volume of fluid (VOF) are essential to model flow around a sharp bend.

The objectives of this chapter is to obtain a comparative assessment of the predictions of bend flow characteristics based on two commercial CFD codes (Phoenics and FLUENT), using 3 different turbulence models (Renormalization Group (RNG) k-ε, Reynolds stress model (RSM) and LES).The assessment will verify the effectiveness of both Cartesian and body-fitted coordinates (BFC) grids using three water surface treatments: rigid lid, porosity and VOF. The simulated flow field in each case is compared with laboratory measurements of velocity and water surface elevation.

4.2 Description of model parameters

Both FLUENT and Phoenics codes are based on the full three dimensional form of Navier-Stokes equations, and both use a finite volume method (FVM). In FVM, the physical space of the domain is split into small volumes and the balance or transport

equations are integrated over a finite volume defined by a grid. The scalar values are stored in the cell centres. For the solution requiring transient simulation such as free surface modelling (VOF and height of liquid (HOL)) or LES, the governing equations are discretized in both space and time. FVM converts a general scalar transport or balance equation for an arbitrary control volume of the physical domain in integral form to an algebraic equation that can be solved numerically for each control volume or cell in the computational domain (Tannehill et al. 1997). A set of algebraic equations with a coefficient matrix is formed with the equations for each cell in the grid. The equation is cast into a correction form to obtain a solution. In the correction form, the sources are replaced by the errors in the original differential equation. The correction tends to be zero as convergence is approached.

This study adopted SIMPLEST (SIMPLE ShorTened), a variation of the SIMPLE (Semi-Implicit Method for Pressure–Linked Equations) algorithm (Caretto et al. 1972; Patankar and Spalding 1972) for Phoenics and PISO (Pressure Implicit with Splitting of Operators), proposed by Issa (1986), for FLUENT.

The iterative numerical solution requires criteria for determining the convergence of the acquired solution. The numerical solution was considered converged when the residuals of the discretized transport equation reached a value of 0.001 or when the solution did not change with further iterations. During the calculation, the amount of change of variables was controlled to promote the convergence of the solution. For the simulations with an unsteady solver, the difference in the mass flow rates at the flow inlet and outlet was monitored to be less than 0.01% in the final solution. Also, sufficient number of extra time steps was added to verify the steadiness of the flow field in the final solution.

Setting initial conditions as close as possible to the final solution can promote convergence. Several techniques were used in this study. Extrapolated pressure and velocity fields obtained from a simulation with a coarse grid were used as the initial fields for these two variables. Rather than specifying the whole domain as water for the initial condition, average water depth was used for the VOF model. Also, the solution was started with a simpler turbulence model (k-ε or RNG k-ε). After the convergence was ensured, results of the simpler models were used as initial values for more complex turbulence models such as the Reynolds stress model.

RNG k-ε models are known to be more accurate and reliable for a wider class of flows than the standard k-ε model (Yakhot et al. 1992). They provide an improved performance for several types of flows, including flows with separation zones and flows around curved geometry (Choudhury 1993). RSM computes all the stresses of anisotropic turbulent flows. In LES, large eddies are resolved directly, while small eddies are modeled. The default values of closure coefficients for all models were chosen from the FLUENT manual. Details of the RNG k-ε model, RSM model, and LES model can be found in Wilcox (2004).

Grid generation

Grid generation is often considered as the most critical part of the numerical modeling process, and generating a good quality mesh requires efforts and skills (Thompson 1982; Biron et al. 2007). Several mesh types were tested for this study. Although the studied open-channel bend has a rectangular cross section shape which is convenient to generate

a mesh, the curvature of the bend can generate a grid aspect ratio problem. Thus, special care near the bend section was needed.

Phoenics uses a structured grid with either boundary or body fitted coordinate (BFC), Cartesian or polar coordinates. In a Cartesian coordinate grid, all cells except the domain occupied by the flow are blocked. Phoenics uses the so called 'cut-cell technique' to avoid the stepping of the cells which would not be a realistic representation of the smooth curvature of the boundary. Using the Cartesian coordinate system instead of BFC resulted in a larger number of cells near the bend with about 50 % of the grid cells that had to be blocked. This results in an increase of CPU time for program execution. Although BFC grids require additional memory for the coordinate transformation, they were still computationally less expensive than Cartesian grids for this bend study.

Both BFC and Cartesian coordinates were tested in the study. BFC grids were all generated using ANSYS ICEM-CFD to render the grid dimensions identical for both codes. The local density, smoothness in distribution, aspect ratio, and skewness of the cells were checked for all cell configurations. The grid spacing was controlled to place the first grid cells next to the walls so that generally they were well within the logarithmic region $30 < u_\tau z / v < 100$ to satisfy the use of the non-equilibrium law-of-the-wall (Viegas et al. 1985).

To ensure that results were grid independent, several simulations using various grid resolutions were compared. Starting from a coarse grid, the number of cells in each direction was increased by steps of 20% to obtain a finer grid. The final grid chosen was

such that the resulting deviations of velocities and pressures were generally much less than 1% between the final grid the penultimate grid.

Free Surface modeling

To investigate the interaction between the flow field and the free surface, several water surface treatment methods were selected for the study. Phoenics offers the height of liquid (HOL) approach and the scalar equation model (SEM). This study adopted the HOL model which is computationally less expensive than the SEM. The porosity correction concept (Ouillon and Dartus 1997) was also tested in Phoenics. The porosity correction concept has previously been successfully used in Phoenics for the simulations of junction flows and natural confluences (Bradbrook et al. 2000a;b; Biron et al. 2002, 2004). In FLUENT, the volume of fluid (VOF) model was adopted. In this approach, two or more fluids can be modeled by solving a single set of momentum equations and tracking the volume fraction of each of the fluids throughout the domain. This model was initially proposed by Hirt and Nicholls (1981). The VOF formulation relies on the fact that two or more fluids are not interpenetrating. In each control volume, the volume fractions of all phases add to unity. The fields for all variables and properties are shared by the phases and represent volume-averaged values, as long as the volume fraction of each of the phases is known at each location. Thus the variables and properties in any given cell are either purely representative of one of the phases, or representative of a mixture of the phases, depending upon the volume fraction values between 0 and 1.

Boundary conditions

Inlet velocity was defined either as a mean velocity at the inlet cross section with known water depth or as a velocity field measured at a specific cross section. The dimension of the mesh for several simulations for this study, especially simulations using LES and VOF, was restricted by the available computer resources. To limit computational cost, the channel lengths of the upstream and downstream sections were reduced, and inlet and outlet velocity measured from the experiment (described below) were used as the boundary conditions. Also, several simulations of this study were carried out using parallel processing, with up to 64 processors. In these cases, the whole channel length could be simulated, and the pressure outlet boundary condition was used to specify a static gauge pressure at the boundary. For the simulations with VOF model, the inlet conditions for air and water needed to be set separately.

The presence of a wall significantly affects turbulent flows. It is known that integrating the k-ε models through the near wall region and applying no-slip condition yields unsatisfactory results (Rodi, 1984). A direct approach would require many cells towards the wall to resolve the viscous sub-layer, which would be computationally expensive due to the increased number of cells. Hence, a wall function was used for the study. Launder and Spalding (1974) provide details of wall functions, which can be classified into the standard equilibrium log-law and non-equilibrium wall functions. The non-equilibrium wall function is capable of accounting for the effects of pressure gradients and departure from equilibrium. Hence, the non-equilibrium wall function was used for the study, as it was expected to produce better predictions of flows with separation, reattachment, and

impingement, where the mean flow and turbulence are subject to severe pressure gradients and change rapidly.

4.3 Laboratory setup and measurements

Laboratory experiments in a small flume were carried out to identify the key parameters characterizing the flow. The flow condition chosen for the comparison of the codes with different models for turbulence closure and water surface treatment are presented in Table 4.1.

Methods

The rectangular open channel flume with a 90° bend section was constructed using 12mm Plexiglas sheets as shown in Fig 3.1. The upstream and downstream rectangular channel sections are connected by a bend section with an inner radius $R_1 = 0.22$ m and an outer radius $R_2 = 0.50$ m, with a width of 0.28m. U and V velocity components, and the corresponding fluctuating velocity components u' and v' were measured using a Dantec 2D 300-mw LDA unit by placing the fiber-optic probe below the channel bed pointing upward. An automated traverse system which has three axes was used to position the probe with linear motions in steps of 0.0025mm. The measuring points were distributed densely near the inner radius of the bend. The measurements were taken at 6 different flow depths between 0.5cm and 10.5cm (Fig. 4.2). Overall there were 936 LDA measuring points.

Mean values of the free water surface levels were collected using a point gauge which could measure depths to the nearest 0.1mm. Visualization of the flow was facilitated by the use of dye to identify the zone of flow separation along the inner wall. Thus, detailed

2D velocity data and water surface profiles in the vicinity of the bend were obtained. The flow was fully turbulent and subcritical. Key parameters were chosen for the comparison between simulations and laboratory measurements: 1) the length of the separation zone (L_s), 2) the predicted maximum and minimum mean streamwise velocities (U_{max} and U_{min}, respectively), and 3) maximum turbulent kinetic energy (ke).

Mean streamwise and lateral velocities

Fig. 4.3 presents the contour plots of measured velocity magnitude (U_T), presented as non-dimensional values. Since W was not measured, U_T was estimated as:

$$U_T = \sqrt{(U^2 + V^2)} \tag{4.1}$$

The flow at the bottom of the channel is moving towards the inner radius passing the 90 degree bend (Fig. 4.3a), and the flow at the water surface is moving towards the outer radius (Fig. 4.3f). These vectors clearly indicate that there is strong secondary flow. Also, there is strong acceleration of the flow at the inner radius, and the U-V vectors indicate that the lateral velocity is strongest near the inner radius of the bend at the bend exit (Fig. 4.3).The zone of flow separation along the inner wall is identifiable from the contour plots at the water levels of z/Z = 0.83 (Fig. 4.3f) and z/Z = 0.67 (Fig. 4.3e). Dye tests indicated that the flow starts separating at about 45° of the bend, and the observed L_s and B_s were 0.52B (= 15.0cm) and 0.08B (= 2.4cm), respectively. The extent of the flow separation zone is much smaller compared to the one observed in the wider open-channel bend used in Chapter 3. Also, the flow separation did not reach the bed in this small flume.

Other flow characteristics

Turbulence characteristics such as turbulence energy of the bend flow were estimated using 2D LDA data. As a first approximation, the turbulent kinetic energy was extrapolated from the measured values of u' and v' for the bend flow, assuming w' to be equal to v'.

An example of estimating *ke* from two dimensional velocity data using a pseudo isotropic assumption is presented by Poelma (2004) who used eq. 4.2 to estimate *ke*.

$$ke \approx \frac{1}{2}(\overline{u'^2} + 2\overline{v'^2}) \qquad (4.2)$$

The contour plots of *ke* (Fig. 4.4) show that a high shear zone exists between the separation zone and the accelerated flow near the inner radius. Fig. 4.5 shows the measured water surface profile near the bend region. The maximum water surface variation recorded was 2.1cm. This is 16.5 % of the average water depth.

4.4 Results

Code comparison

The results of the experimental study described above were compared with the predicted results from different turbulence model and free surface approximation methods in Phoenics and FLUENT code.

As mentioned earlier, grids with both BFC and Cartesian coordinates were tested in the study. Similar cell size and density near the inner wall of the bend were maintained for both grids, and the cell number of the grid with Cartesian coordinates was 2.37 times that with BFC. For the grid with Cartesian coordinates, the cells in the grey and yellow zones were blocked (Fig. 4.6a). The grid with Cartesian coordinates system required considerably more computer memory for the configuration used in this study. The grid for the simulations treating water surface with a rigid-lid assumption for both FLUENT and Phoenics is shown in Fig. 4.6b. All simulation results using a rigid-lid assumption were not able to predict the flow separation zone along the inner wall which was measured in the laboratory experiments, except for the LES model. However, the general pattern of high velocity near the inner wall of the bend was predicted reasonably well by all models. The contour plots of U_T/U_i and vectors of U-V velocity components from the results of simulation using RSM from FLUENT are shown in Figs. 4.7a-c. Also, the model generally underestimated the velocity magnitude near the inner wall of the bend region by ignoring the reduced cross-sectional area due to the depression of the free surface and the zone of flow separation.

The test of the LES model was also done using the grid shown in Fig. 4.6b to avoid excessive computing cost, although LES models ideally require much denser grids. The vector plots of U-V velocity components in Figs. 4.7d-f show that the LES model predicted the flow separation zone along the inner wall. However, the extent of the zone was significantly underestimated due to the absence of a proper water surface treatment.

For the test of the porosity concept in Phoenics, a grid similar to that shown in Fig. 4.6b was constructed with the top cell height of 2.0cm to accommodate the free surface

variation. The porosity correction method was able to some extent to predict the variation of the water surface level near the bend area (Fig. 4.8a). However, the value of L_s was significantly under predicted by the porosity correction method (Fig. 4.9). This is due to the limited capability of the model to accommodate large fluctuations of the water surface level. However, the computational cost of this method was far less compared to other methods such as HOL or VOF, since the flow was treated as a single phase flow, and the solution was obtained in a steady-state solution.

The VOF model was also tested using the grid in Fig. 4.6b with increased domain height and cell numbers in the z direction to simulate air flow above water. Fig. 4.8b presents the contour plots of the predicted water surface level from VOF model with RSM model in FLUENT. The predicted maximum water surface variation was 1.9cm, which is 86% of the measured value. The contour plots of U_T/U_i and the vector plots of U and V (Fig. 4.10) show that the model was able to predict the measured data with reasonable accuracy. The reversed flow near the inner wall downstream of the bend indicates that the model was able to predict the flow separation zone (Fig. 4.10c). The extent of the predicted flow separation zone is shown with streamlines at z = 10.5cm above the channel bed in Fig. 4.11.

Fig. 4.12 shows the predicted pattern of the secondary flow cells at several cross sections located downstream of the bend exit using the RSM and VOF model. In addition to the main strong secondary flow cell, the weaker counter locating cell is also identified near the outer wall close to the water surface. However, it was difficult to make a comparison with the 2D LDA data due to the missing vertical velocity component in the laboratory measurements.

Table 4.2 highlights the differences in some of the variables describing the flow field for simulations using different turbulence models and free surface treatments from FLUENT and Phoenics. The results of the simulations using the rigid-lid assumption with the RNG k-ε model or the RSM model were not able to predict a flow separation zone along the inner wall. Only LES model predicted the flow separation zone with about 70% of the measured size. The use of VOF model improved the accuracy of the simulations. Table 4.2 indicates that the RSM and VOF model is the most suitable for the study of flow around this sharp open-channel bend.

Some of the simulation results with various parameters for the 0.61m-wide flume were also compared with the experimental data, although not to the same extent as for the smaller flume. In Chapter 2, the existence of a weaker secondary flow cell near the outer wall close to the water surface was identified with the 3D LDA measurements (Figs. 2.6d-f). To identify the effect of the water surface treatment on the bend flow characteristics, a grid with a rigid lid for which the water surface geometry was taken from the laboratory measurements was designed for the same bend configuration as in Chapter 2 (Figs. 3.13). Fig. 4.14 show the contour plots of U_T and vector plots of U-V at z = 6.5cm (z/Z = 0.72) for the measurements, as well as model predictions from the RNG k-ε model and the LES model using the grid of Fig. 4.13. Using the grid with the measured water surface geometry, even the RNG k-ε model was able to predict the flow separation. However, the extent of the zone and is markedly over predicted. The LES model prediction was not in good agreement with the measured data (Fig. 4.14c). The LES simulation was carried out up to t = 60.0 seconds using time step (Δt) of 0.001 second, and total CPU time using 12 processors was 25 hours. However, the contour plot

of U_T indicates that the solution had not reached a steady state. It should be noted that the reason for inaccurate predictions using the water surface geometry as a rigid lid could be due to the difficulty of generating a realistic surface mesh using interpolation of the measured water depth data.

When the same simulations are carried out using VOF model, both turbulence models predicted a large zone of flow separation along the inner wall (Fig. 4.15). However, Fig 3.16a shows that the RNG k-ε model with the VOF method predicted only the main secondary flow cell. On the other hand, RSM model with VOF method produced the two counter-rotating secondary flow cells which were identified with LDA measurement (Fig. 4.16b).

4.5 Conclusion

The results of the two commercial CFD codes (Phoenics and Fluent) were compared with the LDA measurements related to flow around a sharp open-channel 90° bend. The results showed that the best agreement of the model prediction with LDA data was obtained with FLUENT with RSM and VOF model. Furthermore, the use of the PISO algorithm in conjunction with FLUENT provided a better convergence.

LES model was able to predict the flow separation zone even using the grid with horizontal rigid-lid for water surface level. However, the predicted flow field was not in good agreement with measured data, since the large variations of the water surface level were ignored. The grid with the water surface geometry as a rigid lid was also tried, but generating a realistic grid to represent the water surface shape proved to be difficult. Slight interpolation errors in the region near the inner wall of the bend where large water surface variation exists can be a significant source of uncertainty in the model prediction.

This analysis also reveals that the use of VOF model resulted in much improved agreement between the predicted and measured flow characteristics such as flow separation along the inner wall and the multiple secondary flow cell structures. Using a rigid-lid assumption, neither the RSM nor the RNG k-ε models were able to predict flow separation. Adopting the VOF approach, both turbulence models predicted a large zone of flow separation, indicating that large super-elevation and depression of the water surface in the bend is directly related to the occurrence of the flow separation zone. However, only the RSM with the VOF model correctly predicted the two counter-rotating main and weak secondary flow cells. This indicates that the proper prediction of the weak secondary flow cell requires not only a proper turbulence model that can resolve the anisotropy of the turbulence, but also an appropriate treatment of the free surface.

Table 4.1. Experimental flow conditions

Channel width (B)	Flow depth (Z)	Inner radius (R1)	Outer radius (R2)	Flow rate (Q)	Inlet mean velocity (U)	Reynolds number (Re)	Froude number (Fr)
0.29m	0.13m	0.22m	0.50m	0.013m³/s	0.37m/s	21800	0.38

Table 4.2. Measured and predicted bend flow characteristics

Variables		Grid dimension	Ls, cm	Umax, m/s	Umin, m/s	Ke max, m2/s2
LDA			**15.0**	**0.65**	**-0.09**	**0.018**
PHOENICS	BFC-POR-RNG k-ε	203 x41x 20	8.9	0.62	-0.067	0.005
	BFC-POR-RSM	203 x41x 20	9.2	0.63	-0.08	0.009
	BFC-RL-RNG k-ε	204 x41x 20	0.0	0.56	0.000	0.003
	BFC-HOL-RNG k-ε	203 x41x 30	7.2	0.62	-0.062	0.005
	CAR-POR-RNG	220 x 130 x 30	3.2	0.63	0.053	0.007
FLUENT	BFC-RL-RNG k-ε	203 x41x 20	0.0	0.56	0.000	0.003
	BFC-RL-RSM	203 x41x 20	0.0	0.58	0.000	0.004
	BFC-RL-LES	203 x41x 20	12.4	0.61	-0.03	-
	BFC-VOF-RNG k-ε	213 x 40 x 30	11.2	0.63	-0.08	0.007
	BFC-VOF-RSM	213 x 40 x 30	**13.4**	**0.63**	**-0.09**	**0.011**

Note: BFC (body fitted coordinate); POR (porosity concept); RNG k-ε (renormalized group k- ε model); RSM (Reynolds stress model); RL (rigid lid assumption)
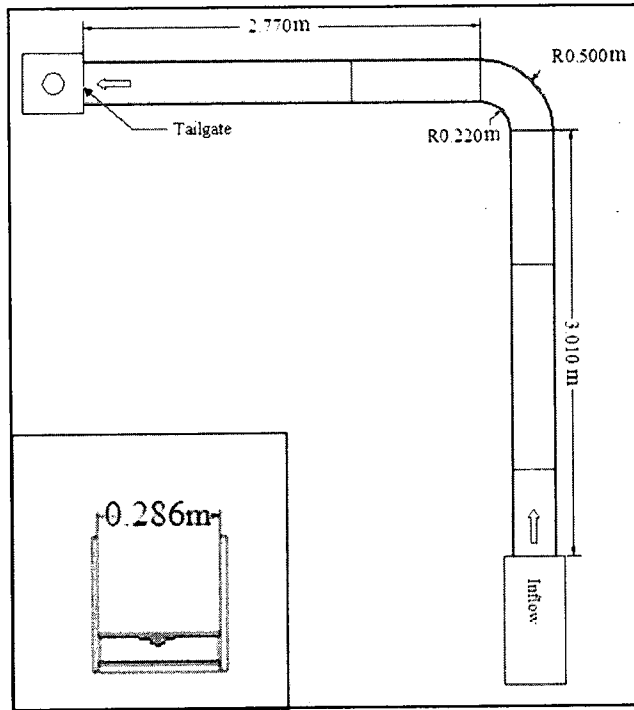
Fig. 4.1. Layout of the small flume (top view and cross section)

(a)

(b)   Inner wall   Outer wall
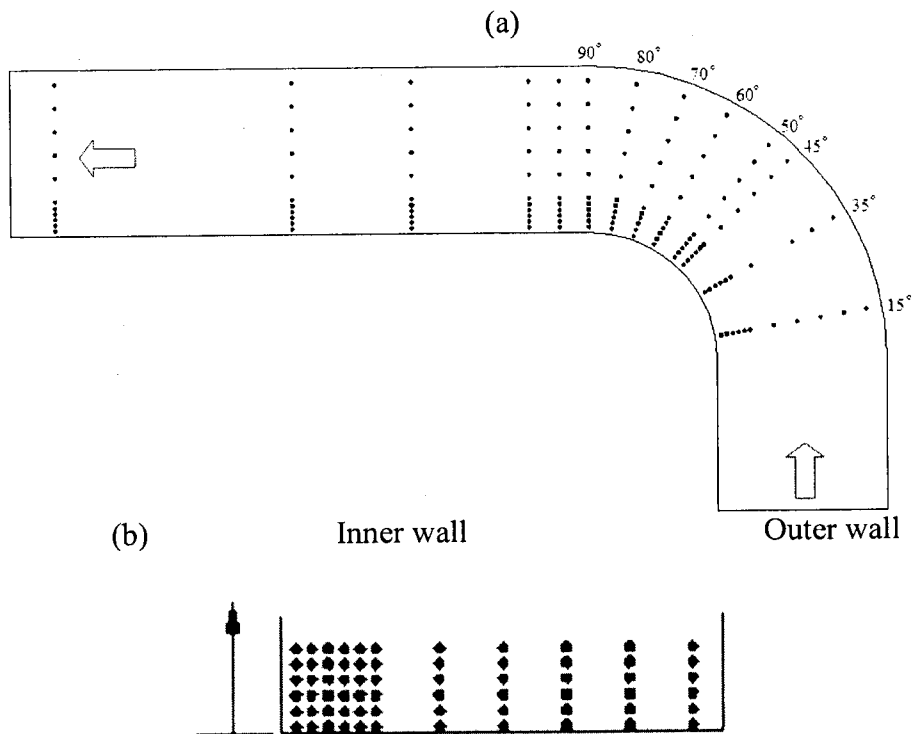
Fig. 4.2. (a) Planform positions for LDA velocity measurements; (b) measuring points in typical cross sections.
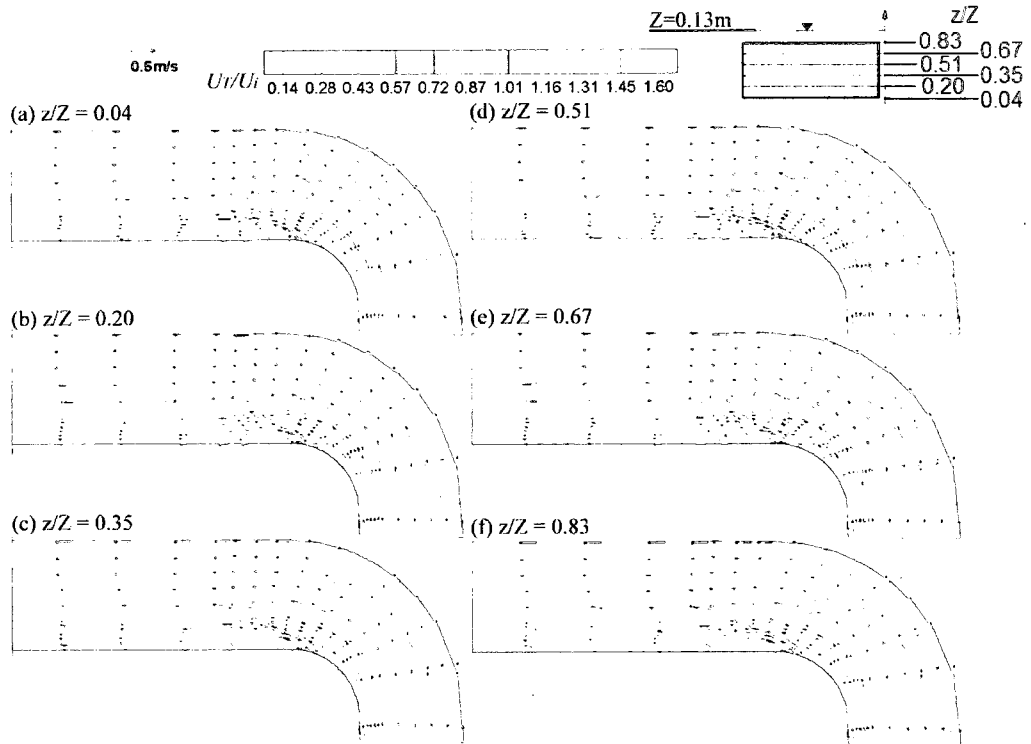
Fig. 4.3. *U-V* vectors with contours of U_T/U_i obtained from LDA measurements at depths: (a) z = 0.05cm; (b) z = 2.5cm; (c) z = 4.5cm; (d) z = 6.5cm; (e) z=8.5cm; (f) z=10.5cm.
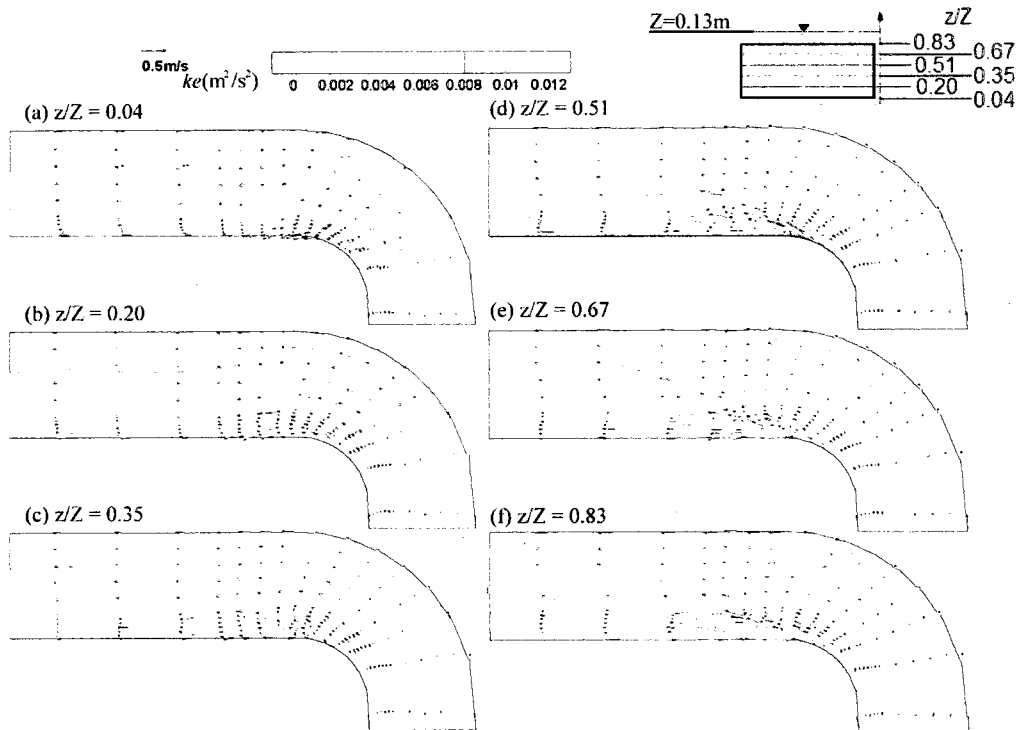
Fig. 4.4. *U-V* vectors with contours of *ke* magnitude obtained from LDA measurements at depths: (a) z = 0.05cm; (b) z = 2.5cm; (c) z = 4.5cm; (d) z = 6.5cm; (e) z=8.5cm; (f) z=10.5cm.

61
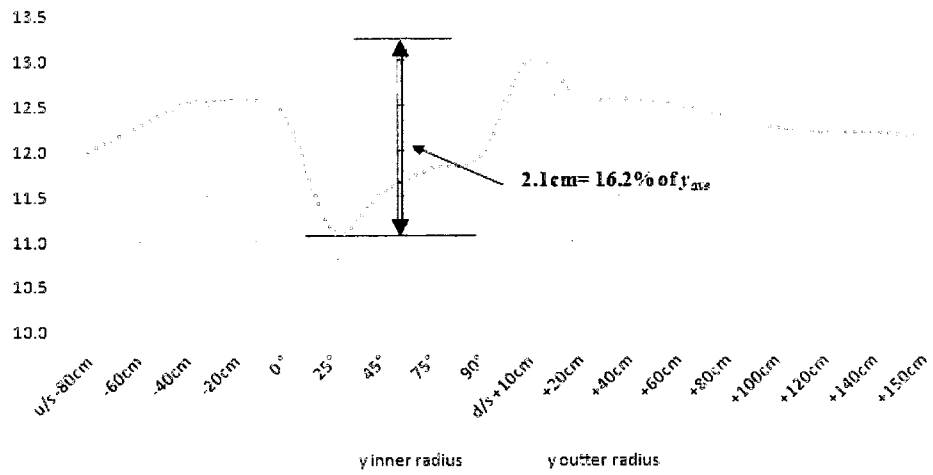
Fig. 4.5. Water surface profiles at the inner and outer radius

(a)

(b)
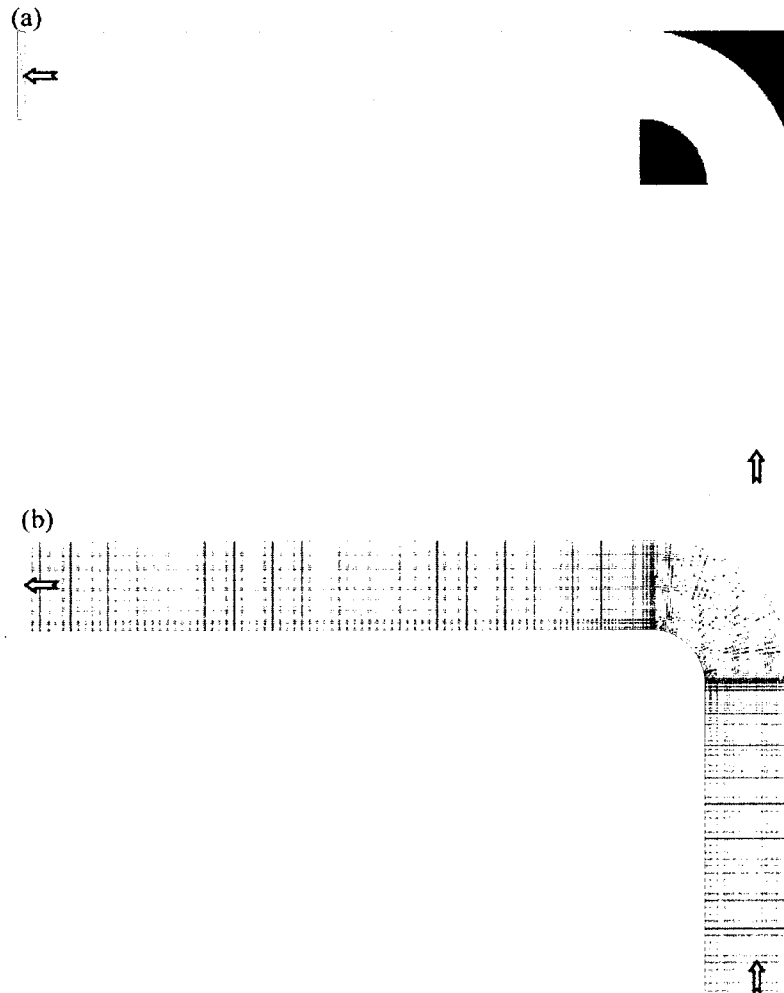
Fig. 4.6. Grids for the 0.29m-wide bend with: (a) Cartesian coordinates (161, 129, 20);
(b) BFC coordinates (214, 41, 20).
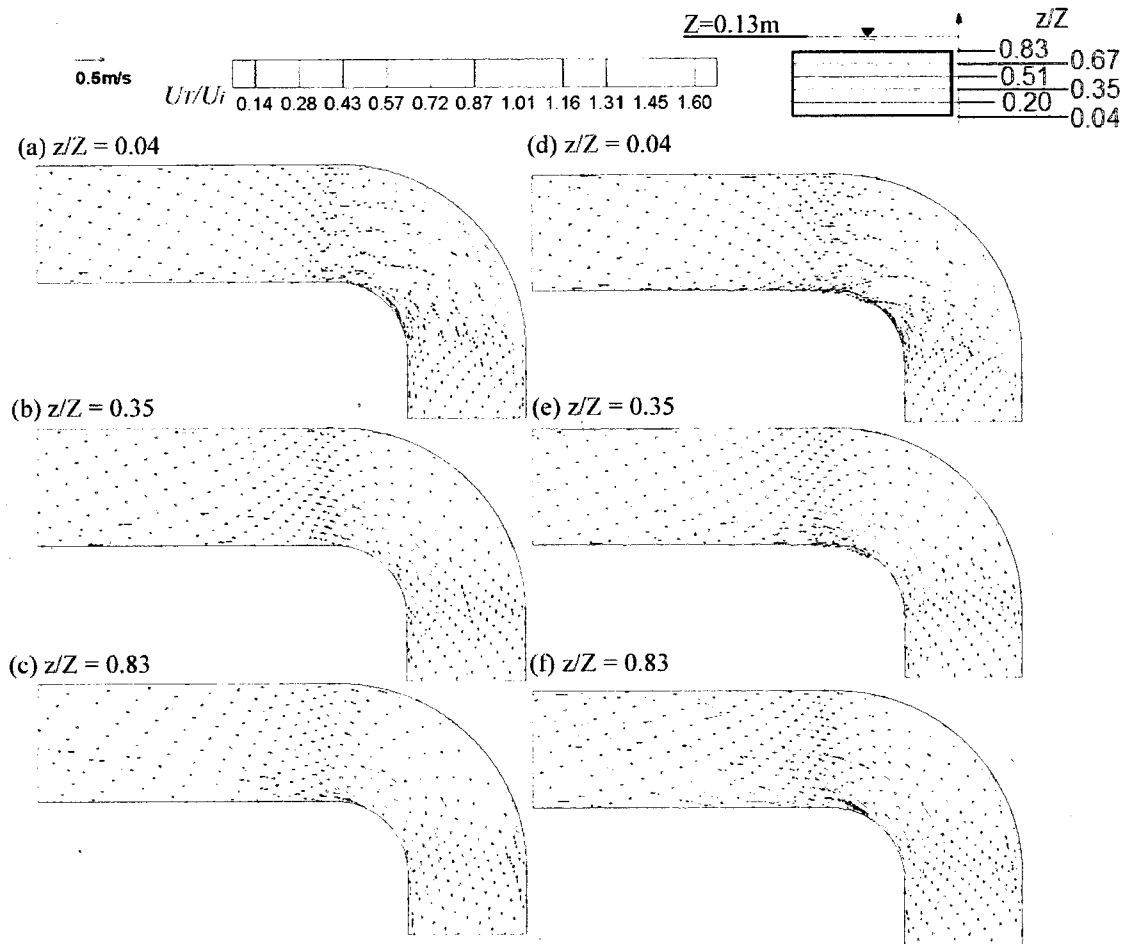
Fig. 4.7. *U-V* vectors with contours of U_T/U_i using horizontal a rigid-lid assumption for the RSM model at: (a) z = 0.05cm (z/Z =0.04); (b) z = 4.5cm (z/Z = 0.35); (c) z = 10.5cm (z/Z=0.83), and for the LES model at: (d) z = 0.05cm (z/Z =0.04); (e) z = 4.5cm (z/Z = 0.35); (f) z = 10.5cm (z/Z=0.83).

(a)

(b)
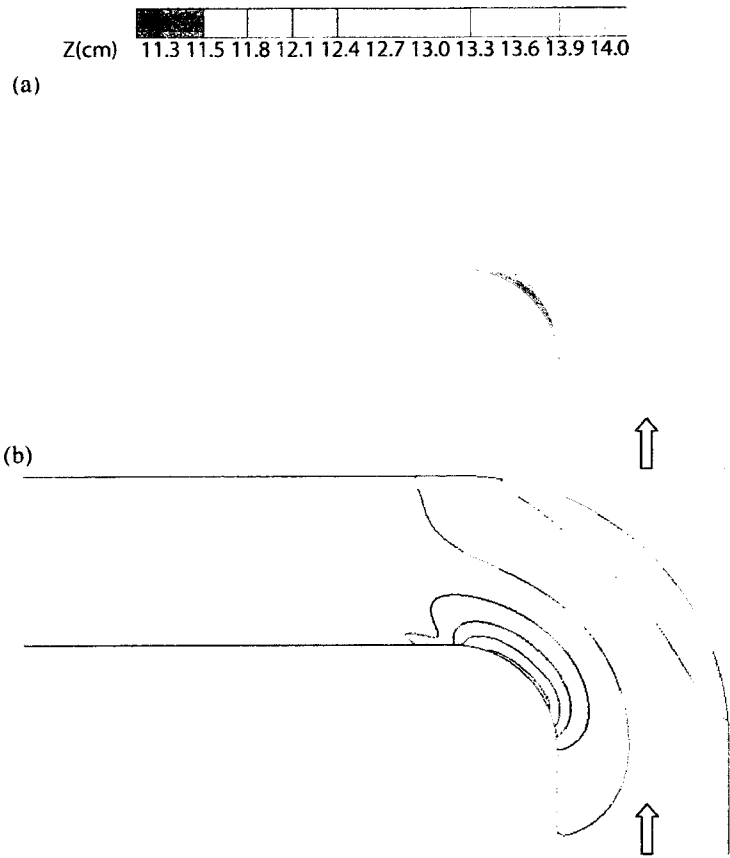
Fig. 4.8. Contours of predicted water surface level from: (a) porosity concept (Phoenics with RSM model); (b) VOF model (FLUENT with RSM model).

U_T/U_i 0.14 0.28 0.43 0.57 0.72 0.87 1.01 1.16 1.31 1.45 1.60

Ls
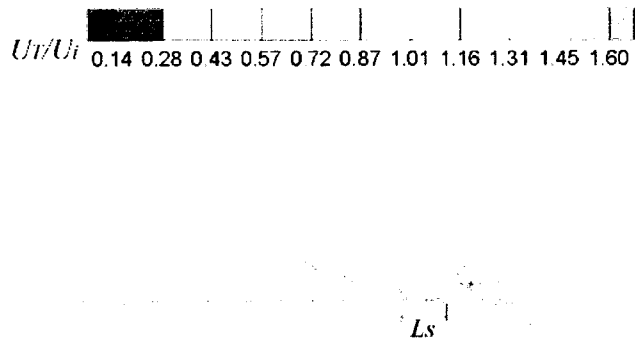
Fig. 4.9. Vector plots of U-V showing *Ls* at z/Z=0.83 using the porosity concept (Phoenics with RSM model).
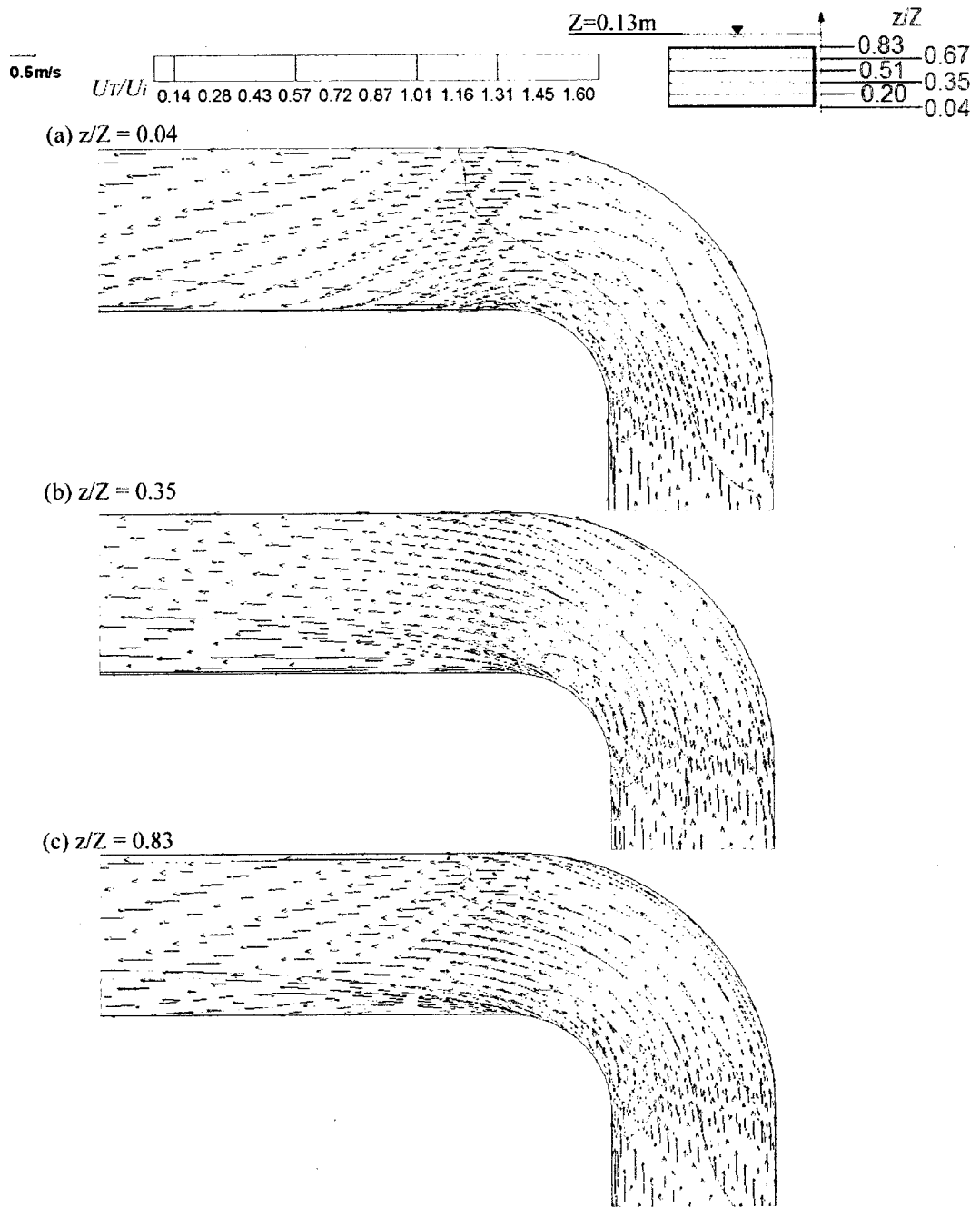
Fig. 4.10. *U-V* vectors with contours of U_T/U_i at depths (FLUENT, VOF, RSM): (a) z = 0.05cm; (b) z = 4.5cm; (c) z =10.5cm.
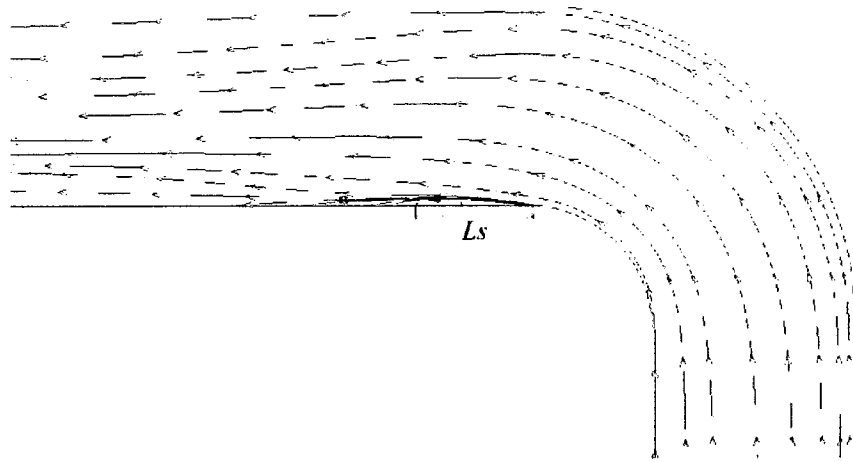
Fig. 4.11. Streamlines showing the flow separation zone near the inner wall based from simulation of RSM and VOF model of FLUENT at z/Z = 0.83 (=10.5cm).
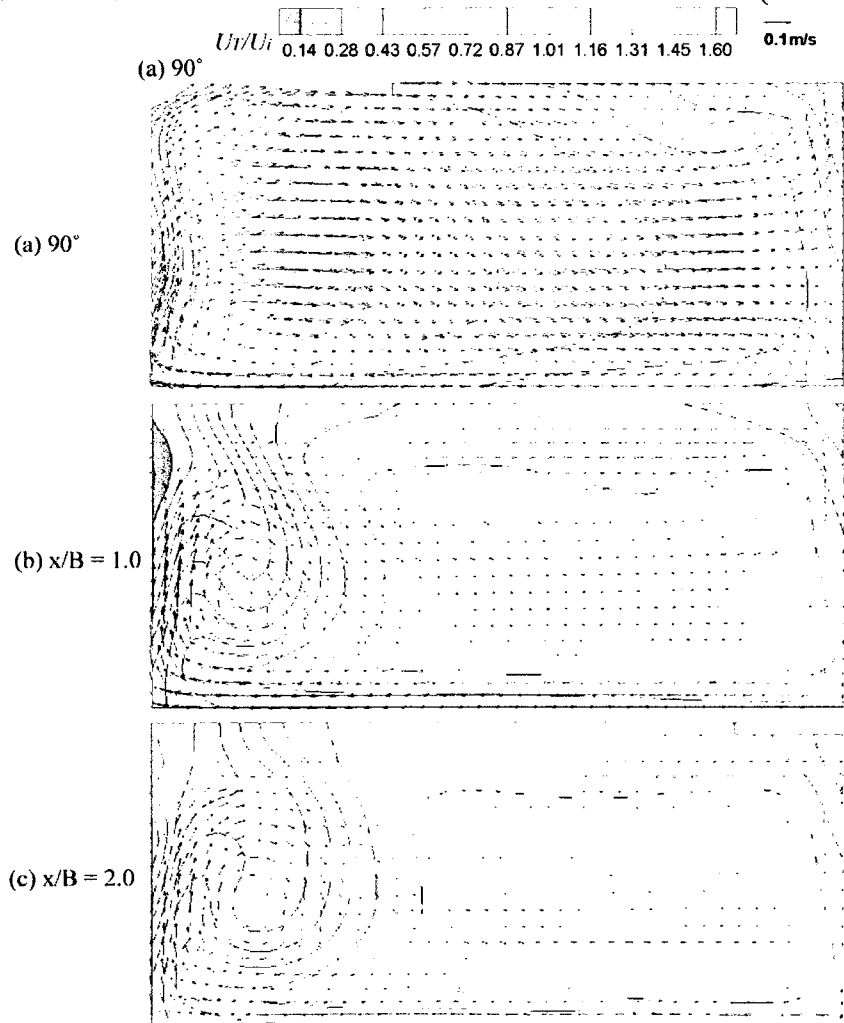
Fig. 4.12. Predicted vector plots of V-W velocity and contours of U_T/U_i from RSM and VOF model of FLUENT at: (a) 90°; (b) x/B=1.0; (c) x/B = 2.0.
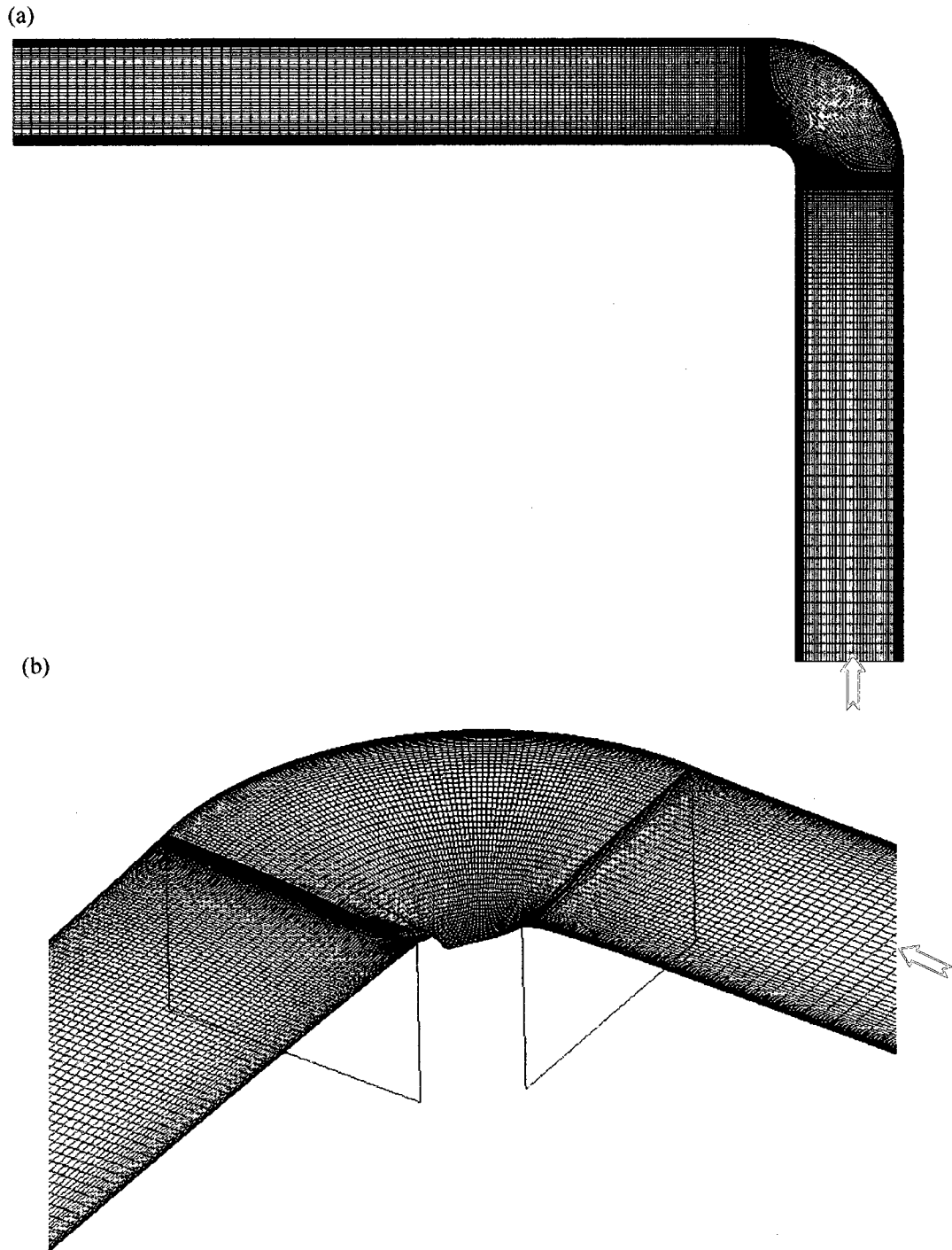
Fig. 4.13. (a) Grid for the simulations with a rigid-lid assumption for the 0.6m wide bend (203, 41, 25); (b) rigid-lid mesh for water surface geometry (vertical exaggeration of 3.0)
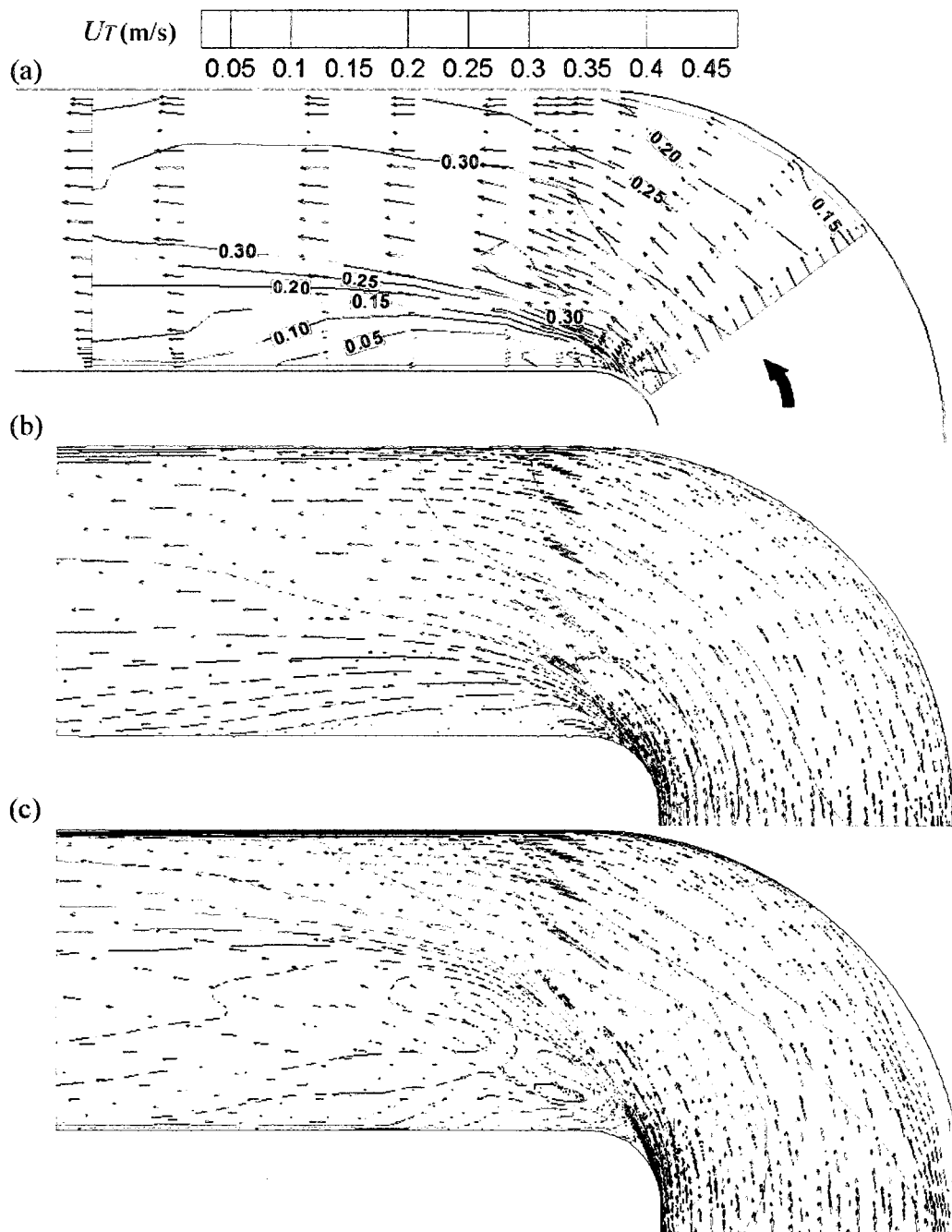
Fig. 4.14. *U-V* vectors with contours of U_T/U_i at z/Z=0.89 for the 0.6m-wide bend: (a) experiment; (b) RNG k-ε model; (c) LES model.
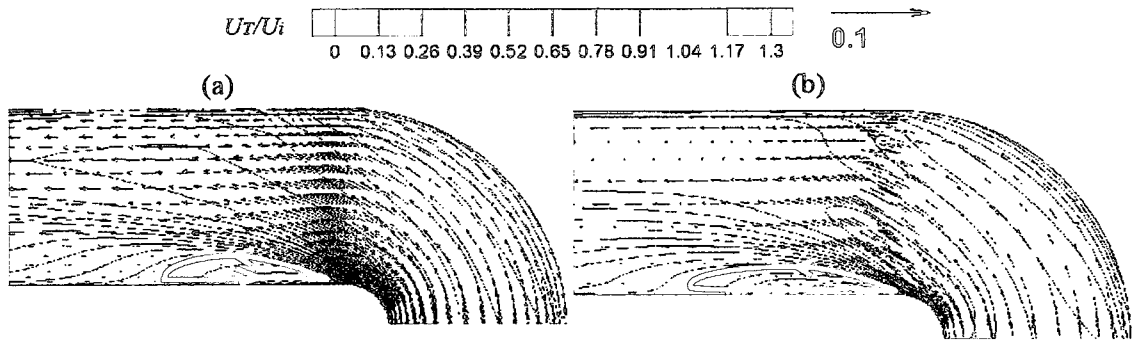
Fig. 4.15. Contour plots of velocity and vector plots of U and V velocity components at z/Z=0.89 for the 0.61m-wide bend: (a) VOF method with RNG k-ε model, (b) VOF method with RSM.
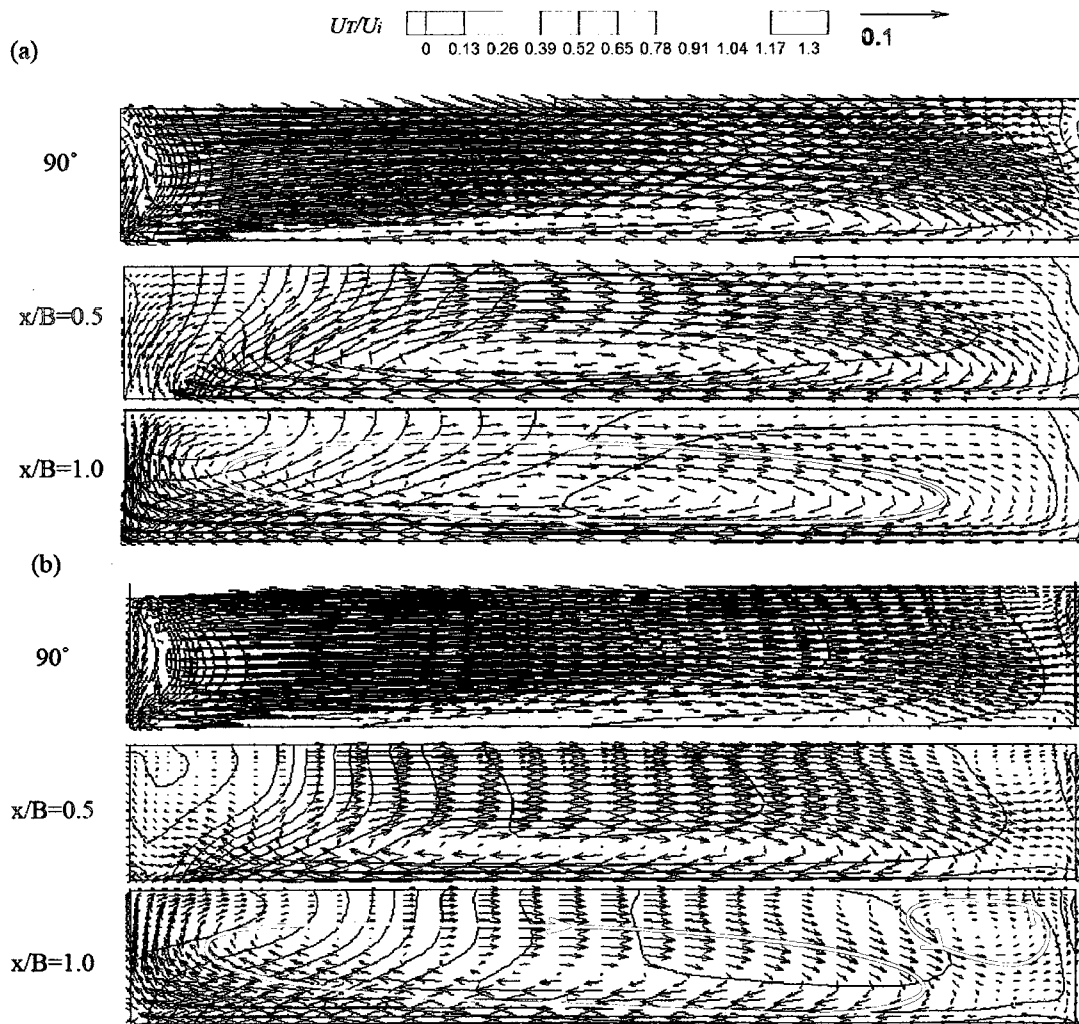
Fig. 4.16. Vector plots of V and W velocity components and contour plots of U_T/U_i at 90°, x/B=0.5, and x/B=1.0 for the 0.61m-wide model: (a) VOF method with RNG k-$ε$, (b) VOF method with RSM.

69

5. THREE-DIMENSIONAL MODELING OF FLOW IN OPEN-CHANNEL SHARP BENDS WITH VANES

5.1 Introduction

The main flow characteristics of sharp bends in rectangular open channels are secondary flows driven by centrifugal forces, a large transverse water surface slope, a zone of flow separation along the inner wall, and high turbulence caused by the flow separation. Several laboratory studies have investigated flow characteristics around bends (Reinauer and Hager 1997; Tominaga et al. 1999; Tominaga and Nagao 2000; Blanckaert and Graf 2001; Booij 2003; Roca 2009). However, the cost and time requirements of physical experiments prompted many investigators to explore the potential of numerical models as a more flexible and inexpensive tool to examine flow behaviour subject to various geometries and boundary conditions.

Earlier numerical studies adopted a two-dimensional (2D) depth-averaged approach (Kuipers and Vreugdenhil 1973; Kalkwijk and de Vriend 1980; Odgaard 1986a,b; Jin and Steffler 1993; Nagata et al. 1997; Kassem and Chaudry 2002). However, both secondary flow and a proper water surface approximation of flow in open-channel bends cannot be truly incorporated in 2D models (Hsieh and Yang 2003; Lu et al. 2004). Thus, fully three-dimensional (3D) models are required to accurately represent these flows (De Vriend 1981; Demuren and Rodi 1986; Cheng and Farokhi 1992; Meselhe and Sotiropoulos 2000; Wu et al. 2000; Wilson et al. 2003).

Many 3D models investigating flow dynamics and sediment transport in channel bends use a rigid-lid assumption (Demuren and Rodi 1986; Pezzinga 1994; Hodskinson 1996;

70

Wu et al. 2000; Huang et al. 2001, Zeng et al. 2008; van Balen et al. 2009). Static pressure is much larger than kinetic pressure for subcritical flow with a large free surface variation such as in open-channel bend flow. With a rigid-lid assumption, an incorrect pressure field is substituted into the momentum equation, leading to errors in the prediction of the flow field (Ouillon and Dartus 1997). Three-dimensional models with a free surface kinematic equation can overcome limitations of the rigid-lid assumption, but known average water depths are still required prior to constructing the numerical grid (Ferguson et al. 2003; Rameshwaran and Naden 2004; Ruether and Olsen 2005). The volume of fluid (VOF) method (Hirt and Nichols 1981) is a successfully-tested alternative to trace large variations in the free surface in numerical simulations without the limitations or requirements of other models described above (Hieu and Tanimoto 2005; Ramamurthy et al. 2006).

Most 3D models are based on Reynolds averaged Navier Stokes (RANS) equations, closed by a k–ε model or a variation such as the renormalized group (RNG) k-ε model, which is known to provide better predictions in situations involving flow separation (Ouillon and Dartus 1997; Biron et al. 2004). However, since the k–ε model is linked to isotropic turbulence, it has limited predicting capabilities for secondary motions of fluids (Booij 2003; Kang and Choi 2006) and it also under-predicts the extent of the flow separation zone (Dargahi 2004). Hence, higher order turbulence models such as the Reynolds stress model (RSM) and large eddy simulation (LES) are required for the study of flow around a bend (Booij 2003; Luo and Razinsky 2009; van Balen et al. 2009). This is particularly true for sharp bend flows, occurring when the ratio of width (B) to the mean radius (R) exceeds 0.33, where a flow separation zone is present along the inner

wall (Marriot 1999; van Balen et al. 2009). Most previous studies investigated open-channel bends with relatively large R, where this flow separation zone was not significant (Shurky, 1949; Rozovskii, 1957; De Vriend, 1977; Booij, 2003).

Several studies have examined the impact of artificial structures to alter the flow field in bends such as bendway weirs (Przedwojski et al. 1995; Jia et al. 2005; Abad et al. 2008) and submerged vanes (Odgaard and Kennedy 1983; Odgaard and Spoljaric 1986, 1989; Odgaard and Wang 1991a,b; Derrick et al. 1994). These structures favour ship navigation and reduce erosion linked to the secondary flow caused by the curvature of the bend. However, studies aiming at reducing the zone of flow separation in open-channel bends have been scarce. Continuous vertical vanes, also called guide vanes, are widely used in water and wind tunnels to limit bend energy losses and obtain a more uniform flow in sections downstream of the bend (Sahlin & Johansson 1991; Wetzel and Arndt 1991; Barlow et al. 1999; Luo and Razinski 2009). Our laboratory experiments revealed that these vertical vanes were successful in considerably decreasing secondary flow in a sharp open-channel bend, besides providing a very uniform flow in the section downstream of the bend (Han et al., in review a). However, our quantitative analysis of the flow field was limited to the area downstream of the bend, since detailed turbulent flow measurements could not be obtained experimentally between vanes. Here, we use a 3D model to provide a more detailed analysis of the impact of using vanes on the mean and turbulent flow field in the bend and downstream zones, and to assess how these modifications can reduce flow separation, secondary flows and energy loss in sharp bends.

5.2 Methods

In Chapter 2, a thorough analysis of the role of turbulence models, grid generation methods and water surface treatment in 3D models was conducted to determine the best modeling parameters to investigate the impact of vanes on the flow field. The best agreement with LDA and water surface topography data was obtained with FLUENT implementation of the RSM in conjunction with the VOF model with a BFC grid. Luo and Razinsky (2009) also observed a better agreement of RSM over RNG k-ε model in their 180° turbulent air duct flow, although some deficiencies for flow separation and re-attachment position were noted. When the model was tested with a rigid-lid assumption, it underestimated the maximum streamwise velocity by 15% compared to laboratory measurements (Han 2009). Furthermore, the rigid-lid model failed to produce the flow separation along the inner wall of the bend and a weaker counter-rotating secondary cell near the outer wall. These preliminary tests highlighted the crucial role of the water surface treatment in simulations of sharp bend flows, even for a low Froude number (0.38).

These modelling parameters were used in 3D simulations of a sharp bend without vane, with one vane and with three vanes, following the experimental conditions described in Chapter 2 (Fig. 5.1). The horizontal flume with rectangular cross-sections has a 90° bend section which is connected to upstream and downstream channels with a width of 0.61m and a mean radius of curvature of 0.46m. The simulation results were compared with 3D LDA velocity data collected at 1638 sampling locations in the bend and downstream sections (Han et al. in review). Flow conditions used to define boundary conditions for

the three simulations are presented in Table 5.1. Numerical grids for the bend with and without vanes are shown in Fig. 5.2. A finer mesh close to the walls was generated using a power law, so that the first grid cell next to the walls was constructed well within the logarithmic region ($30<u_\tau z_w/v<100$, where u_τ = friction velocity; z_w = normal distance to the wall; v = kinematic viscosity), a condition required to satisfy the use of the non-equilibrium law-of-the-wall (Launder and Spalding, 1974). To ensure the independence of grids on the results, series of grids were constructed with the number of cells in each direction increasing by steps of 20%, starting from the coarsest grid. The deviations of velocities and pressures were generally much less than 1% between the results obtained from the final grid and the penultimate grid presented in Fig. 5.2.

FLUENT uses a finite volume solver that employs the Pressure-Implicit with Splitting of Operators (PISO) algorithm for pressure-velocity coupling, a variation of the SIMPLE algorithm, to solve the 3D RANS equations (FLUENT user's guide, 2006). The RSM model computes all the stresses of anisotropic turbulent flows. However, due to the complexity of the model and additional computing cost, the application of the RSM to open-channel flow has been limited (Kang and Choi 2006). At the inlet (Fig. 5.1), uniform velocity was assumed for all simulations. The average inlet velocity and turbulence intensity (4.6%) were obtained from LDA measurements taken at the inlet. The outlet of the numerical model was defined as a pressure boundary that allows the water and air to flow out freely with the same opening area as in the physical model of Han et al. (in review). The grid has a vertical domain height of 0.18m allowing air to occupy the top half of the domain. The time step of the unsteady simulations was set to get a Courant number less than one. The simulation was assumed to have reached a

steady state solution when the difference in the mass flow rates at the flow inlet and outlet was less than 0.01% in the final solution. However, sufficient extra time steps were provided to confirm that the steadiness of the flow field was achieved. All the solid boundaries of the channels (bed, walls and vanes) were assumed to be smooth.

5.3 Results

5.3.1 No-vane system (validation)

The results of simulations for the no-vane system (Fig. 5.1) were compared with the 3D LDA mean and turbulence velocity data (Han et al. in review a). The streamwise, lateral, and vertical velocity components (U, V, and W, respectively) were used to compute the mean velocity vector $U_T = \sqrt{(U^2 + V^2 + W^2)}$. There is a good agreement between the predicted velocity and LDA measurements (Fig. 5.3). In particular, zones of flow acceleration near the inner wall and deceleration near the outer wall of the bend ($\theta = 45°$) are well depicted by the simulation (Fig. 5.3). These zones are associated with favorable and unfavorable streamwise pressure gradients that can be seen from both the measured and simulated water surface topography distribution (Fig. 5.4a,b). As the flow enters the bend, water surface becomes super elevated at the outer wall and depressed at the inner wall. The lateral slope of the water surface reaches its largest value near the central section of the bend ($45°<\theta<50°$), and it starts to recover as the flow leaves the bend. The simulated spatial distribution of water surface elevation (Fig. 5.4b) follows very well the laboratory observations (Fig. 5.4a), with a coefficient of determination (R^2) value of 0.93 and a regression slope of 0.90 (Fig. 5.4c), indicating a high level of agreement with the VOF method.

Table 5.2 provides R^2 and regression slope values for the comparison between the simulated and measured velocities (U, V, W) and the turbulent kinetic energy (ke). Equation 1 was used to obtain the turbulent kinetic energy (ke):

$$ke = \frac{1}{2}\left(\overline{u'^2} + \overline{v'^2} + \overline{w'^2}\right) \tag{5.1}$$

where, u', v' and w' are the fluctuating velocity components in the streamwise, lateral and vertical direction, respectively. The simulations generally agree well with the experimental data for the streamwise and lateral velocity. However, the agreement for the vertical velocity and ke is less good. Note that a lower correlation for the W component is commonly observed, since vertical velocities are typically very close to 0 (Bradbrook et al. 2001). Here, the range for W is generally below 0.01 m/s. Lower correlation for ke is also frequently noted in the literature since ke values involve squares of velocity terms (Booij 2003; Zeng et al. 2008). An LES model may have provided better results. However, only the rigid-lid water surface treatment is available with LES in FLUENT. Based on our preliminary tests which showed a marked impact of the rigid-lid assumption on the simulated flow field, it was decided not to use this approach.

The development of secondary flow circulation in the bend is clearly identified from the lateral and vertical velocity vector plots (Fig. 5.5). The model was able to predict the existence of the main secondary flow cell caused by the centrifugal force in the sharp bend. The weak secondary flow cell near the outer wall which is apparent in the LDA measurements too (Fig. 5.5a) was well reproduced by the RSM model (Fig. 5.5b). Note that the RNG k-ε model, which was also tested for this flow configuration, it failed to predict the full rotating motion of the cell (Han 2009).

The zone of flow separation along the inner wall is generated due to the accelerating flow and an adverse pressure gradient in this zone. It is linked to the recovery of the horizontal water surface slope in the downstream section of the bend (Fig. 5.4a,b). The experimental data (Han et al., in review) indicate that the upstream location of the flow separation zone is close to $\theta \approx 50°$ for all heights above the bed, and the flow separation zone length (L_s) and width (B_s) reach their maximum values near the free surface (Fig. 5.6b). The simulated flow field with the RSM model was close to the measurements in this zone, with predicted L_s and B_s values near the water surface corresponding to 107% and 111% of the measured values, respectively. However, the model markedly over-predicted the L_s and B_s values near the bed (Fig. 5.6c). Also, the model predicts a starting point further downstream (near 85°) compared to laboratory measurements.

5.3.2 Bend with vanes

The validated 3D model was used to examine the impact on the flow field of 1-vane and 3-vane configurations in the bend. As seen above, flow features in the sharp open-channel bend are closely linked to the accelerated flow near the inner wall resulting in a highly non-uniform flow, with a depression of the water surface and flow separation along the inner wall (Figs. 3, 4, 6). For the 1-vane and the 3-vane systems, Fig. 5.7 shows that the mean flow field near the bed and near the water surface is clearly more uniform than for the bend with no vane, particularly for the 3-vane case which very effectively redistributes the flow.

The contour plots of the predicted free surface level indicate that the depth variation is markedly reduced by the presence of vanes (Figs 4a,b and 8). The predicted maximum

variations of the free surface level in the bend are 8.0 mm, 5.0 mm, and 3.0 mm for bends with no vane, 1 vane and 3 vanes, respectively. The predicted maximum variations for all three cases are found close to the inner wall of the bend. Freeboard requirement for the case with vanes is thus less since the free surface levels at the outer wall are reduced. Hence, channel construction cost for bends with vanes would be correspondingly reduced.

Lateral and vertical velocity plots (Fig. 5.9) show that the sectional flows moving through the sub-areas between the vanes produce their own secondary flow cells. These cells rotate in the same direction. There are two and four secondary flow cells for the 1-vane and the 3-vane systems, respectively (Fig. 5.9b,c). At the immediate section downstream of the vane tips, these cells lead to increased shear-induced turbulence (Fig. 5.10). Compared to the no-vane case (Fig. 5.9a), the strength of the secondary flow, which can be identified from the length of the vectors, is much weaker, especially in the 3-vane case (Fig. 5.9c). Flow recovers rapidly to form a nearly uniform flow, after a short distance from the bend exit (x/B = 4.0), in particular for the 3-vane system (Fig. 5.9c).

The simulation results show that the dimensions of the separation zone are also markedly reduced in the presence of vanes, as was the case in the experimental study (Han et al. in review). The zone of flow separation was identified only near the inner wall for the bends with vanes. No flow separation was predicted close to any of the vanes. The simulations also show that the flow separation zone is smallest for the bend with 3 vanes. For the 1-vane case, the predicted values of L_s and B_s near the water surface are 0.24m (= 0.40B) and 0.04m (= 0.07B), respectively. The extent of the separation zone is further reduced in the 3-vane case, and the predicted values of L_s and B_s are 0.16m (=0.26B) and 0.02m

(0.03B) near the water surface. These dimensions are in close agreement with those obtained from dye observations (Han et al. in review). However, as in the no-vane case, the location of flow separation is delayed further downstream of the bend.

The contour plots of ke show that the high turbulence zone associated with the flow separation zone at the inner wall is noticeably reduced for bends with vanes (Fig. 5.10). Local shear-induced high turbulence zones downstream of the vanes dissipate rapidly in the downstream section, in particular for the 3-vane system (Fig. 5.10c). However, the shear-induced high turbulence zone due to flow separation along the inner wall persists farther downstream.

Fig. 5.11 shows the distribution of bed shear stress (τ_w) for the bend with and without vane, which illustrates the major impact of the vanes on the near-bed flow field. The initial value of τ_w in the approach channel for all three cases is quite low and uniform. However, the extent and magnitude of the high shear zone is markedly different among the three bed configurations. For the no-vane case, τ_w increases rapidly along the inner wall in the bend and progressively decreases downstream of the bend, creating a large zone of high shear stress values. By adding vanes in the bend, this zone shrinks and the shear level is reduced, particularly for the 3-vane case (Fig. 5.11c). This leads to reduced chances of channel erosion in these zones.

Following Sudo et al. (2001), the intensity of secondary flow (I_s) and turbulence energy (K_a) in an open channel system with a bend are defined as:

$$I_s = \frac{1}{R_h^2 U_i^2} \int_0^Z \int_0^B (V^2 + W^2) dB \, dZ \tag{5.2}$$

$$K_a = \frac{1}{R_h{}^2 U_i^2} \int_0^Z \int_0^B \frac{1}{2}\left(\overline{u'^2} + \overline{v'^2} + \overline{w'^2}\right) dB \, dZ \qquad (5.3)$$

where R_h is the hydraulic radius and overbars indicate time averages. Experimental LDA velocity measurements for the vane configurations (Han et al., in review a) were limited to sections downstream of the bend, preventing a quantitative analysis of secondary flow, turbulence, and energy loss in the bend section. The detailed simulated flow field from the 3D model permits a broader understanding of secondary flow and turbulence energy in the bend region (Fig. 5.12).

The intensity of secondary flow (I_s) and turbulence energy (K_a) are calculated using equations 2.1 and 2.2, respectively. The trends of I_s are similar for the flow with and without vanes. I_s values start to increase as the flow approaches the bend section (-1.0 < x/B < θ = 0.0°), and they reach their maximum value at the bend exit (θ = 90°) (Fig. 5.12a). However, the maximum values of I_s are markedly reduced for the vane cases, with maximum values at the bend exit of 1.9, 0.7, and 0.3 for a bend with no vane, 1 vane, and 3 vanes, respectively. This indicates that the 3-vane configuration is most effective in controlling secondary flow. Large negative slopes for I_s downstream of the bend for all three cases indicate that the strength of the secondary flow weakens rapidly, as the flow moves into the straight channel section downstream of the bend (θ = 90°< x/B <2.0).

Fig. 5.12b shows that, similarly to Is, turbulence energy K_a increases for the three configurations until the flow reaches the exit of the bend (θ = 90°). For the no-vane case, the further increase of K_a (up to 0.14) between the bend exit (θ = 90°) and x/B=1.0 is due to the high turbulence associated with the flow separation zone. However, the pattern is

different in bends with vanes. The K_a values for both vane cases show a rapid decay as the flow enters the downstream straight channel after the bend ($\theta = 90°< x/B < 5.0$). This is due to the reduced turbulence level associated with smaller flow separation zone along the inner wall of the bend which was described earlier. The 3-vane case shows the lowest overall K_a level in the entire channel length. However, a smaller decay rate of K_a between x/B = 1.0 and x/B = 2.0 is noticed for the 3-vane case (Fig. 5.12b). This could be linked to the local intense shear generated by the adjacent three pairs of secondary flow cells that emerge from the subareas of the 3-vane system. For both vane cases, the lowest values of K_a are reached at x/B=5.0. However, for the no-vane case, the residual turbulence is relatively high (K_a =0.09) at x/B = 4.0, and has not reached the asymptotic value of K_a = 0.06. Values of both I_s (Fig. 5.12a) and K_a (Fig. 5.12b) are lowest for the 3-vane system, indicating that this bend-vane configuration is very effective in reducing intensities of both secondary flow and turbulence.

The specific energy (E) at any cross-section for channels with zero bed slopes is computed as:

$$E = Z + \alpha \frac{U^2}{2g} \tag{5.4}$$

where the velocity distribution coefficient, α, is:

$$\alpha = \frac{\sum_{i=1}^{n} U_a^3 A_i}{U^3 A},$$

where U_a is the average velocity for any segment of the cross section, and A_a is the area for that segment (Strum, 2001). Fig. 5.12c shows the pattern of change in E along the channel. The slope of the specific energy line is largest between x/B = -1.0 and x/B = 1.0,

indicating that the presence of the bend causes large energy losses. The no-vane case shows the largest energy loss, and the energy loss is smaller for both vane cases (Fig. 5.12c). Although the 3-vane case shows a more uniform flow compared to the 1-vane case, boundary friction losses might also be increased in the former, resulting in similar energy loss for both cases. As such, in practice, there is no need to use a large number of vanes in the bend if energy conservation is a primary goal.

5.4 Summary and conclusions

This study analyzed the effect of curved vanes in an open-channel sharp 90° bend using a 3D numerical model. To simulate the complex flow features of the open channel bend flow such as large free surface variation, flow separation, secondary flow, and energy loss, a VOF method and RSM model were adopted. The predicted water surface elevation from VOF model shows a very good agreement with the measured water surface data and highlight that a proper treatment of the water surface is critical for the numerical study of flow in an open-channel sharp bend. Also, among other tested turbulence models, RSM model provides the closest agreement with the experimental data, with only slight discrepancies in the upstream location of the flow separation zone.

The results show that the vanes can greatly improve the adverse impacts of the bend in the channel system. By placing vanes in the bend, the flow distribution through the bend becomes more uniform, and the size of the flow separation zone becomes smaller compared to the bend with no vanes. The strength of the secondary flow and turbulence level also get reduced. Furthermore, a reduction in energy loss in a bend can be achieved by using vanes. The improved performance in bend flows when vanes are present could

be due to the reduced ratio of width to depth in the subsections of the bend (Han et al. in review a).

The bed shear stress distribution patterns clearly show that vanes also reduce shear stress in the bend. Lower bed shear stress values in the vane configurations should result in reduced bedload transport in the bend zone. These improved flow features could contribute to a decrease in the tendency for channel erosion in unlined channels. Future studies should use a 3D numerical model to investigate the impact of vanes on more complex, non-rectangular bends, ideally over a mobile bed using a coupled sediment transport module.

Table 5.1. Experimental flow conditions

Channel width (B), m	Flow depth (Z), m	Inner radius (R1), m	Outer radius (R2), m	Flow rate (Q), m³/s	Inlet mean velocity (U), m/s	Reynolds number (Re)	Froude number (Fr)
0.61	0.091	0.15	0.76	0.013	0.238	15870	0.252

Table 5.2. Coefficient of determination values (R^2) and slope of the regression line between the simulated and measured flow variables

	U	V	W	ke
R^2	0.91	0.90	0.40	0.52
Slope of the regression line	0.82	0.78	0.55	0.52

(where U is streamwise direction velocity, V is lateral direction velocity, W is the vertical direction velocity, and ke is turbulent kinetic energy.)
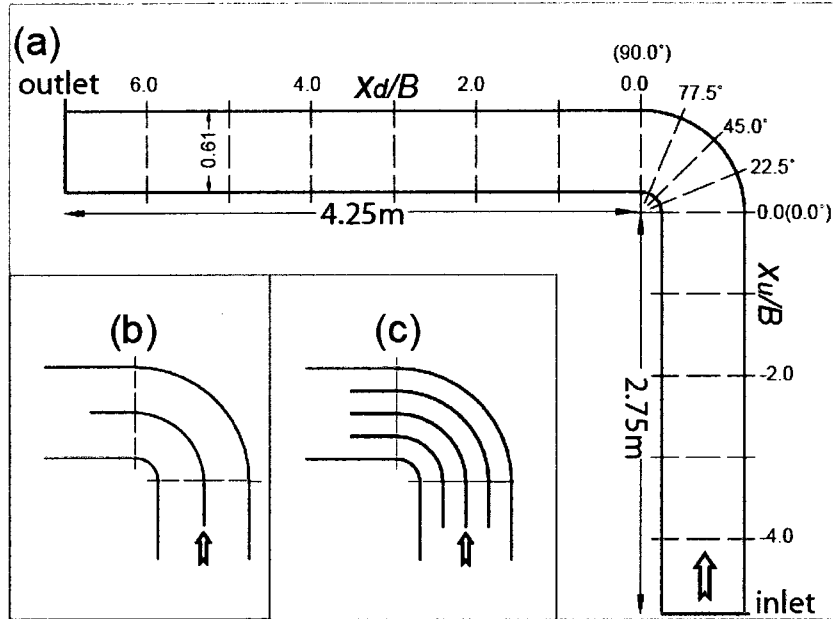
Fig. 5.1. a) Entire numerical domain for the 90° sharp bend with dimensions and positions of cross-sections, b) bend with 1 vane and c) bend with 3 vanes.
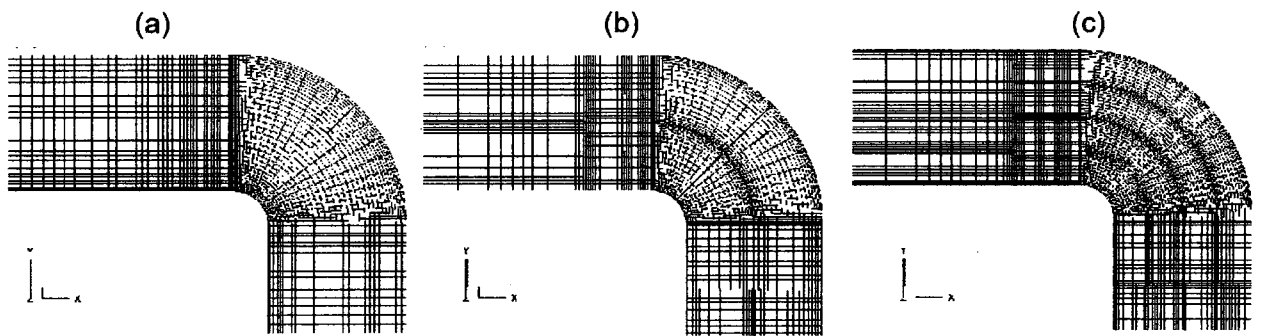
Fig. 5.2. Numerical BFC grids in the bend area for the configurations with: (a) no vane (203, 41, 29); (b) 1 vane (203, 48, 29); (c) 3 vanes (203, 69, 29).
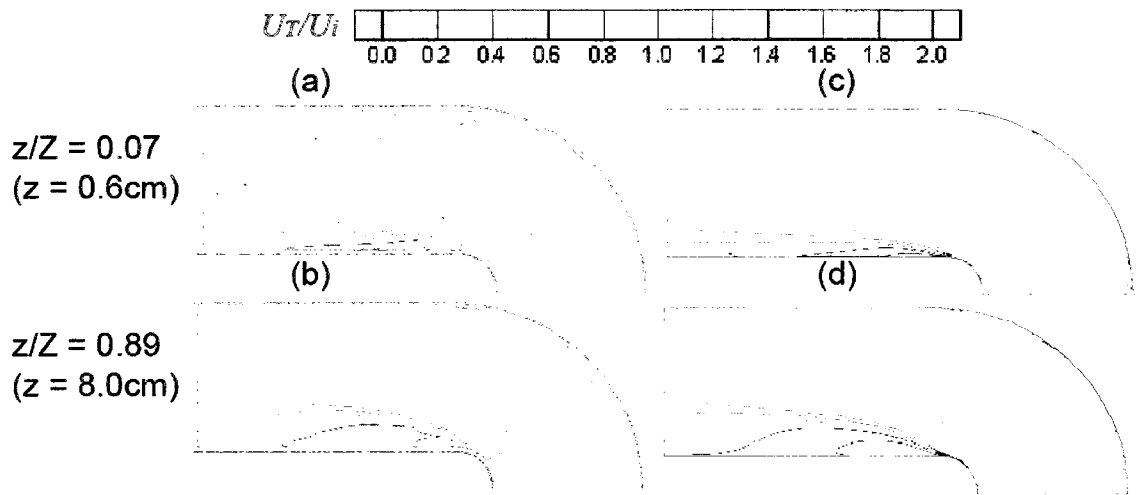
Fig. 5.3. Non-dimensional mean velocity (U_T / U_i) obtained from LDA measurements near the bed (a) and near the water surface (b), and from the 3D model near the bed (c) and near the water surface (d). Flow is to the left.
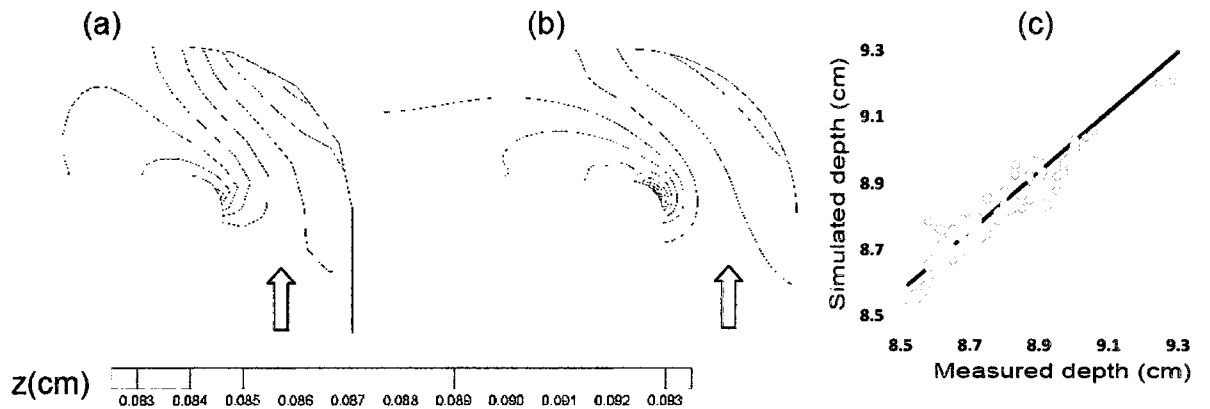
Fig. 5.4. Water surface level from laboratory measurement (a) and from VOF model prediction (b); (c) comparison of flow depth from VOF model predictions versus laboratory measurements.

86
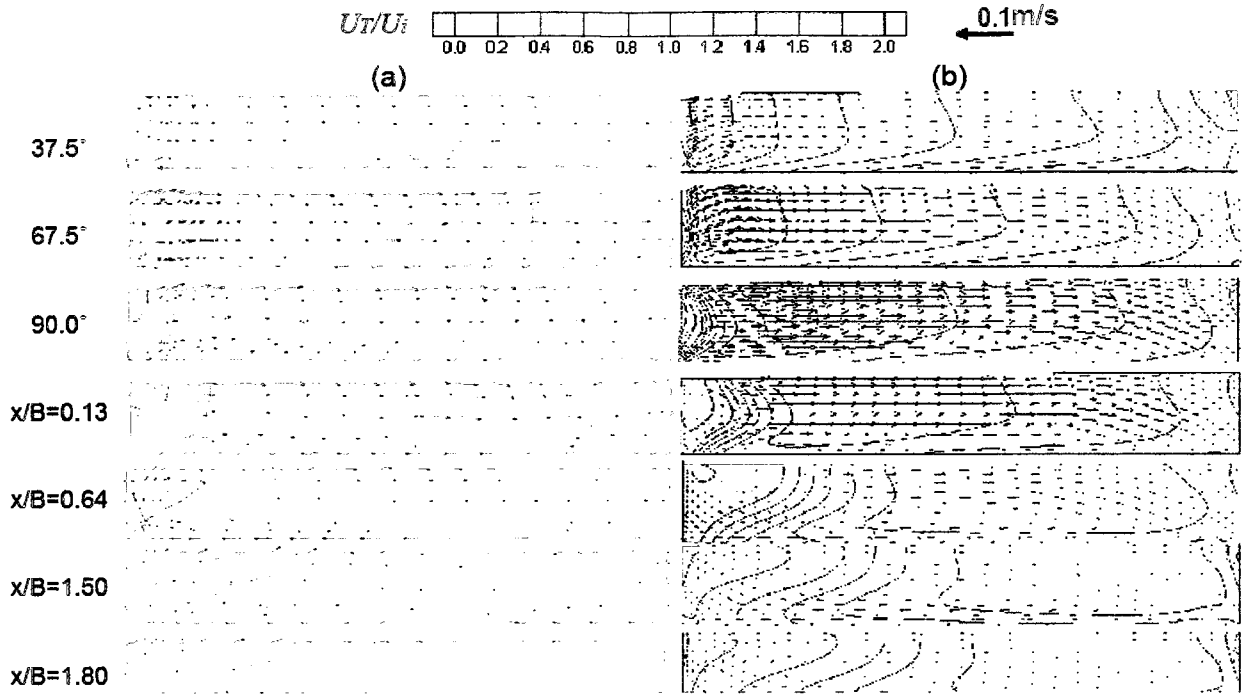
Fig. 5.5. Vector plots of lateral and vertical velocity superimposed on contours of velocity magnitude (looking downstream) in the bend and downstream cross-sections: (a) laboratory experiment; (b) 3D model.
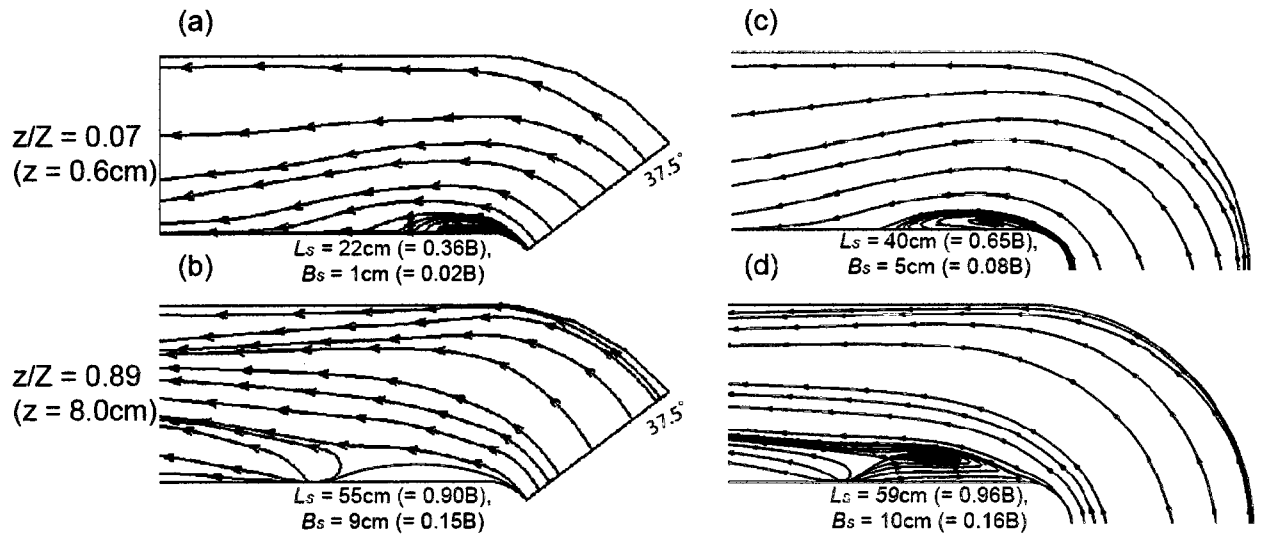
Fig. 5. 6. Streamlines showing the flow separation zone near the inner wall based on experimental data near the bed (a) and near the water surface (b), and based on 3D simulations near the bed (c) and near the water surface (d).

(a)   (b)   (c)

z/Z = 0.067
(z = 0.6cm)

z/Z = 0.89
(z = 8.0cm)
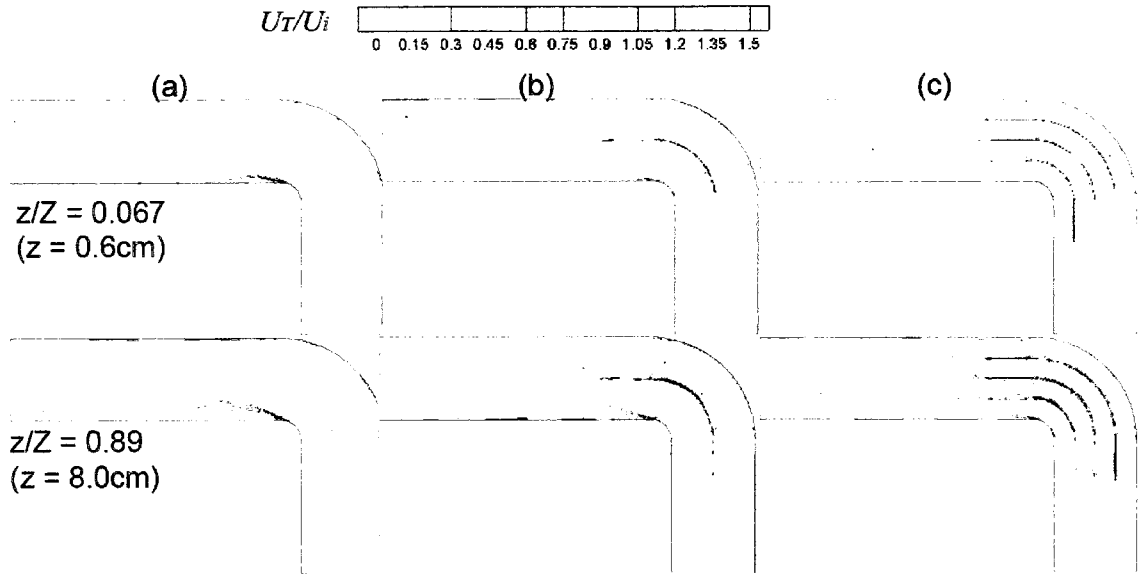
Fig. 5.7. Contours of predicted velocity near the bed and near the water surface for the configurations with (a) no vane, (b) 1 vane and (c) 3 vanes.

z(cm) ☐☐☐☐☐☐☐☐☐☐☐

0.083 0.084 0.085 0.086 0.087 0.088 0.089 0.090 0.091 0.092 0.093

(a)   (b)
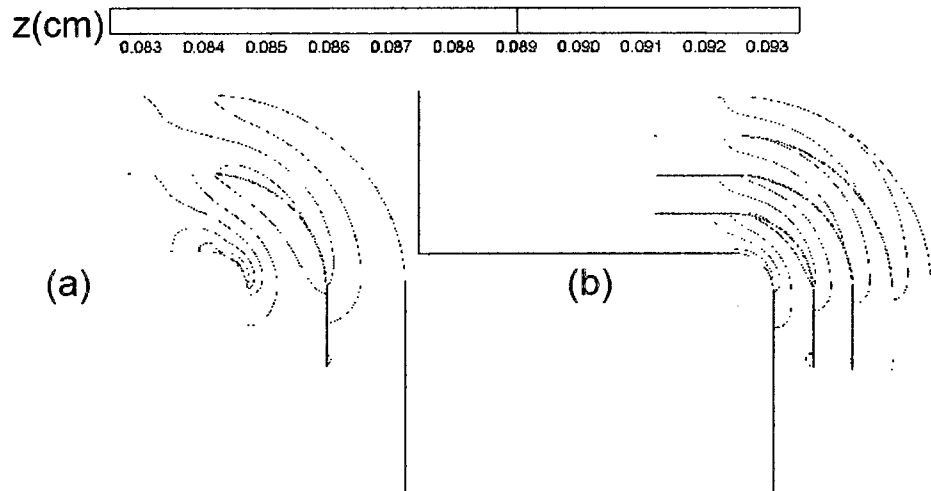
Fig. 5.8. Contours of predicted water surface level for the configuration with (a) 1 vane and (b) 3 vanes. Note that the range of water surface level is the same as for the no-vane case (Fig. 5.4).

UT/Ui

0   0.13 0.26 0.39 0.52 0.65 0.78 0.91 1.04 1.17 1.3

0.1 m/s

(a)

(b)

(c)

x/B=-3

x/B=-1

x/B=-0.5

0°

22.5°

45°

67.5°

90°

x/B=0.5

x/B=1

x/B=2

x/B=3

x/B=4

x/B=6
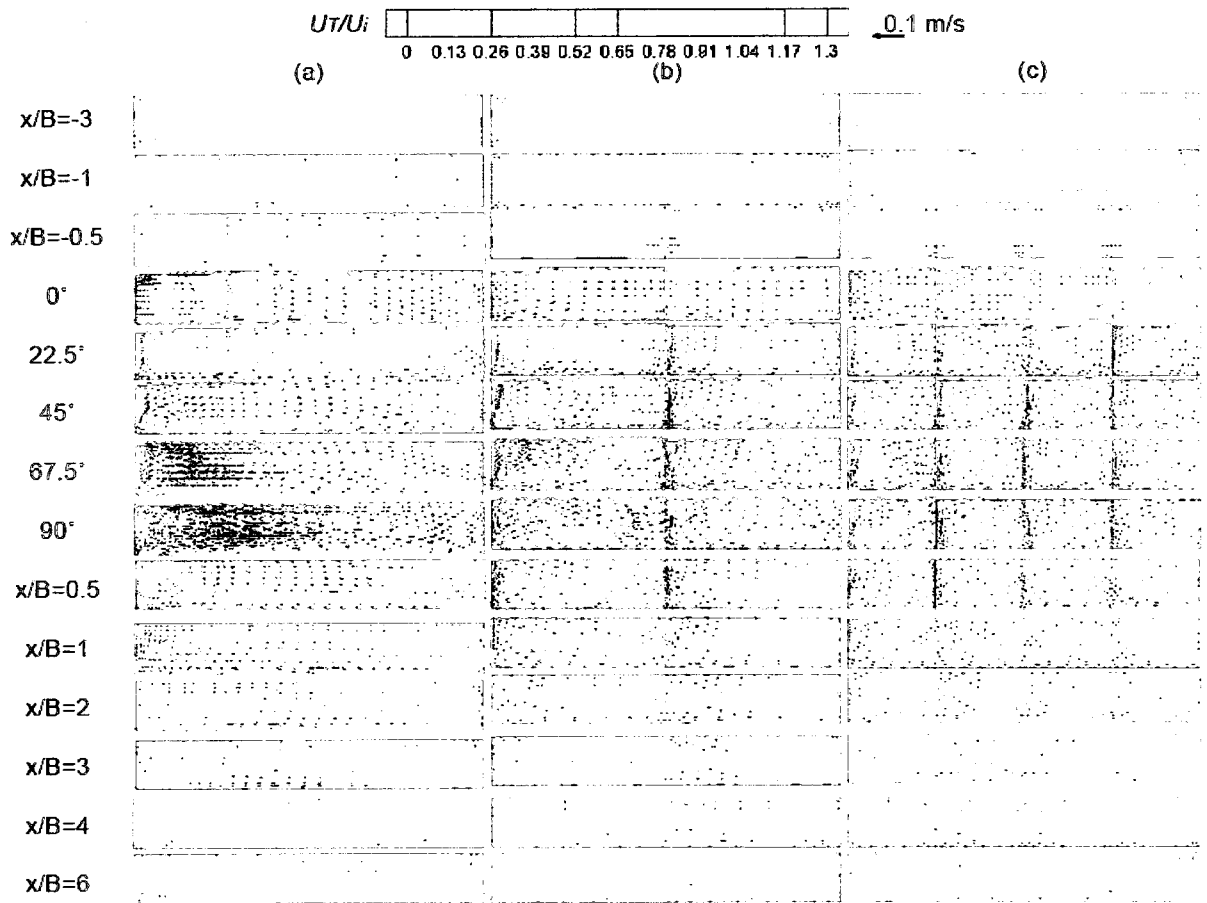
Fig. 5.9. V-W vectors with non-dimensional velocity magnitude at several cross-sections (-3<x/B< 0, 0<θ<90 and 0<x/B<6) for the configuration with (a) no vane, (b) 1 vane and (c) 3 vanes (looking downstream).

89

Fig. 5.10. Contours of ke at various cross-sections ($-3 < x/B < 0$, $0° < \theta < 90°$ and $0 < x/B < 6$) for the configuration with (a) no vane, (b) 1 vane and (c) 3 vanes (looking downstream).
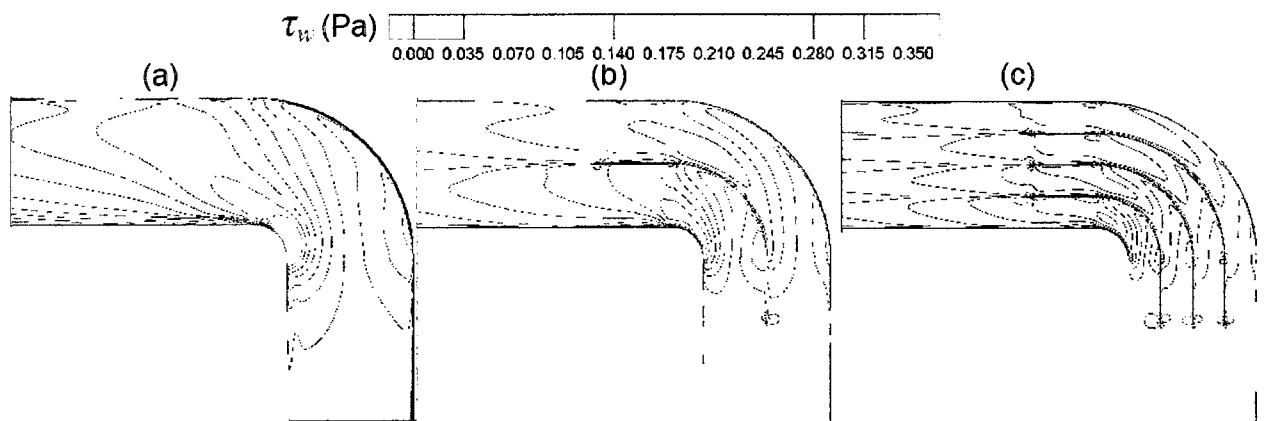
Fig. 5.11. Bed shear stress (τ_w) for the configuration with (a) no vane, b), 1 vane and c) 3 vanes.
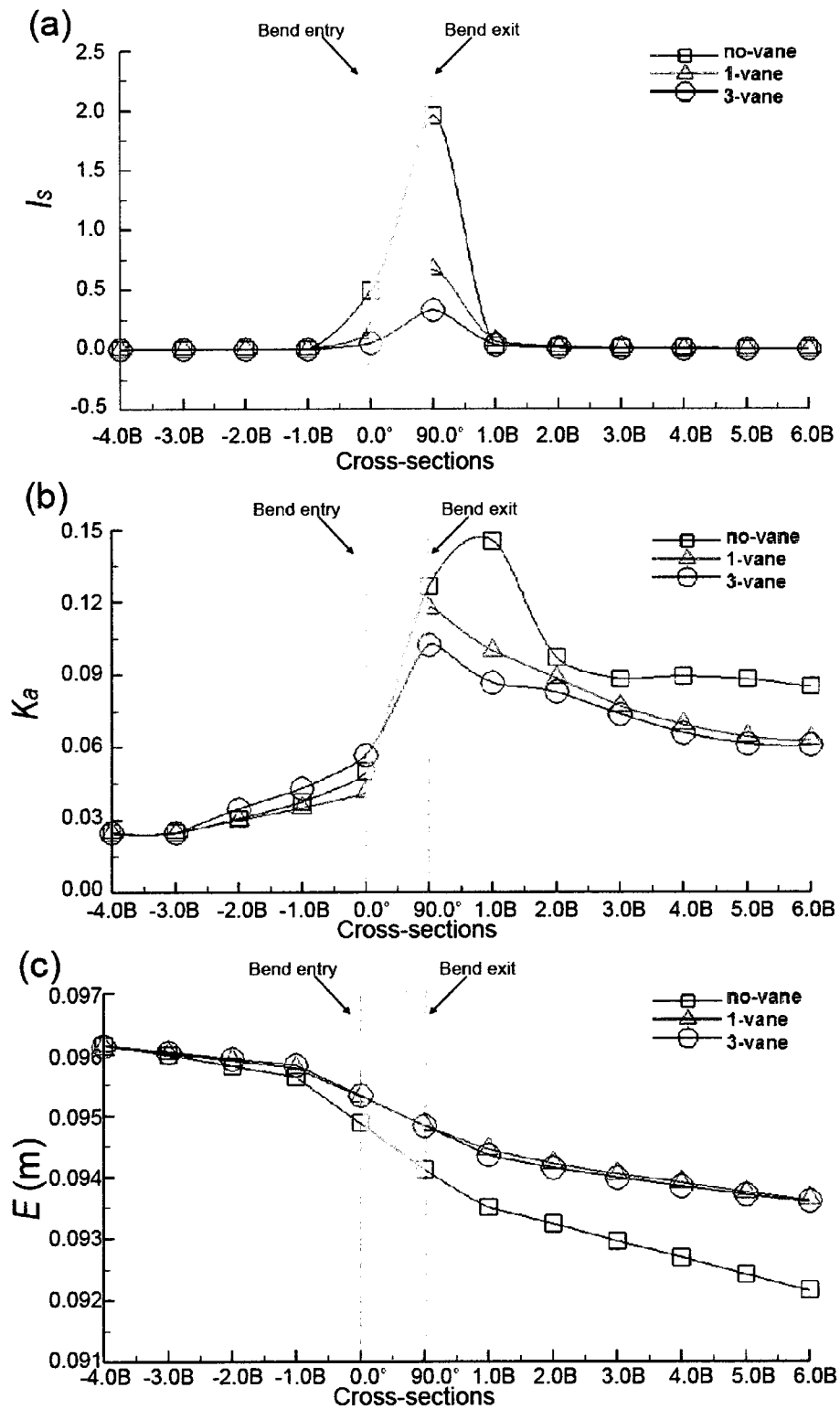
Fig. 5.12. Cross-sectional average values of (a) *Is*, (b) *Ka* and (c) *E* along the channel for the configuration with no vane (red open squares), 1 vane (green open triangles), and 3 vanes (blue open circles).

6. CONCLUSION AND SCOPE OF FURTHER STUDIES

6.1 Conclusion

Sharp bends are characterized by secondary flows, flow separation, energy losses and water surface variations caused by the bend curvature. Flow separation in turn leads to large scale turbulence which may increase energy losses. This study was able to reproduce these key flow characteristics both experimentally and virtually using a 3D numerical model and to test the effects of various designs changes such as the use of vertical vanes to reduce secondary flow impacts. Experimentally, 3D velocity data obtained from LDA measurements revealed marked differences in the mean and turbulent flow characteristics for flows in bends with and without vanes. The 3D flow characteristics in a rectangular open-channel 90° bend (no-vane system) compared well with the large number of studies that have highlighted the existence of multiple secondary flow cell structures in open-channel bends. The existence of a main inner bank cell and a counter-rotating, weaker outer bank cell in the channel downstream of the bend has been confirmed.

Numerically, the 3D model tested was successful in quantifying the effects of curved vanes in an open-channel sharp 90° bend in much more detail than what was obtained experimentally due to the difficulty of measuring the flow in the vicinity of the vanes. To simulate the complex flow features of the open-channel bend such as large free surface variation, flow separation, secondary flow, and energy loss, a VOF method and RSM model were adopted after assessment of results related to modelling based on different turbulence models and water surface treatment methods. The predicted water surface

elevation from VOF model showed a very good agreement with the measured water surface data and highlighted that a proper treatment of the water surface is critical for the numerical study of flow in an open-channel sharp bend. Also, among other tested turbulence models, RSM model provided the closest agreement with the experimental data, with only slight discrepancies in the upstream location of the flow separation zone. However, computational limitations did not allow LES simulations with a finer grid and a VOF approach to be tested. Further research on improved LES simulations may reveal a better agreement with experimental data.

The data of both the experiments and numerical simulations revealed that the vanes are very effective in reducing the adverse effects of the bends in the open channel system. By placing vanes in the bend section, the ratio of width to depth in the subsections of the bend gets reduced. More uniform flow can be established both in the bend and in the downstream channel, and the extent of flow separation zone is drastically reduced along the inner wall, especially for the 3-vane system. Also, the vanes in the bends can contribute to lowering the strength of the secondary flow, decreasing the tendency for channel erosion in unlined channels. Furthermore, a reduction in energy loss in a bend can be achieved by using vanes.

6.2 Scope of further studies

The presence of vanes alters the bed shear stress distribution patterns. Lowering bed shear stress values by the use of vanes in the bend could reduce bedload transport in the bend zone, resulting in a decreased tendency for channel erosion in unlined channels. However, this would need to be further tested using mobile-bed experiments. It could

also be tested numerically with the use of a 3D hydrodynamic model coupled with a bedload transport module. These types of models are increasingly being used in engineering and fluvial geomorphology applications (Olsen and Stokesth 1995; Olsen and Kjellesvig 1998; Nagata et al. 2000, 2005; Olsen 2007).

The major advantage of using a validated 3D numerical model is that other designs to reduce the impacts of secondary flow can be tested at low cost. For example, Ramamurthy and Basak (1973) used a linearly raised bed to reduce the flow separation in subcritical flow in rectangular channel expansions. The idea of a linearized hump may be applicable for the flow separation in open channel bend to suppress or reduce flow separation. Preliminary tests to examine the potential of bed geometry changes as a tool to limit the impact of secondary flows were made using the 3D RSM VOF model. These results, presented in Appendix A, show that a slight reduction of the flow separation zone was achieved using this method, but that it was not as effective as vanes. Compared to the flow expansion case (Ramamurthy and Basak 1973), the open channel bend flow is highly 3D dimensional with large variation of streamwise velocity in lateral direction and strong secondary flow motion. A larger number of bed configurations would need to be tested to produce an optimal design. This would be prohibitively expensive using an experimental approach, but using parallel processing, the time requirement for 3D simulations was reduced drastically to a few hours for each run.

Future research should also concentrate on how vertical vanes could be used in irrigation channels or other shapes of channels with bends. This implies working with a series of straight vanes that would eventually form a vane system. It also implies a major

difference in scale and in width-to-depth ratio. In these cases, channel performance would ideally be evaluated with a 3D numerical model that is capable of also simulating bed and bank adjustments. With ever-growing computer resources, such models will realistically be available in the near future. For example, the Virtual StreamLab (Sotiropolous, 2009) code can simulate turbulence, sediment transport processes, and flow / biota interactions in real-life streams. The model simulates turbulence using a coherent structure-resolving hybrid Unsteady Reynolds Averaged Numerical Simulations/Large Eddy Simulations (URANS/LES) model—the so-called Detached-Eddy Simulation (DES) approach (Spalart et al. 1997). The model can also discretize arbitrarily complex multi-connected domains and the impact of large-scale coherent structures on bedload transport can be investigated using a Lagrangian and Eulerian model. This is just one example of the very rapid developments occurring in the field of 3D numerical modelling which will greatly help improve our understanding of complex flow dynamics such as those occurring in sharp bends.

REFERENCES

Abad, J. D., Rhoads, B. L., Guneralp, I., García, M. H. (2008). "Flow structure at different stages in a meander-bend with bendway weirs." *J. Hydraulic Engineering*, ASCE, 138(8), 1052-1063.

Ambrosi D, Corti S, Pennati V, and Saleri F. (1996). "Numerical simulation of unsteady flow at Pr River Delta." *J. Hydraulic Engineering*, ASCE, 122, 735–43.

Barlow. J. B, Rae, W. H, Jr., and Pope, A. (1999). "Low-Speed Wind Tunnel Testing", 3rd Edition, New York: John Wiley & Sons, Inc.

Bathurst, J., Thorne, C., and Hey, R. (1977). "Direct measurements of secondary currents in river bends." *Nature* (London), 269, 504–506.

Barkdoll, B. D., Ettema, R., Odgaard, A. J. (1999). "Sediment control at lateral diversions: limits and enhancements to vane use." *J. Hydraulic Engineering*, ASCE, 125 (8), 862-870.

Binns, A.D. and da Silva, A.M.F. (2009). "On the quantification of the bed development time of alluvial meandering streams". *J. Hydraulic Engineering*, ASCE, 135(5), 350-360.

Biron, P.B., Rucher, A, Kirkbride, A.D., Roy, A.G., and Han, S. (2002). "Spacial patterns of water surface at a river confluence." *Earth surface process and Landforms*, 27(9), 913-928.

Biron, P. M., Ramamurthy, A. S., and Han, S. (2004). "Three-Dimensional Numerical Modeling of Mixing at River Confluences." *J. Hydraulic Engineering*, ASCE, 130(3), 243-253.

Biron, P.M., Haltigin, T.W., Hardy, R.J. and Lapointe, M.F. (2007). "Assessing different methods of generating a three-dimensional numerical model mesh for a complex stream bed topography." *International Journal of Computational Fluid Dynamics*, 21(1), 37-47.

Blanckaert, K. (2009). "Saturation of curvature-induced secondary flow, energy losses, and turbulence in sharp open-channel bends: Laboratory experiments, analysis, and modeling." *J. Geophysical Research*, 114.

Blanckaert. K. and Graf, W.H. (2001). "Mean flow and turbulence in open-channel bend." *J. Hydraulic Engineering*, ASCE, 127(10), 835-847.

Blanckaert, K. and Graf, W.H. (2004). "Momentum transport in sharp open-channel bends." *J. Hydraulic Engineering*, ASCE, 130(3), 186-198.

Blanckaert, K., and Lemmin, U. (2006). "Means of noise reduction in acoustic turbulence measurements." *J. Hydraulic Research*, IAHR, 44(1), 3 – 17.

Blanckaert, K. and de Vriend, H. J. (2004). "Secondary flow in sharp open-channel bends." *J. Fluid Mechanics*, Cambr. Univ. Press, 498, 353-380.

Blanckaert, K. and de Vriend, H. J. (2005a). "Turbulence structure in sharp open-channel bends." *J. Fluid Mechanics*, Cambr. Univ. Press, 536, 27-48.

Blanckaert, K. and de Vriend, H. J. (2005b). "Turbulence characteristics in sharp open-channel bends." *Physics of Fluids*, Am. Inst. Phys, 17(5), 55-102.

Booij, R. (2003). "Measurements and large eddy simulations of the flows in some curved flumes". *J. Turbulence*, 4, 1–17.

Booij, R. and Tukker J. (1996). "3-Dimensional laser Doppler measurements in a curved flume.", in "Developments in Laser Techniques and Applications to Fluid Mechanics.", Eds. R.J. Adrian, et al., 98-114, Springer, Berlin.

Bradbrook, K.F., Lane, S.N., and Richards, K.S. (2000a). "Numerical simulation of thee-dimensional, time averaged flow at river confluences." *Water Resources Research*, 9, 2731-2746.

Bradbrook, K. F., Lane, S.N., Richards, K.S., Biron, P.M, and Roy, A.G. (2000b)."Large eddy simulation of periodic flow characteristics at river confluences." *J. Hydraulic Research*, 38, 207-215.

Bradbrook, K.F., Lane, S.N., Biron, P.M. and Roy, A.G. (2001). "Role of bed discordance at asymmetrical river confluences." *J. Hydraulic Engineering.* ASCE, 127(5), 351-368.

Brizuela, E. A. (1993). "Potential flow in elbows." *J. Wind Engineering and industrial Aerodynamics*, Elsevier, 45, 125-137.

Caretto, L. S., Gosman, A. D., Patankar, S. V., and Spalding, D. (1972). "Two calculation Proceures for Steady, Three-Dimensional flows with Recirculation." *Proc. Third. Int. Conf. Num. Methods Fluid Mech.*, Lect. Notes Phys., 19, 60-68.

Chang, H.H. (1988). "Fluvial processes in river engineering". Wiley-Interscience, ISBN 0-471-63139-6

Cheng, G.C., Farokhi, S., (1992). "On turbulent flows dominated by curvature effects." *J. Fluid Engineering*, ASME, 114, 52–57.

Choudhury, D. (1993). "Introduction to the Renormalization Group Method and Turbulence Modeling." Technical Memorandum, Fluent Inc, TM-107.

Chow, V. T. (1959). "Open-Channel Hydraulics." McGraw-Hill, Inc

Chu., S. S. (2003). "Separated flow in bends of arbitrary turning angles, using the hodograph method and Kirchhoff's free streamline theory." *J. Fluid Engineering*, ASME, 125, 438-442.

Da Silva, A.M.A.F. (1999). "Friction factor of meandering flows". *J. Hydraulic Engineering*, ASCE, 125(7), 779-783.

Dargahi, B. (2004). "Three-dimensional flow modelling and sediment transport in the river Klarälven." *Earth Surface Processes and Landforms*, 29, 821–852.

Demuren A. O., and Rodi W. (1986). "Calculation of flow and pollutant dispersion in meandering channels." *J. Fluid Mechanics*, 72(11), 65– 92.

Derrick, D.L., Pokrefke, T.J., Boyd, M.B., Crutchfield, J.P., and Henderson, R.R. (1994). "Design and development of bendway weirs for the dogtooth bend reach, Mississippi River." Technical Rep. No. HL-94-10, U.S. Army Corps of Engineers, Washington, D.C.

Derrick, D.L. (1997). "Harland creek bendway weir/willow post bank stabilization demonstration project." Management of landscapes disturbed by channel incision, S. S. Y. Wang, E. J. Langendoen, and F. D. Shields, Jr., eds., University of Mississippi Press, Oxford, Miss., 351–356.

De Vriend, H.J. (1977). "A mathematical model of steady flow in curve shallow channels." *J. Hydraulic Research*, 15(1), 37-53.

De Vriend, H.J. (1981). "Velocity redistribution in curved rectangle channels." *J. Fluid Mechanics*, 107(6), 423-439.

Demuren, A.O., and Rodi, W. (1986). "Calculation of flow and pollutant dispersion in meandering channels." *J. Fluid Mechanics*, 172(11), 65-92.

Dietrich, W.E. and Smith, J.D. (1983). "Influence of the point bar on flow through curved Channels." *Water Resources Research*, 19(5), 1173-1192.

Duan, J,G. (2004). "Simulation of flow and mass dispersion in meandering channels." *J. Hydraulic Engineering*, ASCE, 130 (10), 964-976.

Durbin, P.A. (1993). "On modeling three-dimensional turbulent wall layers." *Physics of Fluids A*, Fluid Dynamics, 5(5), 1231.

Edward, T. J., Jeremiah, D. W., Jennifer, S. (2004). "Application of stereoscopic particle image velocimetry to studies of transport in a dusty (complex) plasma." Physics of Plasmas, 11 (7), L37-L40.

Engelund, F. (1974). "Flow and bed topography in channel bends." *J. Hydraulic Divison*, ASCE, 100(HY11), 1631-1648.

Ferguson, R.I., Parsons, D.R., Lane, S.N., and Hardy, R.J. (2003). "Flow in meander bends with recirculation at the inner bank." *Water Resource Research*, 39(11), 1322.

Ferziger, J.H. and Peric, M. (2002). "Computational Methods for Fluid Dynamics.", third ed. Springer Verlag, New York

Flokstra, C. (2006). "Modelling of submerged vanes." J. Hydraulic Research, 44 (5), 591-602.

Fluent Inc. (2006). "FLUENT 6.3 User's guide", Lebanon, New Hampshire.

Galmes J.M. and Lakshminarayana, B. (1984), "Turbulence modeling for three dimensional shear flows over cured rotating bodies." *AIAA J.* 22(10), 1420–1428.

Gibson, M.M. and Launder, B.E. (1978). "Ground Effects on Pressure Fluctuations in the Atmospheric Boundary Layer." *J. Fluid Mechanics*, 86,491-511.

Han, S.S (2010). "Use of vanes in sharp bends to improve open-channel flow characteristics: laboratory and numerical experiments." PhD thesis, Dept. of Building, Civil, and Environmental Engineering, Concordia University, Montreal, Quebec.

Han, S.S., Ramamurthy, A.S. and Biron, P.M. (in review a) "Characteristics of flow around open channel 90° bends with vanes." *J. Irrigation and Drainage Engineering.*

Han, S.S., Biron, P.M. and Ramamurthy, A.S (in review b) "Three-dimensional modeling of flow in open-channel sharp bends with vanes." *J. Hydraulic Research.*

Hersberger, D. (2002). "Wall roughness effects on flow and scouring in curved channels with gravel bed." Ph.D. thesis Nr 2632, École Polytechnique Fédérate Lausanne, Switzerland.

Hieu, P.D., and Tanimoto, K. (2006). "Verification of a VOF-based two-phase flow model for wave breaking and wave–structure interactions." *Ocean Engineering*, 33(11-12), 1565-1588.

Hinze, J. O. (1975). "Turbulence", Second Ed. , McGraw-Hill, New York.

Hirt, C.W. and Nicholls, B.D. (1981). "Volume of Fluid (VOF) method for dynamics of free boundaries." *J. Computational Physics*, 39, 201-221.

Hodskinson, A. (1996). "Computational fluid dynamics as a tool for investigating separated flow in river bends." *Earth surface processes and landforms*, 21, 993-1000.

Hooke, R.L. (1974). "Shear stress and sediment distribution in a meander bend." Ungi report 30, University of Uppsala, Sweden, 55-60

Huang, J, Lai, Y.G., and Patel, V.C. (2001) "Verification and validation of a 3-D numerical model for open-channel flows." *Numerical Heat Transfer*, Part B, 40, 431-449.

Hunt, J. C. R., Sandham, N. D., Vassilicos, J. C., Launder, B. E, Monkewitz, P. A., and Hewitt, G. F. (2001). "Developments in turbulence research: a review based on the 1999 Programme of the Isaac Newton Institute, Cambridge." *J. Fluid Mechanics*, 436, 353-391.

Hsieh, T.Y. and Yang, J.C. (2003). "Investigation on the suitability of two-dimensional depth-averaged models for bend-flow simulation." *J. of Hydraulic Engineering*, 129 (8), 597–612

Hyun, B.S., Balachandar, R., Yu, K. and Patel, V.C. (2003). "Assessment of PIV to measure mean velocity and turbulence in open-channel flow." *Experiments in Fluids,* 35(3), 262-267.

Ippen, A. and Drinker, P.A. (1962). "Boundary shear stresses in curved trapezoidal channels." *J. Hydraulics Division*, ASCE, 143-179.

Issa, R.I. (1986), "Solution of the implicitly discretized fluid flow equations by operator splitting", *J. Computational Physics*, 62, 40-65.

ITRC (Irrigation Training and Research Center) (1998). "Water level sensor and data logger testing and demonstration." Cal Poly.

Jia, Y., Scott, S. H., Xu, Y., Huang, S., Wang, S.S.Y, (2005). "Three-dimensional numerical simulation and analysis of flows around a submerged weir in a channel bendway." *J. Hydraulic Engineering*, 131 (8), 682-693.

Jiao, J., Liu, Z, and Zheng, Y. (2007). " Evaluations and Modifications on Reynolds Stress Model in Cyclone Simulations." , Chem. Eng. Technol. 2007, 30, No. 1, 15–20

Jin, Y.C. and Steffler, P.M. (1993). "Predicting flow in curved open channels by depth-averaged method." *J. Hydraulic Engineering*, 119(1), 109–124.

Julien, P.Y. (2002). "River Mechanics". Cambridge University Press, ISBN 0521562848

Kalkwijk, J.P. and de Vriend, H.J. (1980). "Computation of the flow in shallow river bends." *J. Hydraulic Research*, IAHR, 18(4), 327-341.

Kang, H. and Choi, S. (2006). "Reynolds stress modelling of rectangular open-channel flow." *International Journal for Numerical Methods in Fluids*, 51, 1319–1334.

Kassem, E, Chaudhry, M.H. (2002). "Numerical modeling of bed evolution in channel bends." *J. Hydraulic Engineering*, 128(5), 507-514.

Khan, F.R., Rielly, C. D., and Brown, D. A. R. (2006). "Angle resolved stereo-PIV measurement close to a down pumping pitched-blade turbine." *Chemical Engineering Science.*, 61, 2799-2806.

Khosronejad, A., Rennie, C. D., Neyshabouri, A. A. S., and Townsend, R. D. (2007). "3D numerical modeling of flow and sediment transport in laboratory channel bends." *J. Hydraulic Engineering*, ASCE, 133(10), 1123-1134.

Klonidis, A. J., and Soulis, J. V. (2001). "An implicit scheme for steady two-dimensional free surface flow calculations." *J. Hydraulic Research*, 39(4), 393–402.

Knupp, P. and Steiberg, S. (1993). Fundamentals of grid generation, CRC press. Inc

Kuipers, J., and Vreugdenhil, C. B. (1973). "Calculation of two dimensional horizontal flow." Report S163, part 1, Delft Hydraulics Lab., Delft, The Netherlands.

Lai, Y. G., Weber, L. J., and Patel, V. C. (2003). "Nonhydrostatic three dimensional model for hydraulic flow simulation, I: Formulation and verification." *J. Hydraulic Engineering*, ASCE, 129(3), 196–205.

Launder, B. E., Reece, G. J., and Rodi, W. (1975). "Progress in the Development of a Reynolds-Stress Turbulence Closure." *J. Fluid Mechanics,* 68(3),537-566.

Launder, B. E., and Spalding, D. B. (1974). "The numerical computation of turbulent flows." co*mp. Methods Appl. Mech. Eng.*, 3,269-289.

Leeder, M. R., and Bridges, P. H. (1975). "Flow separation in meander bends." *Nature,* 253, 338 – 339.

Leschziner, M. A., and Rodi, W. (1979). "Calculation of strongly curved open channel flow." *J. Hydraulic Division*, ASCE., 105(10), 1297–1314.

Lichtarowicz, A., and *Markland*, E., *(1963)*. "Calculation of potential flow with separation in a right-angled elbow with unequal branches," *J. Fluid Mechanic*, 17(4), 596-606.

Lien, H.C., Hsieh, T.Y., Yang, J.C., and Yeh, K.C. (1999). "Bend flow simulation using 2D depth-averaged model." *J. Hydraulic Engineering*, ASCE, 125(10), 1097–1108.

Lien, F. S., and Leschziner, M. A. (1994). "Assessment of Turbulent Transport Models Including Non-Linear RNG Eddy-Viscosity Formulation and Second-Moment Closure." *Computers and Fluids*, 23(8), 983-1004.

Liu, X. and Garcia, M.H. (2007). "Three dimension numerical model with free surface and mesh deformation for local sediment scour." J. waterways, Port, Costal, and Ocean Engineering,134(4), 203-217.

Luo. J. and Razinsky, E.H. (2009). "Analysis of turbulent flow in 180 deg turning ducts with and without guide vanes." *J. Turbomachinery*, ASME, **131**(2), 021011

Lu, W.Z., Zhang, W.S., Cui, C.Z., and Leung, A.Y.T. (2004) "A numerical analysis of free surface flow in curved open channel with velocity pressure free surface correction." *Computational Mechanics*, 33, 215-224.

Mankbadi, R.R., and Zaki, S.S. (1986). "Computations of the contraction coefficient of unsymmetrical bends." AIAA Journal,24(8), 1285-1289,

Marriott, M.J. (1998). "Hydrodynamics of flow around bends in meandering and compound channels". PhD thesis, University of Hertfordshire, UK

Marriott, M.J. (1999). "The effect of overbank flow on the conveyance of the inbank zone in meandering compound channels." 28th IAHR Congress, Graz, Austria

Meselhe, E.A., and Sotiropoulos, F. (2000). "Three-dimensional numerical model for open-channels with free-surface variations." *J. Hydraulic Research*, 38 (2), 115-121.

Molls, T., and Chaudhry, M.H. (1995). "Depth-averaged open-channel flow model." J. Hydraulic Engineering, ASCE, 121(6), 453-465.

Morvan, H., Pender, G., Wright, N.G., and Ervine, D.A. (2002). "Three dimensional hydrodynamics of meandering compound channels." J. Hydraulic Engineering, ASCE, 128(7), 674–682.

Nagata, T., Hosoda, T., Muramoto, Y., and Rahman, M.M. (1997). "Development of the numerical model to forecast the channel processes with bank erosion." Proc., 4th Japan-Chinese (Taipei) Joint Seminar on Natural Hazard Mitigation, 167–176.

Nagata, N., Hosoda, T. and Muramoto, Y. (2000). "Numerical analysis of river channel processes with bank erosion." J. Hydraulic Engineering, 126(4), 243-252.

Nagata, N., Hosoda, T. and Nakato, T. (2005). "Three-dimensional numerical model for flow and bed deformation around river hydraulic structures." *J. Hydraulic Engineering*, 131(12), 1074-1087.

Naot, D. and Rodi, W. (1982). "Calculation of secondary currents in channel flow." *J. Hydraulic Division*, ASCE, 108(8), 948–968.

Nezu, I and Sanjou, M. (2008). "Turbulence structure and coherent motion in vegetated canopy open-channel flows". *J. Hydro-environment Research*. 2(2), 62-90.

Nichols, B.D. and Hirt, C. W. (1975). "Methods for calculating multidimensional, transient free surface flows past bodies." Proc., 1st Int. Conf. Ship Hydrodynamics, J.W.

Schot and N. Salvesen, eds., Naval Ship Research and Development Center, Bethesda, Md., 253–277.

Odgaard, A.J. (1981). "Traverse bed slope in alluvial channel bends." J. Hydr. Div., ASCE, 107 (HY12), 1677-1694.

Odgaard, A. (1989a). "River meander model. I: Development." *J. Hydraulic Engineering*, 15(11), 1433–1450.

Odgaard, A. (1989b). "River meander model. II: Application." *J. Hydraulic Engineering*, ASCE, 115(11), 1451–1464.

Odgaard, A. J. and Kennedy, J. F. (1982). "Analysis of Sacramento River Bend Flows and Development of a New Method for Bank Protection." Iowa Inst. of Hydr. Res., Univ. of Iowa, Report No. 241.

Odgaard, A.J. and Kennedy. J. F. (1983). "River-bend bank protection by submerged vanes." J. Hydraulic Engineering, 109(8), 1161-1173.

Odgaard, A.J. and Spoljarec, A. (1986). "Sediment Control by Submerged Vanes." *J. Hydraulic Engineering,* ASCE, 112(12), 1164–1181.

Odgaard, A.J. and Spoljarec, A. (1989). "Sediment Control by Submerged Vanes." In: Ikeda, S. and Parker, G.(eds), Design Basis. River Meandering, Water Resources Monograph No. 12, American Geophysical Union, 127–151.

Odgaard, A.J., and Mosconi, C. E. (1987). "Stream bank protection by submerged vanes." *J. Hydraulic Engineering*, ASCE, 113(4), 520–536.

Odgaard, A.J., and Wang, Y. (1991). "Sediment management with submerged vanes. I: Theory." *J. Hydraulic Engineering*, ASCE, 117(3), 267-283.

Odgaard, A.J., and Wang, Y. (1991). "Sediment management with submerged vanes. II: Applications." *J. Hydraulic Engineering*, ASCE, 117(3), 284-302.

Olsen, N.R.B. (2003). "Three-dimensional CFD modeling of self forming meandering channel." *J. Hydraulic Engineering*, ASCE, 129(5), 366–372.

Olsen, N.R.B and Stoketh. S. (1995) "Three-dimensional numerical modelling of water flow of water flow in a river with large bed roughness." J. Hydraulic Research, 33, 571-581.

Olsen, N.R.B. and Kjellesvig, V.M. (1998). "Three-dimensional numerical flow modeling for estimation of maximum local scour depth." J. Hydraulic Research, 36, 579-590.

Ouillon, S. and Dartus, D. (1997). "Three-dimensional computation of flow around groyne." *J. Hydraulic Engineering*, ASCE, 123(11), 962-970.

Patankar, S. V. (1980). "Numerical heat transfer and fluid flow." Hemisphere, New York

Patankar, S.V., and Spalding, D.B. (1972), "A calculation procedure for heat, mass and momentum transfer in three-dimensional parabolic flows.", *International Journal of Heat and Mass Transfer*, 15.

Pezzinga, G. (1994), "Velocity distribution in compound channel flows by numerical modeling." *J. Hydraulic Engineering*, ASCE, 120(10), 1176–1198.

Peolma C. (2004). "Experiments in particle laden turbulence." Ph. D Thesis, U. of Delft.

Przedwojski, B., Blazejewski, R., and Pilarczyk, K.W. (1995). "River Training Techniques: Fundamentals, Techniques and Applications." *Balkema, Rotterdam*, The Netherlands.

Raisee, M., Alemi, H., Iacovides, H. (2006) "Prediction of developing turbulent flow in 90°-curved ducts using linear and non-linear low-Re k-ε models" International Journal for Numerical Methods in Fluids, 51(12), 1379-1405.

Ramamurthy, A. S. and Basak, S. (1973). "Control of flow separation in a wide channel expansion." Proceedings of Canadian hydraulics conference, CSCE, 515-522.

Ramamurthy, A.S., Qu, J., and Vo, D. (2006) "VOF model for simulation of a free overfall in trapezoidal channels." *J. Irrigation and Drainage Engineering*, 132(4), 425-428.

Rameshwaran, P. and Naden, P.S. (2004). "Three dimensional modeling of free surface variation in a meandering channel." *J. Hydraulic Research*, 42(6), 603-615.

Rozovskii, I. L. (1957). "Flow and water in bends open channels." Academy of Sciences of the Ukrainian SSr, Isr. Progr. Sc. Transl, Jerusalem, Israel.

Reinauer, R. and Hager, W. H. (1997). "Supercritical bend flow." *J. Hydraulic Engineering*, ASCE, 123(3), 208-218.

Roca, M., Martin Vide, J. P., and Blanckaert, K. (2007). "Reduction of bend scour by an outer bank footing: Footing design and bed topography." *J. Hydraulic Engineering*, ASCE, 133(2), 139-147.

Ruether, N. and Olsen. N.R.B. (2005) "Three dimensional modeling of sediment transport in a narrow 90° channel bend", *J. Hydraulic Engineering*, 131, 917-920

Sahlin, A. and Johansson, A. V. (1991). "Design of guide vanes for minimizing the pressure loss in sharp bends." *Physics of Fluids* A3, 1934-1940.

Sanjou, M and Nezu, I. (2009). "Turbulence structure and coherent motion in meandering compound open-channel flows", *J. Hydraulic Research*, 47(5), 598-610.

Shao, X., Wang, H., and Chen Z. (2003). "Numerical modeling of turbulent flow in curved channels of compound cross section." Advances in water resources, 26(5), 525-539.

Shimizu, Y., Yamaguchi, H., and Itakura, T. (1990). "Three-dimensional computation of flow and bed deformation." J. Hydra. Eng., ASCE, 116(9), 1090–1107.

Shukry, A. (1949). "Flow around bends in an open flume." *Transactions*, ASCE, 115, 751-788.

Spalart, P.R., Jou, W.H., Stretlets, M., and Allmaras, S.R. (1997), "Comments on the Feasibility of LES for Wings and on the Hybrid RANS/LES Approach", Advances in DNS/LES, Proceedings of the First AFOSR International Conference on DNS/LES.

Speziale, C. G., Sarkar, S. and Gatski, T. B. (1991). "Modelling the Pressure-Strain Correlation of Turbulence: An Invariant Dynamical Systems Approach." J. Fluid Mech., 227, 245-272.

Steffler, P. M. (1984). "Turbulent flow in a curved rectangular channel." PhD thesis, University of Alberta, Canada.

Sotiropolous, F. (2009.) "Coherent-structure resolving simulations of turbulence in natural streams with the curvilinear immersed-boundary method." 62nd Meeting of the American Physical Society, Nov. 22-24, Minneapolis.

Sudo, K., Sumida, M., and Hibara, H. (2001). "Experimental investigation on turbulent flow in a square-sectioned 90° bend", Experiments in Fluids, 30, 246-52.

Svendsen, I. A. (1987). "Analysis of surf zone turbulence." J. Geophys.Res. 92, 5115–5124.

Tannehill, J.C., Anderson, D.A., and Pletcher, R.H. (1997). "Computational Fluid Mechanics and Heat transfer." Second edition, Taylor & Francis. ISBN 1-56032-046-X

Tarek, M.S., Jasim, I, and Chaudry, M.H. (2004). "Numerical modeling of three-dimensional flow field around circular piers." J. Hydraulic Engineering. 130(2), 91-100.

Thompson, J. F. (1982). "Numerical grid generation". North Holland, New York.

Tominaga, A. and Nezu, I. (1991). "Turbulent structure in compound open channel flows". J. Hydraulic Engineering, ASCE, 117(1), 21-41.

Tominaga, A., Nagao, M., and Nezu, I. (1999). "Flow structure and momentum transport processes in curved open-channels with vegetation." Proc., 28th Congr. Int. Assoc. Hydr. Res., Technical University of Graz, Austria

Tominaga, A. and Nagao, M. (2000). "Secondary flow structure in bends of narrow open channels with various cross sections." 4th international conference on hydro-science and engineering.

US Army Corps of Engineers, 1994. "Hydraulic Design of Flood Control Channels.", US Army Corps of Engineers Engineer Manual EM 1110-2-1601.

Van Balen, W, Uijttewaal, W.S.J., and Blanckaert, K. (2009). "Large-eddy simulation of a mildly curved open-channel flow." *J. Fluid Mechanics*, 630, 413–442.

Viegas, J.R., Rubesin, M.W., and Horstman, C.C. (1985)."On the use of wall functions as boundary conditions for two-dimensional separated compressible flows." Technical Report AIAA-85-0180, AIAA 23rd Aerospace Sciences Meeting, Reno, Nevada

Vreugdenhil, C.B., and Wijbenga, J.H.A. (1982). "Computation of flow patterns in rivers". J. *Hydraulic Engineering*. ASCE, 110(1), 90-101.

Waterway Simulation Technology, Inc. (1999). "A physical model test plan for bendway weir design criteria," *Project report to U.S. Army Engineer Waterways Experiment Station.*

Wernet, M.P. , Subramanian, A., Mu, H., Kadambi, J.R. (2000). "Comparison of particle image velocimetry and laser Doppler anemometry measurements in turbulent fluid flow." Annals of Biomedical Engineering, 28 (11), 1393-1394.

Wetzel, J. and Arndt, R.E.A. (1994)."Hydro dynamic design considerations for hydroacoustic facilities: I flow quality.", *J. Fluid Engineering*, 116(2), 324-331.

Wilcox, D.C. (2004). "Turbulence modeling for CFD." .DCW industries.

Wilson, C. A. M. E., Boxall, J. B., Guymer, I., and Olsen, N. R. B. (2003). "Validation of a three-dimensional numerical code in the simulation of pseudo-natural meandering flows." *J. Hydraulic Engineering*, ASCE, 129(10), 758–768.

Wu, W., Rodi, W, and Wenka, T. (2000). "3D modeling of flow and sediment transport in open channels. *" J. Hydraulic Engineering*, ASCE,126, 4-15.

Yakhot, V., and Orszag, S.A. (1986). "Renormalization Group Analysis of Turbulence: I. Basic Theory." *Journal of Scientific Computing*, 1(1), 51.

Ye, J. and McCorquodale, J.A. (1997). "Three dimensional numerical modeling of mass transport in curved channels." Can. J. Civ. Eng, 24, 471-479.

Yen, B.C. (1965). "Characteristics of subcritical flow in a meandering channel." Ph.D. Thesis, Dept. Mechanics and Hydraulics, The Univ. of Iowa, Iowa City, IA.

Yen, C.L., and Ho, S. Y. (1990). "Bed evolution of channel bends." *J. Hydraulic Engineering*, ASCE, 116(4), 544–562.

Zhou, J.G., and Goodwill, I.M. (1997). "A finite volume method for state 2D shallow water flows." *International J. Numerical Methods in Heat Fluid Flow*, 7(1), 4–23.

Zeng, J., Constantinescu, G., and Weber, L. (2008). "A 3D non-hydrostatic model to predict flow and sediment transport in loose-bed channel bends." J. Hydraulic Research, 46 (3), 356-372.

APPENDIX A. USE OF A LINEAR HUMP TO CONTROL BEND FLOW CHARACTERISTICS

A.1 Introduction

As seen from the previous chapters, curved open channel flow is characterized by the secondary flow, the zone of flow separation at the inner bank, and large water depth variation in the bend. Scientists and engineers have been trying to alter these characteristics to formulate the flow condition favourable to the engineering practices such as reducing outer bank erosion and energy loss using submerged vanes (Odgaard et al. 1987), and groynes (Przedwojoski et al. 1995) to counteract the secondary flow and control sediment. Ramamurthy and Basak (1973) used a linearly raised bed to reduce the flow separation in subcritical flow in rectangular open channel expansions. The idea of the linearly raised bed may be applicable in open channel bend to suppress flow separation. The effects of the hump (partially raised channel bed) on the flow separation and the secondary circulation were investigated using the numerical models.

A.2 Theoretical consideration

Adverse pressure gradient is responsible for the flow separation. Considering a flow past a channel expansion, one may assume that the energy loss in the short reach of the expansion is negligible. In the specific energy diagram, the flow follows the path 1-2 when the bed is horizontal in Fig. A.1. When the bed is raised linearly towards the exit of the expansion, the path of the flow is 1-3-2 in Figure A.1. The energy loss from 1-3 is equal to the gain in datum energy due to the raised bed (Ramamurthy and Basak 1973). The linearly raised bed may reduce the adverse pressure gradient while the flow

negotiates the expansion and thus inhibits flow separation. Similar principle may possibly be applied to reduce the flow separation in the open channel bend flow. By adding the linearly raised bed to reduce the flow deceleration at the inner wall region, the flow separation may be reduced.

The flow in the bend (flat bed) achieves the maximum velocity near the middle of the bend along the inner wall, and decelerates in the short reach of the downstream section where boundary friction losses are negligible. Head loss in this section is due to the flow turbulence generated through separation caused by the deceleration of the flow (adverse pressure gradient). By providing a hump, the datum head is increased and hence the specific energy gets reduced. However, compared to the flow expansion in a straight open channel (Fig. A.1), the open channel bend flow is highly three dimensional with large variation of streamwise velocity in lateral direction and strong secondary flow motion. The geometry of open channel bend (flat bed) and flow conditions of the experimental study (chapter 3) were used for these numerical simulations.

A. 3 Simulation results

The maximum velocity measured from the lab and predicted from the model near the bend was 0.43m/s which is 0.94cm in hydraulic head. So the heights of the hump to raise the bed were chosen among 0.05Z (=0.5cm), 0.11Z (= 1.0cm), and 0.17Z (=1.5cm) with three different configurations as shown in Figure A.2. The height of the bed was raised from the 45° of the bend at the inner bank keeping bed height of the outer bank to 0.0cm. The raised bed height was maintained for the length of the channel width 1.0B (= 0.61m) toward the downstream and goes back to the original bed height linearly with another

length of the channel width (1.0B = 0.61m). The results presented here are from three different configurations of 1.0cm height of the raised bed which was most effective in reducing the size of the flow separation.

The typical numerical grid for the raised bed simulations is shown in Fig. A.3. The grid dimension is 250, 42, 20, and the whole downstream length was simulated. The sizes of the flow separation zone at the free water surface for the three cases of the bed change are shown in Fig. A.4. It clearly indicates that the length of the flow separation zone has been reduced to 54.5% comparing to the flat bed case. The width of the separation did show noticeable change.
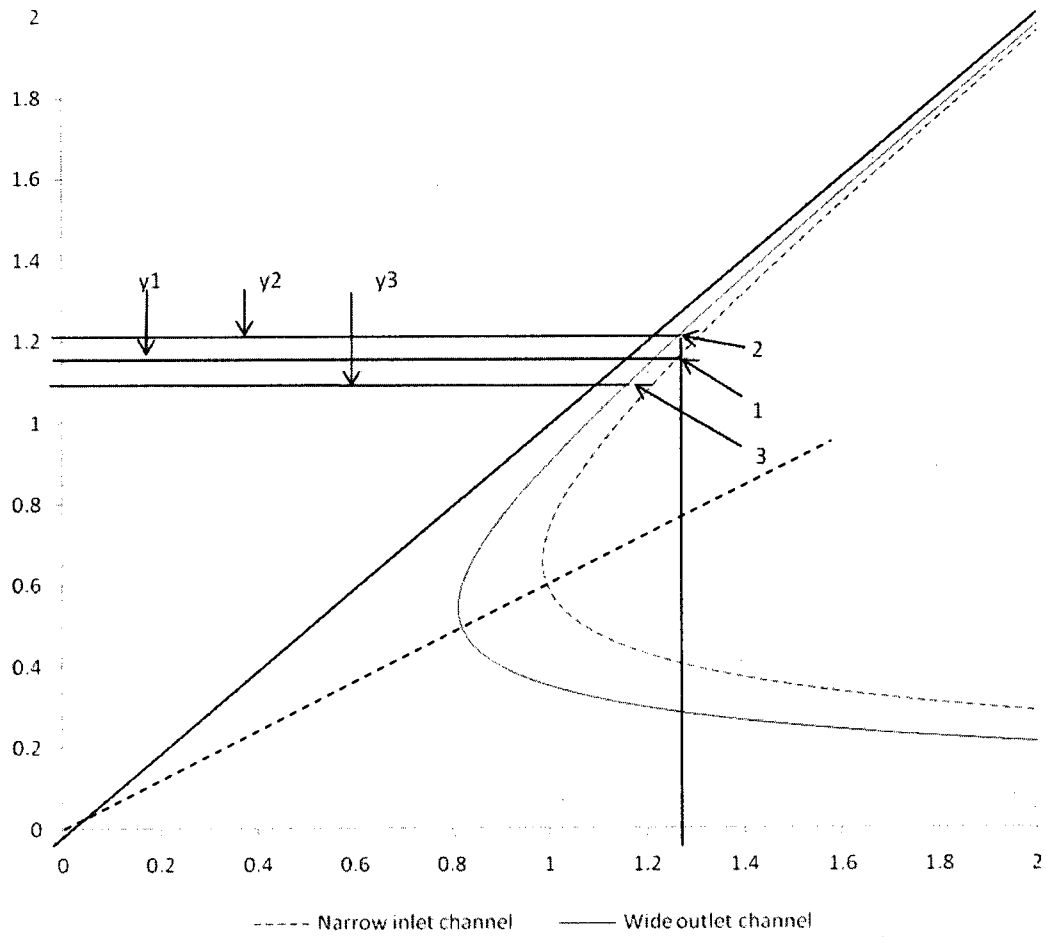
Fig. A.1. Specific energy diagram for the flow expansion with a linearly raised bed
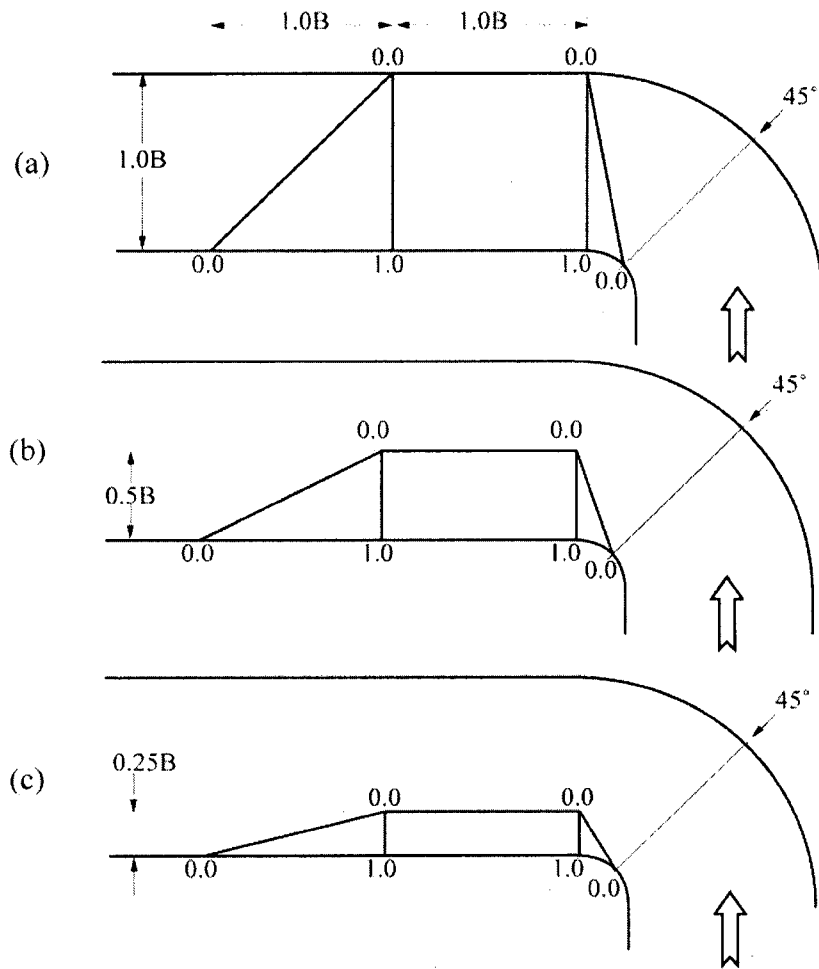
Fig. A.2. Bed forms: (a) configuration A1; (b) configuration A2; (c) configuration A3. Numbers denote height of the modified bed in mm above horizontal bed.

115
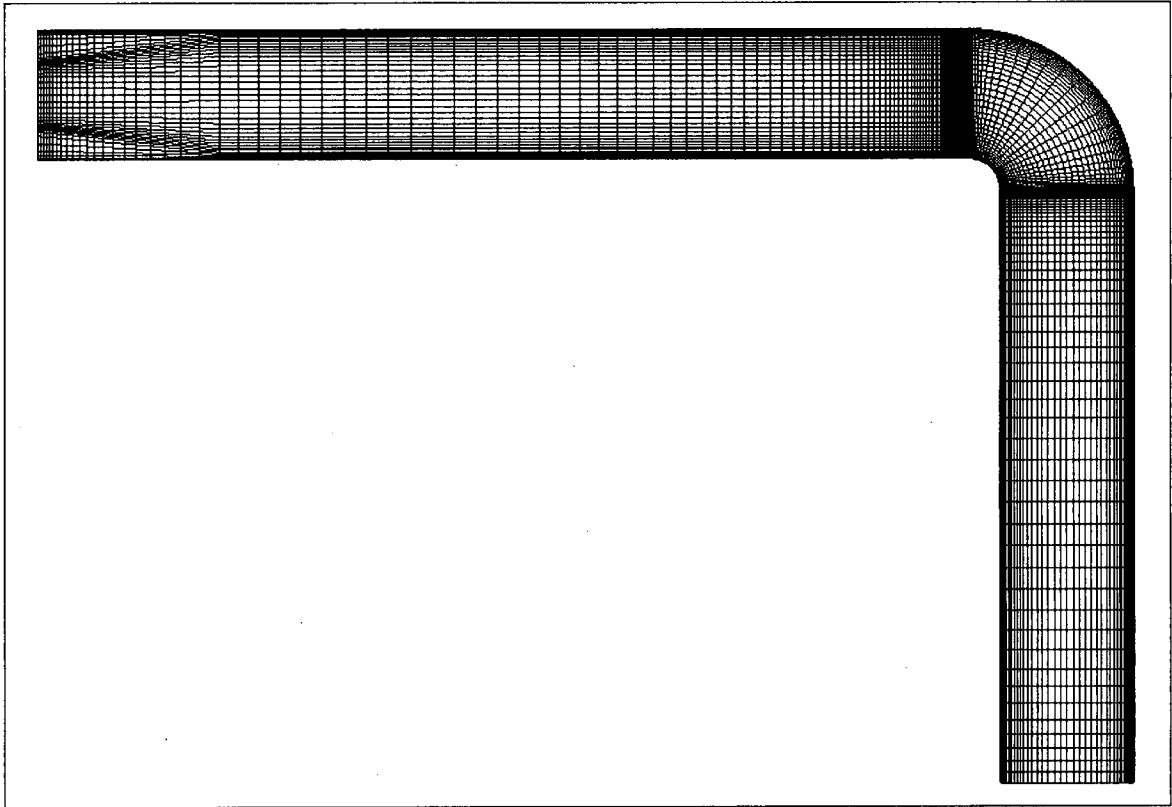
Fig. A.3. Numerical grid for raised bed
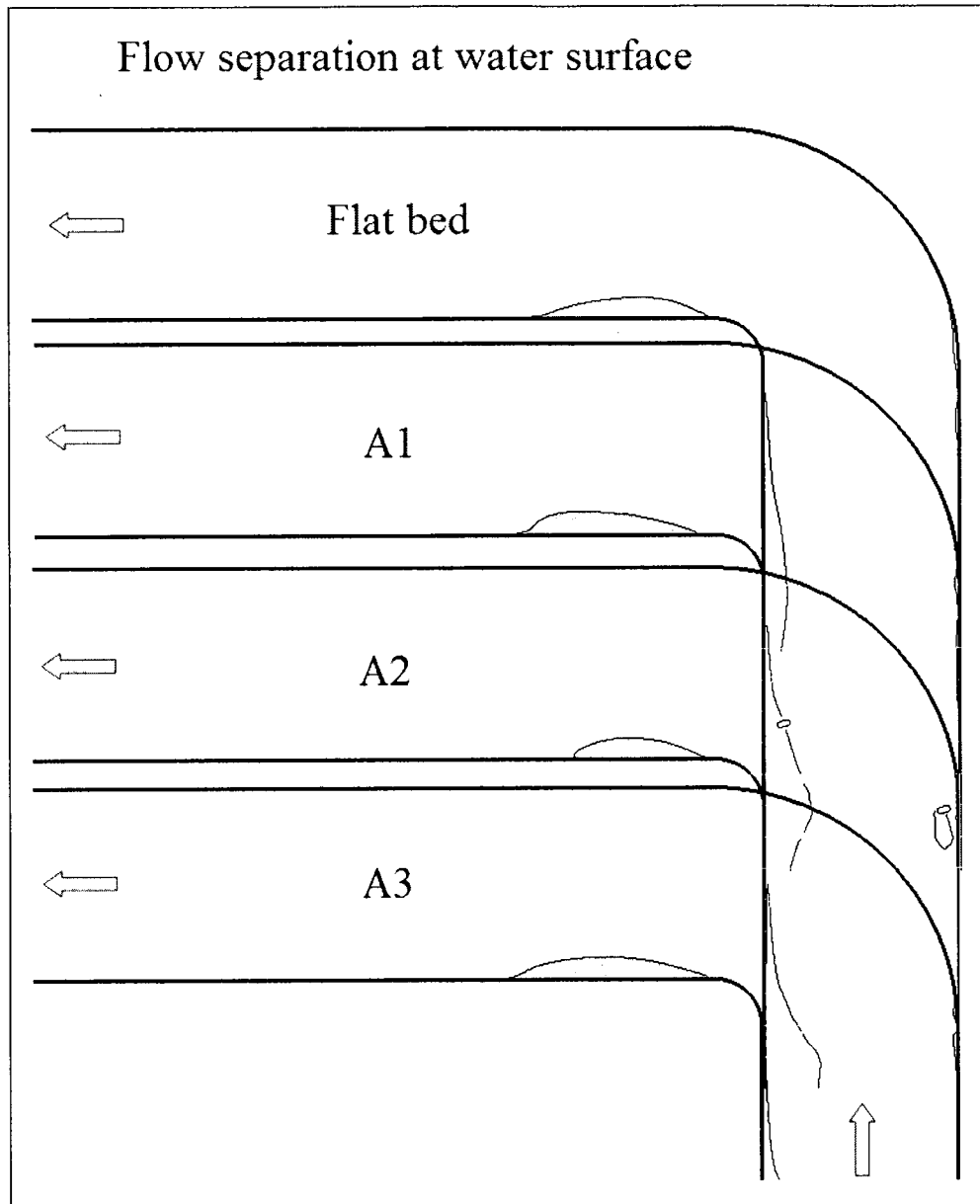
Fig. A.4. Zone of flow separation for different bed configurations

APPENDIX B. LDA EXPERIMENTAL DATA
Table B.1 Flow field data for the bend width 0.60m (Q=0.013m^3/s)

x (m)	y (m)	z (m)	Urms (m/s)	Vrms (m/s)	Wrms (m/s)	U (m/s)	V (m/s)	W (m/s)	U$_T$(m/s)	Ke (m^2/s^2)
2.1270	1.2494	0.0060	0.0269	0.0330	0.0300	-0.1186	0.1447	0.0331	0.3403	0.0010
2.1349	1.2555	0.0060	0.0293	0.0140	0.0246	-0.1891	0.2431	0.0168	0.3533	0.0009
2.1429	1.2616	0.0060	0.0251	0.0220	0.0300	-0.2234	0.2748	0.0078	0.3730	0.0008
2.1509	1.2677	0.0060	0.0267	0.0130	0.0237	-0.2270	0.2909	0.0020	0.3785	0.0008
2.1588	1.2738	0.0060	0.0249	0.0270	0.0204	-0.2312	0.2751	0.0022	0.3707	0.0007
2.1748	1.2860	0.0060	0.0250	0.0200	0.0227	-0.2091	0.1143	0.0012	0.3302	0.0007
2.1907	1.2981	0.0060	0.0245	0.0160	0.0228	-0.1931	0.1577	0.0014	0.3169	0.0007
2.2226	1.3225	0.0060	0.0297	0.0240	0.0204	-0.1843	0.2040	0.0012	0.3058	0.0008
2.2544	1.3468	0.0060	0.0250	0.0190	0.0156	-0.1561	0.1903	0.0008	0.2777	0.0007
2.2863	1.3712	0.0060	0.0250	0.0280	0.0181	-0.1706	0.1451	0.0002	0.2506	0.0008
2.3181	1.3955	0.0060	0.0231	0.0200	0.0130	-0.0974	0.1105	0.0000	0.2124	0.0006
2.3500	1.4199	0.0060	0.0262	0.0220	0.0146	-0.0470	0.1019	-0.0003	0.1861	0.0006
2.3819	1.4442	0.0060	0.0236	0.0230	0.0155	-0.0415	0.1031	-0.0005	0.1751	0.0006
2.4137	1.4686	0.0060	0.0229	0.0270	0.0115	-0.1149	0.1021	-0.0009	0.1764	0.0007
2.4456	1.4929	0.0060	0.0270	0.0250	0.0163	-0.1082	0.0934	-0.0015	0.1651	0.0007
2.4774	1.5173	0.0060	0.0229	0.0270	0.0172	-0.1181	0.0997	-0.0018	0.1661	0.0007
2.5093	1.5416	0.0060	0.0229	0.0220	0.0135	-0.0655	0.0607	-0.0024	0.1443	0.0006
2.5412	1.5660	0.0060	0.0289	0.0180	0.0110	-0.0781	0.0951	-0.0016	0.1505	0.0007
2.5730	1.5903	0.0060	0.0292	0.0050	0.0100	0.0044	0.0848	-0.0014	0.1125	0.0006
2.5890	1.6025	0.0060	0.0300	0.0250	0.0145	-0.0620	0.0759	-0.0027	0.0923	0.0006
2.6009	1.6117	0.0060	0.0230	0.0110	0.0138	-0.0262	0.0391	-0.0038	0.0737	0.0006
2.1270	1.2494	0.0150	0.0180	0.0170	0.0213	-0.2370	0.3664	-0.0028	0.3814	0.0008
2.1349	1.2555	0.0150	0.0190	0.0190	0.0172	-0.2402	0.3640	0.0477	0.3971	0.0008
2.1429	1.2616	0.0150	0.0200	0.0200	0.0254	-0.2383	0.3516	0.0214	0.4052	0.0007
2.1509	1.2677	0.0150	0.0180	0.0210	0.0033	-0.2301	0.3377	0.0103	0.4006	0.0007
2.1588	1.2738	0.0150	0.0200	0.0220	0.0037	-0.2280	0.3267	0.0042	0.3864	0.0007
2.1748	1.2860	0.0150	0.0210	0.0220	0.0037	-0.2206	0.3072	0.0038	0.3454	0.0007
2.1907	1.2981	0.0150	0.0220	0.0220	0.0038	-0.2110	0.2881	0.0029	0.3288	0.0007
2.2226	1.3225	0.0150	0.0250	0.0220	0.0038	-0.1976	0.2542	0.0030	0.3131	0.0008
2.2544	1.3468	0.0150	0.0280	0.0250	0.0044	-0.1845	0.2240	0.0029	0.2848	0.0007
2.2863	1.3712	0.0150	0.0300	0.0240	0.0043	-0.1700	0.1985	0.0019	0.2580	0.0007
2.3181	1.3955	0.0150	0.0300	0.0240	0.0044	-0.1652	0.1808	0.0012	0.2228	0.0006
2.3500	1.4199	0.0150	0.0280	0.0260	0.0048	-0.1540	0.1629	0.0004	0.1978	0.0006
2.3819	1.4442	0.0150	0.0280	0.0250	0.0047	-0.1440	0.1466	-0.0002	0.1861	0.0006
2.4137	1.4686	0.0150	0.0270	0.0270	0.0052	-0.1322	0.1280	-0.0008	0.1841	0.0007
2.4456	1.4929	0.0150	0.0300	0.0260	0.0050	-0.1213	0.1187	-0.0019	0.1718	0.0007
2.4774	1.5173	0.0150	0.0277	0.0330	0.0063	-0.1223	0.1167	-0.0027	0.1720	0.0007
2.5093	1.5416	0.0150	0.0270	0.0260	0.0047	-0.1082	0.1262	-0.0045	0.1531	0.0007

Table B.1 Flow field data for the bend width 0.60m (Q=0.013m^3/s, continued)

x (m)	y (m)	z (m)	Urms (m/s)	Vrms (m/s)	Wrms (m/s)	U (m/s)	V (m/s)	W (m/s)	U$_T$(m/s)	Ke (m^2/s^2)
2.5412	1.5660	0.0150	0.0250	0.0280	0.0048	-0.0928	0.1406	-0.0045	0.1562	0.0007
2.5730	1.5903	0.0150	0.0261	0.0320	0.0054	-0.0688	0.1061	-0.0035	0.1181	0.0006
2.5890	1.6025	0.0150	0.0220	0.0230	0.0041	-0.0509	0.0794	-0.0013	0.0975	0.0007
2.6009	1.6117	0.0150	0.0260	0.0140	0.0025	-0.0368	0.0562	-0.0028	0.0796	0.0006
2.1270	1.2494	0.0350	0.0230	0.0160	0.0145	-0.2385	0.3716	0.0436	0.4374	0.0006
2.1349	1.2555	0.0350	0.0110	0.0170	0.0182	-0.2348	0.3832	0.0204	0.4418	0.0006
2.1429	1.2616	0.0350	0.0120	0.0190	0.0252	-0.2312	0.3835	0.0102	0.4400	0.0006
2.1509	1.2677	0.0350	0.0140	0.0190	0.0291	-0.2228	0.3774	0.0048	0.4326	0.0006
2.1588	1.2738	0.0350	0.0150	0.0180	0.0286	-0.2148	0.3671	0.0041	0.4206	0.0006
2.1748	1.2860	0.0350	0.0140	0.0190	0.0304	-0.2034	0.3456	0.0034	0.3922	0.0006
2.1907	1.2981	0.0350	0.0140	0.0200	0.0322	-0.1965	0.3333	0.0036	0.3707	0.0006
2.2226	1.3225	0.0350	0.0150	0.0170	0.0279	-0.1768	0.3093	0.0037	0.3419	0.0006
2.2544	1.3468	0.0350	0.0160	0.0180	0.0303	-0.1621	0.2852	0.0031	0.3135	0.0006
2.2863	1.3712	0.0350	0.0160	0.0180	0.0308	-0.1509	0.2624	0.0014	0.2885	0.0006
2.3181	1.3955	0.0350	0.0210	0.0210	0.0115	-0.1447	0.2444	0.0008	0.2647	0.0005
2.3500	1.4199	0.0350	0.0220	0.0210	0.0119	-0.1369	0.2227	0.0002	0.2449	0.0005
2.3819	1.4442	0.0350	0.0220	0.0200	0.0115	-0.1302	0.2140	-0.0004	0.2311	0.0005
2.4137	1.4686	0.0350	0.0220	0.0220	0.0111	-0.1191	0.1947	-0.0014	0.2171	0.0006
2.4456	1.4929	0.0350	0.0206	0.0230	0.0130	-0.1020	0.1789	-0.0031	0.2010	0.0006
2.4774	1.5173	0.0350	0.0181	0.0250	0.0143	-0.1036	0.1827	-0.0042	0.1969	0.0007
2.5093	1.5416	0.0350	0.0180	0.0190	0.0233	-0.0979	0.1883	-0.0057	0.1869	0.0007
2.5412	1.5660	0.0350	0.0098	0.0220	0.0142	-0.0874	0.1812	-0.0041	0.1769	0.0008
2.5730	1.5903	0.0350	0.0108	0.0199	0.0167	-0.0632	0.1267	-0.0010	0.1399	0.0008
2.5890	1.6025	0.0350	0.0123	0.0161	0.0161	-0.0661	0.1157	-0.0019	0.1187	0.0008
2.6009	1.6117	0.0350	0.0370	0.0150	0.0188	-0.0511	0.0780	-0.0005	0.1046	0.0008
2.1270	1.2494	0.0550	0.0230	0.0160	0.0199	-0.2376	0.3786	0.0152	0.4439	0.0007
2.1349	1.2555	0.0550	0.0110	0.0170	0.0155	-0.2317	0.3857	0.0162	0.4476	0.0006
2.1429	1.2616	0.0550	0.0240	0.0150	0.0149	-0.2265	0.3921	0.0086	0.4481	0.0005
2.1509	1.2677	0.0550	0.0100	0.0150	0.0153	-0.2201	0.3920	0.0062	0.4440	0.0005
2.1588	1.2738	0.0550	0.0110	0.0150	0.0166	-0.2165	0.3872	0.0033	0.4346	0.0005
2.1748	1.2860	0.0550	0.0110	0.0180	0.0202	-0.2034	0.3620	0.0032	0.4102	0.0006
2.1907	1.2981	0.0550	0.0100	0.0220	0.0258	-0.1956	0.3403	0.0031	0.3886	0.0006
2.2226	1.3225	0.0550	0.0110	0.0150	0.0182	-0.1736	0.3231	0.0048	0.3575	0.0006
2.2544	1.3468	0.0550	0.0100	0.0140	0.0174	-0.1573	0.3003	0.0059	0.3294	0.0005
2.2863	1.3712	0.0550	0.0120	0.0160	0.0200	-0.1437	0.2792	0.0034	0.3063	0.0005
2.3181	1.3955	0.0550	0.0120	0.0150	0.0183	-0.1383	0.2657	0.0005	0.2874	0.0005
2.3500	1.4199	0.0550	0.0130	0.0140	0.0173	-0.1290	0.2552	-0.0023	0.2716	0.0005
2.3819	1.4442	0.0550	0.0120	0.0140	0.0183	-0.1237	0.2417	-0.0020	0.2579	0.0005

119

Table B.1 Flow field data for the bend width 0.60m (Q=0.013m^3/s, continued)

x (m)	y (m)	z (m)	Urms (m/s)	Vrms (m/s)	Wrms (m/s)	U (m/s)	V (m/s)	W (m/s)	U$_T$(m/s)	Ke (m^2/s^2)
2.4137	1.4686	0.0550	0.0140	0.0150	0.0200	-0.1113	0.2272	-0.0028	0.2390	0.0005
2.4456	1.4929	0.0550	0.0130	0.0160	0.0218	-0.1005	0.2115	-0.0035	0.2195	0.0005
2.4774	1.5173	0.0550	0.0120	0.0150	0.0207	-0.0938	0.1978	-0.0041	0.2119	0.0006
2.5093	1.5416	0.0550	0.0160	0.0180	0.0255	-0.0896	0.1972	-0.0055	0.1997	0.0009
2.5412	1.5660	0.0550	0.0095	0.0197	0.0455	-0.0855	0.1739	-0.0067	0.1813	0.0010
2.5730	1.5903	0.0550	0.0162	0.0192	0.0416	-0.0680	0.1609	-0.0052	0.1455	0.0010
2.5890	1.6025	0.0550	0.0130	0.0195	0.0429	-0.0589	0.1162	0.0006	0.1248	0.0009
2.6009	1.6117	0.0550	0.0390	0.0140	0.0225	-0.0565	0.0852	0.0069	0.1132	0.0009
2.1270	1.2494	0.0750	0.0332	0.0160	0.0146	-0.2218	0.3630	-0.0110	0.4318	0.0011
2.1349	1.2555	0.0750	0.0285	0.0170	0.0172	-0.2333	0.3895	-0.0011	0.4414	0.0010
2.1429	1.2616	0.0750	0.0280	0.0150	0.0156	-0.2307	0.3877	-0.0020	0.4453	0.0008
2.1509	1.2677	0.0750	0.0110	0.0150	0.0167	-0.2246	0.3848	-0.0006	0.4422	0.0008
2.1588	1.2738	0.0750	0.0170	0.0150	0.0168	-0.2218	0.3794	-0.0005	0.4346	0.0007
2.1748	1.2860	0.0750	0.0120	0.0230	0.0266	-0.2125	0.3575	0.0000	0.4118	0.0007
2.1907	1.2981	0.0750	0.0140	0.0250	0.0297	-0.2166	0.3266	0.0000	0.3905	0.0006
2.2226	1.3225	0.0750	0.0110	0.0180	0.0218	-0.1800	0.3118	0.0000	0.3606	0.0005
2.2544	1.3468	0.0750	0.0100	0.0160	0.0199	-0.1610	0.2886	0.0000	0.3317	0.0005
2.2863	1.3712	0.0750	0.0110	0.0150	0.0190	-0.1498	0.2758	0.0000	0.3103	0.0005
2.3181	1.3955	0.0750	0.0130	0.0140	0.0184	-0.1386	0.2579	0.0000	0.2920	0.0005
2.3500	1.4199	0.0750	0.0110	0.0130	0.0168	-0.1301	0.2468	-0.0053	0.2787	0.0004
2.3819	1.4442	0.0750	0.0130	0.0150	0.0194	-0.1268	0.2392	-0.0053	0.2661	0.0005
2.4137	1.4686	0.0750	0.0130	0.0150	0.0201	-0.1142	0.2212	-0.0053	0.2458	0.0004
2.4456	1.4929	0.0750	0.0130	0.0140	0.0195	-0.1012	0.2009	-0.0044	0.2234	0.0005
2.4774	1.5173	0.0750	0.0140	0.0160	0.0230	-0.1037	0.1927	-0.0039	0.2149	0.0006
2.5093	1.5416	0.0750	0.0230	0.0190	0.0310	-0.0983	0.1691	-0.0020	0.1928	0.0010
2.5412	1.5660	0.0750	0.0280	0.0250	0.0396	-0.0917	0.1540	-0.0019	0.1685	0.0012
2.5730	1.5903	0.0750	0.0248	0.0270	0.0396	-0.0696	0.1104	0.0016	0.1312	0.0011
2.5890	1.6025	0.0750	0.0104	0.0240	0.0338	-0.0622	0.0909	0.0000	0.1106	0.0010
2.6009	1.6117	0.0750	0.0380	0.0160	0.0195	-0.0592	0.0920	0.0000	0.1041	0.0009
2.1270	1.2494	0.0850	0.0421	0.0270	0.0246	-0.2086	0.3441	0.0000	0.4244	0.0013
2.1349	1.2555	0.0850	0.0330	0.0160	0.0171	-0.2284	0.3831	-0.0047	0.4354	0.0012
2.1429	1.2616	0.0850	0.0355	0.0170	0.0207	-0.2290	0.3789	-0.0068	0.4412	0.0011
2.1509	1.2677	0.0850	0.0370	0.0210	0.0267	-0.2201	0.3756	-0.0037	0.4390	0.0010
2.1588	1.2738	0.0850	0.0230	0.0190	0.0241	-0.2236	0.3768	-0.0024	0.4328	0.0009
2.1748	1.2860	0.0850	0.0310	0.0139	0.0174	-0.2196	0.3470	0.0000	0.4111	0.0008
2.1907	1.2981	0.0850	0.0170	0.0150	0.0188	-0.2310	0.3093	0.0000	0.3902	0.0006
2.2226	1.3225	0.0850	0.0170	0.0180	0.0215	-0.2041	0.2972	0.0000	0.3605	0.0005
2.2544	1.3468	0.0850	0.0140	0.0180	0.0215	-0.1667	0.2830	0.0000	0.3314	0.0005

Table B.1 Flow field data for the bend width 0.60m (Q=0.013m³/s, continued)

x (m)	y (m)	z (m)	Urms (m/s)	Vrms (m/s)	Wrms (m/s)	U (m/s)	V (m/s)	W (m/s)	U$_T$(m/s)	Ke (m²/s²)
2.2863	1.3712	0.0850	0.0160	0.0160	0.0221	-0.1543	0.2635	0.0000	0.3103	0.0005
2.3181	1.3955	0.0850	0.0170	0.0150	0.0220	-0.1433	0.2492	0.0000	0.2919	0.0005
2.3500	1.4199	0.0850	0.0130	0.0150	0.0205	-0.1410	0.2397	0.0000	0.2791	0.0004
2.3819	1.4442	0.0850	0.0160	0.0160	0.0215	-0.1281	0.2294	0.0000	0.2667	0.0004
2.4137	1.4686	0.0850	0.0130	0.0150	0.0205	-0.1191	0.2111	0.0000	0.2462	0.0004
2.4456	1.4929	0.0850	0.0130	0.0150	0.0211	-0.1037	0.1877	0.0000	0.2232	0.0004
2.4774	1.5173	0.0850	0.0170	0.0160	0.0232	-0.1092	0.1834	0.0000	0.2147	0.0006
2.5093	1.5416	0.0850	0.0340	0.0200	0.0319	-0.1059	0.1380	0.0000	0.1898	0.0011
2.5412	1.5660	0.0850	0.0340	0.0210	0.0331	-0.0904	0.1046	-0.0001	0.1640	0.0012
2.5730	1.5903	0.0850	0.0280	0.0210	0.0311	-0.0693	0.0854	0.0000	0.1259	0.0011
2.5890	1.6025	0.0850	0.0280	0.0200	0.0268	-0.0458	0.0695	0.0000	0.1049	0.0009
2.6009	1.6117	0.0850	0.0280	0.0130	0.0159	-0.0494	0.0693	0.0000	0.1002	0.0008
2.0970	1.2789	0.0060	0.0357	0.0150	0.0217	-0.0292	0.0211	0.0383	0.2911	0.0010
2.1031	1.2868	0.0060	0.0509	0.0270	0.0154	-0.1890	0.2239	0.0219	0.3147	0.0010
2.1092	1.2947	0.0060	0.0288	0.0160	0.0087	-0.2026	0.2300	0.0074	0.3453	0.0009
2.1153	1.3027	0.0060	0.0350	0.0130	0.0069	-0.2804	0.2344	0.0013	0.3628	0.0007
2.1214	1.3106	0.0060	0.0320	0.0090	0.0047	-0.2635	0.2255	0.0002	0.3647	0.0007
2.1336	1.3265	0.0060	0.0280	0.0120	0.0062	-0.2414	0.1272	0.0001	0.3326	0.0006
2.1457	1.3423	0.0060	0.0350	0.0140	0.0071	-0.2242	0.1506	0.0004	0.3167	0.0007
2.1701	1.3741	0.0060	0.0230	0.0230	0.0114	-0.2118	0.1704	0.0001	0.2995	0.0007
2.1944	1.4058	0.0060	0.0354	0.0220	0.0107	-0.2417	0.1708	-0.0003	0.2883	0.0008
2.2188	1.4375	0.0060	0.0332	0.0280	0.0134	-0.2285	0.1404	-0.0006	0.2641	0.0009
2.2431	1.4693	0.0060	0.0320	0.0310	0.0147	-0.1892	0.0885	-0.0006	0.2327	0.0010
2.2675	1.5010	0.0060	0.0310	0.0290	0.0137	-0.1795	0.0634	-0.0003	0.2126	0.0009
2.2918	1.5327	0.0060	0.0330	0.0300	0.0144	-0.1603	0.0674	-0.0006	0.1973	0.0010
2.3162	1.5645	0.0060	0.0351	0.0320	0.0158	-0.1435	0.0646	-0.0012	0.1819	0.0011
2.3405	1.5962	0.0060	0.0310	0.0310	0.0160	-0.1477	0.0604	-0.0022	0.1797	0.0010
2.3649	1.6279	0.0060	0.0300	0.0270	0.0143	-0.1467	0.0634	-0.0026	0.1738	0.0009
2.3892	1.6597	0.0060	0.0347	0.0250	0.0136	-0.0987	0.0555	-0.0026	0.1499	0.0009
2.4136	1.6914	0.0060	0.0354	0.0160	0.0082	-0.0719	0.0576	-0.0002	0.1366	0.0008
2.4379	1.7231	0.0060	0.0228	0.0230	0.0113	-0.0838	0.0517	-0.0003	0.1249	0.0008
2.4501	1.7390	0.0060	0.0233	0.0100	0.0060	-0.0649	0.0485	-0.0042	0.1065	0.0013
2.4593	1.7509	0.0060	0.0870	0.0120	0.0109	-0.0381	0.0292	-0.0031	0.0952	0.0021
2.0970	1.2789	0.0150	0.0200	0.0160	0.0145	-0.2951	0.2807	-0.0016	0.3389	0.0009
2.1031	1.2868	0.0150	0.0200	0.0210	0.0308	-0.2953	0.2821	0.0596	0.3642	0.0009
2.1092	1.2947	0.0150	0.0200	0.0230	0.0182	-0.2830	0.2751	0.0273	0.3796	0.0008
2.1153	1.3027	0.0150	0.0220	0.0240	0.0153	-0.2835	0.2679	0.0087	0.3835	0.0007
2.1214	1.3106	0.0150	0.0160	0.0220	0.0131	-0.2612	0.3101	0.0015	0.3772	0.0006

121

Table B.1 Flow field data for the bend width 0.60m (Q=0.013m³/s, continued)

x (m)	y (m)	z (m)	Urms (m/s)	Vrms (m/s)	Wrms (m/s)	U (m/s)	V (m/s)	W (m/s)	U_T (m/s)	Ke (m²/s²)
2.1336	1.3265	0.0150	0.0250	0.0250	0.0144	-0.2683	0.2450	0.0014	0.3439	0.0007
2.1457	1.3423	0.0150	0.0250	0.0260	0.0147	-0.2547	0.2282	0.0017	0.3259	0.0007
2.1701	1.3741	0.0150	0.0290	0.0280	0.0154	-0.2380	0.1990	0.0019	0.3058	0.0007
2.1944	1.4058	0.0150	0.0290	0.0300	0.0161	-0.2190	0.1680	0.0009	0.2925	0.0008
2.2188	1.4375	0.0150	0.0280	0.0300	0.0158	-0.2072	0.1489	0.0000	0.2682	0.0009
2.2431	1.4693	0.0150	0.0280	0.0300	0.0157	-0.2040	0.1301	-0.0003	0.2383	0.0009
2.2675	1.5010	0.0150	0.0290	0.0310	0.0160	-0.1882	0.1129	-0.0001	0.2191	0.0009
2.2918	1.5327	0.0150	0.0300	0.0300	0.0153	-0.1777	0.0986	-0.0001	0.2044	0.0009
2.3162	1.5645	0.0150	0.0270	0.0300	0.0154	-0.1684	0.0877	-0.0014	0.1883	0.0010
2.3405	1.5962	0.0150	0.0250	0.0280	0.0148	-0.1610	0.0958	-0.0033	0.1851	0.0009
2.3649	1.6279	0.0150	0.0270	0.0290	0.0157	-0.1574	0.0905	-0.0045	0.1781	0.0008
2.3892	1.6597	0.0150	0.0330	0.0280	0.0163	-0.1364	0.0933	-0.0061	0.1565	0.0009
2.4136	1.6914	0.0150	0.0320	0.0280	0.0171	-0.1233	0.0972	-0.0041	0.1439	0.0008
2.4379	1.7231	0.0150	0.0340	0.0310	0.0183	-0.1120	0.0922	-0.0014	0.1313	0.0008
2.4501	1.7390	0.0150	0.0320	0.0280	0.0145	-0.1020	0.0707	0.0012	0.1160	0.0012
2.4593	1.7509	0.0150	0.0300	0.0180	0.0096	-0.0904	0.0694	-0.0045	0.1051	0.0019
2.0970	1.2789	0.0350	0.0190	0.0170	0.0250	-0.2779	0.3015	0.0591	0.4024	0.0011
2.1031	1.2868	0.0350	0.0160	0.0180	0.0189	-0.2808	0.3125	0.0221	0.4115	0.0009
2.1092	1.2947	0.0350	0.0170	0.0200	0.0168	-0.2777	0.3165	0.0072	0.4118	0.0008
2.1153	1.3027	0.0350	0.0240	0.0210	0.0148	-0.2647	0.3039	0.0015	0.4061	0.0007
2.1214	1.3106	0.0350	0.0170	0.0210	0.0132	-0.2575	0.3034	0.0016	0.3978	0.0008
2.1336	1.3265	0.0350	0.0170	0.0200	0.0120	-0.2453	0.2979	0.0022	0.3753	0.0009
2.1457	1.3423	0.0350	0.0230	0.0210	0.0123	-0.2320	0.2890	0.0027	0.3575	0.0010
2.1701	1.3741	0.0350	0.0160	0.0220	0.0126	-0.2153	0.2648	0.0021	0.3312	0.0008
2.1944	1.4058	0.0350	0.0160	0.0210	0.0117	-0.2028	0.2514	0.0008	0.3115	0.0007
2.2188	1.4375	0.0350	0.0190	0.0220	0.0121	-0.1875	0.2271	0.0000	0.2870	0.0007
2.2431	1.4693	0.0350	0.0220	0.0220	0.0120	-0.1819	0.1950	-0.0001	0.2627	0.0007
2.2675	1.5010	0.0350	0.0230	0.0260	0.0139	-0.1776	0.1842	0.0007	0.2469	0.0007
2.2918	1.5327	0.0350	0.0200	0.0230	0.0122	-0.1748	0.1795	-0.0004	0.2345	0.0007
2.3162	1.5645	0.0350	0.0280	0.0260	0.0139	-0.1535	0.1531	-0.0025	0.2165	0.0008
2.3405	1.5962	0.0350	0.0230	0.0260	0.0144	-0.1525	0.1511	-0.0053	0.2077	0.0007
2.3649	1.6279	0.0350	0.0200	0.0250	0.0142	-0.1420	0.1418	-0.0065	0.1964	0.0007
2.3892	1.6597	0.0350	0.0200	0.0220	0.0136	-0.1330	0.1487	-0.0074	0.1811	0.0008
2.4136	1.6914	0.0350	0.0250	0.0230	0.0144	-0.1254	0.1504	-0.0020	0.1710	0.0008
2.4379	1.7231	0.0350	0.0236	0.0226	0.0191	-0.1063	0.1144	0.0021	0.1551	0.0008
2.4501	1.7390	0.0350	0.0233	0.0170	0.0158	-0.1109	0.1166	-0.0030	0.1467	0.0009
2.4593	1.7509	0.0350	0.0200	0.0169	0.0199	-0.1016	0.0943	0.0004	0.1390	0.0010
2.0970	1.2789	0.0550	0.0340	0.0190	0.0173	-0.2811	0.2989	0.0142	0.4001	0.0023

Table B.1 Flow field data for the bend width 0.60m (Q=0.013m^3/s, continued)

x (m)	y (m)	z (m)	Urms (m/s)	Vrms (m/s)	Wrms (m/s)	U (m/s)	V (m/s)	W (m/s)	U$_T$(m/s)	Ke (m^2/s^2)
2.1031	1.2868	0.0550	0.0220	0.0180	0.0260	-0.2779	0.3229	0.0310	0.4127	0.0021
2.1092	1.2947	0.0550	0.0300	0.0170	0.0201	-0.2704	0.3260	0.0157	0.4172	0.0019
2.1153	1.3027	0.0550	0.0290	0.0200	0.0220	-0.2650	0.3281	0.0071	0.4134	0.0017
2.1214	1.3106	0.0550	0.0250	0.0200	0.0201	-0.2546	0.3252	0.0023	0.4041	0.0018
2.1336	1.3265	0.0550	0.0206	0.0190	0.0171	-0.2336	0.3116	0.0023	0.3794	0.0019
2.1457	1.3423	0.0550	0.0200	0.0210	0.0173	-0.2289	0.2979	0.0026	0.3660	0.0019
2.1701	1.3741	0.0550	0.0250	0.0170	0.0129	-0.2083	0.2821	0.0030	0.3446	0.0013
2.1944	1.4058	0.0550	0.0110	0.0180	0.0133	-0.1965	0.2680	0.0016	0.3243	0.0007
2.2188	1.4375	0.0550	0.0120	0.0180	0.0132	-0.1813	0.2500	-0.0001	0.3004	0.0006
2.2431	1.4693	0.0550	0.0120	0.0170	0.0129	-0.1721	0.2291	-0.0008	0.2794	0.0005
2.2675	1.5010	0.0550	0.0120	0.0170	0.0137	-0.1658	0.2192	-0.0024	0.2657	0.0005
2.2918	1.5327	0.0550	0.0130	0.0160	0.0119	-0.1613	0.2120	0.0007	0.2547	0.0005
2.3162	1.5645	0.0550	0.0150	0.0180	0.0128	-0.1516	0.1983	-0.0010	0.2362	0.0005
2.3405	1.5962	0.0550	0.0130	0.0180	0.0121	-0.1455	0.1898	-0.0033	0.2217	0.0005
2.3649	1.6279	0.0550	0.0140	0.0170	0.0111	-0.1358	0.1647	-0.0048	0.2075	0.0006
2.3892	1.6597	0.0550	0.0240	0.0210	0.0128	-0.1281	0.1550	-0.0084	0.1881	0.0009
2.4136	1.6914	0.0550	0.0230	0.0230	0.0127	-0.1217	0.1551	-0.0094	0.1779	0.0009
2.4379	1.7231	0.0550	0.0240	0.0270	0.0157	-0.1122	0.1314	-0.0048	0.1639	0.0009
2.4501	1.7390	0.0550	0.0250	0.0260	0.0161	-0.1130	0.1271	0.0051	0.1574	0.0008
2.4593	1.7509	0.0550	0.0259	0.0190	0.0115	-0.1045	0.1004	0.0094	0.1515	0.0008
2.0970	1.2789	0.0750	0.1470	0.0260	0.0372	-0.2152	0.2584	0.0040	0.3272	0.0052
2.1031	1.2868	0.0750	0.0800	0.0210	0.0244	-0.2606	0.3109	0.0067	0.3631	0.0057
2.1092	1.2947	0.0750	0.0920	0.0220	0.0239	-0.2532	0.3090	0.0043	0.3880	0.0058
2.1153	1.3027	0.0750	0.0930	0.0220	0.0219	-0.2486	0.3068	0.0018	0.3913	0.0054
2.1214	1.3106	0.0750	0.0490	0.0230	0.0208	-0.2540	0.3146	0.0020	0.3846	0.0050
2.1336	1.3265	0.0750	0.0408	0.0230	0.0192	-0.2062	0.2767	0.0027	0.3548	0.0044
2.1457	1.3423	0.0750	0.0240	0.0250	0.0199	-0.2213	0.2833	0.0039	0.3542	0.0038
2.1701	1.3741	0.0750	0.0240	0.0210	0.0160	-0.2162	0.2768	0.0029	0.3459	0.0020
2.1944	1.4058	0.0750	0.0120	0.0190	0.0144	-0.2027	0.2614	0.0000	0.3277	0.0008
2.2188	1.4375	0.0750	0.0110	0.0180	0.0131	-0.1867	0.2429	0.0004	0.3041	0.0005
2.2431	1.4693	0.0750	0.0100	0.0160	0.0115	-0.1761	0.2272	-0.0053	0.2852	0.0004
2.2675	1.5010	0.0750	0.0110	0.0160	0.0111	-0.1696	0.2159	-0.0016	0.2722	0.0004
2.2918	1.5327	0.0750	0.0120	0.0160	0.0114	-0.1615	0.2084	0.0014	0.2618	0.0003
2.3162	1.5645	0.0750	0.0160	0.0170	0.0117	-0.1539	0.1937	-0.0002	0.2429	0.0004
2.3405	1.5962	0.0750	0.0120	0.0160	0.0105	-0.1452	0.1656	-0.0014	0.2232	0.0004
2.3649	1.6279	0.0750	0.0150	0.0180	0.0112	-0.1443	0.1586	-0.0021	0.2101	0.0005
2.3892	1.6597	0.0750	0.0350	0.0290	0.0162	-0.1259	0.1168	-0.0035	0.1786	0.0010
2.4136	1.6914	0.0750	0.0270	0.0290	0.0189	-0.1200	0.1097	-0.0083	0.1660	0.0011

123

Table B.1 Flow field data for the bend width 0.60m (Q=0.013m^3/s, continued)

x (m)	y (m)	z (m)	Urms (m/s)	Vrms (m/s)	Wrms (m/s)	U (m/s)	V (m/s)	W (m/s)	U$_T$(m/s)	Ke (m^2/s^2)
2.4379	1.7231	0.0750	0.0270	0.0250	0.0185	-0.1223	0.1166	-0.0008	0.1569	0.0010
2.4501	1.7390	0.0750	0.0270	0.0240	0.0183	-0.1104	0.1074	0.0088	0.1507	0.0009
2.4593	1.7509	0.0750	0.0350	0.0170	0.0156	-0.1105	0.0974	0.0174	0.1472	0.0008
2.0970	1.2789	0.0850	0.0380	0.0250	0.0358	0.0226	0.0344	-0.0090	0.2838	0.0057
2.1031	1.2868	0.0850	0.1380	0.0300	0.0301	-0.2395	0.2644	0.0019	0.3225	0.0066
2.1092	1.2947	0.0850	0.1380	0.0290	0.0260	-0.2310	0.2706	-0.0041	0.3613	0.0074
2.1153	1.3027	0.0850	0.1340	0.0350	0.0289	-0.2368	0.2712	-0.0040	0.3736	0.0072
2.1214	1.3106	0.0850	0.1130	0.0340	0.0267	-0.2385	0.2838	-0.0006	0.3728	0.0064
2.1336	1.3265	0.0850	0.1121	0.0330	0.0254	-0.1838	0.2368	0.0023	0.3455	0.0053
2.1457	1.3423	0.0850	0.1020	0.0350	0.0272	-0.2210	0.2590	0.0043	0.3496	0.0044
2.1701	1.3741	0.0850	0.0580	0.0310	0.0254	-0.2224	0.2589	0.0029	0.3453	0.0022
2.1944	1.4058	0.0850	0.0100	0.0250	0.0204	-0.2097	0.2491	-0.0010	0.3277	0.0008
2.2188	1.4375	0.0850	0.0140	0.0210	0.0157	-0.1909	0.2309	0.0003	0.3042	0.0005
2.2431	1.4693	0.0850	0.0100	0.0180	0.0120	-0.1818	0.2164	-0.0051	0.2858	0.0003
2.2675	1.5010	0.0850	0.0130	0.0170	0.0111	-0.1721	0.2077	-0.0001	0.2728	0.0003
2.2918	1.5327	0.0850	0.0110	0.0170	0.0118	-0.1690	0.2003	0.0016	0.2624	0.0003
2.3162	1.5645	0.0850	0.0130	0.0170	0.0114	-0.1576	0.1789	0.0000	0.2435	0.0003
2.3405	1.5962	0.0850	0.0150	0.0170	0.0112	-0.1487	0.1594	-0.0008	0.2225	0.0004
2.3649	1.6279	0.0850	0.0160	0.0160	0.0101	-0.1443	0.1536	-0.0012	0.2101	0.0005
2.3892	1.6597	0.0850	0.0370	0.0310	0.0179	-0.1299	0.1034	-0.0024	0.1754	0.0011
2.4136	1.6914	0.0850	0.0360	0.0330	0.0213	-0.1251	0.0784	-0.0077	0.1618	0.0012
2.4379	1.7231	0.0850	0.0360	0.0280	0.0206	-0.1080	0.0778	-0.0040	0.1537	0.0011
2.4501	1.7390	0.0850	0.0280	0.0260	0.0216	-0.1069	0.0808	0.0028	0.1471	0.0009
2.4593	1.7509	0.0850	0.0290	0.0170	0.0155	-0.1097	0.0854	0.0094	0.1446	0.0008
2.0610	1.2997	0.0060	0.0340	0.0250	0.0144	-0.3039	0.1497	0.0172	0.3224	0.0017
2.0648	1.3089	0.0060	0.0300	0.0270	0.0324	-0.3178	0.1630	0.0024	0.3449	0.0016
2.0687	1.3181	0.0060	0.0330	0.0300	0.0391	-0.3097	0.1694	-0.0033	0.3566	0.0016
2.0725	1.3274	0.0060	0.0360	0.0310	0.0411	-0.3021	0.1565	-0.0024	0.3553	0.0016
2.0763	1.3366	0.0060	0.0340	0.0310	0.0411	-0.3029	0.1547	-0.0010	0.3532	0.0016
2.0840	1.3551	0.0060	0.0349	0.0374	0.0264	-0.2964	0.1420	-0.0004	0.3444	0.0016
2.0916	1.3736	0.0060	0.0350	0.0320	0.0422	-0.2876	0.1289	-0.0004	0.3349	0.0017
2.1069	1.4105	0.0060	0.0320	0.0350	0.0458	-0.2671	0.1202	-0.0008	0.3131	0.0019
2.1222	1.4475	0.0060	0.0290	0.0310	0.0404	-0.2599	0.1270	-0.0010	0.3017	0.0017
2.1375	1.4844	0.0060	0.0280	0.0350	0.0453	-0.2401	0.0930	-0.0011	0.2694	0.0018
2.1528	1.5214	0.0060	0.0340	0.0330	0.0427	-0.2218	0.0367	-0.0011	0.2466	0.0019
2.1682	1.5584	0.0060	0.0310	0.0290	0.0373	-0.2123	0.0414	-0.0011	0.2273	0.0017
2.1835	1.5953	0.0060	0.0270	0.0290	0.0367	-0.2083	0.0224	-0.0013	0.2199	0.0016
2.1988	1.6323	0.0060	0.0270	0.0290	0.0361	-0.1822	0.0278	-0.0020	0.2117	0.0014

Table B.1 Flow field data for the bend width 0.60m (Q=0.013m³/s, continued)

x (m)	y (m)	z (m)	Urms (m/s)	Vrms (m/s)	Wrms (m/s)	U (m/s)	V (m/s)	W (m/s)	U_T(m/s)	Ke (m²/s²)
2.2141	1.6692	0.0060	0.0280	0.0260	0.0317	-0.1959	0.0444	-0.0027	0.2062	0.0012
2.2294	1.7062	0.0060	0.0270	0.0280	0.0337	-0.1814	0.0481	-0.0029	0.1884	0.0013
2.2447	1.7431	0.0060	0.0290	0.0230	0.0274	-0.1577	0.0556	-0.0030	0.1857	0.0012
2.2600	1.7801	0.0060	0.0290	0.0250	0.0295	-0.1353	0.0496	-0.0022	0.1624	0.0013
2.2753	1.8170	0.0060	0.0270	0.0150	0.0177	-0.1423	0.0535	0.0018	0.1620	0.0009
2.2830	1.8355	0.0060	0.0280	0.0120	0.0129	-0.1332	0.0573	-0.0047	0.1564	0.0007
2.2887	1.8494	0.0060	0.0290	0.0140	0.0118	-0.1095	0.0518	-0.0032	0.1494	0.0007
2.0610	1.2997	0.0150	0.0490	0.0290	0.0270	-0.2168	0.1612	0.0194	0.3163	0.0020
2.0648	1.3089	0.0150	0.0170	0.0300	0.0369	-0.3002	0.2239	-0.0007	0.3425	0.0018
2.0687	1.3181	0.0150	0.0160	0.0260	0.0360	-0.2949	0.2315	-0.0048	0.3624	0.0016
2.0725	1.3274	0.0150	0.0190	0.0250	0.0359	-0.2923	0.2272	-0.0026	0.3651	0.0015
2.0763	1.3366	0.0150	0.0210	0.0260	0.0374	-0.2933	0.2222	-0.0006	0.3614	0.0015
2.0840	1.3551	0.0150	0.0210	0.0290	0.0417	-0.2901	0.2089	0.0002	0.3500	0.0016
2.0916	1.3736	0.0150	0.0240	0.0290	0.0415	-0.2804	0.2038	0.0000	0.3399	0.0018
2.1069	1.4105	0.0150	0.0250	0.0330	0.0470	-0.2679	0.1737	-0.0007	0.3181	0.0019
2.1222	1.4475	0.0150	0.0280	0.0340	0.0482	-0.2640	0.1570	-0.0010	0.3061	0.0017
2.1375	1.4844	0.0150	0.0300	0.0330	0.0464	-0.2362	0.1249	-0.0013	0.2751	0.0018
2.1528	1.5214	0.0150	0.0270	0.0390	0.0548	-0.2366	0.0926	-0.0015	0.2523	0.0018
2.1682	1.5584	0.0150	0.0280	0.0394	0.0601	-0.2141	0.0659	-0.0014	0.2331	0.0017
2.1835	1.5953	0.0150	0.0310	0.0380	0.0527	-0.2083	0.0668	-0.0020	0.2253	0.0015
2.1988	1.6323	0.0150	0.0240	0.0290	0.0399	-0.2096	0.0793	-0.0031	0.2169	0.0014
2.2141	1.6692	0.0150	0.0220	0.0290	0.0395	-0.1961	0.0650	-0.0042	0.2098	0.0012
2.2294	1.7062	0.0150	0.0300	0.0290	0.0393	-0.1753	0.0499	-0.0046	0.1913	0.0013
2.2447	1.7431	0.0150	0.0250	0.0310	0.0416	-0.1669	0.1092	-0.0047	0.1881	0.0012
2.2600	1.7801	0.0150	0.0270	0.0320	0.0426	-0.1454	0.0775	-0.0037	0.1664	0.0013
2.2753	1.8170	0.0150	0.0270	0.0230	0.0301	-0.1497	0.0750	0.0025	0.1655	0.0009
2.2830	1.8355	0.0150	0.0290	0.0180	0.0236	-0.1502	0.0763	-0.0058	0.1614	0.0008
2.2887	1.8494	0.0150	0.0320	0.0170	0.0143	-0.1442	0.0673	-0.0024	0.1549	0.0007
2.0610	1.2997	0.0350	0.0970	0.0420	0.0286	-0.1140	0.0959	-0.0066	0.2909	0.0031
2.0648	1.3089	0.0350	0.0420	0.0240	0.0158	-0.2707	0.2507	-0.0091	0.3236	0.0026
2.0687	1.3181	0.0350	0.0170	0.0180	0.0121	-0.2866	0.2724	-0.0069	0.3645	0.0019
2.0725	1.3274	0.0350	0.0150	0.0220	0.0163	-0.2859	0.2635	-0.0025	0.3808	0.0015
2.0763	1.3366	0.0350	0.0150	0.0240	0.0214	-0.2861	0.2657	0.0011	0.3792	0.0015
2.0840	1.3551	0.0350	0.0140	0.0240	0.0270	-0.2670	0.2491	0.0020	0.3670	0.0020
2.0916	1.3736	0.0350	0.0200	0.0190	0.0254	-0.2665	0.2554	0.0019	0.3568	0.0023
2.1069	1.4105	0.0350	0.0130	0.0250	0.0372	-0.2531	0.2434	0.0003	0.3363	0.0024
2.1222	1.4475	0.0350	0.0150	0.0240	0.0363	-0.2458	0.2349	-0.0004	0.3225	0.0020
2.1375	1.4844	0.0350	0.0160	0.0250	0.0387	-0.2283	0.2093	-0.0013	0.2984	0.0018

Table B.1 Flow field data for the bend width 0.60m (Q=0.013m³/s, continued)

x (m)	y (m)	z (m)	Urms (m/s)	Vrms (m/s)	Wrms (m/s)	U (m/s)	V (m/s)	W (m/s)	U_T(m/s)	Ke (m²/s²)
2.1528	1.5214	0.0350	0.0220	0.0290	0.0453	-0.2225	0.1788	-0.0024	0.2770	0.0016
2.1682	1.5584	0.0350	0.0240	0.0310	0.0483	-0.2165	0.1568	-0.0024	0.2584	0.0014
2.1835	1.5953	0.0350	0.0220	0.0300	0.0463	-0.2082	0.1533	-0.0033	0.2490	0.0013
2.1988	1.6323	0.0350	0.0210	0.0280	0.0429	-0.2037	0.1407	-0.0058	0.2391	0.0012
2.2141	1.6692	0.0350	0.0180	0.0250	0.0382	-0.1899	0.1295	-0.0074	0.2257	0.0011
2.2294	1.7062	0.0350	0.0210	0.0230	0.0352	-0.1756	0.0987	-0.0083	0.2044	0.0012
2.2447	1.7431	0.0350	0.0180	0.0200	0.0311	-0.1650	0.1268	-0.0093	0.1959	0.0013
2.2600	1.7801	0.0350	0.0250	0.0290	0.0466	-0.1523	0.1237	-0.0085	0.1811	0.0014
2.2753	1.8170	0.0350	0.0240	0.0270	0.0417	-0.1484	0.1069	0.0027	0.1782	0.0011
2.2830	1.8355	0.0350	0.0240	0.0190	0.0324	-0.1624	0.0965	0.0034	0.1770	0.0009
2.2887	1.8494	0.0350	0.0340	0.0160	0.0135	-0.1512	0.0697	0.0061	0.1725	0.0008
2.0610	1.2997	0.0550	0.0750	0.0430	0.0211	-0.1790	0.1402	-0.0062	0.2833	0.0037
2.0648	1.3089	0.0550	0.0340	0.0250	0.0140	-0.2788	0.2519	0.0031	0.3238	0.0034
2.0687	1.3181	0.0550	0.0390	0.0230	0.0139	-0.2814	0.2692	0.0051	0.3665	0.0029
2.0725	1.3274	0.0550	0.0280	0.0250	0.0170	-0.2854	0.2752	0.0035	0.3824	0.0029
2.0763	1.3366	0.0550	0.0380	0.0280	0.0228	-0.2810	0.2701	0.0025	0.3799	0.0034
2.0840	1.3551	0.0550	0.0450	0.0260	0.0265	-0.2703	0.2646	0.0027	0.3662	0.0044
2.0916	1.3736	0.0550	0.0420	0.0240	0.0293	-0.2644	0.2632	0.0020	0.3563	0.0048
2.1069	1.4105	0.0550	0.0340	0.0200	0.0278	-0.2469	0.2506	-0.0006	0.3377	0.0042
2.1222	1.4475	0.0550	0.0270	0.0170	0.0242	-0.2367	0.2464	-0.0013	0.3248	0.0029
2.1375	1.4844	0.0550	0.0220	0.0190	0.0280	-0.2272	0.2381	-0.0021	0.3087	0.0023
2.1528	1.5214	0.0550	0.0130	0.0200	0.0283	-0.2074	0.2180	-0.0054	0.2931	0.0014
2.1682	1.5584	0.0550	0.0140	0.0170	0.0237	-0.2015	0.1982	-0.0065	0.2759	0.0012
2.1835	1.5953	0.0550	0.0140	0.0190	0.0268	-0.1975	0.1922	-0.0039	0.2652	0.0011
2.1988	1.6323	0.0550	0.0140	0.0180	0.0253	-0.1921	0.1791	-0.0053	0.2529	0.0010
2.2141	1.6692	0.0550	0.0120	0.0190	0.0271	-0.1876	0.1665	-0.0050	0.2370	0.0009
2.2294	1.7062	0.0550	0.0160	0.0200	0.0297	-0.1732	0.1410	-0.0055	0.2122	0.0010
2.2447	1.7431	0.0550	0.0220	0.0240	0.0388	-0.1579	0.1206	-0.0063	0.1946	0.0013
2.2600	1.7801	0.0550	0.0230	0.0280	0.0457	-0.1453	0.1197	-0.0063	0.1836	0.0015
2.2753	1.8170	0.0550	0.0210	0.0260	0.0393	-0.1521	0.1085	-0.0013	0.1803	0.0012
2.2830	1.8355	0.0550	0.0240	0.0190	0.0304	-0.1567	0.0920	0.0137	0.1780	0.0009
2.2887	1.8494	0.0550	0.0320	0.0190	0.0160	-0.1464	0.0655	0.0175	0.1727	0.0009
2.0610	1.2997	0.0750	0.0950	0.0470	0.0277	-0.0513	0.0537	0.0196	0.2028	0.0062
2.0648	1.3089	0.0750	0.1030	0.0390	0.0243	-0.2334	0.2049	0.0178	0.2616	0.0070
2.0687	1.3181	0.0750	0.0690	0.0320	0.0224	-0.2762	0.2530	0.0154	0.3246	0.0080
2.0725	1.3274	0.0750	0.0750	0.0340	0.0282	-0.2725	0.2568	0.0132	0.3482	0.0087
2.0763	1.3366	0.0750	0.0630	0.0380	0.0387	-0.2745	0.2544	0.0105	0.3479	0.0094
2.0840	1.3551	0.0750	0.0860	0.0350	0.0430	-0.2568	0.2503	0.0071	0.3350	0.0102

Table B.1 Flow field data for the bend width 0.60m (Q=0.013m^3/s, continued)

x (m)	y (m)	z (m)	Urms (m/s)	Vrms (m/s)	Wrms (m/s)	U (m/s)	V (m/s)	W (m/s)	U$_T$(m/s)	Ke (m^2/s^2)
2.0916	1.3736	0.0750	0.0820	0.0310	0.0417	-0.2527	0.2497	0.0031	0.3312	0.0096
2.1069	1.4105	0.0750	0.0740	0.0310	0.0361	-0.2387	0.2363	-0.0028	0.3196	0.0072
2.1222	1.4475	0.0750	0.0880	0.0260	0.0280	-0.2177	0.2244	-0.0037	0.3101	0.0045
2.1375	1.4844	0.0750	0.0270	0.0210	0.0223	-0.2256	0.2158	-0.0028	0.3014	0.0034
2.1528	1.5214	0.0750	0.0110	0.0190	0.0216	-0.2160	0.2129	-0.0067	0.2974	0.0015
2.1682	1.5584	0.0750	0.0090	0.0190	0.0227	-0.2067	0.2014	-0.0113	0.2816	0.0009
2.1835	1.5953	0.0750	0.0100	0.0200	0.0254	-0.1985	0.1872	-0.0020	0.2702	0.0008
2.1988	1.6323	0.0750	0.0100	0.0200	0.0256	-0.1958	0.1753	-0.0024	0.2553	0.0010
2.2141	1.6692	0.0750	0.0110	0.0180	0.0241	-0.1887	0.1507	0.0006	0.2394	0.0008
2.2294	1.7062	0.0750	0.0210	0.0270	0.0394	-0.1771	0.1134	0.0016	0.2126	0.0009
2.2447	1.7431	0.0750	0.0260	0.0280	0.0443	-0.1600	0.0814	0.0019	0.1850	0.0014
2.2600	1.7801	0.0750	0.0270	0.0260	0.0414	-0.1582	0.0753	-0.0008	0.1759	0.0016
2.2753	1.8170	0.0750	0.0220	0.0220	0.0329	-0.1591	0.0811	-0.0038	0.1731	0.0012
2.2830	1.8355	0.0750	0.0230	0.0180	0.0212	-0.1633	0.0839	0.0102	0.1692	0.0009
2.2887	1.8494	0.0750	0.0270	0.0170	0.0143	-0.1377	0.0600	0.0161	0.1604	0.0008
2.0610	1.2997	0.0850	0.0900	0.0320	0.0210	-0.0523	0.0357	0.0000	0.1705	0.0075
2.0648	1.3089	0.0850	0.1630	0.0510	0.0383	-0.1760	0.1292	0.0015	0.2256	0.0093
2.0687	1.3181	0.0850	0.1570	0.0610	0.0565	-0.2286	0.1564	0.0019	0.2872	0.0113
2.0725	1.3274	0.0850	0.1590	0.0640	0.0724	-0.2197	0.1700	0.0020	0.3129	0.0123
2.0763	1.3366	0.0850	0.1490	0.0650	0.0852	-0.2273	0.1699	0.0014	0.3229	0.0122
2.0840	1.3551	0.0850	0.1590	0.0670	0.0919	-0.2063	0.1580	0.0066	0.3202	0.0121
2.0916	1.3736	0.0850	0.1490	0.0620	0.0768	-0.2160	0.1631	0.0006	0.3217	0.0109
2.1069	1.4105	0.0850	0.1320	0.0550	0.0526	-0.2088	0.1753	-0.0062	0.3134	0.0080
2.1222	1.4475	0.0850	0.0890	0.0450	0.0421	-0.2273	0.1699	-0.0063	0.3052	0.0049
2.1375	1.4844	0.0850	0.0910	0.0390	0.0385	-0.2048	0.1746	-0.0042	0.2981	0.0038
2.1528	1.5214	0.0850	0.0320	0.0290	0.0319	-0.2180	0.1975	-0.0031	0.2974	0.0015
2.1682	1.5584	0.0850	0.0180	0.0240	0.0281	-0.2043	0.1810	-0.0043	0.2820	0.0009
2.1835	1.5953	0.0850	0.0100	0.0220	0.0280	-0.2046	0.1724	0.0007	0:2704	0.0008
2.1988	1.6323	0.0850	0.0270	0.0240	0.0308	-0.1872	0.1544	0.0010	0.2548	0.0009
2.2141	1.6692	0.0850	0.0120	0.0220	0.0278	-0.1918	0.1379	0.0024	0.2392	0.0008
2.2294	1.7062	0.0850	0.0140	0.0210	0.0280	-0.1757	0.1193	0.0030	0.2121	0.0009
2.2447	1.7431	0.0850	0.0290	0.0250	0.0368	-0.1601	0.0707	0.0029	0.1824	0.0014
2.2600	1.7801	0.0850	0.0290	0.0280	0.0429	-0.1540	0.0594	0.0014	0.1735	0.0016
2.2753	1.8170	0.0850	0.0280	0.0220	0.0333	-0.1464	0.0542	-0.0001	0.1703	0.0012
2.2830	1.8355	0.0850	0.0330	0.0170	0.0196	-0.1428	0.0656	0.0040	0.1652	0.0009
2.2887	1.8494	0.0850	0.0300	0.0210	0.0177	-0.1211	0.0577	0.0066	0.1560	0.0008
2.0208	1.3104	0.0060	0.0280	0.0350	0.0256	-0.2503	0.0067	0.0005	0.2296	0.0025
2.0221	1.3204	0.0060	0.0580	0.0270	0.0172	-0.2798	0.0580	-0.0015	0.2449	0.0025

Table B.1 Flow field data for the bend width 0.60m (Q=0.013m³/s, continued)

x (m)	y (m)	z (m)	Urms (m/s)	Vrms (m/s)	Wrms (m/s)	U (m/s)	V (m/s)	W (m/s)	U$_T$(m/s)	Ke (m²/s²)
2.0234	1.3303	0.0060	0.0510	0.0330	0.0183	-0.2927	0.0678	0.0017	0.2767	0.0024
2.0247	1.3402	0.0060	0.0360	0.0370	0.0190	-0.3016	0.0841	0.0054	0.3061	0.0021
2.0260	1.3501	0.0060	0.0360	0.0320	0.0158	-0.3047	0.0684	0.0060	0.3203	0.0019
2.0286	1.3699	0.0060	0.0350	0.0360	0.0175	-0.3023	0.0862	0.0040	0.3309	0.0016
2.0313	1.3898	0.0060	0.0360	0.0300	0.0146	-0.3072	0.0566	0.0013	0.3312	0.0014
2.0365	1.4294	0.0060	0.0310	0.0320	0.0157	-0.2928	0.0517	-0.0005	0.3163	0.0013
2.0417	1.4691	0.0060	0.0340	0.0320	0.0157	-0.2807	0.0359	-0.0008	0.3019	0.0012
2.0469	1.5087	0.0060	0.0290	0.0320	0.0157	-0.2698	0.0194	-0.0009	0.2851	0.0011
2.0521	1.5484	0.0060	0.0395	0.0240	0.0120	-0.2600	0.0044	-0.0012	0.2730	0.0011
2.0574	1.5880	0.0060	0.0280	0.0287	0.0177	-0.2503	0.0067	-0.0014	0.2635	0.0010
2.0626	1.6277	0.0060	0.0240	0.0269	0.0204	-0.2407	-0.0046	-0.0020	0.2532	0.0010
2.0678	1.6674	0.0060	0.0360	0.0240	0.0131	-0.2378	0.0091	-0.0026	0.2393	0.0010
2.0730	1.7070	0.0060	0.0270	0.0287	0.0225	-0.2311	-0.0089	-0.0029	0.2350	0.0010
2.0782	1.7467	0.0060	0.0230	0.0240	0.0144	-0.2133	0.0422	-0.0033	0.2294	0.0007
2.0835	1.7863	0.0060	0.0240	0.0290	0.0178	-0.2024	0.0488	-0.0033	0.2156	0.0008
2.0887	1.8260	0.0060	0.0230	0.0270	0.0165	-0.1845	0.0162	-0.0023	0.1947	0.0007
2.0939	1.8657	0.0060	0.0250	0.0200	0.0108	-0.1934	0.0174	0.0029	0.1949	0.0006
2.0965	1.8855	0.0060	0.0250	0.0170	0.0113	-0.1917	0.0151	-0.0046	0.1904	0.0006
2.0985	1.9004	0.0060	0.0240	0.0170	0.0244	-0.1455	0.0212	-0.0049	0.1780	0.0007
2.0208	1.3104	0.0150	0.0830	0.0180	0.0202	-0.2251	0.0367	-0.0077	0.1963	0.0029
2.0221	1.3204	0.0150	0.0930	0.0450	0.0405	-0.1373	0.0604	-0.0048	0.2088	0.0031
2.0234	1.3303	0.0150	0.0830	0.0380	0.0269	-0.2404	0.1355	0.0033	0.2482	0.0030
2.0247	1.3402	0.0150	0.0440	0.0310	0.0178	-0.2837	0.1665	0.0100	0.2922	0.0026
2.0260	1.3501	0.0150	0.0290	0.0340	0.0176	-0.2990	0.1654	0.0106	0.3161	0.0022
2.0286	1.3699	0.0150	0.0290	0.0320	0.0160	-0.3070	0.1655	0.0070	0.3326	0.0018
2.0313	1.3898	0.0150	0.0270	0.0310	0.0156	-0.3128	0.1521	0.0027	0.3336	0.0015
2.0365	1.4294	0.0150	0.0330	0.0370	0.0187	-0.3021	0.1184	-0.0001	0.3194	0.0014
2.0417	1.4691	0.0150	0.0280	0.0390	0.0197	-0.2914	0.1080	-0.0007	0.3056	0.0013
2.0469	1.5087	0.0150	0.0270	0.0380	0.0191	-0.2766	0.0828	-0.0010	0.2892	0.0011
2.0521	1.5484	0.0150	0.0320	0.0380	0.0192	-0.2695	0.0597	-0.0017	0.2771	0.0011
2.0574	1.5880	0.0150	0.0350	0.0380	0.0193	-0.2665	0.0442	-0.0020	0.2669	0.0010
2.0626	1.6277	0.0150	0.0300	0.0370	0.0193	-0.2560	0.0398	-0.0031	0.2567	0.0010
2.0678	1.6674	0.0150	0.0330	0.0340	0.0186	-0.2281	0.0371	-0.0042	0.2432	0.0010
2.0730	1.7070	0.0150	0.0260	0.0300	0.0172	-0.2302	0.0364	-0.0047	0.2381	0.0009
2.0782	1.7467	0.0150	0.0300	0.0310	0.0185	-0.2363	0.0210	-0.0053	0.2320	0.0007
2.0835	1.7863	0.0150	0.0240	0.0260	0.0162	-0.2102	0.0579	-0.0055	0.2178	0.0008
2.0887	1.8260	0.0150	0.0240	0.0310	0.0195	-0.1843	0.0485	-0.0038	0.1980	0.0007
2.0939	1.8657	0.0150	0.0200	0.0270	0.0147	-0.1912	0.0413	0.0042	0.1962	0.0006

Table B.1 Flow field data for the bend width 0.60m (Q=0.013m³/s, continued)

x (m)	y (m)	z (m)	Urms (m/s)	Vrms (m/s)	Wrms (m/s)	U (m/s)	V (m/s)	W (m/s)	U$_T$(m/s)	Ke (m²/s²)
2.0965	1.8855	0.0150	0.0200	0.0190	0.0104	-0.2013	0.0265	-0.0059	0.1927	0.0007
2.0985	1.9004	0.0150	0.0300	0.0190	0.0272	-0.1778	0.0285	-0.0046	0.1820	0.0007
2.0208	1.3104	0.0350	0.0770	0.0410	0.0582	-0.0953	0.0267	-0.0101	0.0931	0.0038
2.0221	1.3204	0.0350	0.0730	0.0410	0.0489	-0.0101	0.0225	-0.0061	0.1001	0.0041
2.0234	1.3303	0.0350	0.0950	0.0450	0.0455	-0.0578	0.0590	0.0030	0.1471	0.0043
2.0247	1.3402	0.0350	0.0940	0.0370	0.0359	-0.1857	0.1374	0.0160	0.2194	0.0040
2.0260	1.3501	0.0350	0.0550	0.0340	0.0331	-0.2749	0.1724	0.0169	0.2770	0.0035
2.0286	1.3699	0.0350	0.0180	0.0410	0.0394	-0.2986	0.1755	0.0115	0.3255	0.0027
2.0313	1.3898	0.0350	0.0170	0.0330	0.0295	-0.2980	0.1804	0.0064	0.3354	0.0023
2.0365	1.4294	0.0350	0.0150	0.0310	0.0236	-0.2908	0.1815	0.0019	0.3270	0.0019
2.0417	1.4691	0.0350	0.0200	0.0250	0.0164	-0.2782	0.1778	0.0013	0.3174	0.0015
2.0469	1.5087	0.0350	0.0190	0.0280	0.0163	-0.2721	0.1629	0.0008	0.3046	0.0012
2.0521	1.5484	0.0350	0.0260	0.0320	0.0180	-0.2611	0.1544	-0.0019	0.2932	0.0012
2.0574	1.5880	0.0350	0.0240	0.0330	0.0187	-0.2498	0.1327	-0.0032	0.2812	0.0011
2.0626	1.6277	0.0350	0.0220	0.0340	0.0196	-0.2442	0.1219	-0.0065	0.2717	0.0010
2.0678	1.6674	0.0350	0.0250	0.0320	0.0187	-0.2415	0.1195	-0.0087	0.2598	0.0009
2.0730	1.7070	0.0350	0.0250	0.0320	0.0186	-0.2321	0.1062	-0.0089	0.2511	0.0009
2.0782	1.7467	0.0350	0.0160	0.0240	0.0137	-0.2260	0.1064	-0.0096	0.2417	0.0007
2.0835	1.7863	0.0350	0.0200	0.0240	0.0132	-0.2195	0.0945	-0.0102	0.2246	0.0008
2.0887	1.8260	0.0350	0.0190	0.0230	0.0124	-0.2042	0.1035	-0.0085	0.2096	0.0007
2.0939	1.8657	0.0350	0.0190	0.0270	0.0159	-0.1884	0.0702	0.0047	0.2012	0.0006
2.0965	1.8855	0.0350	0.0200	0.0250	0.0134	-0.1918	0.0525	0.0040	0.1990	0.0007
2.0985	1.9004	0.0350	0.0270	0.0170	0.0244	-0.2012	0.0426	0.0040	0.1943	0.0008
2.0208	1.3104	0.0550	0.0260	0.0190	0.0278	0.0504	-0.0076	-0.0076	0.0825	0.0032
2.0221	1.3204	0.0550	0.0860	0.0420	0.0584	-0.0595	0.0381	-0.0026	0.1024	0.0037
2.0234	1.3303	0.0550	0.0990	0.0440	0.0592	-0.1205	0.0885	0.0011	0.1591	0.0045
2.0247	1.3402	0.0550	0.0840	0.0360	0.0467	-0.2162	0.1505	0.0037	0.2279	0.0048
2.0260	1.3501	0.0550	0.0650	0.0500	0.0627	-0.2662	0.1541	0.0019	0.2762	0.0046
2.0286	1.3699	0.0550	0.0280	0.0590	0.0701	-0.3093	0.1406	-0.0004	0.3207	0.0039
2.0313	1.3898	0.0550	0.0280	0.0600	0.0667	-0.3104	0.1246	-0.0013	0.3321	0.0033
2.0365	1.4294	0.0550	0.0400	0.0510	0.0494	-0.2904	0.1613	0.0003	0.3235	0.0027
2.0417	1.4691	0.0550	0.0260	0.0380	0.0323	-0.2783	0.1768	0.0016	0.3185	0.0021
2.0469	1.5087	0.0550	0.0330	0.0250	0.0177	-0.2654	0.1832	0.0020	0.3114	0.0015
2.0521	1.5484	0.0550	0.0250	0.0190	0.0129	-0.2543	0.1828	-0.0006	0.3030	0.0015
2.0574	1.5880	0.0550	0.0110	0.0200	0.0139	-0.2463	0.1746	-0.0025	0.2915	0.0013
2.0626	1.6277	0.0550	0.0130	0.0170	0.0118	-0.2421	0.1761	-0.0091	0.2824	0.0013
2.0678	1.6674	0.0550	0.0130	0.0190	0.0120	-0.2328	0.1547	-0.0098	0.2722	0.0009
2.0730	1.7070	0.0550	0.0150	0.0240	0.0137	-0.2295	0.1412	-0.0073	0.2600	0.0009

Table B.1 Flow field data for the bend width 0.60m (Q=0.013m³/s, continued)

x (m)	y (m)	z (m)	Urms (m/s)	Vrms (m/s)	Wrms (m/s)	U (m/s)	V (m/s)	W (m/s)	U$_T$(m/s)	Ke (m²/s²)
2.0782	1.7467	0.0550	0.0130	0.0210	0.0113	-0.2290	0.1149	-0.0065	0.2452	0.0008
2.0835	1.7863	0.0550	0.0210	0.0290	0.0148	-0.2049	0.0835	-0.0060	0.2228	0.0008
2.0887	1.8260	0.0550	0.0260	0.0240	0.0128	-0.1992	0.0878	-0.0063	0.2108	0.0007
2.0939	1.8657	0.0550	0.0190	0.0210	0.0130	-0.1904	0.0705	-0.0019	0.2021	0.0007
2.0965	1.8855	0.0550	0.0180	0.0220	0.0145	-0.1989	0.0595	0.0140	0.1989	0.0007
2.0985	1.9004	0.0550	0.0280	0.0180	0.0259	-0.1789	0.0357	0.0177	0.1947	0.0008
2.0208	1.3104	0.0750	0.0320	0.0180	0.0232	0.0613	-0.0091	-0.0095	0.0589	0.0030
2.0221	1.3204	0.0750	0.0580	0.0290	0.0334	-0.0065	0.0120	-0.0073	0.0866	0.0038
2.0234	1.3303	0.0750	0.0960	0.0410	0.0453	-0.1560	0.1022	-0.0057	0.1589	0.0050
2.0247	1.3402	0.0750	0.0820	0.0430	0.0469	-0.2315	0.1495	-0.0078	0.2350	0.0059
2.0260	1.3501	0.0750	0.0650	0.0560	0.0605	-0.2876	0.1367	-0.0086	0.2816	0.0060
2.0286	1.3699	0.0750	0.0460	0.0590	0.0617	-0.3120	0.1127	-0.0076	0.3183	0.0051
2.0313	1.3898	0.0750	0.0270	0.0580	0.0571	-0.3127	0.1148	-0.0049	0.3248	0.0044
2.0365	1.4294	0.0750	0.0247	0.0610	0.0537	-0.2807	0.1277	-0.0015	0.3077	0.0036
2.0417	1.4691	0.0750	0.0221	0.0490	0.0400	-0.2664	0.1601	0.0010	0.3065	0.0028
2.0469	1.5087	0.0750	0.0209	0.0280	0.0216	-0.2551	0.1768	0.0034	0.3055	0.0020
2.0521	1.5484	0.0750	0.0420	0.0310	0.0213	-0.2545	0.1737	0.0042	0.3018	0.0021
2.0574	1.5880	0.0750	0.0390	0.0250	0.0159	-0.2415	0.1730	0.0040	0.2917	0.0018
2.0626	1.6277	0.0750	0.0330	0.0210	0.0120	-0.2324	0.1657	-0.0073	0.2825	0.0018
2.0678	1.6674	0.0750	0.0130	0.0220	0.0127	-0.2341	0.1529	-0.0074	0.2758	0.0011
2.0730	1.7070	0.0750	0.0180	0.0290	0.0173	-0.2336	0.1256	-0.0036	0.2609	0.0010
2.0782	1.7467	0.0750	0.0200	0.0300	0.0178	-0.2255	0.0872	-0.0013	0.2410	0.0008
2.0835	1.7863	0.0750	0.0270	0.0280	0.0163	-0.2012	0.0497	-0.0007	0.2143	0.0008
2.0887	1.8260	0.0750	0.0270	0.0260	0.0149	-0.1918	0.0444	-0.0033	0.2036	0.0007
2.0939	1.8657	0.0750	0.0200	0.0210	0.0147	-0.1940	0.0356	-0.0057	0.1990	0.0006
2.0965	1.8855	0.0750	0.0200	0.0200	0.0214	-0.1942	0.0417	0.0082	0.1952	0.0007
2.0985	1.9004	0.0750	0.0260	0.0180	0.0260	-0.1841	0.0343	0.0163	0.1883	0.0008
2.0208	1.3104	0.0850	0.0650	0.0250	0.0275	0.0154	0.0020	0.0091	0.0504	0.0033
2.0221	1.3204	0.0850	0.0510	0.0290	0.0309	-0.0247	0.0194	0.0077	0.0770	0.0042
2.0234	1.3303	0.0850	0.1020	0.0420	0.0437	-0.1271	0.0692	0.0074	0.1487	0.0056
2.0247	1.3402	0.0850	0.1070	0.0540	0.0551	-0.2030	0.1054	0.0054	0.2250	0.0066
2.0260	1.3501	0.0850	0.0980	0.0590	0.0571	-0.2755	0.0988	0.0002	0.2756	0.0066
2.0286	1.3699	0.0850	0.0510	0.0540	0.0476	-0.3125	0.0936	-0.0048	0.3151	0.0055
2.0313	1.3898	0.0850	0.0590	0.0530	0.0442	-0.3062	0.0877	-0.0078	0.3219	0.0047
2.0365	1.4294	0.0850	0.0319	0.0600	0.0519	-0.2653	0.0995	-0.0061	0.3030	0.0038
2.0417	1.4691	0.0850	0.0307	0.0560	0.0492	-0.2493	0.1367	-0.0021	0.3026	0.0030
2.0469	1.5087	0.0850	0.0253	0.0480	0.0386	-0.2473	0.1516	0.0025	0.3030	0.0021
2.0521	1.5484	0.0850	0.0540	0.0430	0.0301	-0.2486	0.1497	0.0039	0.3004	0.0022

130

Table B.1 Flow field data for the bend width 0.60m (Q=0.013m^3/s, continued)

x (m)	y (m)	z (m)	Urms (m/s)	Vrms (m/s)	Wrms (m/s)	U (m/s)	V (m/s)	W (m/s)	U$_T$(m/s)	Ke (m^2/s^2)
2.0574	1.5880	0.0850	0.0470	0.0400	0.0256	-0.2412	0.1447	0.0042	0.2908	0.0019
2.0626	1.6277	0.0850	0.0620	0.0370	0.0200	-0.2301	0.1443	0.0010	0.2815	0.0020
2.0678	1.6674	0.0850	0.0290	0.0320	0.0173	-0.2371	0.1371	-0.0013	0.2757	0.0011
2.0730	1.7070	0.0850	0.0400	0.0290	0.0173	-0.2300	0.1069	-0.0014	0.2603	0.0011
2.0782	1.7467	0.0850	0.0330	0.0230	0.0143	-0.2213	0.0735	-0.0008	0.2393	0.0009
2.0835	1.7863	0.0850	0.0290	0.0230	0.0140	-0.2047	0.0542	-0.0008	0.2121	0.0008
2.0887	1.8260	0.0850	0.0220	0.0240	0.0136	-0.2006	0.0012	-0.0019	0.2014	0.0007
2.0939	1.8657	0.0850	0.0220	0.0220	0.0148	-0.1979	0.0139	-0.0021	0.1980	0.0006
2.0965	1.8855	0.0850	0.0270	0.0160	0.0159	-0.1948	0.0297	0.0020	0.1938	0.0007
2.0985	1.9004	0.0850	0.0310	0.0180	0.0258	-0.1680	0.0262	0.0057	0.1863	0.0008
2.0000	1.3118	0.0059	0.0600	0.0170	0.0350	-0.1720	0.0020	0.0052	0.1429	0.0024
2.0000	1.3218	0.0059	0.0580	0.0220	0.0407	-0.2140	0.0090	0.0049	0.1656	0.0026
2.0000	1.3318	0.0059	0.0610	0.0290	0.0446	-0.2430	0.0130	0.0059	0.1939	0.0027
2.0000	1.3418	0.0059	0.0530	0.0260	0.0324	-0.2720	-0.0120	0.0000	0.2250	0.0027
2.0000	1.3518	0.0059	0.0490	0.0170	0.0352	-0.2930	-0.0160	0.0000	0.2514	0.0026
2.0000	1.3718	0.0059	0.0450	0.0220	0.0354	-0.3140	-0.0140	0.0000	0.3087	0.0021
2.0000	1.3918	0.0059	0.0400	0.0150	0.0336	-0.3180	-0.0101	0.0000	0.3280	0.0016
2.0000	1.4318	0.0059	0.0350	0.0190	0.0386	-0.3110	-0.0130	0.0000	0.3337	0.0015
2.0000	1.4718	0.0059	0.0350	0.0200	0.0377	-0.2900	-0.0170	0.0000	0.3158	0.0017
2.0000	1.5118	0.0059	0.0310	0.0230	0.0000	-0.2820	-0.0190	0.0000	0.2992	0.0010
2.0000	1.5518	0.0059	0.0320	0.0240	0.0000	-0.2720	-0.0100	-0.0017	0.2882	0.0010
2.0000	1.5918	0.0059	0.0290	0.0310	0.0000	-0.2530	-0.0190	-0.0017	0.2709	0.0010
2.0000	1.6318	0.0059	0.0290	0.0330	0.0176	-0.2490	-0.0260	-0.0022	0.2634	0.0012
2.0000	1.6718	0.0059	0.0265	0.0320	0.0180	-0.2450	-0.0310	-0.0029	0.2591	0.0011
2.0000	1.7118	0.0059	0.0245	0.0390	0.0230	-0.2360	-0.0320	-0.0029	0.2483	0.0012
2.0000	1.7518	0.0059	0.0224	0.0070	0.0043	-0.2130	-0.0010	-0.0032	0.1928	0.0006
2.0000	1.7918	0.0059	0.0224	0.0140	0.0088	-0.1890	-0.0010	-0.0025	0.2185	0.0006
2.0000	1.8318	0.0059	0.0200	0.0180	0.0100	-0.1930	-0.0050	-0.0034	0.2093	0.0006
2.0000	1.8718	0.0059	0.0180	0.0010	0.0005	-0.1980	-0.0010	-0.0041	0.1721	0.0004
2.0000	1.8918	0.0059	0.0270	0.0120	0.0079	-0.2030	-0.0090	-0.0046	0.1974	0.0006
2.0000	1.9068	0.0059	0.0390	0.0100	0.0163	-0.1680	-0.0010	-0.0053	0.1925	0.0008
2.0000	1.3118	0.0148	0.0475	0.0215	0.0371	-0.0805	-0.0020	-0.0206	0.0995	0.0024
2.0000	1.3218	0.0148	0.0490	0.0290	0.0328	-0.0960	0.0010	-0.0068	0.1106	0.0026
2.0000	1.3318	0.0148	0.0565	0.0335	0.0304	-0.1205	0.0070	-0.0037	0.1341	0.0029
2.0000	1.3418	0.0148	0.0610	0.0355	0.0311	-0.1650	0.0225	0.0068	0.1733	0.0030
2.0000	1.3518	0.0148	0.0630	0.0295	0.0239	-0.2150	0.0355	0.0184	0.2203	0.0029
2.0000	1.3718	0.0148	0.0460	0.0280	0.0187	-0.3080	0.0640	0.0216	0.3061	0.0024
2.0000	1.3918	0.0148	0.0330	0.0260	0.0145	-0.3240	0.0615	0.0165	0.3327	0.0018

Table B.1 Flow field data for the bend width 0.60m (Q=0.013m³/s, continued)

x (m)	y (m)	z (m)	Urms (m/s)	Vrms (m/s)	Wrms (m/s)	U (m/s)	V (m/s)	W (m/s)	U$_T$(m/s)	Ke (m²/s²)
2.0000	1.4318	0.0148	0.0295	0.0260	0.0135	-0.3300	0.0575	0.0024	0.3400	0.0016
2.0000	1.4718	0.0148	0.0305	0.0290	0.0152	-0.3150	0.0475	-0.0015	0.3232	0.0017
2.0000	1.5118	0.0148	0.0295	0.0315	0.0164	-0.3000	0.0325	-0.0018	0.3057	0.0011
2.0000	1.5518	0.0148	0.0305	0.0325	0.0169	-0.2890	0.0290	-0.0021	0.2945	0.0011
2.0000	1.5918	0.0148	0.0285	0.0335	0.0176	-0.2710	0.0165	-0.0032	0.2768	0.0011
2.0000	1.6318	0.0148	0.0305	0.0327	0.0199	-0.2645	0.0030	-0.0048	0.2684	0.0012
2.0000	1.6718	0.0148	0.0295	0.0320	0.0188	-0.2605	0.0005	-0.0063	0.2637	0.0011
2.0000	1.7118	0.0148	0.0310	0.0269	0.0226	-0.2520	-0.0055	-0.0063	0.2536	0.0012
2.0000	1.7518	0.0148	0.0320	0.0200	0.0119	-0.1355	0.0180	-0.0069	0.2018	0.0006
2.0000	1.7918	0.0148	0.0323	0.0220	0.0139	-0.2220	0.0360	-0.0058	0.2270	0.0006
2.0000	1.8318	0.0148	0.0270	0.0235	0.0136	-0.2135	0.0280	-0.0057	0.2155	0.0006
2.0000	1.8718	0.0148	0.0195	0.0160	0.0080	-0.1115	0.0150	-0.0040	0.1767	0.0005
2.0000	1.8918	0.0148	0.0250	0.0165	0.0082	-0.2105	-0.0010	-0.0042	0.2032	0.0006
2.0000	1.9068	0.0148	0.0320	0.0125	0.0204	-0.1915	0.0035	-0.0058	0.1977	0.0008
2.0000	1.3118	0.0236	0.0350	0.0260	0.0358	0.0110	-0.0060	0.0037	0.0554	0.0025
2.0000	1.3218	0.0236	0.0400	0.0360	0.0357	0.0220	-0.0070	-0.0014	0.0535	0.0027
2.0000	1.3318	0.0236	0.0520	0.0380	0.0515	0.0020	0.0010	0.0020	0.0704	0.0031
2.0000	1.3418	0.0236	0.0690	0.0450	0.0531	-0.0580	0.0330	0.0044	0.1137	0.0034
2.0000	1.3518	0.0236	0.0770	0.0420	0.0571	-0.1370	0.0650	0.0136	0.1794	0.0034
2.0000	1.3718	0.0236	0.0470	0.0340	0.0550	-0.3020	0.1240	0.0241	0.2939	0.0028
2.0000	1.3918	0.0236	0.0260	0.0370	0.0365	-0.3300	0.1220	0.0191	0.3368	0.0022
2.0000	1.4318	0.0236	0.0240	0.0330	0.0426	-0.3490	0.1180	0.0210	0.3479	0.0018
2.0000	1.4718	0.0236	0.0260	0.0380	0.0439	-0.3400	0.1020	0.0136	0.3348	0.0018
2.0000	1.5118	0.0236	0.0280	0.0400	0.0165	-0.3180	0.0740	0.0040	0.3172	0.0013
2.0000	1.5518	0.0236	0.0290	0.0410	0.0245	-0.3060	0.0680	0.0055	0.3059	0.0012
2.0000	1.5918	0.0236	0.0280	0.0360	0.0245	-0.2890	0.0520	0.0055	0.2891	0.0012
2.0000	1.6318	0.0236	0.0320	0.0410	0.0130	-0.2800	0.0320	0.0076	0.2787	0.0013
2.0000	1.6718	0.0236	0.0290	0.0350	0.0195	-0.2760	0.0320	0.0125	0.2726	0.0012
2.0000	1.7118	0.0236	0.0310	0.0390	0.0227	-0.2680	0.0210	-0.0077	0.2626	0.0011
2.0000	1.7518	0.0236	0.0240	0.0330	0.0092	-0.2630	0.0370	-0.0050	0.2234	0.0007
2.0000	1.7918	0.0236	0.0200	0.0300	0.0092	-0.2550	0.0720	-0.0050	0.2388	0.0008
2.0000	1.8318	0.0236	0.0230	0.0290	0.0173	-0.2340	0.0510	-0.0059	0.2238	0.0008
2.0000	1.8718	0.0236	0.0210	0.0310	0.0158	-0.2180	0.0300	-0.0074	0.1921	0.0006
2.0000	1.8918	0.0236	0.0230	0.0210	0.0104	-0.2180	0.0070	-0.0016	0.2100	0.0007
2.0000	1.9068	0.0236	0.0250	0.0150	0.0244	-0.2150	0.0080	-0.0033	0.2075	0.0008
2.0000	1.3118	0.0471	0.0260	0.0110	0.0473	0.0420	-0.0020	0.0038	0.0483	0.0022
2.0000	1.3218	0.0471	0.0310	0.0210	0.0568	0.0490	-0.0050	0.0030	0.0482	0.0024
2.0000	1.3318	0.0471	0.0290	0.0270	0.0299	0.0500	-0.0060	-0.0258	0.0535	0.0030

Table B.1 Flow field data for the bend width 0.60m (Q=0.013m^3/s, continued)

x (m)	y (m)	z (m)	Urms (m/s)	Vrms (m/s)	Wrms (m/s)	U (m/s)	V (m/s)	W (m/s)	U$_T$(m/s)	Ke (m^2/s^2)
2.0000	1.3418	0.0471	0.0610	0.0330	0.0483	0.0090	0.0050	0.0024	0.0762	0.0035
2.0000	1.3518	0.0471	0.0800	0.0360	0.0531	-0.0660	0.0450	0.0074	0.1310	0.0039
2.0000	1.3718	0.0471	0.0660	0.0360	0.0539	-0.2630	0.1200	0.0246	0.2552	0.0041
2.0000	1.3918	0.0471	0.0200	0.0450	0.0318	-0.3250	0.1090	0.0220	0.3220	0.0037
2.0000	1.4318	0.0471	0.0130	0.0420	0.0343	-0.3280	0.1140	0.0155	0.3440	0.0031
2.0000	1.4718	0.0471	0.0140	0.0370	0.0315	-0.3230	0.1230	0.0063	0.3420	0.0026
2.0000	1.5118	0.0471	0.0150	0.0360	0.0000	-0.3150	0.1240	0.0000	0.3307	0.0019
2.0000	1.5518	0.0471	0.0150	0.0310	0.0000	-0.3100	0.1320	0.0000	0.3223	0.0019
2.0000	1.5918	0.0471	0.0160	0.0300	0.0000	-0.2970	0.1260	0.0000	0.3100	0.0017
2.0000	1.6318	0.0471	0.0200	0.0320	0.0146	-0.2800	0.1150	0.0046	0.2979	0.0017
2.0000	1.6718	0.0471	0.0220	0.0360	0.0125	-0.2730	0.1010	0.0004	0.2888	0.0015
2.0000	1.7118	0.0471	0.0160	0.0260	0.0292	-0.2700	0.0990	0.0034	0.2805	0.0011
2.0000	1.7518	0.0471	0.0170	0.0270	0.0157	-0.2670	0.0890	0.0073	0.2620	0.0010
2.0000	1.7918	0.0471	0.0200	0.0270	0.0157	-0.2530	0.0760	0.0073	0.2472	0.0013
2.0000	1.8318	0.0471	0.0240	0.0260	0.0158	-0.2340	0.0580	-0.0030	0.2304	0.0013
2.0000	1.8718	0.0471	0.0210	0.0280	0.0172	-0.2240	0.0460	-0.0020	0.2176	0.0012
2.0000	1.8918	0.0471	0.0190	0.0240	0.0147	-0.2230	0.0340	-0.0010	0.2199	0.0010
2.0000	1.9068	0.0471	0.0230	0.0160	0.0261	-0.2230	0.0160	-0.0020	0.2162	0.0009
2.0000	1.3118	0.0701	0.0490	0.0140	0.0268	0.0480	-0.0020	0.0030	0.0401	0.0020
2.0000	1.3218	0.0701	0.0510	0.0200	0.0385	0.0350	0.0010	0.0040	0.0385	0.0023
2.0000	1.3318	0.0701	0.0420	0.0270	0.0283	0.0200	0.0070	-0.0014	0.0457	0.0030
2.0000	1.3418	0.0701	0.0560	0.0310	0.0473	-0.0090	0.0200	0.0218	0.0744	0.0040
2.0000	1.3518	0.0701	0.0860	0.0380	0.0525	-0.0910	0.0590	0.0263	0.1295	0.0049
2.0000	1.3718	0.0701	0.0738	0.0430	0.0521	-0.2400	0.1150	0.0204	0.2459	0.0058
2.0000	1.3918	0.0701	0.0770	0.0510	0.0414	-0.3090	0.1010	0.0172	0.3114	0.0056
2.0000	1.4318	0.0701	0.0830	0.0430	0.0364	-0.2930	0.1100	0.0110	0.3274	0.0048
2.0000	1.4718	0.0701	0.0710	0.0460	0.0178	-0.3170	0.1080	0.0057	0.3324	0.0041
2.0000	1.5118	0.0701	0.0658	0.0420	0.0154	-0.2990	0.1160	-0.0006	0.3260	0.0027
2.0000	1.5518	0.0701	0.0690	0.0370	0.0319	-0.2890	0.1320	0.0074	0.3191	0.0028
2.0000	1.5918	0.0701	0.0470	0.0310	0.0319	-0.2840	0.1340	0.0074	0.3104	0.0024
2.0000	1.6318	0.0701	0.0410	0.0280	0.0217	-0.2790	0.1310	0.0088	0.2994	0.0025
2.0000	1.6718	0.0701	0.0240	0.0270	0.0158	-0.2750	0.1180	0.0056	0.2907	0.0020
2.0000	1.7118	0.0701	0.0160	0.0260	0.0139	-0.2700	0.1050	0.0012	0.2841	0.0013
2.0000	1.7518	0.0701	0.0160	0.0300	0.0150	-0.2640	0.0730	0.0009	0.2682	0.0012
2.0000	1.7918	0.0701	0.0480	0.0290	0.0150	-0.2260	0.0280	0.0009	0.2314	0.0020
2.0000	1.8318	0.0701	0.0500	0.0290	0.0197	-0.2130	0.0130	0.0009	0.2167	0.0021
2.0000	1.8718	0.0701	0.0430	0.0230	0.0190	-0.2190	0.0150	-0.0001	0.2124	0.0020
2.0000	1.8918	0.0701	0.0430	0.0210	0.0215	-0.2180	0.0160	-0.0010	0.2057	0.0016

133

Table B.1 Flow field data for the bend width 0.60m (Q=0.013m³/s, continued)

x (m)	y (m)	z (m)	Urms (m/s)	Vrms (m/s)	Wrms (m/s)	U (m/s)	V (m/s)	W (m/s)	U$_T$(m/s)	Ke (m²/s²)
2.0000	1.9068	0.0701	0.0220	0.0140	0.0229	-0.1922	0.0100	-0.0020	0.1972	0.0012
2.0000	1.3118	0.0823	0.0460	0.0150	0.0318	0.0350	-0.0030	0.0037	0.0333	0.0020
2.0000	1.3218	0.0823	0.0350	0.0200	0.0397	0.0140	0.0010	0.0000	0.0314	0.0023
2.0000	1.3318	0.0823	0.0360	0.0250	0.0331	-0.0050	0.0060	0.0000	0.0435	0.0032
2.0000	1.3418	0.0823	0.0680	0.0350	0.0500	-0.0500	0.0310	0.0000	0.0796	0.0044
2.0000	1.3518	0.0823	0.0980	0.0400	0.0500	-0.1250	0.0690	0.0000	0.1353	0.0054
2.0000	1.3718	0.0823	0.1240	0.0480	0.0469	-0.2330	0.1020	0.0000	0.2439	0.0064
2.0000	1.3918	0.0823	0.1150	0.0462	0.0317	-0.3150	0.1000	0.0000	0.3065	0.0062
2.0000	1.4318	0.0823	0.1064	0.0457	0.0406	-0.3010	0.1010	0.0000	0.3215	0.0053
2.0000	1.4718	0.0823	0.1064	0.0355	0.0363	-0.3000	0.1030	0.0000	0.3281	0.0045
2.0000	1.5118	0.0823	0.0783	0.0158	0.0000	-0.3000	0.1080	0.0000	0.3231	0.0029
2.0000	1.5518	0.0823	0.0950	0.0136	0.0000	-0.2850	0.1200	0.0000	0.3164	0.0031
2.0000	1.5918	0.0823	0.0830	0.0126	0.0000	-0.2690	0.1250	0.0000	0.3084	0.0027
2.0000	1.6318	0.0823	0.0830	0.0320	0.0253	-0.2530	0.1190	0.0000	0.2978	0.0028
2.0000	1.6718	0.0823	0.0740	0.0300	0.0197	-0.2500	0.1130	0.0000	0.2895	0.0022
2.0000	1.7118	0.0823	0.0370	0.0300	0.0139	-0.2630	0.0850	0.0000	0.2833	0.0013
2.0000	1.7518	0.0823	0.0380	0.0310	0.0089	-0.2580	0.0590	0.0000	0.2668	0.0013
2.0000	1.7918	0.0823	0.0780	0.0260	0.0089	-0.1990	0.0100	0.0000	0.2254	0.0022
2.0000	1.8318	0.0823	0.0730	0.0250	0.0170	-0.1940	-0.0120	0.0000	0.2115	0.0023
2.0000	1.8718	0.0823	0.0760	0.0210	0.0176	-0.1930	-0.0150	0.0000	0.2078	0.0022
2.0000	1.8918	0.0823	0.0770	0.0190	0.0203	-0.1860	0.0000	0.0000	0.1971	0.0018
2.0000	1.9068	0.0823	0.0210	0.0150	0.0245	-0.1521	0.0020	-0.0020	0.1880	0.0013
1.9600	1.3118	0.0059	0.0200	0.0060	0.0019	-0.0020	0.0000	0.0009	0.0788	0.0016
1.9600	1.3218	0.0059	0.0700	0.0130	0.0020	-0.1930	0.0010	0.0017	0.1241	0.0020
1.9600	1.3318	0.0059	0.0650	0.0070	0.0024	-0.2220	0.0010	0.0022	0.1670	0.0025
1.9600	1.3418	0.0059	0.0610	0.0140	0.0159	-0.2410	0.0040	0.0026	0.1950	0.0028
1.9600	1.3518	0.0059	0.0660	0.0180	0.0287	-0.2550	0.0060	0.0068	0.2147	0.0030
1.9600	1.3718	0.0059	0.0570	0.0210	0.0284	-0.2920	0.0050	0.0089	0.2746	0.0028
1.9600	1.3918	0.0059	0.0440	0.0210	0.0275	-0.3160	0.0010	0.0074	0.3212	0.0021
1.9600	1.4318	0.0059	0.0390	0.0220	0.0297	-0.3120	-0.0050	0.0085	0.3332	0.0017
1.9600	1.4718	0.0059	0.0370	0.0210	0.0113	-0.2990	-0.0070	0.0011	0.3205	0.0040
1.9600	1.5118	0.0059	0.0350	0.0270	0.0000	-0.2790	-0.0180	-0.0072	0.3036	0.0014
1.9600	1.5518	0.0059	0.0320	0.0140	0.0000	-0.2850	-0.0060	0.0000	0.3026	0.0009
1.9600	1.5918	0.0059	0.0330	0.0220	0.0000	-0.2670	-0.0160	0.0000	0.2870	0.0010
1.9600	1.6318	0.0059	0.0370	0.0300	0.0163	-0.2560	-0.0240	-0.0023	0.2764	0.0012
1.9600	1.6718	0.0059	0.0320	0.0320	0.0182	-0.2580	-0.0330	-0.0030	0.2749	0.0012
1.9600	1.7118	0.0059	0.0310	0.0270	0.0157	-0.2550	-0.0180	-0.0030	0.2653	0.0011
1.9600	1.7518	0.0059	0.0300	0.0140	0.0086	-0.2105	-0.0040	-0.0033	0.2027	0.0007

Table B.1 Flow field data for the bend width 0.60m (Q=0.013m³/s, continued)

x (m)	y (m)	z (m)	Urms (m/s)	Vrms (m/s)	Wrms (m/s)	U (m/s)	V (m/s)	W (m/s)	U$_T$(m/s)	Ke (m²/s²)
1.9600	1.7918	0.0059	0.0300	0.0170	0.0108	-0.1960	-0.0030	-0.0027	0.2261	0.0007
1.9600	1.8318	0.0059	0.0300	0.0020	0.0011	-0.2060	0.0010	0.0034	0.1917	0.0006
1.9600	1.8718	0.0059	0.0310	0.0120	0.0064	-0.2160	-0.0050	0.0012	0.2213	0.0006
1.9600	1.8918	0.0059	0.0220	0.0170	0.0112	-0.2310	-0.0180	-0.0046	0.2274	0.0006
1.9600	1.9068	0.0059	0.0310	0.0140	0.0228	-0.2050	-0.0100	-0.0056	0.2199	0.0008
1.9600	1.3118	0.0148	0.0380	0.0235	0.0384	-0.0235	-0.0010	0.0096	0.0560	0.0018
1.9600	1.3218	0.0148	0.0645	0.0320	0.0350	-0.1045	0.0010	0.0015	0.0893	0.0023
1.9600	1.3318	0.0148	0.0660	0.0335	0.0296	-0.1195	0.0045	-0.0001	0.1197	0.0028
1.9600	1.3418	0.0148	0.0670	0.0350	0.0301	-0.1470	0.0135	0.0058	0.1484	0.0032
1.9600	1.3518	0.0148	0.0740	0.0350	0.0292	-0.1810	0.0225	0.0151	0.1818	0.0033
1.9600	1.3718	0.0148	0.0665	0.0310	0.0230	-0.2675	0.0455	0.0212	0.2632	0.0031
1.9600	1.3918	0.0148	0.0425	0.0275	0.0167	-0.3235	0.0595	0.0184	0.3229	0.0023
1.9600	1.4318	0.0148	0.0325	0.0290	0.0150	-0.3330	0.0510	0.0048	0.3399	0.0017
1.9600	1.4718	0.0148	0.0320	0.0295	0.0156	-0.3215	0.0405	-0.0017	0.3277	0.0036
1.9600	1.5118	0.0148	0.0315	0.0330	0.0173	-0.3050	0.0230	-0.0018	0.3107	0.0013
1.9600	1.5518	0.0148	0.0310	0.0270	0.0141	-0.3065	0.0250	-0.0020	0.3093	0.0010
1.9600	1.5918	0.0148	0.0330	0.0315	0.0167	-0.2905	0.0085	-0.0032	0.2939	0.0010
1.9600	1.6318	0.0148	0.0330	0.0330	0.0180	-0.2795	-0.0005	-0.0051	0.2828	0.0012
1.9600	1.6718	0.0148	0.0315	0.0340	0.0193	-0.2790	-0.0090	-0.0067	0.2807	0.0012
1.9600	1.7118	0.0148	0.0310	0.0305	0.0176	-0.2725	-0.0040	-0.0067	0.2714	0.0011
1.9600	1.7518	0.0148	0.0265	0.0225	0.0134	-0.1460	0.0125	-0.0070	0.2133	0.0007
1.9600	1.7918	0.0148	0.0324	0.0225	0.0142	-0.2320	0.0275	-0.0060	0.2356	0.0007
1.9600	1.8318	0.0148	0.0290	0.0160	0.0094	-0.1340	0.0275	0.0058	0.1994	0.0006
1.9600	1.8718	0.0148	0.0260	0.0205	0.0103	-0.2260	0.0130	0.0056	0.2254	0.0006
1.9600	1.8918	0.0148	0.0215	0.0205	0.0101	-0.2345	-0.0025	-0.0040	0.2309	0.0007
1.9600	1.9068	0.0148	0.0275	0.0175	0.0285	-0.2190	-0.0030	-0.0066	0.2231	0.0009
1.9600	1.3118	0.0236	0.0560	0.0410	0.0020	-0.0450	-0.0020	0.0012	0.0405	0.0021
1.9600	1.3218	0.0236	0.0590	0.0510	0.0021	-0.0160	0.0010	0.0016	0.0492	0.0025
1.9600	1.3318	0.0236	0.0670	0.0600	0.0021	-0.0170	0.0080	0.0019	0.0641	0.0030
1.9600	1.3418	0.0236	0.0730	0.0560	0.0176	-0.0530	0.0230	0.0023	0.0921	0.0034
1.9600	1.3518	0.0236	0.0820	0.0520	0.0478	-0.1070	0.0390	0.0049	0.1367	0.0036
1.9600	1.3718	0.0236	0.0760	0.0410	0.0580	-0.2430	0.0860	0.0071	0.2364	0.0034
1.9600	1.3918	0.0236	0.0410	0.0340	0.0519	-0.3310	0.1180	0.0188	0.3137	0.0027
1.9600	1.4318	0.0236	0.0260	0.0360	0.0244	-0.3540	0.1070	0.0170	0.3476	0.0018
1.9600	1.4718	0.0236	0.0270	0.0380	0.0301	-0.3440	0.0880	0.0068	0.3385	0.0029
1.9600	1.5118	0.0236	0.0280	0.0390	0.0254	-0.3310	0.0640	0.0066	0.3229	0.0014
1.9600	1.5518	0.0236	0.0300	0.0400	0.0198	-0.3280	0.0560	-0.0043	0.3195	0.0011
1.9600	1.5918	0.0236	0.0330	0.0410	0.0177	-0.3140	0.0330	-0.0059	0.3057	0.0011

Table B.1 Flow field data for the bend width 0.60m (Q=0.013m³/s, continued)

x (m)	y (m)	z (m)	Urms (m/s)	Vrms (m/s)	Wrms (m/s)	U (m/s)	V (m/s)	W (m/s)	U_T(m/s)	Ke (m²/s²)
1.9600	1.6318	0.0236	0.0290	0.0360	0.0199	-0.3030	0.0230	-0.0063	0.2942	0.0012
1.9600	1.6718	0.0236	0.0310	0.0360	0.0207	-0.3000	0.0150	-0.0083	0.2897	0.0012
1.9600	1.7118	0.0236	0.0310	0.0340	0.0198	-0.2900	0.0100	-0.0082	0.2797	0.0011
1.9600	1.7518	0.0236	0.0230	0.0310	0.0183	-0.2860	0.0290	-0.0083	0.2371	0.0008
1.9600	1.7918	0.0236	0.0200	0.0280	0.0169	-0.2680	0.0580	-0.0073	0.2489	0.0008
1.9600	1.8318	0.0236	0.0200	0.0300	0.0181	-0.2560	0.0540	0.0058	0.2176	0.0007
1.9600	1.8718	0.0236	0.0210	0.0290	0.0149	-0.2360	0.0310	0.0078	0.2307	0.0007
1.9600	1.8918	0.0236	0.0210	0.0240	0.0119	-0.2380	0.0130	-0.0013	0.2341	0.0008
1.9600	1.9068	0.0236	0.0240	0.0210	0.0342	-0.2330	0.0040	-0.0042	0.2289	0.0009
1.9600	1.3118	0.0471	0.0360	0.0240	0.0019	0.0500	0.0020	0.0010	0.0495	0.0014
1.9600	1.3218	0.0471	0.0310	0.0230	0.0020	0.0470	-0.0080	0.0017	0.0514	0.0015
1.9600	1.3318	0.0471	0.0280	0.0220	0.0024	0.0640	-0.0120	0.0012	0.0539	0.0018
1.9600	1.3418	0.0471	0.0280	0.0220	0.0060	0.0560	-0.0120	0.0017	0.0585	0.0023
1.9600	1.3518	0.0471	0.0470	0.0260	0.0282	0.0470	0.0010	-0.0020	0.0777	0.0030
1.9600	1.3718	0.0471	0.0860	0.0350	0.0569	-0.0830	0.0410	0.0123	0.1637	0.0038
1.9600	1.3918	0.0471	0.0590	0.0400	0.0647	-0.2860	0.1030	0.0237	0.2643	0.0039
1.9600	1.4318	0.0471	0.0160	0.0410	0.0225	-0.3430	0.1230	0.0164	0.3466	0.0027
1.9600	1.4718	0.0471	0.0130	0.0390	0.0248	-0.3370	0.1210	0.0119	0.3506	0.0024
1.9600	1.5118	0.0471	0.0150	0.0340	0.0276	-0.3240	0.1230	0.0133	0.3407	0.0016
1.9600	1.5518	0.0471	0.0170	0.0340	0.0110	-0.3260	0.1260	-0.0097	0.3335	0.0013
1.9600	1.5918	0.0471	0.0200	0.0340	0.0000	-0.3190	0.1210	0.0000	0.3255	0.0013
1.9600	1.6318	0.0471	0.0240	0.0370	0.0244	-0.3090	0.1080	-0.0082	0.3149	0.0013
1.9600	1.6718	0.0471	0.0190	0.0320	0.0207	-0.3000	0.1000	-0.0135	0.3048	0.0013
1.9600	1.7118	0.0471	0.0200	0.0310	0.0190	-0.2870	0.0880	-0.0126	0.2956	0.0011
1.9600	1.7518	0.0471	0.0130	0.0240	0.0130	-0.2850	0.0830	-0.0081	0.2763	0.0010
1.9600	1.7918	0.0471	0.0160	0.0250	0.0130	-0.2690	0.0700	-0.0060	0.2612	0.0010
1.9600	1.8318	0.0471	0.0200	0.0250	0.0152	-0.2520	0.0580	-0.0007	0.2421	0.0011
1.9600	1.8718	0.0471	0.0200	0.0280	0.0173	-0.2410	0.0490	0.0099	0.2380	0.0010
1.9600	1.8918	0.0471	0.0200	0.0270	0.0165	-0.2420	0.0310	0.0141	0.2363	0.0010
1.9600	1.9068	0.0471	0.0200	0.0200	0.0326	-0.2360	0.0180	0.0164	0.2304	0.0010
1.9600	1.3118	0.0701	0.0370	0.0160	0.0020	0.0610	0.0030	0.0024	0.0593	0.0014
1.9600	1.3218	0.0701	0.0430	0.0210	0.0032	0.0660	0.0030	0.0017	0.0560	0.0015
1.9600	1.3318	0.0701	0.0450	0.0250	0.0074	0.0550	0.0020	-0.0010	0.0475	0.0018
1.9600	1.3418	0.0701	0.0490	0.0340	0.0427	0.0310	0.0050	0.0017	0.0414	0.0024
1.9600	1.3518	0.0701	0.0540	0.0320	0.0419	-0.0050	0.0080	-0.0003	0.0511	0.0031
1.9600	1.3718	0.0701	0.0850	0.0380	0.0545	-0.1060	0.0460	0.0187	0.1263	0.0044
1.9600	1.3918	0.0701	0.0830	0.0400	0.0552	-0.2660	0.1060	0.0233	0.2352	0.0049
1.9600	1.4318	0.0701	0.0610	0.0490	0.0223	-0.3350	0.1130	0.0086	0.3401	0.0037

Table B.1 Flow field data for the bend width 0.60m (Q=0.013m³/s, continued)

x (m)	y (m)	z (m)	Urms (m/s)	Vrms (m/s)	Wrms (m/s)	U (m/s)	V (m/s)	W (m/s)	U$_T$(m/s)	Ke (m²/s²)
1.9600	1.4718	0.0701	0.0390	0.0510	0.0163	-0.3340	0.1090	0.0101	0.3482	0.0029
1.9600	1.5118	0.0701	0.0480	0.0390	0.0190	-0.3180	0.1280	0.0077	0.3413	0.0019
1.9600	1.5518	0.0701	0.0450	0.0370	0.0157	-0.2950	0.1300	0.0055	0.3281	0.0015
1.9600	1.5918	0.0701	0.0462	0.0330	0.0000	-0.3050	0.1340	0.0000	0.3253	0.0014
1.9600	1.6318	0.0701	0.0480	0.0270	0.0159	-0.2990	0.1350	-0.0026	0.3175	0.0015
1.9600	1.6718	0.0701	0.0450	0.0290	0.0160	-0.2890	0.1160	-0.0142	0.3048	0.0014
1.9600	1.7118	0.0701	0.0260	0.0250	0.0138	-0.2880	0.1070	-0.0132	0.2983	0.0013
1.9600	1.7518	0.0701	0.0200	0.0340	0.0194	-0.2810	0.0730	-0.0037	0.2798	0.0014
1.9600	1.7918	0.0701	0.0361	0.0310	0.0178	-0.2440	0.0270	-0.0022	0.2465	0.0013
1.9600	1.8318	0.0701	0.0400	0.0270	0.0183	-0.2340	0.0070	-0.0061	0.2341	0.0015
1.9600	1.8718	0.0701	0.0429	0.0260	0.0213	-0.2240	0.0130	0.0019	0.2273	0.0015
1.9600	1.8918	0.0701	0.0400	0.0210	0.0217	-0.2310	0.0070	0.0110	0.2196	0.0014
1.9600	1.9068	0.0701	0.0415	0.0190	0.0311	-0.1922	0.0060	0.0203	0.2058	0.0013
1.9600	1.3118	0.0823	0.0550	0.0200	0.0021	0.0710	-0.0030	0.0022	0.0579	0.0015
1.9600	1.3218	0.0823	0.0470	0.0220	0.0020	0.0590	-0.0020	0.0022	0.0516	0.0016
1.9600	1.3318	0.0823	0.0560	0.0310	0.0124	-0.0010	-0.0080	0.0021	0.0413	0.0019
1.9600	1.3418	0.0823	0.0450	0.0190	0.0324	0.0500	0.0080	-0.0003	0.0369	0.0024
1.9600	1.3518	0.0823	0.0450	0.0290	0.0496	-0.0190	-0.0090	0.0074	0.0467	0.0031
1.9600	1.3718	0.0823	0.0680	0.0330	0.0497	-0.0670	0.0060	0.0136	0.1173	0.0045
1.9600	1.3918	0.0823	0.0920	0.0370	0.0424	-0.1670	0.0420	0.0133	0.2252	0.0052
1.9600	1.4318	0.0823	0.0770	0.0358	0.0221	-0.3280	0.1010	0.0050	0.3364	0.0040
1.9600	1.4718	0.0823	0.0772	0.0347	0.0170	-0.3240	0.1150	0.0084	0.3462	0.0031
1.9600	1.5118	0.0823	0.0509	0.0253	0.0123	-0.3280	0.1030	0.0069	0.3401	0.0019
1.9600	1.5518	0.0823	0.0319	0.0276	0.0139	-0.2900	0.1260	0.0059	0.3251	0.0015
1.9600	1.5918	0.0823	0.0430	0.0156	0.0000	-0.2900	0.1240	0.0000	0.3233	0.0014
1.9600	1.6318	0.0823	0.0388	0.0248	0.0220	-0.2940	0.1100	-0.0023	0.3160	0.0015
1.9600	1.6718	0.0823	0.0399	0.0300	0.0156	-0.2720	0.1030	-0.0094	0.3030	0.0015
1.9600	1.7118	0.0823	0.0410	0.0320	0.0167	-0.2800	0.0880	-0.0089	0.2973	0.0014
1.9600	1.7518	0.0823	0.0530	0.0330	0.0191	-0.2620	0.0290	-0.0029	0.2776	0.0015
1.9600	1.7918	0.0823	0.0390	0.0280	0.0161	-0.2170	0.0000	-0.0018	0.2407	0.0014
1.9600	1.8318	0.0823	0.0540	0.0230	0.0157	-0.2230	-0.0210	-0.0044	0.2297	0.0016
1.9600	1.8718	0.0823	0.0560	0.0200	0.0170	-0.2190	-0.0160	-0.0018	0.2226	0.0016
1.9600	1.8918	0.0823	0.0490	0.0200	0.0218	-0.2230	-0.0090	0.0024	0.2119	0.0015
1.9600	1.9068	0.0823	0.0440	0.0150	0.0245	-0.1522	-0.0080	0.0100	0.1963	0.0014
1.9200	1.3118	0.0059	0.0640	0.0250	0.0102	-0.0660	-0.0060	0.0065	0.0811	0.0025
1.9200	1.3218	0.0059	0.0690	0.0190	0.0041	-0.1230	-0.0020	0.0025	0.1024	0.0026
1.9200	1.3318	0.0059	0.0690	0.0180	0.0083	-0.1570	-0.0020	0.0047	0.1281	0.0028
1.9200	1.3418	0.0059	0.0760	0.0180	0.0156	-0.1740	0.0010	-0.0032	0.1507	0.0031

Table B.1 Flow field data for the bend width 0.60m (Q=0.013m^3/s, continued)

x (m)	y (m)	z (m)	Urms (m/s)	Vrms (m/s)	Wrms (m/s)	U (m/s)	V (m/s)	W (m/s)	U$_T$(m/s)	Ke (m^2/s^2)
1.9200	1.3518	0.0059	0.0660	0.0210	0.0238	-0.2110	0.0000	0.0002	0.1689	0.0033
1.9200	1.3718	0.0059	0.0610	0.0240	0.0333	-0.2720	0.0030	0.0060	0.2361	0.0033
1.9200	1.3918	0.0059	0.0520	0.0220	0.0346	-0.3010	-0.0030	0.0057	0.2934	0.0027
1.9200	1.4318	0.0059	0.0390	0.0240	0.0265	-0.3160	-0.0100	0.0014	0.3358	0.0018
1.9200	1.4718	0.0059	0.0360	0.0260	0.0104	-0.3050	-0.0190	0.0045	0.3284	0.0037
1.9200	1.5118	0.0059	0.0330	0.0300	0.0000	-0.2920	-0.0380	0.0000	0.3135	0.0014
1.9200	1.5518	0.0059	0.0350	0.0270	0.0000	-0.2870	-0.0430	0.0000	0.3083	0.0011
1.9200	1.5918	0.0059	0.0300	0.0260	0.0000	-0.2760	-0.0440	0.0000	0.2980	0.0010
1.9200	1.6318	0.0059	0.0310	0.0300	0.0165	-0.2640	-0.0560	-0.0023	0.2831	0.0011
1.9200	1.6718	0.0059	0.0410	0.0280	0.0163	-0.2470	-0.0510	-0.0031	0.2745	0.0013
1.9200	1.7118	0.0059	0.0547	0.0290	0.0176	-0.2465	-0.0470	-0.0030	0.2686	0.0015
1.9200	1.7518	0.0059	0.0350	0.0200	0.0125	-0.2460	-0.0130	-0.0032	0.2622	0.0010
1.9200	1.7918	0.0059	0.0260	0.0280	0.0182	-0.2540	0.0080	-0.0028	0.2654	0.0008
1.9200	1.8318	0.0059	0.0260	0.0310	0.0178	-0.2300	-0.0010	0.0036	0.2454	0.0009
1.9200	1.8718	0.0059	0.0220	0.0200	0.0109	-0.2360	-0.0170	0.0015	0.2394	0.0006
1.9200	1.8918	0.0059	0.0210	0.0180	0.0121	-0.2420	-0.0240	-0.0044	0.2406	0.0006
1.9200	1.9068	0.0059	0.0250	0.0160	0.0261	-0.2260	-0.0130	-0.0062	0.2383	0.0007
1.9200	1.3118	0.0148	0.0590	0.0315	0.0513	-0.0575	-0.0030	0.0046	0.0672	0.0025
1.9200	1.3218	0.0148	0.0605	0.0325	0.0353	-0.0860	-0.0045	-0.0029	0.0827	0.0027
1.9200	1.3318	0.0148	0.0605	0.0340	0.0298	-0.1020	-0.0005	-0.0021	0.1015	0.0030
1.9200	1.3418	0.0148	0.0760	0.0350	0.0295	-0.1235	0.0005	0.0046	0.1202	0.0033
1.9200	1.3518	0.0148	0.0700	0.0375	0.0308	-0.1340	0.0045	0.0137	0.1408	0.0036
1.9200	1.3718	0.0148	0.0695	0.0380	0.0288	-0.2285	0.0220	0.0201	0.2193	0.0035
1.9200	1.3918	0.0148	0.0530	0.0300	0.0193	-0.2950	0.0415	0.0188	0.2879	0.0029
1.9200	1.4318	0.0148	0.0345	0.0315	0.0164	-0.3395	0.0395	0.0064	0.3414	0.0018
1.9200	1.4718	0.0148	0.0320	0.0320	0.0170	-0.3300	0.0275	-0.0016	0.3351	0.0034
1.9200	1.5118	0.0148	0.0330	0.0355	0.0188	-0.3150	0.0055	-0.0019	0.3198	0.0014
1.9200	1.5518	0.0148	0.0335	0.0330	0.0174	-0.3105	0.0010	-0.0019	0.3148	0.0011
1.9200	1.5918	0.0148	0.0300	0.0315	0.0168	-0.3005	-0.0065	-0.0030	0.3043	0.0010
1.9200	1.6318	0.0148	0.0305	0.0315	0.0173	-0.2830	-0.0230	-0.0051	0.2886	0.0011
1.9200	1.6718	0.0148	0.0345	0.0315	0.0181	-0.2760	-0.0190	-0.0070	0.2807	0.0013
1.9200	1.7118	0.0148	0.0347	0.0305	0.0180	-0.2685	-0.0200	-0.0067	0.2744	0.0015
1.9200	1.7518	0.0148	0.0330	0.0255	0.0153	-0.2660	-0.0080	-0.0070	0.2676	0.0010
1.9200	1.7918	0.0148	0.0225	0.0270	0.0170	-0.2680	0.0320	-0.0062	0.2697	0.0008
1.9200	1.8318	0.0148	0.0235	0.0300	0.0179	-0.2470	0.0230	0.0058	0.2497	0.0009
1.9200	1.8718	0.0148	0.0230	0.0240	0.0122	-0.2390	0.0045	0.0059	0.2414	0.0007
1.9200	1.8918	0.0148	0.0215	0.0215	0.0106	-0.2425	-0.0090	-0.0035	0.2427	0.0007
1.9200	1.9068	0.0148	0.0235	0.0170	0.0277	-0.2395	-0.0080	-0.0076	0.2408	0.0008

Table B.1 Flow field data for the bend width 0.60m (Q=0.013m^3/s, continued)

x (m)	y (m)	z (m)	Urms (m/s)	Vrms (m/s)	Wrms (m/s)	U (m/s)	V (m/s)	W (m/s)	U$_T$(m/s)	Ke (m^2/s^2)
1.9200	1.3118	0.0236	0.0540	0.0380	0.0023	-0.0490	0.0000	0.0010	0.0531	0.0024
1.9200	1.3218	0.0236	0.0520	0.0460	0.0025	-0.0490	-0.0070	0.0016	0.0588	0.0026
1.9200	1.3318	0.0236	0.0520	0.0500	0.0034	-0.0470	0.0010	0.0022	0.0691	0.0030
1.9200	1.3418	0.0236	0.0760	0.0520	0.0217	-0.0730	0.0000	-0.0015	0.0824	0.0035
1.9200	1.3518	0.0236	0.0740	0.0540	0.0553	-0.0570	0.0090	0.0093	0.1050	0.0038
1.9200	1.3718	0.0236	0.0780	0.0520	0.0603	-0.1850	0.0410	0.0095	0.1850	0.0038
1.9200	1.3918	0.0236	0.0540	0.0380	0.0504	-0.2890	0.0860	0.0140	0.2662	0.0033
1.9200	1.4318	0.0236	0.0300	0.0390	0.0253	-0.3630	0.0890	0.0100	0.3447	0.0021
1.9200	1.4718	0.0236	0.0280	0.0380	0.0267	-0.3550	0.0740	-0.0018	0.3450	0.0028
1.9200	1.5118	0.0236	0.0330	0.0410	0.0217	-0.3380	0.0490	-0.0035	0.3311	0.0014
1.9200	1.5518	0.0236	0.0320	0.0390	0.0222	-0.3340	0.0450	-0.0037	0.3257	0.0012
1.9200	1.5918	0.0236	0.0300	0.0370	0.0145	-0.3250	0.0310	-0.0017	0.3149	0.0011
1.9200	1.6318	0.0236	0.0300	0.0330	0.0184	-0.3020	0.0100	-0.0063	0.2988	0.0011
1.9200	1.6718	0.0236	0.0280	0.0350	0.0204	-0.3050	0.0130	-0.0087	0.2916	0.0012
1.9200	1.7118	0.0236	0.0280	0.0320	0.0190	-0.2960	0.0070	-0.0082	0.2846	0.0014
1.9200	1.7518	0.0236	0.0310	0.0310	0.0185	-0.2860	-0.0030	-0.0084	0.2763	0.0010
1.9200	1.7918	0.0236	0.0190	0.0260	0.0156	-0.2820	0.0560	-0.0074	0.2745	0.0008
1.9200	1.8318	0.0236	0.0210	0.0290	0.0177	-0.2640	0.0470	0.0056	0.2557	0.0009
1.9200	1.8718	0.0236	0.0240	0.0280	0.0146	-0.2420	0.0260	0.0080	0.2453	0.0007
1.9200	1.8918	0.0236	0.0220	0.0250	0.0124	-0.2430	0.0060	-0.0007	0.2458	0.0007
1.9200	1.9068	0.0236	0.0220	0.0180	0.0293	-0.2530	-0.0030	-0.0054	0.2444	0.0008
1.9200	1.3118	0.0471	0.0400	0.0240	0.0030	0.0200	0.0050	0.0028	0.0409	0.0016
1.9200	1.3218	0.0471	0.0310	0.0220	0.0067	0.0310	-0.0070	0.0014	0.0448	0.0018
1.9200	1.3318	0.0471	0.0360	0.0350	0.0529	0.0570	-0.0050	-0.0043	0.0529	0.0022
1.9200	1.3418	0.0471	0.0350	0.0300	0.0453	0.0810	-0.0090	-0.0079	0.0550	0.0028
1.9200	1.3518	0.0471	0.0680	0.0390	0.0398	-0.0020	0.0120	-0.0067	0.0583	0.0033
1.9200	1.3718	0.0471	0.0680	0.0400	0.0484	-0.0210	0.0100	0.0088	0.1056	0.0041
1.9200	1.3918	0.0471	0.0930	0.0380	0.0628	-0.1540	0.0450	0.0184	0.1971	0.0043
1.9200	1.4318	0.0471	0.0240	0.0340	0.0266	-0.3430	0.1170	0.0121	0.3343	0.0030
1.9200	1.4718	0.0471	0.0180	0.0330	0.0171	-0.3520	0.1230	0.0001	0.3553	0.0022
1.9200	1.5118	0.0471	0.0160	0.0330	0.0234	-0.3420	0.1200	0.0032	0.3486	0.0015
1.9200	1.5518	0.0471	0.0160	0.0290	0.0183	-0.3390	0.1310	-0.0086	0.3422	0.0013
1.9200	1.5918	0.0471	0.0170	0.0310	0.0206	-0.3320	0.1210	-0.0017	0.3306	0.0011
1.9200	1.6318	0.0471	0.0180	0.0320	0.0206	-0.3210	0.1110	-0.0072	0.3151	0.0011
1.9200	1.6718	0.0471	0.0210	0.0290	0.0185	-0.3040	0.0920	-0.0137	0.3082	0.0012
1.9200	1.7118	0.0471	0.0200	0.0310	0.0181	-0.3020	0.0870	-0.0120	0.3009	0.0014
1.9200	1.7518	0.0471	0.0160	0.0240	0.0131	-0.2870	0.0760	-0.0092	0.2895	0.0010
1.9200	1.7918	0.0471	0.0200	0.0290	0.0151	-0.2800	0.0610	-0.0061	0.2749	0.0010

Table B.1 Flow field data for the bend width 0.60m (Q=0.013m³/s, continued)

x (m)	y (m)	z (m)	Urms (m/s)	Vrms (m/s)	Wrms (m/s)	U (m/s)	V (m/s)	W (m/s)	U$_T$(m/s)	Ke (m²/s²)
1.9200	1.8318	0.0471	0.0210	0.0280	0.0172	-0.2660	0.0630	-0.0010	0.2571	0.0010
1.9200	1.8718	0.0471	0.0170	0.0260	0.0162	-0.2600	0.0450	0.0095	0.2497	0.0010
1.9200	1.8918	0.0471	0.0190	0.0240	0.0148	-0.2570	0.0270	0.0142	0.2486	0.0010
1.9200	1.9068	0.0471	0.0220	0.0210	0.0343	-0.2520	0.0120	0.0160	0.2430	0.0011
1.9200	1.3118	0.0701	0.0340	0.0190	0.0189	0.0580	0.0030	0.0123	0.0620	0.0013
1.9200	1.3218	0.0701	0.0360	0.0210	0.0308	0.0800	0.0070	0.0026	0.0645	0.0015
1.9200	1.3318	0.0701	0.0390	0.0230	0.0486	0.0670	0.0040	-0.0091	0.0635	0.0018
1.9200	1.3418	0.0701	0.0400	0.0280	0.0355	0.0660	0.0020	-0.0186	0.0558	0.0023
1.9200	1.3518	0.0701	0.0490	0.0240	0.0392	0.0450	0.0070	-0.0016	0.0497	0.0030
1.9200	1.3718	0.0701	0.0690	0.0400	0.0455	-0.0410	0.0080	0.0120	0.0829	0.0044
1.9200	1.3918	0.0701	0.0820	0.0380	0.0593	-0.1620	0.0480	0.0213	0.1759	0.0054
1.9200	1.4318	0.0701	0.0776	0.0430	0.0342	-0.3430	0.1180	0.0019	0.3331	0.0040
1.9200	1.4718	0.0701	0.0710	0.0370	0.0194	-0.3340	0.1280	0.0000	0.3523	0.0021
1.9200	1.5118	0.0701	0.0600	0.0360	0.0182	-0.3320	0.1260	-0.0022	0.3469	0.0015
1.9200	1.5518	0.0701	0.0533	0.0340	0.0133	-0.3140	0.1310	-0.0046	0.3384	0.0013
1.9200	1.5918	0.0701	0.0347	0.0310	0.0101	-0.2940	0.1290	-0.0056	0.3249	0.0012
1.9200	1.6318	0.0701	0.0375	0.0280	0.0168	-0.2880	0.1230	-0.0004	0.3070	0.0012
1.9200	1.6718	0.0701	0.0429	0.0280	0.0152	-0.2980	0.1120	-0.0118	0.3049	0.0012
1.9200	1.7118	0.0701	0.0340	0.0240	0.0131	-0.2950	0.0840	-0.0126	0.3009	0.0017
1.9200	1.7518	0.0701	0.0170	0.0270	0.0151	-0.2900	0.0650	-0.0070	0.2882	0.0012
1.9200	1.7918	0.0701	0.0375	0.0300	0.0173	-0.2560	0.0240	-0.0035	0.2621	0.0012
1.9200	1.8318	0.0701	0.0366	0.0270	0.0184	-0.2420	0.0010	-0.0060	0.2391	0.0013
1.9200	1.8718	0.0701	0.0372	0.0260	0.0214	-0.2400	0.0040	0.0028	0.2338	0.0013
1.9200	1.8918	0.0701	0.0410	0.0220	0.0233	-0.2500	0.0070	0.0112	0.2266	0.0014
1.9200	1.9068	0.0701	0.0390	0.0170	0.0278	-0.1925	0.0020	0.0201	0.2125	0.0015
1.9200	1.3118	0.0823	0.0460	0.0160	0.0131	0.0630	0.0070	0.0000	0.0632	0.0013
1.9200	1.3218	0.0823	0.0420	0.0160	0.0234	0.0620	0.0060	0.0001	0.0627	0.0015
1.9200	1.3318	0.0823	0.0420	0.0170	0.0292	0.0590	0.0060	0.0000	0.0572	0.0018
1.9200	1.3418	0.0823	0.0440	0.0250	0.0453	0.0390	-0.0070	0.0032	0.0473	0.0023
1.9200	1.3518	0.0823	0.0430	0.0290	0.0502	0.0060	0.0020	0.0000	0.0444	0.0029
1.9200	1.3718	0.0823	0.0690	0.0350	0.0474	-0.0740	0.0090	0.0000	0.0818	0.0045
1.9200	1.3918	0.0823	0.1100	0.0350	0.0536	-0.1900	0.0540	0.0000	0.1742	0.0057
1.9200	1.4318	0.0823	0.0900	0.0400	0.0303	-0.3250	0.1000	-0.0029	0.3316	0.0043
1.9200	1.4718	0.0823	0.0335	0.0320	0.0169	-0.3210	0.1110	-0.0023	0.3498	0.0021
1.9200	1.5118	0.0823	0.0430	0.0136	0.0212	-0.3120	0.1030	-0.0053	0.3447	0.0015
1.9200	1.5518	0.0823	0.0471	0.0123	0.0123	-0.3025	0.1190	-0.0056	0.3356	0.0013
1.9200	1.5918	0.0823	0.0459	0.0108	0.0143	-0.2925	0.1130	-0.0016	0.3214	0.0012
1.9200	1.6318	0.0823	0.0430	0.0104	0.0208	-0.2470	0.1080	-0.0001	0.3027	0.0012

Table B.1 Flow field data for the bend width 0.60m (Q=0.013m³/s, continued)

x (m)	y (m)	z (m)	Urms (m/s)	Vrms (m/s)	Wrms (m/s)	U (m/s)	V (m/s)	W (m/s)	U$_T$(m/s)	Ke (m²/s²)
1.9200	1.6718	0.0823	0.0338	0.0280	0.0148	-0.2670	0.0820	-0.0071	0.3020	0.0013
1.9200	1.7118	0.0823	0.0680	0.0270	0.0142	-0.2820	0.0630	-0.0098	0.2992	0.0018
1.9200	1.7518	0.0823	0.0380	0.0280	0.0157	-0.2729	0.0480	-0.0067	0.2864	0.0013
1.9200	1.7918	0.0823	0.0438	0.0250	0.0143	-0.2521	-0.0020	-0.0034	0.2577	0.0012
1.9200	1.8318	0.0823	0.0441	0.0280	0.0192	-0.1990	-0.0290	-0.0033	0.2328	0.0014
1.9200	1.8718	0.0823	0.0417	0.0270	0.0239	-0.2040	-0.0150	0.0009	0.2269	0.0014
1.9200	1.8918	0.0823	0.0417	0.0220	0.0259	-0.2140	-0.0140	0.0039	0.2159	0.0015
1.9200	1.9068	0.0823	0.0590	0.0160	0.0261	-0.1523	-0.0080	0.0106	0.2005	0.0016
1.8100	1.3118	0.0059	0.0210	0.0030	0.0007	0.0010	-0.0020	-0.0005	0.0145	0.0008
1.8100	1.3218	0.0059	0.0360	0.0240	0.0012	-0.0150	-0.0160	0.0008	0.0204	0.0010
1.8100	1.3318	0.0059	0.0420	0.0250	0.0024	-0.0220	-0.0130	-0.0004	0.0282	0.0014
1.8100	1.3418	0.0059	0.0570	0.0140	0.0086	-0.0440	-0.0080	0.0011	0.0334	0.0016
1.8100	1.3518	0.0059	0.0070	0.0060	0.0142	-0.0020	-0.0020	0.0008	0.0412	0.0020
1.8100	1.3718	0.0059	0.0790	0.0280	0.0154	-0.1160	-0.0090	0.0016	0.1054	0.0031
1.8100	1.3918	0.0059	0.0620	0.0290	0.0155	-0.2250	-0.0080	0.0015	0.1928	0.0030
1.8100	1.4318	0.0059	0.0490	0.0310	0.0182	-0.2880	-0.0210	0.0081	0.2948	0.0024
1.8100	1.4718	0.0059	0.0530	0.0410	0.0191	-0.2960	-0.0240	0.0098	0.3305	0.0029
1.8100	1.5118	0.0059	0.0408	0.0230	0.0299	-0.2960	-0.0120	0.0098	0.3238	0.0016
1.8100	1.5518	0.0059	0.0430	0.0260	0.0000	-0.2960	-0.0170	-0.0078	0.3166	0.0014
1.8100	1.5918	0.0059	0.0645	0.0220	0.0000	-0.2890	-0.0100	0.0000	0.3101	0.0018
1.8100	1.6318	0.0059	0.0440	0.0300	0.0169	-0.2680	-0.0220	-0.0019	0.2986	0.0015
1.8100	1.6718	0.0059	0.0330	0.0320	0.0195	-0.2820	-0.0270	-0.0031	0.3039	0.0013
1.8100	1.7118	0.0059	0.0421	0.0210	0.0131	-0.2840	-0.0110	-0.0030	0.3011	0.0012
1.8100	1.7518	0.0059	0.0390	0.0210	0.0135	-0.2790	-0.0110	-0.0027	0.2978	0.0010
1.8100	1.7918	0.0059	0.0290	0.0250	0.0167	-0.2850	-0.0090	-0.0026	0.3009	0.0008
1.8100	1.8318	0.0059	0.0270	0.0210	0.0126	-0.2740	-0.0050	0.0037	0.2856	0.0008
1.8100	1.8718	0.0059	0.0820	0.0160	0.0093	-0.3070	-0.0190	0.0018	0.2437	0.0019
1.8100	1.8918	0.0059	0.0220	0.0160	0.0115	-0.2720	-0.0190	-0.0038	0.2681	0.0010
1.8100	1.9068	0.0059	0.0370	0.0110	0.0179	-0.2400	-0.0060	-0.0070	0.2630	0.0009
1.8100	1.3118	0.0148	0.0350	0.0155	0.0007	0.0080	-0.0060	-0.0005	0.0160	0.0010
1.8100	1.3218	0.0148	0.0420	0.0285	0.0079	-0.0100	-0.0195	0.0005	0.0220	0.0013
1.8100	1.3318	0.0148	0.0485	0.0305	0.0145	-0.0225	-0.0185	0.0017	0.0298	0.0017
1.8100	1.3418	0.0148	0.0600	0.0270	0.0189	-0.0365	-0.0150	0.0030	0.0359	0.0020
1.8100	1.3518	0.0148	0.0730	0.0265	0.0210	-0.0270	-0.0115	0.0035	0.0422	0.0023
1.8100	1.3718	0.0148	0.0770	0.0420	0.0195	-0.0955	-0.0070	0.0057	0.0993	0.0033
1.8100	1.3918	0.0148	0.0690	0.0415	0.0204	-0.1955	0.0025	0.0075	0.1832	0.0031
1.8100	1.4318	0.0148	0.0550	0.0370	0.0174	-0.3015	0.0035	0.0056	0.2925	0.0025
1.8100	1.4718	0.0148	0.0455	0.0420	0.0141	-0.3340	-0.0260	0.0014	0.3367	0.0028

Table B.1 Flow field data for the bend width 0.60m (Q=0.013m^3/s, continued)

x (m)	y (m)	z (m)	Urms (m/s)	Vrms (m/s)	Wrms (m/s)	U (m/s)	V (m/s)	W (m/s)	U$_T$(m/s)	Ke (m^2/s^2)
1.8100	1.5118	0.0148	0.0412	0.0320	0.0166	-0.3260	-0.0030	0.0019	0.3321	0.0016
1.8100	1.5518	0.0148	0.0390	0.0330	0.0154	-0.3105	-0.0025	0.0017	0.3253	0.0014
1.8100	1.5918	0.0148	0.0397	0.0305	0.0142	-0.3095	-0.0055	0.0000	0.3180	0.0017
1.8100	1.6318	0.0148	0.0395	0.0330	0.0183	-0.3015	-0.0145	-0.0041	0.3061	0.0015
1.8100	1.6718	0.0148	0.0315	0.0345	0.0206	-0.3075	-0.0150	-0.0069	0.3099	0.0013
1.8100	1.7118	0.0148	0.0412	0.0285	0.0174	-0.3035	-0.0135	-0.0068	0.3062	0.0012
1.8100	1.7518	0.0148	0.0325	0.0245	0.0150	-0.3005	-0.0025	-0.0060	0.3025	0.0010
1.8100	1.7918	0.0148	0.0235	0.0250	0.0157	-0.3035	0.0220	-0.0055	0.3050	0.0008
1.8100	1.8318	0.0148	0.0245	0.0250	0.0153	-0.2890	0.0080	0.0060	0.2889	0.0008
1.8100	1.8718	0.0148	0.0358	0.0225	0.0118	-0.1625	-0.0020	0.0058	0.2456	0.0017
1.8100	1.8918	0.0148	0.0205	0.0185	0.0094	-0.2800	-0.0125	-0.0029	0.2724	0.0009
1.8100	1.9068	0.0148	0.0305	0.0130	0.0212	-0.2620	-0.0065	-0.0092	0.2672	0.0008
1.8100	1.3118	0.0236	0.0490	0.0280	0.0008	0.0150	-0.0100	-0.0004	0.0213	0.0013
1.8100	1.3218	0.0236	0.0480	0.0330	0.0140	-0.0050	-0.0230	0.0051	0.0253	0.0016
1.8100	1.3318	0.0236	0.0550	0.0360	0.0161	-0.0230	-0.0240	0.0027	0.0318	0.0020
1.8100	1.3418	0.0236	0.0630	0.0400	0.0191	-0.0290	-0.0220	0.0050	0.0392	0.0023
1.8100	1.3518	0.0236	0.0660	0.0470	0.0229	-0.0520	-0.0210	0.0022	0.0478	0.0026
1.8100	1.3718	0.0236	0.0750	0.0560	0.0230	-0.0750	-0.0050	0.0069	0.0900	0.0032
1.8100	1.3918	0.0236	0.0760	0.0540	0.0243	-0.1660	0.0130	0.0079	0.1581	0.0032
1.8100	1.4318	0.0236	0.0610	0.0430	0.0201	-0.3150	0.0280	0.0078	0.2774	0.0027
1.8100	1.4718	0.0236	0.0380	0.0430	0.0152	-0.3720	0.0220	0.0047	0.3416	0.0025
1.8100	1.5118	0.0236	0.0380	0.0410	0.0142	-0.3650	0.0060	-0.0003	0.3453	0.0016
1.8100	1.5518	0.0236	0.0350	0.0400	0.0167	-0.3650	0.0120	-0.0023	0.3401	0.0014
1.8100	1.5918	0.0236	0.0330	0.0390	0.0148	-0.3500	-0.0010	-0.0006	0.3311	0.0016
1.8100	1.6318	0.0236	0.0350	0.0360	0.0201	-0.3350	-0.0070	-0.0051	0.3190	0.0014
1.8100	1.6718	0.0236	0.0300	0.0370	0.0223	-0.3330	-0.0030	-0.0086	0.3189	0.0012
1.8100	1.7118	0.0236	0.0340	0.0360	0.0222	-0.3230	-0.0160	-0.0085	0.3141	0.0012
1.8100	1.7518	0.0236	0.0260	0.0280	0.0172	-0.3220	0.0060	-0.0073	0.3094	0.0010
1.8100	1.7918	0.0236	0.0180	0.0250	0.0148	-0.3220	0.0530	-0.0064	0.3090	0.0008
1.8100	1.8318	0.0236	0.0220	0.0290	0.0181	-0.3040	0.0210	0.0056	0.2922	0.0008
1.8100	1.8718	0.0236	0.0240	0.0290	0.0156	-0.2880	0.0150	0.0075	0.2558	0.0014
1.8100	1.8918	0.0236	0.0190	0.0210	0.0107	-0.2880	-0.0060	-0.0002	0.2761	0.0009
1.8100	1.9068	0.0236	0.0240	0.0150	0.0244	-0.2840	-0.0070	-0.0072	0.2740	0.0008
1.8100	1.3118	0.0471	0.0390	0.0250	0.0020	0.0320	0.0060	-0.0004	0.0313	0.0012
1.8100	1.3218	0.0471	0.0370	0.0310	0.0011	0.0320	-0.0010	-0.0003	0.0322	0.0014
1.8100	1.3318	0.0471	0.0450	0.0310	0.0061	0.0260	-0.0070	0.0011	0.0348	0.0016
1.8100	1.3418	0.0471	0.0510	0.0360	0.0155	0.0390	0.0000	0.0018	0.0392	0.0019
1.8100	1.3518	0.0471	0.0544	0.0280	0.0204	0.0400	0.0080	0.0010	0.0443	0.0022

142

1.8100	1.3718	0.0471	0.0534	0.0330	0.0143	0.0460	0.0250	-0.0012	0.0566	0.0027
1.8100	1.3918	0.0471	0.0560	0.0420	0.0232	0.0000	0.0260	0.0054	0.0898	0.0030
1.8100	1.4318	0.0471	0.0710	0.0430	0.0275	-0.1790	0.0380	0.0060	0.2158	0.0033
1.8100	1.4718	0.0471	0.0380	0.0310	0.0178	-0.3500	0.0830	0.0056	0.3305	0.0023
1.8100	1.5118	0.0471	0.0230	0.0300	0.0119	-0.3740	0.0950	0.0001	0.3606	0.0015
1.8100	1.5518	0.0471	0.0170	0.0280	0.0111	-0.3760	0.0990	-0.0021	0.3620	0.0013
1.8100	1.5918	0.0471	0.0170	0.0290	0.0115	-0.3580	0.0890	-0.0034	0.3511	0.0013
1.8100	1.6318	0.0471	0.0240	0.0340	0.0220	-0.3490	0.0830	-0.0047	0.3342	0.0012
1.8100	1.6718	0.0471	0.0180	0.0310	0.0188	-0.3420	0.0750	-0.0106	0.3256	0.0011
1.8100	1.7118	0.0471	0.0140	0.0260	0.0158	-0.3380	0.0710	-0.0127	0.3201	0.0011
1.8100	1.7518	0.0471	0.0180	0.0230	0.0127	-0.3240	0.0570	-0.0088	0.3121	0.0011
1.8100	1.7918	0.0471	0.0170	0.0230	0.0120	-0.3180	0.0500	-0.0045	0.3025	0.0010
1.8100	1.8318	0.0471	0.0190	0.0250	0.0157	-0.3060	0.0390	-0.0016	0.2876	0.0010
1.8100	1.8718	0.0471	0.0200	0.0260	0.0168	-0.2980	0.0180	0.0072	0.2691	0.0011
1.8100	1.8918	0.0471	0.0220	0.0240	0.0154	-0.2910	0.0160	0.0122	0.2732	0.0009
1.8100	1.9068	0.0471	0.0250	0.0170	0.0277	-0.2890	-0.0020	0.0139	0.2681	0.0009
1.8100	1.3118	0.0701	0.0300	0.0180	0.0065	0.0290	0.0170	0.0020	0.0409	0.0009
1.8100	1.3218	0.0701	0.0330	0.0190	0.0093	0.0390	0.0200	0.0028	0.0434	0.0010
1.8100	1.3318	0.0701	0.0330	0.0220	0.0146	0.0530	0.0180	0.0016	0.0472	0.0011
1.8100	1.3418	0.0701	0.0320	0.0230	0.0163	0.0480	0.0210	-0.0030	0.0497	0.0013
1.8100	1.3518	0.0701	0.0430	0.0320	0.0192	0.0620	0.0190	-0.0065	0.0477	0.0016
1.8100	1.3718	0.0701	0.0480	0.0360	0.0196	0.0400	0.0080	-0.0060	0.0384	0.0022
1.8100	1.3918	0.0701	0.0470	0.0410	0.0237	0.0060	0.0130	-0.0013	0.0481	0.0028
1.8100	1.4318	0.0701	0.0568	0.0440	0.0257	-0.1500	0.0290	0.0116	0.1687	0.0041
1.8100	1.4718	0.0701	0.0636	0.0320	0.0196	-0.3380	0.0830	0.0019	0.3137	0.0022
1.8100	1.5118	0.0701	0.0473	0.0310	0.0094	-0.3630	0.1030	-0.0012	0.3536	0.0015
1.8100	1.5518	0.0701	0.0428	0.0290	0.0096	-0.3460	0.1070	-0.0015	0.3600	0.0014
1.8100	1.5918	0.0701	0.0421	0.0270	0.0093	-0.3390	0.1060	-0.0023	0.3490	0.0013
1.8100	1.6318	0.0701	0.0392	0.0260	0.0174	-0.3137	0.0990	-0.0008	0.3234	0.0012
1.8100	1.6718	0.0701	0.0355	0.0270	0.0148	-0.2934	0.0890	-0.0031	0.3097	0.0011
1.8100	1.7118	0.0701	0.0379	0.0250	0.0131	-0.3032	0.0680	-0.0083	0.3058	0.0010
1.8100	1.7518	0.0701	0.0350	0.0310	0.0168	-0.2932	0.0340	-0.0068	0.2984	0.0014
1.8100	1.7918	0.0701	0.0364	0.0280	0.0161	-0.2725	0.0070	-0.0015	0.2818	0.0012
1.8100	1.8318	0.0701	0.0436	0.0280	0.0199	-0.2570	-0.0030	-0.0076	0.2671	0.0012
1.8100	1.8718	0.0701	0.0405	0.0250	0.0223	-0.2221	-0.0060	-0.0017	0.2451	0.0012
1.8100	1.8918	0.0701	0.0436	0.0190	0.0222	-0.2319	-0.0080	0.0061	0.2305	0.0011
1.8100	1.9068	0.0701	0.0300	0.0150	0.0245	-0.1928	-0.0060	0.0159	0.2187	0.0010
1.8100	1.3118	0.0823	0.0380	0.0150	0.0084	0.0450	0.0090	0.0037	0.0426	0.0009
1.8100	1.3218	0.0823	0.0410	0.0180	0.0086	0.0420	0.0190	0.0020	0.0438	0.0009
1.8100	1.3318	0.0823	0.0300	0.0230	0.0118	0.0340	0.0180	-0.0009	0.0448	0.0011
1.8100	1.3418	0.0823	0.0400	0.0270	0.0133	0.0350	0.0280	-0.0017	0.0449	0.0012

143

Table B.1 Flow field data for the bend width 0.60m (Q=0.013m^3/s, continued)

x (m)	y (m)	z (m)	Urms (m/s)	Vrms (m/s)	Wrms (m/s)	U (m/s)	V (m/s)	W (m/s)	U$_T$(m/s)	Ke (m^2/s^2)
1.8100	1.3518	0.0823	0.0370	0.0330	0.0147	0.0320	0.0180	-0.0043	0.0432	0.0015
1.8100	1.3718	0.0823	0.0420	0.0360	0.0177	0.0090	0.0030	-0.0033	0.0335	0.0020
1.8100	1.3918	0.0823	0.0570	0.0320	0.0223	-0.0300	-0.0010	0.0020	0.0409	0.0028
1.8100	1.4318	0.0823	0.1040	0.0320	0.0258	-0.1370	0.0210	0.0076	0.1588	0.0042
1.8100	1.4718	0.0823	0.0446	0.0322	0.0167	-0.2710	0.0730	-0.0005	0.3075	0.0022
1.8100	1.5118	0.0823	0.0477	0.0239	0.0104	-0.2980	0.0940	-0.0022	0.3491	0.0015
1.8100	1.5518	0.0823	0.0496	0.0232	0.0085	-0.3380	0.0860	-0.0021	0.3570	0.0014
1.8100	1.5918	0.0823	0.0452	0.0226	0.0082	-0.3260	0.0860	-0.0036	0.3464	0.0013
1.8100	1.6318	0.0823	0.0329	0.0236	0.0238	-0.2790	0.0760	-0.0012	0.3184	0.0012
1.8100	1.6718	0.0823	0.0323	0.0300	0.0170	-0.2740	0.0680	-0.0008	0.3036	0.0011
1.8100	1.7118	0.0823	0.0288	0.0230	0.0119	-0.2704	0.0500	-0.0028	0.3003	0.0010
1.8100	1.7518	0.0823	0.0580	0.0270	0.0142	-0.2850	0.0160	-0.0032	0.2935	0.0015
1.8100	1.7918	0.0823	0.0392	0.0270	0.0155	-0.2621	-0.0210	-0.0009	0.2754	0.0012
1.8100	1.8318	0.0823	0.0433	0.0250	0.0178	-0.2518	-0.0370	-0.0060	0.2608	0.0013
1.8100	1.8718	0.0823	0.0440	0.0240	0.0240	-0.2413	-0.0220	-0.0040	0.2371	0.0013
1.8100	1.8918	0.0823	0.0433	0.0190	0.0261	-0.2135	-0.0170	-0.0011	0.2179	0.0012
1.8100	1.9068	0.0823	0.0270	0.0180	0.0293	-0.1627	-0.0090	0.0056	0.2045	0.0011
1.6100	1.3118	0.0059	0.0570	0.0080	0.0000	-0.0090	-0.0010	0.0000	0.0584	0.0021
1.6100	1.3218	0.0059	0.0520	0.0040	0.0000	0.0080	0.0000	0.0000	0.0305	0.0020
1.6100	1.3318	0.0059	0.0610	0.0110	0.0000	-0.0120	-0.0010	0.0000	0.0297	0.0020
1.6100	1.3418	0.0059	0.0590	0.0090	0.0000	-0.0380	-0.0030	0.0000	0.0545	0.0023
1.6100	1.3518	0.0059	0.0620	0.0190	0.0000	-0.0880	-0.0090	0.0000	0.0854	0.0029
1.6100	1.3718	0.0059	0.0790	0.0410	0.0000	-0.1580	-0.0350	0.0016	0.1387	0.0041
1.6100	1.3918	0.0059	0.0520	0.0540	0.0000	-0.1870	-0.0410	0.0000	0.1788	0.0039
1.6100	1.4318	0.0059	0.0640	0.0510	0.0000	-0.2560	-0.0470	0.0000	0.2544	0.0038
1.6100	1.4718	0.0059	0.0400	0.0400	0.0000	-0.3220	-0.0650	0.0000	0.3238	0.0022
1.6100	1.5118	0.0059	0.0410	0.0390	0.0000	-0.3200	-0.0710	0.0000	0.3395	0.0018
1.6100	1.5518	0.0059	0.0400	0.0390	0.0000	-0.3040	-0.0860	0.0000	0.3363	0.0017
1.6100	1.5918	0.0059	0.0350	0.0360	0.0000	-0.2910	-0.0850	0.0000	0.3336	0.0014
1.6100	1.6318	0.0059	0.0360	0.0360	0.0000	-0.2870	-0.0540	0.0000	0.3172	0.0013
1.6100	1.6718	0.0059	0.0310	0.0270	0.0000	-0.2830	-0.0190	0.0000	0.3188	0.0009
1.6100	1.7118	0.0059	0.0400	0.0260	0.0000	-0.3040	-0.0210	0.0000	0.3266	0.0010
1.6100	1.7518	0.0059	0.0323	0.0230	0.0000	-0.2640	-0.0230	0.0000	0.3080	0.0008
1.6100	1.7918	0.0059	0.0240	0.0240	0.0000	-0.3440	0.0010	0.0000	0.3442	0.0006
1.6100	1.8318	0.0059	0.0300	0.0180	0.0000	-0.3130	0.0010	0.0000	0.3269	0.0005
1.6100	1.8718	0.0059	0.0320	0.0180	0.0000	-0.3010	-0.0150	0.0000	0.3147	0.0007
1.6100	1.8918	0.0059	0.0320	0.0100	0.0000	-0.3090	-0.0030	0.0000	0.3062	0.0015
1.6100	1.9068	0.0059	0.1022	0.0060	0.0000	-0.2615	-0.0010	0.0000	0.2801	0.0026

Table B.1 Flow field data for the bend width 0.60m ($Q=0.013m^3/s$, continued)

x (m)	y (m)	z (m)	Urms (m/s)	Vrms (m/s)	Wrms (m/s)	U (m/s)	V (m/s)	W (m/s)	U_T(m/s)	Ke (m²/s²)
1.6100	1.3118	0.0148	0.0695	0.0115	0.0192	-0.1268	0.0020	0.0041	0.0856	0.0024
1.6100	1.3218	0.0148	0.0555	0.0170	0.0149	-0.0110	-0.0085	0.0091	0.0489	0.0023
1.6100	1.3318	0.0148	0.0600	0.0205	0.0141	-0.0210	-0.0090	0.0183	0.0386	0.0023
1.6100	1.3418	0.0148	0.0625	0.0270	0.0160	-0.0570	-0.0185	0.0254	0.0601	0.0026
1.6100	1.3518	0.0148	0.0670	0.0385	0.0209	-0.0820	-0.0255	0.0215	0.0856	0.0032
1.6100	1.3718	0.0148	0.0785	0.0490	0.0269	-0.1310	-0.0385	0.0131	0.1313	0.0042
1.6100	1.3918	0.0148	0.0630	0.0580	0.0336	-0.1735	-0.0370	0.0074	0.1704	0.0041
1.6100	1.4318	0.0148	0.0670	0.0530	0.0315	-0.2530	-0.0340	0.0028	0.2478	0.0039
1.6100	1.4718	0.0148	0.0420	0.0415	0.0230	-0.3260	-0.0410	0.0004	0.3196	0.0023
1.6100	1.5118	0.0148	0.0400	0.0405	0.0228	-0.3405	-0.0415	-0.0016	0.3410	0.0019
1.6100	1.5518	0.0148	0.0405	0.0385	0.0218	-0.3330	-0.0650	-0.0021	0.3415	0.0017
1.6100	1.5918	0.0148	0.0360	0.0365	0.0210	-0.3340	-0.0555	-0.0033	0.3416	0.0014
1.6100	1.6318	0.0148	0.0350	0.0390	0.0235	-0.3170	-0.0405	-0.0055	0.3247	0.0013
1.6100	1.6718	0.0148	0.0290	0.0295	0.0190	-0.3235	-0.0165	-0.0069	0.3270	0.0009
1.6100	1.7118	0.0148	0.0325	0.0260	0.0173	-0.3325	-0.0040	-0.0063	0.3335	0.0009
1.6100	1.7518	0.0148	0.0373	0.0240	0.0158	-0.3100	-0.0015	-0.0047	0.3157	0.0008
1.6100	1.7918	0.0148	0.0215	0.0220	0.0138	-0.3485	0.0190	-0.0033	0.3462	0.0006
1.6100	1.8318	0.0148	0.0215	0.0185	0.0119	-0.3280	0.0205	0.0066	0.3294	0.0005
1.6100	1.8718	0.0148	0.0265	0.0215	0.0121	-0.3165	0.0050	0.0054	0.3188	0.0007
1.6100	1.8918	0.0148	0.0265	0.0170	0.0097	-0.3215	0.0040	-0.0018	0.3137	0.0012
1.6100	1.9068	0.0148	0.0409	0.0150	0.0244	-0.2445	0.0050	-0.0098	0.2876	0.0023
1.6100	1.3118	0.0236	0.0820	0.0150	0.0000	-0.2445	0.0050	0.0000	0.1017	0.0028
1.6100	1.3218	0.0236	0.0590	0.0300	0.0097	-0.0300	-0.0170	0.0026	0.0734	0.0027
1.6100	1.3318	0.0236	0.0590	0.0300	0.0143	-0.0300	-0.0170	0.0040	0.0536	0.0028
1.6100	1.3418	0.0236	0.0660	0.0450	0.0260	-0.0760	-0.0340	0.0056	0.0629	0.0030
1.6100	1.3518	0.0236	0.0720	0.0580	0.0162	-0.0760	-0.0420	0.0009	0.0790	0.0034
1.6100	1.3718	0.0236	0.0780	0.0570	0.0388	-0.1040	-0.0420	0.0113	0.1124	0.0043
1.6100	1.3918	0.0236	0.0740	0.0620	0.0457	-0.1600	-0.0330	0.0076	0.1485	0.0043
1.6100	1.4318	0.0236	0.0700	0.0550	0.0477	-0.2500	-0.0210	0.0145	0.2267	0.0040
1.6100	1.4718	0.0236	0.0440	0.0430	0.0401	-0.3300	-0.0170	-0.0010	0.3019	0.0026
1.6100	1.5118	0.0236	0.0390	0.0420	0.0303	-0.3610	-0.0120	0.0054	0.3384	0.0020
1.6100	1.5518	0.0236	0.0410	0.0380	0.0297	-0.3620	-0.0440	-0.0026	0.3476	0.0017
1.6100	1.5918	0.0236	0.0370	0.0370	0.0291	-0.3770	-0.0260	0.0131	0.3521	0.0014
1.6100	1.6318	0.0236	0.0340	0.0420	0.0000	-0.3470	-0.0270	0.0000	0.3376	0.0013
1.6100	1.6718	0.0236	0.0270	0.0320	0.0000	-0.3640	-0.0140	0.0000	0.3391	0.0010
1.6100	1.7118	0.0236	0.0250	0.0260	0.0000	-0.3610	0.0130	0.0000	0.3420	0.0009
1.6100	1.7518	0.0236	0.0230	0.0250	0.0000	-0.3560	0.0200	0.0000	0.3274	0.0008
1.6100	1.7918	0.0236	0.0190	0.0200	0.0000	-0.3530	0.0370	0.0000	0.3442	0.0006

Table B.1 Flow field data for the bend width 0.60m (Q=0.013m^3/s, continued)

x (m)	y (m)	z (m)	Urms (m/s)	Vrms (m/s)	Wrms (m/s)	U (m/s)	V (m/s)	W (m/s)	U$_T$(m/s)	Ke (m^2/s^2)
1.6100	1.8318	0.0236	0.0130	0.0190	0.0000	-0.3430	0.0400	0.0000	0.3303	0.0005
1.6100	1.8718	0.0236	0.0210	0.0250	0.0000	-0.3320	0.0250	0.0000	0.3227	0.0006
1.6100	1.8918	0.0236	0.0210	0.0240	0.0000	-0.3340	0.0050	0.0000	0.3205	0.0009
1.6100	1.9068	0.0236	0.0210	0.0240	0.0000	-0.3340	0.0110	0.0000	0.3039	0.0016
1.6100	1.3118	0.0471	0.0873	0.0140	0.0000	-0.0630	-0.0070	0.0000	0.0666	0.0030
1.6100	1.3218	0.0471	0.0873	0.0140	0.0164	-0.0630	-0.0070	0.0362	0.0540	0.0030
1.6100	1.3318	0.0471	0.0530	0.0320	0.0342	0.0070	-0.0030	0.0132	0.0372	0.0031
1.6100	1.3418	0.0471	0.0560	0.0330	0.0474	-0.0070	-0.0050	0.0112	0.0308	0.0032
1.6100	1.3518	0.0471	0.0590	0.0400	0.0529	-0.0210	-0.0130	0.0097	0.0352	0.0034
1.6100	1.3718	0.0471	0.0660	0.0480	0.0530	-0.0210	-0.0120	0.0014	0.0522	0.0038
1.6100	1.3918	0.0471	0.0930	0.0620	0.0517	-0.0290	-0.0170	-0.0031	0.0779	0.0040
1.6100	1.4318	0.0471	0.0740	0.0510	0.0602	-0.1270	0.0070	0.0145	0.1493	0.0038
1.6100	1.4718	0.0471	0.0590	0.0450	0.0513	-0.2060	0.0250	0.0119	0.2363	0.0028
1.6100	1.5118	0.0471	0.0460	0.0310	0.0367	-0.3020	0.0400	0.0100	0.3164	0.0023
1.6100	1.5518	0.0471	0.0310	0.0280	0.0210	-0.3690	0.0410	0.0028	0.3431	0.0018
1.6100	1.5918	0.0471	0.0250	0.0250	0.0218	-0.3880	0.0560	-0.0014	0.3547	0.0015
1.6100	1.6318	0.0471	0.0220	0.0280	0.0000	-0.3850	0.0550	0.0000	0.3501	0.0013
1.6100	1.6718	0.0471	0.0220	0.0280	0.0000	-0.3670	0.0490	0.0000	0.3465	0.0011
1.6100	1.7118	0.0471	0.0190	0.0240	0.0000	-0.3670	0.0510	0.0000	0.3422	0.0009
1.6100	1.7518	0.0471	0.0180	0.0210	0.0000	-0.3500	0.0390	0.0000	0.3277	0.0009
1.6100	1.7918	0.0471	0.0240	0.0280	0.0000	-0.3470	0.0220	0.0000	0.3214	0.0008
1.6100	1.8318	0.0471	0.0200	0.0240	0.0000	-0.3380	0.0200	0.0000	0.3109	0.0006
1.6100	1.8718	0.0471	0.0200	0.0260	0.0000	-0.3440	0.0100	0.0000	0.3073	0.0007
1.6100	1.8918	0.0471	0.0220	0.0240	0.0000	-0.3330	0.0030	0.0000	0.3102	0.0007
1.6100	1.9068	0.0471	0.0220	0.0240	0.0000	-0.3330	0.0050	0.0000	0.3038	0.0008
1.6100	1.3118	0.0701	0.0530	0.0164	0.0000	-0.0380	-0.0170	0.0000	0.0366	0.0016
1.6100	1.3218	0.0701	0.0530	0.0164	0.0000	-0.0380	-0.0170	0.0000	0.0357	0.0017
1.6100	1.3318	0.0701	0.0420	0.0250	0.0354	0.0320	0.0110	0.0151	0.0343	0.0019
1.6100	1.3418	0.0701	0.0430	0.0240	0.0510	0.0360	0.0100	0.0106	0.0323	0.0020
1.6100	1.3518	0.0701	0.0390	0.0310	0.0440	0.0260	0.0230	0.0095	0.0298	0.0022
1.6100	1.3718	0.0701	0.0440	0.0430	0.0391	0.0270	0.0190	0.0017	0.0294	0.0025
1.6100	1.3918	0.0701	0.0480	0.0520	0.0394	0.0140	0.0270	-0.0110	0.0388	0.0028
1.6100	1.4318	0.0701	0.0650	0.0410	0.0566	-0.0410	-0.0040	0.0020	0.0933	0.0030
1.6100	1.4718	0.0701	0.0760	0.0400	0.0554	-0.1650	0.0180	0.0080	0.1890	0.0025
1.6100	1.5118	0.0701	0.0711	0.0300	0.0409	-0.3227	0.0400	-0.0001	0.3022	0.0023
1.6100	1.5518	0.0701	0.0740	0.0230	0.0234	-0.3036	0.0560	0.0014	0.3244	0.0018
1.6100	1.5918	0.0701	0.0445	0.0270	0.0161	-0.3135	0.0580	0.0018	0.3336	0.0015
1.6100	1.6318	0.0701	0.0367	0.0220	0.0000	-0.3237	0.0560	0.0000	0.3341	0.0015

146

Table B.1 Flow field data for the bend width 0.60m (Q=0.013m^3/s, continued)

x (m)	y (m)	z (m)	Urms (m/s)	Vrms (m/s)	Wrms (m/s)	U (m/s)	V (m/s)	W (m/s)	U$_T$(m/s)	Ke (m^2/s^2)
1.6100	1.6718	0.0701	0.0340	0.0230	0.0000	-0.3237	0.0450	0.0000	0.3277	0.0013
1.6100	1.7118	0.0701	0.0270	0.0230	0.0000	-0.3136	0.0360	0.0000	0.3206	0.0011
1.6100	1.7518	0.0701	0.0430	0.0210	0.0000	-0.2935	0.0210	0.0000	0.3015	0.0010
1.6100	1.7918	0.0701	0.0415	0.0260	0.0000	-0.2632	0.0010	0.0000	0.2855	0.0009
1.6100	1.8318	0.0701	0.0335	0.0230	0.0000	-0.2297	-0.0180	0.0000	0.2752	0.0008
1.6100	1.8718	0.0701	0.0270	0.0180	0.0000	-0.2327	-0.0090	0.0000	0.2573	0.0009
1.6100	1.8918	0.0701	0.0366	0.0160	0.0000	-0.2324	0.0030	0.0000	0.2443	0.0009
1.6100	1.9068	0.0701	0.0366	0.0160	0.0000	-0.2324	0.0030	0.0000	0.2368	0.0009
1.6100	1.3118	0.0823	0.0120	0.0140	0.0000	0.0010	-0.0010	0.0000	0.0206	0.0010
1.6100	1.3218	0.0823	0.0120	0.0140	0.0000	0.0010	-0.0010	0.0000	0.0207	0.0010
1.6100	1.3318	0.0823	0.0440	0.0180	0.0263	0.0290	0.0090	0.0068	0.0243	0.0013
1.6100	1.3418	0.0823	0.0350	0.0210	0.0397	0.0190	0.0100	0.0083	0.0253	0.0015
1.6100	1.3518	0.0823	0.0060	0.0220	0.0363	0.0020	0.0110	0.0029	0.0246	0.0017
1.6100	1.3718	0.0823	0.0100	0.0250	0.0371	0.0020	0.0110	-0.0045	0.0244	0.0020
1.6100	1.3918	0.0823	0.0100	0.0250	0.0376	0.0020	0.0120	-0.0098	0.0319	0.0023
1.6100	1.4318	0.0823	0.0090	0.0190	0.0584	-0.1000	0.0010	-0.0007	0.0825	0.0028
1.6100	1.4718	0.0823	0.0160	0.0190	0.0426	-0.1722	0.0050	0.0067	0.1797	0.0023
1.6100	1.5118	0.0823	0.0520	0.0250	0.0329	-0.3000	0.0170	0.0023	0.2989	0.0023
1.6100	1.5518	0.0823	0.0370	0.0320	0.0212	-0.3120	0.0400	0.0002	0.3184	0.0018
1.6100	1.5918	0.0823	0.0408	0.0330	0.0140	-0.3139	0.0380	0.0055	0.3261	0.0015
1.6100	1.6318	0.0823	0.0541	0.0290	0.0000	-0.3090	0.0440	0.0000	0.3276	0.0015
1.6100	1.6718	0.0823	0.0528	0.0220	0.0000	-0.2973	0.0260	0.0000	0.3208	0.0013
1.6100	1.7118	0.0823	0.0459	0.0230	0.0000	-0.2978	0.0120	0.0000	0.3133	0.0011
1.6100	1.7518	0.0823	0.0452	0.0220	0.0000	-0.2720	0.0010	0.0000	0.2931	0.0011
1.6100	1.7918	0.0823	0.0417	0.0230	0.0000	-0.2650	-0.0150	0.0000	0.2758	0.0010
1.6100	1.8318	0.0823	0.0351	0.0170	0.0000	-0.2910	-0.0070	0.0000	0.2657	0.0008
1.6100	1.8718	0.0823	0.0480	0.0140	0.0000	-0.2319	-0.0070	0.0000	0.2429	0.0010
1.6100	1.8918	0.0823	0.0443	0.0160	0.0000	-0.2152	-0.0090	0.0000	0.2241	0.0010
1.6100	1.9068	0.0823	0.0443	0.0160	0.0000	-0.1520	-0.0090	0.0000	0.2156	0.0010
1.4200	1.3118	0.0059	0.0420	0.0040	0.0000	-0.0170	0.0000	0.0000	0.0118	0.0017
1.4200	1.3218	0.0059	0.0560	0.0100	0.0000	-0.0030	0.0000	0.0000	0.0202	0.0019
1.4200	1.3318	0.0059	0.0640	0.0110	0.0000	-0.0490	-0.0010	0.0000	0.0465	0.0021
1.4200	1.3418	0.0059	0.0630	0.0160	0.0000	-0.0500	-0.0040	0.0000	0.0715	0.0023
1.4200	1.3518	0.0059	0.0530	0.0240	0.0000	-0.0720	-0.0130	0.0000	0.0975	0.0025
1.4200	1.3718	0.0059	0.0690	0.0530	0.0000	-0.1440	-0.0460	0.0000	0.1605	0.0033
1.4200	1.3918	0.0059	0.0570	0.0440	0.0000	-0.2310	-0.0580	0.0000	0.2189	0.0034
1.4200	1.4318	0.0059	0.0660	0.0410	0.0000	-0.2350	-0.0550	0.0000	0.2322	0.0033
1.4200	1.4718	0.0059	0.0430	0.0370	0.0000	-0.3050	-0.0600	0.0000	0.2946	0.0023

Table B.1 Flow field data for the bend width 0.60m (Q=0.013m³/s, continued)

x (m)	y (m)	z (m)	Urms (m/s)	Vrms (m/s)	Wrms (m/s)	U (m/s)	V (m/s)	W (m/s)	U$_T$(m/s)	Ke (m²/s²)
1.4200	1.5118	0.0059	0.0390	0.0410	0.0000	-0.2930	-0.0760	0.0000	0.3219	0.0018
1.4200	1.5518	0.0059	0.0410	0.0360	0.0000	-0.2860	-0.0890	0.0000	0.3246	0.0016
1.4200	1.5918	0.0059	0.0370	0.0350	0.0000	-0.2960	-0.0810	0.0000	0.3271	0.0014
1.4200	1.6318	0.0059	0.0360	0.0370	0.0000	-0.2960	-0.0560	0.0000	0.3289	0.0013
1.4200	1.6718	0.0059	0.0370	0.0300	0.0000	-0.3180	-0.0650	0.0000	0.3378	0.0011
1.4200	1.7118	0.0059	0.0310	0.0310	0.0000	-0.3230	-0.0500	0.0000	0.3383	0.0009
1.4200	1.7518	0.0059	0.0290	0.0260	0.0000	-0.3270	-0.0250	0.0000	0.3390	0.0007
1.4200	1.7918	0.0059	0.0280	0.0190	0.0000	-0.3210	-0.0040	0.0000	0.3364	0.0006
1.4200	1.8318	0.0059	0.0300	0.0230	0.0000	-0.2980	0.0080	0.0000	0.3233	0.0006
1.4200	1.8718	0.0059	0.0395	0.0170	0.0000	-0.2950	0.0000	0.0000	0.3201	0.0008
1.4200	1.8918	0.0059	0.0390	0.0090	0.0000	-0.2960	0.0010	0.0000	0.3094	0.0007
1.4200	1.9068	0.0059	0.0260	0.0080	0.0000	-0.2830	0.0020	0.0000	0.3048	0.0006
1.4200	1.3118	0.0148	0.0545	0.0205	0.0334	-0.0080	-0.0020	-0.0034	0.0113	0.0020
1.4200	1.3218	0.0148	0.0615	0.0235	0.0194	-0.0010	-0.0020	-0.0009	0.0217	0.0022
1.4200	1.3318	0.0148	0.0640	0.0295	0.0232	-0.0615	-0.0150	-0.0028	0.0558	0.0024
1.4200	1.3418	0.0148	0.0621	0.0305	0.0246	-0.0840	-0.0285	-0.0069	0.0858	0.0025
1.4200	1.3518	0.0148	0.0596	0.0355	0.0288	-0.0995	-0.0285	-0.0066	0.1083	0.0027
1.4200	1.3718	0.0148	0.0630	0.0515	0.0391	-0.1570	-0.0475	0.0032	0.1622	0.0035
1.4200	1.3918	0.0148	0.0630	0.0515	0.0324	-0.2195	-0.0590	0.0134	0.2146	0.0035
1.4200	1.4318	0.0148	0.0655	0.0470	0.0260	-0.2220	-0.0495	0.0063	0.2256	0.0034
1.4200	1.4718	0.0148	0.0555	0.0380	0.0215	-0.2910	-0.0545	0.0024	0.2893	0.0025
1.4200	1.5118	0.0148	0.0385	0.0390	0.0220	-0.3230	-0.0535	-0.0003	0.3232	0.0020
1.4200	1.5518	0.0148	0.0400	0.0395	0.0227	-0.3220	-0.0645	-0.0015	0.3299	0.0017
1.4200	1.5918	0.0148	0.0365	0.0375	0.0225	-0.3245	-0.0600	-0.0037	0.3330	0.0014
1.4200	1.6318	0.0148	0.0350	0.0370	0.0236	-0.3300	-0.0400	-0.0057	0.3354	0.0013
1.4200	1.6718	0.0148	0.0350	0.0325	0.0225	-0.3375	-0.0440	-0.0060	0.3423	0.0011
1.4200	1.7118	0.0148	0.0280	0.0300	0.0217	-0.3385	-0.0280	-0.0041	0.3418	0.0009
1.4200	1.7518	0.0148	0.0250	0.0260	0.0186	-0.3410	-0.0105	-0.0035	0.3421	0.0007
1.4200	1.7918	0.0148	0.0215	0.0215	0.0138	-0.3395	0.0110	-0.0011	0.3404	0.0006
1.4200	1.8318	0.0148	0.0245	0.0220	0.0149	-0.3260	0.0195	0.0065	0.3282	0.0006
1.4200	1.8718	0.0148	0.0326	0.0215	0.0129	-0.3355	0.0130	0.0042	0.3252	0.0008
1.4200	1.8918	0.0148	0.0365	0.0160	0.0104	-0.3150	0.0045	-0.0016	0.3162	0.0008
1.4200	1.9068	0.0148	0.0300	0.0155	0.0252	-0.3085	0.0050	-0.0091	0.3114	0.0007
1.4200	1.3118	0.0236	0.0670	0.0370	0.0000	0.0010	-0.0040	0.0000	0.0171	0.0024
1.4200	1.3218	0.0236	0.0670	0.0370	0.0033	0.0010	-0.0040	0.0020	0.0303	0.0026
1.4200	1.3318	0.0236	0.0640	0.0480	0.0058	-0.0740	-0.0290	0.0036	0.0655	0.0027
1.4200	1.3418	0.0236	0.0440	0.0450	0.0221	-0.1180	-0.0530	0.0037	0.0991	0.0028
1.4200	1.3518	0.0236	0.0480	0.0470	0.0277	-0.1270	-0.0440	0.0113	0.1194	0.0030

148

Table B.1 Flow field data for the bend width 0.60m (Q=0.013m^3/s, continued)

x (m)	y (m)	z (m)	Urms (m/s)	Vrms (m/s)	Wrms (m/s)	U (m/s)	V (m/s)	W (m/s)	U$_T$(m/s)	Ke (m^2/s^2)
1.4200	1.3718	0.0236	0.0570	0.0500	0.0242	-0.1700	-0.0490	0.0043	0.1577	0.0036
1.4200	1.3918	0.0236	0.0690	0.0590	0.0346	-0.2080	-0.0600	0.0022	0.1954	0.0037
1.4200	1.4318	0.0236	0.0650	0.0530	0.0292	-0.2090	-0.0440	0.0015	0.2097	0.0036
1.4200	1.4718	0.0236	0.0602	0.0390	0.0000	-0.2770	-0.0490	0.0000	0.2722	0.0028
1.4200	1.5118	0.0236	0.0380	0.0370	0.0000	-0.3530	-0.0310	0.0000	0.3175	0.0022
1.4200	1.5518	0.0236	0.0390	0.0430	0.0000	-0.3580	-0.0400	0.0000	0.3352	0.0018
1.4200	1.5918	0.0236	0.0360	0.0400	0.0000	-0.3530	-0.0390	0.0000	0.3415	0.0014
1.4200	1.6318	0.0236	0.0340	0.0370	0.0000	-0.3640	-0.0240	0.0000	0.3447	0.0012
1.4200	1.6718	0.0236	0.0330	0.0350	0.0000	-0.3570	-0.0230	0.0000	0.3482	0.0011
1.4200	1.7118	0.0236	0.0250	0.0290	0.0000	-0.3540	-0.0060	0.0000	0.3463	0.0008
1.4200	1.7518	0.0236	0.0210	0.0260	0.0000	-0.3550	0.0040	0.0000	0.3451	0.0007
1.4200	1.7918	0.0236	0.0150	0.0240	0.0000	-0.3580	0.0260	0.0000	0.3436	0.0006
1.4200	1.8318	0.0236	0.0190	0.0210	0.0000	-0.3540	0.0310	0.0000	0.3327	0.0006
1.4200	1.8718	0.0236	0.0250	0.0260	0.0000	-0.3360	0.0260	0.0000	0.3292	0.0008
1.4200	1.8918	0.0236	0.0340	0.0230	0.0000	-0.3340	0.0080	0.0000	0.3242	0.0008
1.4200	1.9068	0.0236	0.0340	0.0230	0.0000	-0.3340	0.0080	0.0000	0.3197	0.0007
1.4200	1.3118	0.0471	0.0530	0.0360	0.0227	-0.0370	-0.0030	0.0200	0.0353	0.0025
1.4200	1.3218	0.0471	0.0530	0.0360	0.0388	-0.0370	-0.0030	0.0184	0.0420	0.0027
1.4200	1.3318	0.0471	0.0540	0.0410	0.0344	-0.0410	-0.0160	0.0162	0.0577	0.0030
1.4200	1.3418	0.0471	0.0640	0.0500	0.0440	-0.0770	-0.0220	0.0253	0.0774	0.0033
1.4200	1.3518	0.0471	0.0540	0.0550	0.0484	-0.1050	-0.0290	0.0225	0.0919	0.0035
1.4200	1.3718	0.0471	0.0820	0.0520	0.0461	-0.1070	-0.0230	0.0155	0.1102	0.0039
1.4200	1.3918	0.0471	0.0690	0.0510	0.0508	-0.1020	-0.0410	0.0139	0.1270	0.0040
1.4200	1.4318	0.0471	0.0680	0.0570	0.0527	-0.1480	-0.0170	0.0173	0.1492	0.0040
1.4200	1.4718	0.0471	0.0740	0.0480	0.0592	-0.2100	-0.0120	0.0306	0.2111	0.0037
1.4200	1.5118	0.0471	0.0460	0.0380	0.0810	-0.2650	0.0010	0.0132	0.2784	0.0029
1.4200	1.5518	0.0471	0.0420	0.0320	0.0369	-0.3380	0.0190	0.0098	0.3261	0.0020
1.4200	1.5918	0.0471	0.0250	0.0290	0.0238	-0.3740	0.0270	-0.0014	0.3451	0.0014
1.4200	1.6318	0.0471	0.0210	0.0260	0.0000	-0.3750	0.0350	0.0000	0.3475	0.0010
1.4200	1.6718	0.0471	0.0210	0.0260	0.0000	-0.3770	0.0340	0.0000	0.3471	0.0008
1.4200	1.7118	0.0471	0.0180	0.0220	0.0000	-0.3730	0.0380	0.0000	0.3424	0.0007
1.4200	1.7518	0.0471	0.0150	0.0210	0.0000	-0.3600	0.0320	0.0000	0.3357	0.0006
1.4200	1.7918	0.0471	0.0200	0.0250	0.0000	-0.3630	0.0360	0.0000	0.3303	0.0005
1.4200	1.8318	0.0471	0.0210	0.0200	0.0000	-0.3500	0.0270	0.0000	0.3157	0.0006
1.4200	1.8718	0.0471	0.0180	0.0220	0.0000	-0.3490	0.0280	0.0000	0.3118	0.0007
1.4200	1.8918	0.0471	0.0193	0.0240	0.0000	-0.3330	0.0250	0.0000	0.3125	0.0007
1.4200	1.9068	0.0471	0.0193	0.0240	0.0000	-0.3330	0.0250	0.0000	0.3086	0.0007
1.4200	1.3118	0.0701	0.0500	0.0320	0.0245	0.0080	0.0050	0.0194	0.0227	0.0020

Table B.1 Flow field data for the bend width 0.60m (Q=0.013m^3/s, continued)

x (m)	y (m)	z (m)	Urms (m/s)	Vrms (m/s)	Wrms (m/s)	U (m/s)	V (m/s)	W (m/s)	U$_T$(m/s)	Ke (m^2/s^2)
1.4200	1.3218	0.0701	0.0500	0.0320	0.0298	0.0080	0.0050	0.0087	0.0242	0.0021
1.4200	1.3318	0.0701	0.0330	0.0340	0.0369	-0.0080	0.0020	0.0376	0.0298	0.0023
1.4200	1.3418	0.0701	0.0540	0.0400	0.0480	-0.0160	0.0170	0.0165	0.0371	0.0026
1.4200	1.3518	0.0701	0.0510	0.0430	0.0473	-0.0230	0.0320	0.0123	0.0454	0.0029
1.4200	1.3718	0.0701	0.0550	0.0430	0.0419	-0.0290	0.0370	0.0169	0.0585	0.0034
1.4200	1.3918	0.0701	0.0600	0.0470	0.0436	-0.0660	-0.0010	0.0092	0.0717	0.0038
1.4200	1.4318	0.0701	0.0500	0.0520	0.0486	-0.0300	0.0210	0.0003	0.0945	0.0040
1.4200	1.4718	0.0701	0.0840	0.0480	0.0437	-0.1210	0.0190	0.0053	0.1600	0.0042
1.4200	1.5118	0.0701	0.0760	0.0420	0.0530	-0.2176	0.0190	0.0100	0.2444	0.0031
1.4200	1.5518	0.0701	0.0337	0.0310	0.0338	-0.3223	0.0360	-0.0021	0.3064	0.0020
1.4200	1.5918	0.0701	0.0427	0.0230	0.0207	-0.3231	0.0470	-0.0057	0.3298	0.0012
1.4200	1.6318	0.0701	0.0430	0.0210	0.0000	-0.3132	0.0520	0.0000	0.3272	0.0007
1.4200	1.6718	0.0701	0.0408	0.0200	0.0000	-0.3133	0.0410	0.0000	0.3256	0.0006
1.4200	1.7118	0.0701	0.0392	0.0210	0.0000	-0.3032	0.0240	0.0000	0.3195	0.0005
1.4200	1.7518	0.0701	0.0342	0.0270	0.0000	-0.2932	0.0010	0.0000	0.3087	0.0004
1.4200	1.7918	0.0701	0.0450	0.0270	0.0000	-0.2734	-0.0050	0.0000	0.2996	0.0005
1.4200	1.8318	0.0701	0.0240	0.0200	0.0000	-0.2335	0.0060	0.0000	0.2760	0.0005
1.4200	1.8718	0.0701	0.0560	0.0270	0.0000	-0.2333	-0.0060	0.0000	0.2618	0.0005
1.4200	1.8918	0.0701	0.0490	0.0200	0.0000	-0.2331	0.0210	0.0000	0.2515	0.0006
1.4200	1.9068	0.0701	0.0490	0.0200	0.0000	-0.2331	0.0210	0.0000	0.2478	0.0007
1.4200	1.3118	0.0823	0.0465	0.0150	0.0183	0.0040	0.0010	0.0230	0.0189	0.0017
1.4200	1.3218	0.0823	0.0465	0.0150	0.0388	0.0040	0.0010	0.0121	0.0187	0.0017
1.4200	1.3318	0.0823	0.0250	0.0240	0.0274	0.0010	0.0120	0.0099	0.0209	0.0018
1.4200	1.3418	0.0823	0.0256	0.0230	0.0482	0.0020	0.0120	0.0120	0.0251	0.0021
1.4200	1.3518	0.0823	0.0291	0.0330	0.0416	0.0010	0.0210	0.0136	0.0323	0.0024
1.4200	1.3718	0.0823	0.0490	0.0380	0.0455	-0.0010	0.0260	0.0118	0.0456	0.0032
1.4200	1.3918	0.0823	0.0528	0.0440	0.0511	0.0000	0.0390	0.0070	0.0594	0.0037
1.4200	1.4318	0.0823	0.0566	0.0390	0.0512	-0.1000	0.0180	0.0063	0.0828	0.0040
1.4200	1.4718	0.0823	0.0579	0.0380	0.0635	-0.1500	0.0230	0.0103	0.1492	0.0042
1.4200	1.5118	0.0823	0.0522	0.0350	0.0348	-0.2550	0.0280	0.0097	0.2370	0.0031
1.4200	1.5518	0.0823	0.0386	0.0300	0.0361	-0.2690	0.0280	0.0060	0.3004	0.0020
1.4200	1.5918	0.0823	0.0340	0.0240	0.0217	-0.3140	0.0290	0.0024	0.3241	0.0012
1.4200	1.6318	0.0823	0.0130	0.0210	0.0000	-0.3030	0.0290	0.0000	0.3201	0.0006
1.4200	1.6718	0.0823	0.0080	0.0210	0.0000	-0.3047	0.0170	0.0000	0.3184	0.0005
1.4200	1.7118	0.0823	0.0090	0.0210	0.0000	-0.3050	-0.0090	0.0000	0.3121	0.0004
1.4200	1.7518	0.0823	0.0120	0.0170	0.0000	-0.2900	-0.0120	0.0000	0.3007	0.0004
1.4200	1.7918	0.0823	0.0060	0.0230	0.0000	-0.2950	-0.0170	0.0000	0.2907	0.0004
1.4200	1.8318	0.0823	0.0040	0.0280	0.0000	-0.2710	-0.0280	0.0000	0.2650	0.0005

Table B.1 Flow field data for the bend width 0.60m (Q=0.013m^3/s, continued)

x (m)	y (m)	z (m)	Urms (m/s)	Vrms (m/s)	Wrms (m/s)	U (m/s)	V (m/s)	W (m/s)	U$_T$(m/s)	Ke (m^2/s^2)
1.4200	1.8718	0.0823	0.0030	0.0160	0.0000	-0.2430	-0.0090	0.0000	0.2482	0.0005
1.4200	1.8918	0.0823	0.0210	0.0140	0.0000	-0.2290	-0.0040	0.0000	0.2354	0.0005
1.4200	1.9068	0.0823	0.0210	0.0140	0.0000	-0.1990	-0.0040	0.0000	0.2313	0.0006
1.1000	1.3118	0.0059	0.0430	0.0060	0.0056	-0.0700	0.0010	0.0012	0.0737	0.0013
1.1000	1.3218	0.0059	0.0510	0.0090	0.0127	-0.0480	0.0010	0.0023	0.0741	0.0015
1.1000	1.3318	0.0059	0.0480	0.0080	0.0366	-0.0680	0.0020	0.0055	0.0843	0.0018
1.1000	1.3418	0.0059	0.0470	0.0070	0.0417	-0.0900	0.0000	0.0074	0.0998	0.0021
1.1000	1.3518	0.0059	0.0470	0.0270	0.0287	-0.0980	0.0030	0.0067	0.1159	0.0023
1.1000	1.3718	0.0059	0.0560	0.0360	0.0262	-0.1330	-0.0150	-0.0038	0.1465	0.0026
1.1000	1.3918	0.0059	0.0590	0.0390	0.0266	-0.1480	-0.0140	0.0019	0.1764	0.0029
1.1000	1.4318	0.0059	0.0530	0.0450	0.0000	-0.1860	-0.0340	0.0000	0.2111	0.0025
1.1000	1.4718	0.0059	0.0520	0.0260	0.0000	-0.2160	-0.0160	0.0000	0.2385	0.0020
1.1000	1.5118	0.0059	0.0720	0.0310	0.0000	-0.2050	-0.0230	0.0000	0.2534	0.0025
1.1000	1.5518	0.0059	0.0370	0.0250	0.0000	-0.2960	0.0150	0.0000	0.3042	0.0014
1.1000	1.5918	0.0059	0.0400	0.0210	0.0000	-0.2410	0.0050	0.0000	0.2849	0.0011
1.1000	1.6318	0.0059	0.0342	0.0130	0.0000	-0.2110	0.0000	0.0000	0.2694	0.0009
1.1000	1.6718	0.0059	0.0349	0.0100	0.0000	-0.2200	0.0020	0.0000	0.2734	0.0008
1.1000	1.7118	0.0059	0.0500	0.0070	0.0000	-0.2120	0.0020	0.0000	0.2714	0.0010
1.1000	1.7518	0.0059	0.0490	0.0117	0.0000	-0.2430	-0.0350	0.0000	0.2903	0.0011
1.1000	1.7918	0.0059	0.0420	0.0098	0.0000	-0.2690	-0.0330	0.0000	0.3064	0.0009
1.1000	1.8318	0.0059	0.0445	0.0090	0.0000	-0.2785	-0.0265	0.0000	0.3000	0.0010
1.1000	1.8718	0.0059	0.0470	0.0082	0.0000	-0.2880	-0.0200	0.0000	0.3007	0.0010
1.1000	1.8918	0.0059	0.0470	0.0089	0.0000	-0.2880	-0.0060	0.0000	0.2990	0.0010
1.1000	1.9068	0.0059	0.0460	0.0170	0.0000	-0.2750	0.0030	0.0000	0.2850	0.0010
1.1000	1.3118	0.0148	0.0440	0.0150	0.0244	-0.0820	-0.0010	-0.0030	0.0843	0.0014
1.1000	1.3218	0.0148	0.0470	0.0200	0.0174	-0.0825	-0.0045	-0.0030	0.0878	0.0016
1.1000	1.3318	0.0148	0.0475	0.0235	0.0165	-0.0975	-0.0045	0.0018	0.0997	0.0020
1.1000	1.3418	0.0148	0.0470	0.0250	0.0150	-0.1155	-0.0070	0.0088	0.1143	0.0023
1.1000	1.3518	0.0148	0.0480	0.0345	0.0186	-0.1230	-0.0080	0.0152	0.1268	0.0025
1.1000	1.3718	0.0148	0.0500	0.0385	0.0194	-0.1500	-0.0190	0.0163	0.1540	0.0027
1.1000	1.3918	0.0148	0.0545	0.0420	0.0213	-0.1820	-0.0280	0.0121	0.1835	0.0029
1.1000	1.4318	0.0148	0.0475	0.0425	0.0252	-0.2120	-0.0400	0.0033	0.2154	0.0026
1.1000	1.4718	0.0148	0.0485	0.0300	0.0181	-0.2420	-0.0325	0.0013	0.2425	0.0021
1.1000	1.5118	0.0148	0.0455	0.0340	0.0203	-0.2570	-0.0180	-0.0006	0.2606	0.0025
1.1000	1.5518	0.0148	0.0385	0.0305	0.0189	-0.3115	-0.0180	-0.0020	0.3083	0.0015
1.1000	1.5918	0.0148	0.0355	0.0260	0.0172	-0.2915	-0.0120	-0.0038	0.2945	0.0012
1.1000	1.6318	0.0148	0.0399	0.0220	0.0156	-0.2775	-0.0098	-0.0048	0.2824	0.0009
1.1000	1.6718	0.0148	0.0400	0.0205	0.0151	-0.2830	-0.0040	-0.0032	0.2868	0.0008

Table B.1 Flow field data for the bend width 0.60m (Q=0.013m³/s, continued)

x (m)	y (m)	z (m)	Urms (m/s)	Vrms (m/s)	Wrms (m/s)	U (m/s)	V (m/s)	W (m/s)	U$_T$(m/s)	Ke (m²/s²)
1.1000	1.7118	0.0148	0.0360	0.0155	0.0115	-0.2795	0.0045	-0.0021	0.2852	0.0010
1.1000	1.7518	0.0148	0.0340	0.0275	0.0204	-0.2970	0.0015	-0.0019	0.3017	0.0010
1.1000	1.7918	0.0148	0.0310	0.0265	0.0181	-0.3135	-0.0020	0.0005	0.3152	0.0009
1.1000	1.8318	0.0148	0.0316	0.0282	0.0203	-0.3022	-0.0052	0.0054	0.3055	0.0009
1.1000	1.8718	0.0148	0.0329	0.0250	0.0165	-0.3030	-0.0080	0.0027	0.3054	0.0010
1.1000	1.8918	0.0148	0.0350	0.0235	0.0178	-0.3110	-0.0010	-0.0019	0.3056	0.0009
1.1000	1.9068	0.0148	0.0360	0.0150	0.0244	-0.2785	0.0060	-0.0068	0.2890	0.0009
1.1000	1.3118	0.0236	0.0450	0.0240	0.0087	-0.0940	-0.0030	0.0017	0.0996	0.0016
1.1000	1.3218	0.0236	0.0430	0.0310	0.0108	-0.1170	-0.0100	0.0019	0.1066	0.0019
1.1000	1.3318	0.0236	0.0470	0.0390	0.0449	-0.1270	-0.0110	0.0080	0.1190	0.0023
1.1000	1.3418	0.0236	0.0470	0.0430	0.0436	-0.1410	-0.0140	0.0069	0.1319	0.0027
1.1000	1.3518	0.0236	0.0490	0.0420	0.0783	-0.1480	-0.0190	0.0117	0.1416	0.0028
1.1000	1.3718	0.0236	0.0440	0.0410	0.0336	-0.1670	-0.0230	0.0087	0.1644	0.0029
1.1000	1.3918	0.0236	0.0500	0.0450	0.0583	-0.2160	-0.0420	0.0172	0.1902	0.0030
1.1000	1.4318	0.0236	0.0420	0.0400	0.0399	-0.2380	-0.0460	0.0162	0.2173	0.0027
1.1000	1.4718	0.0236	0.0450	0.0340	0.0289	-0.2680	-0.0490	0.0085	0.2424	0.0024
1.1000	1.5118	0.0236	0.0370	0.0370	0.0330	-0.3090	-0.0530	0.0091	0.2677	0.0026
1.1000	1.5518	0.0236	0.0400	0.0360	0.0272	-0.3270	-0.0310	0.0063	0.3084	0.0018
1.1000	1.5918	0.0236	0.0310	0.0310	0.0276	-0.3420	-0.0290	0.0096	0.3077	0.0013
1.1000	1.6318	0.0236	0.0275	0.0310	0.0211	-0.3440	-0.0195	-0.0106	0.3022	0.0010
1.1000	1.6718	0.0236	0.0240	0.0310	0.0000	-0.3460	-0.0100	0.0000	0.3065	0.0009
1.1000	1.7118	0.0236	0.0220	0.0240	0.0000	-0.3470	0.0070	0.0000	0.3064	0.0009
1.1000	1.7518	0.0236	0.0190	0.0180	0.0156	-0.3510	0.0380	-0.0148	0.3175	0.0010
1.1000	1.7918	0.0236	0.0200	0.0220	0.0161	-0.3580	0.0290	-0.0048	0.3256	0.0009
1.1000	1.8318	0.0236	0.0262	0.0280	0.0000	-0.3260	0.0160	0.0000	0.3134	0.0009
1.1000	1.8718	0.0236	0.0265	0.0240	0.0000	-0.3180	0.0040	0.0000	0.3116	0.0009
1.1000	1.8918	0.0236	0.0230	0.0190	0.0000	-0.3340	0.0040	0.0000	0.3125	0.0008
1.1000	1.9068	0.0236	0.0260	0.0130	0.0075	-0.2820	0.0090	-0.0004	0.2996	0.0008
1.1000	1.3118	0.0471	0.0460	0.0240	0.0051	-0.1170	-0.0040	0.0018	0.1098	0.0021
1.1000	1.3218	0.0471	0.0690	0.0280	0.0364	-0.1060	-0.0120	0.0065	0.1150	0.0024
1.1000	1.3318	0.0471	0.0670	0.0390	0.0563	-0.1260	-0.0110	0.0120	0.1262	0.0029
1.1000	1.3418	0.0471	0.0460	0.0360	0.0558	-0.1460	-0.0180	0.0160	0.1406	0.0033
1.1000	1.3518	0.0471	0.0450	0.0390	0.0425	-0.1570	-0.0160	0.0180	0.1516	0.0033
1.1000	1.3718	0.0471	0.0530	0.0380	0.0510	-0.1840	-0.0220	0.0203	0.1670	0.0033
1.1000	1.3918	0.0471	0.0550	0.0480	0.0500	-0.1940	-0.0190	0.0143	0.1798	0.0033
1.1000	1.4318	0.0471	0.0520	0.0490	0.0456	-0.2080	-0.0180	0.0146	0.1932	0.0033
1.1000	1.4718	0.0471	0.0580	0.0490	0.0436	-0.2160	-0.0160	0.0167	0.2107	0.0034
1.1000	1.5118	0.0471	0.0530	0.0410	0.0394	-0.2520	-0.0100	0.0173	0.2488	0.0032

Table B.1 Flow field data for the bend width 0.60m (Q=0.013m^3/s, continued)

x (m)	y (m)	z (m)	Urms (m/s)	Vrms (m/s)	Wrms (m/s)	U (m/s)	V (m/s)	W (m/s)	U$_T$(m/s)	Ke (m^2/s^2)
1.1000	1.5518	0.0471	0.0380	0.0370	0.0349	-0.3000	-0.0020	0.0005	0.2886	0.0027
1.1000	1.5918	0.0471	0.0350	0.0340	0.0250	-0.3220	0.0100	-0.0132	0.3157	0.0018
1.1000	1.6318	0.0471	0.0260	0.0280	0.0163	-0.3325	0.0180	-0.0180	0.3221	0.0011
1.1000	1.6718	0.0471	0.0170	0.0220	0.0190	-0.3430	0.0260	-0.0162	0.3260	0.0010
1.1000	1.7118	0.0471	0.0180	0.0220	0.0161	-0.3530	0.0230	-0.0182	0.3252	0.0010
1.1000	1.7518	0.0471	0.0210	0.0210	0.0197	-0.3540	0.0280	-0.0109	0.3249	0.0010
1.1000	1.7918	0.0471	0.0260	0.0210	0.0185	-0.3470	0.0200	0.0004	0.3237	0.0009
1.1000	1.8318	0.0471	0.0240	0.0200	0.0185	-0.3440	0.0230	0.0088	0.3130	0.0009
1.1000	1.8718	0.0471	0.0360	0.0210	0.0152	-0.3340	0.0230	0.0083	0.3078	0.0009
1.1000	1.8918	0.0471	0.0180	0.0180	0.0136	-0.3440	0.0170	0.0006	0.3114	0.0008
1.1000	1.9068	0.0471	0.0180	0.0180	0.0293	-0.3440	0.0170	0.0091	0.3050	0.0008
1.1000	1.3118	0.0701	0.0410	0.0210	0.0054	-0.0980	0.0000	0.0013	0.0916	0.0019
1.1000	1.3218	0.0701	0.0570	0.0240	0.0141	-0.0960	0.0030	0.0029	0.0935	0.0023
1.1000	1.3318	0.0701	0.0570	0.0280	0.0550	-0.1090	-0.0010	0.0134	0.1026	0.0029
1.1000	1.3418	0.0701	0.0560	0.0260	0.0599	-0.1160	-0.0010	0.0171	0.1179	0.0034
1.1000	1.3518	0.0701	0.0470	0.0370	0.0681	-0.1520	-0.0010	0.0208	0.1288	0.0036
1.1000	1.3718	0.0701	0.0490	0.0320	0.0555	-0.1410	0.0140	0.0194	0.1374	0.0035
1.1000	1.3918	0.0701	0.0440	0.0430	0.0405	-0.1460	0.0140	0.0162	0.1460	0.0035
1.1000	1.4318	0.0701	0.0650	0.0480	0.0433	-0.1460	0.0260	0.0120	0.1523	0.0038
1.1000	1.4718	0.0701	0.0610	0.0490	0.0445	-0.1440	0.0280	0.0106	0.1637	0.0044
1.1000	1.5118	0.0701	0.0700	0.0470	0.0456	-0.2015	0.0240	0.0027	0.2146	0.0040
1.1000	1.5518	0.0701	0.0710	0.0450	0.0414	-0.2519	0.0230	0.0021	0.2613	0.0036
1.1000	1.5918	0.0701	0.0527	0.0370	0.0304	-0.3124	0.0270	-0.0047	0.3096	0.0021
1.1000	1.6318	0.0701	0.0505	0.0295	0.0252	-0.3029	0.0310	-0.0057	0.3204	0.0010
1.1000	1.6718	0.0701	0.0503	0.0220	0.0192	-0.3129	0.0350	-0.0115	0.3196	0.0012
1.1000	1.7118	0.0701	0.0397	0.0310	0.0192	-0.3033	0.0050	-0.0125	0.3116	0.0011
1.1000	1.7518	0.0701	0.0390	0.0260	0.0178	-0.2933	0.0010	-0.0166	0.3023	0.0011
1.1000	1.7918	0.0701	0.0403	0.0220	0.0134	-0.2932	-0.0100	-0.0080	0.2977	0.0011
1.1000	1.8318	0.0701	0.0180	0.0200	0.0150	-0.2736	0.0200	-0.0029	0.2890	0.0010
1.1000	1.8718	0.0701	0.0190	0.0190	0.0186	-0.2535	0.0220	0.0060	0.2671	0.0011
1.1000	1.8918	0.0701	0.0220	0.0210	0.0182	-0.2338	0.0220	0.0032	0.2509	0.0011
1.1000	1.9068	0.0701	0.0170	0.0200	0.0124	-0.2343	0.0150	0.0022	0.2433	0.0010
1.1000	1.3118	0.0824	0.0420	0.0230	0.0080	-0.0850	0.0020	0.0018	0.0724	0.0018
1.1000	1.3218	0.0824	0.0520	0.0220	0.0180	-0.0310	0.0020	0.0030	0.0690	0.0022
1.1000	1.3318	0.0824	0.0580	0.0260	0.0551	-0.0380	0.0100	0.0127	0.0768	0.0029
1.1000	1.3418	0.0824	0.0560	0.0220	0.0591	-0.1060	0.0060	0.0145	0.0951	0.0034
1.1000	1.3518	0.0824	0.0600	0.0270	0.0669	-0.0860	0.0170	0.0171	0.1115	0.0037
1.1000	1.3718	0.0824	0.0650	0.0330	0.0385	-0.0870	0.0240	0.0101	0.1238	0.0036

153

Table B.1 Flow field data for the bend width 0.60m (Q=0.013m³/s, continued)

x (m)	y (m)	z (m)	Urms (m/s)	Vrms (m/s)	Wrms (m/s)	U (m/s)	V (m/s)	W (m/s)	U$_T$(m/s)	Ke (m²/s²)
1.1000	1.3918	0.0824	0.0570	0.0390	0.0501	-0.1070	0.0300	0.0165	0.1343	0.0036
1.1000	1.4318	0.0824	0.0670	0.0400	0.0388	-0.1020	0.0330	-0.0009	0.1406	0.0039
1.1000	1.4718	0.0824	0.0680	0.0460	0.0687	-0.1100	0.0350	0.0262	0.1513	0.0046
1.1000	1.5118	0.0824	0.0670	0.0460	0.0492	-0.1920	0.0330	0.0187	0.2053	0.0042
1.1000	1.5518	0.0824	0.0830	0.0470	0.0268	-0.2340	0.0330	0.0017	0.2540	0.0039
1.1000	1.5918	0.0824	0.0367	0.0400	0.0334	-0.3080	0.0200	0.0057	0.3071	0.0022
1.1000	1.6318	0.0824	0.0300	0.0000	0.0265	-0.3350	0.0260	-0.0066	0.3189	0.0010
1.1000	1.6718	0.0824	0.0398	0.0280	0.0225	-0.3110	0.0110	-0.0081	0.3163	0.0012
1.1000	1.7118	0.0824	0.0342	0.0280	0.0230	-0.2940	0.0040	-0.0134	0.3058	0.0012
1.1000	1.7518	0.0824	0.0408	0.0250	0.0169	-0.2730	-0.0120	-0.0132	0.2943	0.0012
1.1000	1.7918	0.0824	0.0421	0.0240	0.0164	-0.2640	-0.0310	-0.0035	0.2891	0.0011
1.1000	1.8318	0.0824	0.0402	0.0210	0.0163	-0.2760	-0.0170	-0.0020	0.2810	0.0010
1.1000	1.8718	0.0824	0.0430	0.0170	0.0189	-0.2420	-0.0080	0.0075	0.2543	0.0012
1.1000	1.8918	0.0824	0.0700	0.0140	0.0182	-0.2170	0.0020	0.0028	0.2315	0.0013
1.1000	1.9068	0.0824	0.0350	0.0130	0.0191	-0.1720	0.0040	0.0000	0.2233	0.0011
0.9000	1.3118	0.0059	0.0080	0.0060	0.0057	0.0020	0.0000	0.0018	0.0501	0.0007
0.9000	1.3218	0.0059	0.0420	0.0090	0.0079	-0.0260	0.0020	0.0028	0.0550	0.0009
0.9000	1.3318	0.0059	0.0550	0.0170	0.0126	-0.0440	0.0050	0.0021	0.0747	0.0011
0.9000	1.3418	0.0059	0.0330	0.0160	0.0188	-0.0990	0.0080	0.0033	0.1025	0.0012
0.9000	1.3518	0.0059	0.0290	0.0230	0.0139	-0.1020	0.0170	0.0098	0.1211	0.0013
0.9000	1.3718	0.0059	0.0340	0.0320	0.0289	-0.1330	-0.0030	0.0085	0.1449	0.0017
0.9000	1.3918	0.0059	0.0570	0.0370	0.0208	-0.1550	-0.0070	0.0081	0.1674	0.0022
0.9000	1.4318	0.0059	0.0430	0.0400	0.0212	-0.2030	-0.0370	0.0075	0.2129	0.0020
0.9000	1.4718	0.0059	0.0550	0.0310	0.0230	-0.2250	-0.0320	0.0003	0.2385	0.0021
0.9000	1.5118	0.0059	0.0380	0.0310	0.0219	-0.2460	-0.0430	-0.0012	0.2561	0.0017
0.9000	1.5518	0.0059	0.0410	0.0260	0.0000	-0.2670	0.0140	0.0000	0.2781	0.0014
0.9000	1.5918	0.0059	0.0440	0.0260	0.0000	-0.2370	-0.0020	0.0000	0.2779	0.0012
0.9000	1.6318	0.0059	0.0367	0.0100	0.0000	-0.2490	-0.0030	0.0000	0.2861	0.0008
0.9000	1.6718	0.0059	0.0430	0.0140	0.0000	-0.2610	-0.0050	0.0000	0.2912	0.0008
0.9000	1.7118	0.0059	0.0310	0.0100	0.0000	-0.2290	0.0000	0.0000	0.2750	0.0006
0.9000	1.7518	0.0059	0.0410	0.0217	0.0000	-0.2750	-0.0430	0.0000	0.2978	0.0009
0.9000	1.7918	0.0059	0.0410	0.0290	0.0000	-0.2790	-0.0400	0.0000	0.2980	0.0011
0.9000	1.8318	0.0059	0.0340	0.0300	0.0000	-0.2980	-0.0300	0.0000	0.2987	0.0010
0.9000	1.8718	0.0059	0.0380	0.0250	0.0000	-0.3000	-0.0140	0.0000	0.2989	0.0009
0.9000	1.8918	0.0059	0.0320	0.0250	0.0000	-0.3120	0.0000	0.0000	0.3042	0.0008
0.9000	1.9068	0.0059	0.0330	0.0210	0.0000	-0.2810	0.0140	0.0000	0.2919	0.0008
0.9000	1.3118	0.0148	0.0230	0.0170	0.0277	-0.0655	-0.0015	-0.0013	0.0749	0.0008
0.9000	1.3218	0.0148	0.0283	0.0185	0.0163	-0.0795	-0.0005	0.0002	0.0821	0.0010

Table B.1 Flow field data for the bend width 0.60m (Q=0.013m³/s, continued)

x (m)	y (m)	z (m)	Urms (m/s)	Vrms (m/s)	Wrms (m/s)	U (m/s)	V (m/s)	W (m/s)	U_T(m/s)	Ke (m²/s²)
0.9000	1.3318	0.0148	0.0385	0.0225	0.0181	-0.0885	0.0010	-0.0002	0.0981	0.0013
0.9000	1.3418	0.0148	0.0375	0.0275	0.0212	-0.1310	-0.0030	-0.0030	0.1203	0.0014
0.9000	1.3518	0.0148	0.0403	0.0305	0.0225	-0.1390	-0.0075	-0.0036	0.1302	0.0015
0.9000	1.3718	0.0148	0.0380	0.0370	0.0258	-0.1545	-0.0125	-0.0002	0.1484	0.0018
0.9000	1.3918	0.0148	0.0408	0.0395	0.0247	-0.1735	-0.0105	0.0056	0.1701	0.0022
0.9000	1.4318	0.0148	0.0395	0.0340	0.0183	-0.2125	-0.0365	0.0060	0.2139	0.0020
0.9000	1.4718	0.0148	0.0445	0.0340	0.0202	-0.2505	-0.0365	0.0022	0.2374	0.0021
0.9000	1.5118	0.0148	0.0422	0.0365	0.0222	-0.2545	-0.0360	0.0000	0.2562	0.0018
0.9000	1.5518	0.0148	0.0390	0.0285	0.0177	-0.2890	-0.0100	-0.0015	0.2783	0.0015
0.9000	1.5918	0.0148	0.0355	0.0260	0.0177	-0.2885	-0.0105	-0.0039	0.2846	0.0012
0.9000	1.6318	0.0148	0.0344	0.0185	0.0135	-0.2920	-0.0090	-0.0044	0.2943	0.0008
0.9000	1.6718	0.0148	0.0320	0.0180	0.0133	-0.3050	-0.0050	-0.0022	0.2975	0.0008
0.9000	1.7118	0.0148	0.0235	0.0135	0.0101	-0.2870	0.0120	-0.0015	0.2816	0.0005
0.9000	1.7518	0.0148	0.0330	0.0300	0.0223	-0.3100	-0.0050	-0.0013	0.3009	0.0009
0.9000	1.7918	0.0148	0.0360	0.0270	0.0190	-0.3080	-0.0080	0.0008	0.2989	0.0011
0.9000	1.8318	0.0148	0.0335	0.0280	0.0206	-0.3055	-0.0060	0.0047	0.2969	0.0010
0.9000	1.8718	0.0148	0.0315	0.0245	0.0169	-0.3050	-0.0060	0.0019	0.2955	0.0009
0.9000	1.8918	0.0148	0.0280	0.0215	0.0172	-0.3195	0.0010	-0.0020	0.3018	0.0008
0.9000	1.9068	0.0148	0.0320	0.0210	0.0342	-0.2850	0.0085	-0.0056	0.2898	0.0008
0.9000	1.3118	0.0236	0.0380	0.0280	0.0097	-0.1330	-0.0030	0.0020	0.1096	0.0011
0.9000	1.3218	0.0236	0.0380	0.0280	0.0200	-0.1330	-0.0030	0.0026	0.1179	0.0013
0.9000	1.3318	0.0236	0.0340	0.0280	0.0221	-0.1330	-0.0030	0.0031	0.1279	0.0015
0.9000	1.3418	0.0236	0.0420	0.0390	0.0352	-0.1630	-0.0140	0.0035	0.1382	0.0017
0.9000	1.3518	0.0236	0.0438	0.0380	0.0317	-0.1260	-0.0320	-0.0010	0.1408	0.0017
0.9000	1.3718	0.0236	0.0420	0.0420	0.0328	-0.1460	-0.0220	0.0060	0.1540	0.0020
0.9000	1.3918	0.0236	0.0360	0.0420	0.0325	-0.1700	-0.0140	0.0115	0.1746	0.0022
0.9000	1.4318	0.0236	0.0360	0.0280	0.0370	-0.2220	-0.0360	0.0169	0.2125	0.0021
0.9000	1.4718	0.0236	0.0382	0.0370	0.0296	-0.2200	-0.0410	0.0121	0.2328	0.0021
0.9000	1.5118	0.0236	0.0400	0.0420	0.0371	-0.2630	-0.0290	0.0154	0.2532	0.0020
0.9000	1.5518	0.0236	0.0370	0.0310	0.0324	-0.2800	-0.0260	0.0024	0.2750	0.0016
0.9000	1.5918	0.0236	0.0270	0.0260	0.0000	-0.3200	-0.0190	0.0000	0.2932	0.0014
0.9000	1.6318	0.0236	0.0280	0.0270	0.0000	-0.3380	-0.0150	0.0000	0.3049	0.0009
0.9000	1.6718	0.0236	0.0210	0.0220	0.0000	-0.3200	-0.0050	0.0000	0.3054	0.0008
0.9000	1.7118	0.0236	0.0160	0.0170	0.0000	-0.3100	0.0240	0.0000	0.2921	0.0006
0.9000	1.7518	0.0236	0.0250	0.0230	0.0000	-0.3100	0.0330	0.0000	0.3036	0.0009
0.9000	1.7918	0.0236	0.0310	0.0250	0.0000	-0.3000	0.0240	0.0000	0.2991	0.0010
0.9000	1.8318	0.0236	0.0330	0.0260	0.0000	-0.2800	0.0180	0.0000	0.2934	0.0010
0.9000	1.8718	0.0236	0.0250	0.0240	0.0000	-0.2700	0.0020	0.0000	0.2902	0.0008

155

Table B.1 Flow field data for the bend width 0.60m (Q=0.013m³/s, continued)

x (m)	y (m)	z (m)	Urms (m/s)	Vrms (m/s)	Wrms (m/s)	U (m/s)	V (m/s)	W (m/s)	U$_T$(m/s)	Ke (m²/s²)
0.9000	1.8918	0.0236	0.0240	0.0180	0.0000	-0.2900	0.0020	0.0000	0.2933	0.0008
0.9000	1.9068	0.0236	0.0310	0.0210	0.0000	-0.2890	0.0030	0.0000	0.2863	0.0008
0.9000	1.3118	0.0471	0.0460	0.0300	0.0107	-0.1390	-0.0090	0.0020	0.1265	0.0018
0.9000	1.3218	0.0471	0.0460	0.0300	0.0260	-0.1390	-0.0090	0.0038	0.1337	0.0019
0.9000	1.3318	0.0471	0.0440	0.0290	0.0551	-0.1510	-0.0090	0.0083	0.1419	0.0021
0.9000	1.3418	0.0471	0.0420	0.0310	0.0315	-0.1660	-0.0170	0.0025	0.1478	0.0021
0.9000	1.3518	0.0471	0.0416	0.0300	0.0307	-0.1270	-0.0050	0.0106	0.1504	0.0022
0.9000	1.3718	0.0471	0.0490	0.0310	0.0317	-0.1690	-0.0170	0.0152	0.1624	0.0023
0.9000	1.3918	0.0471	0.0370	0.0390	0.0400	-0.2080	-0.0220	0.0162	0.1771	0.0025
0.9000	1.4318	0.0471	0.0474	0.0430	0.0366	-0.2020	0.0000	0.0231	0.1967	0.0026
0.9000	1.4718	0.0471	0.0460	0.0360	0.0415	-0.2260	-0.0100	0.0168	0.2093	0.0026
0.9000	1.5118	0.0471	0.0480	0.0460	0.0000	-0.2390	-0.0060	0.0000	0.2316	0.0026
0.9000	1.5518	0.0471	0.0460	0.0450	0.0000	-0.2400	0.0000	0.0000	0.2559	0.0022
0.9000	1.5918	0.0471	0.0424	0.0330	0.0231	-0.2880	0.0080	0.0175	0.2965	0.0020
0.9000	1.6318	0.0471	0.0330	0.0320	0.0000	-0.3190	0.0150	0.0000	0.3102	0.0012
0.9000	1.6718	0.0471	0.0210	0.0240	0.0000	-0.3100	0.0210	0.0000	0.3122	0.0009
0.9000	1.7118	0.0471	0.0190	0.0230	0.0000	-0.3000	0.0230	0.0000	0.3001	0.0007
0.9000	1.7518	0.0471	0.0190	0.0210	0.0000	-0.3000	0.0250	0.0000	0.3012	0.0008
0.9000	1.7918	0.0471	0.0220	0.0230	0.0000	-0.2900	0.0220	0.0000	0.2937	0.0009
0.9000	1.8318	0.0471	0.0280	0.0240	0.0000	-0.2950	0.0210	0.0000	0.2843	0.0009
0.9000	1.8718	0.0471	0.0300	0.0210	0.0000	-0.2950	0.0190	0.0000	0.2758	0.0008
0.9000	1.8918	0.0471	0.0190	0.0200	0.0000	-0.2800	0.0200	0.0000	0.2698	0.0007
0.9000	1.9068	0.0471	0.0260	0.0190	0.0000	-0.2700	0.0110	0.0000	0.2645	0.0007
0.9000	1.3118	0.0701	0.0650	0.0210	0.0129	-0.0610	0.0020	0.0023	0.0667	0.0020
0.9000	1.3218	0.0701	0.0650	0.0210	0.0392	-0.0610	0.0020	0.0078	0.0745	0.0022
0.9000	1.3318	0.0701	0.0740	0.0220	0.0397	-0.0880	0.0000	0.0142	0.0968	0.0025
0.9000	1.3418	0.0701	0.0500	0.0260	0.0358	-0.1460	-0.0050	0.0171	0.1235	0.0026
0.9000	1.3518	0.0701	0.0450	0.0300	0.0319	-0.1560	0.0030	0.0048	0.1388	0.0026
0.9000	1.3718	0.0701	0.0510	0.0370	0.0340	-0.1620	0.0070	0.0145	0.1501	0.0027
0.9000	1.3918	0.0701	0.0510	0.0350	0.0440	-0.1680	0.0120	0.0163	0.1599	0.0029
0.9000	1.4318	0.0701	0.0670	0.0400	0.0399	-0.1730	0.0160	0.0182	0.1718	0.0031
0.9000	1.4718	0.0701	0.0440	0.0370	0.0328	-0.1600	0.0350	0.0168	0.1795	0.0031
0.9000	1.5118	0.0701	0.0660	0.0430	0.0000	-0.1960	0.0170	0.0000	0.2066	0.0032
0.9000	1.5518	0.0701	0.0495	0.0420	0.0420	-0.2300	0.0220	0.0025	0.2377	0.0028
0.9000	1.5918	0.0701	0.0495	0.0400	0.0347	-0.3128	0.0270	0.0113	0.2969	0.0028
0.9000	1.6318	0.0701	0.0411	0.0350	0.0000	-0.2900	0.0240	0.0000	0.3064	0.0015
0.9000	1.6718	0.0701	0.0397	0.0300	0.0000	-0.3190	0.0200	0.0000	0.3135	0.0010
0.9000	1.7118	0.0701	0.0407	0.0260	0.0000	-0.2931	0.0060	0.0000	0.2967	0.0008

Table B.1 Flow field data for the bend width 0.60m (Q=0.013m^3/s, continued)

x (m)	y (m)	z (m)	Urms (m/s)	Vrms (m/s)	Wrms (m/s)	U (m/s)	V (m/s)	W (m/s)	U$_T$(m/s)	Ke (m^2/s^2)
0.9000	1.7518	0.0701	0.0390	0.0210	0.0000	-0.2953	-0.0020	0.0000	0.2969	0.0008
0.9000	1.7918	0.0701	0.0364	0.0210	0.0000	-0.2900	-0.0070	0.0000	0.2871	0.0009
0.9000	1.8318	0.0701	0.0390	0.0210	0.0000	-0.2600	0.0050	0.0000	0.2739	0.0009
0.9000	1.8718	0.0701	0.0411	0.0180	0.0000	-0.2535	0.0130	0.0000	0.2519	0.0009
0.9000	1.8918	0.0701	0.0430	0.0190	0.0000	-0.2200	0.0130	0.0000	0.2272	0.0010
0.9000	1.9068	0.0701	0.0230	0.0110	0.0000	-0.2100	-0.0090	0.0000	0.2190	0.0009
0.9000	1.3118	0.0824	0.0330	0.0130	0.0153	-0.0190	0.0020	0.0027	0.0424	0.0017
0.9000	1.3218	0.0824	0.0330	0.0130	0.0413	-0.0190	0.0020	0.0082	0.0476	0.0020
0.9000	1.3318	0.0824	0.0520	0.0170	0.0561	-0.0450	0.0020	0.0161	0.0709	0.0024
0.9000	1.3418	0.0824	0.0700	0.0250	0.0385	-0.0990	0.0070	0.0106	0.1022	0.0027
0.9000	1.3518	0.0824	0.0540	0.0270	0.0337	-0.1230	0.0040	0.0116	0.1250	0.0028
0.9000	1.3718	0.0824	0.0640	0.0340	0.0316	-0.1140	0.0080	0.0120	0.1411	0.0029
0.9000	1.3918	0.0824	0.0640	0.0340	0.0396	-0.1200	0.0200	0.0115	0.1520	0.0031
0.9000	1.4318	0.0824	0.0680	0.0360	0.0361	-0.1370	0.0340	0.0129	0.1644	0.0033
0.9000	1.4718	0.0824	0.0660	0.0410	0.0309	-0.1500	0.0390	0.0094	0.1715	0.0032
0.9000	1.5118	0.0824	0.0720	0.0340	0.0398	-0.1900	0.0160	0.0177	0.2002	0.0033
0.9000	1.5518	0.0824	0.0600	0.0340	0.0377	-0.2200	0.0250	0.0013	0.2338	0.0030
0.9000	1.5918	0.0824	0.0810	0.0390	0.0190	-0.2963	0.0350	0.0022	0.2967	0.0030
0.9000	1.6318	0.0824	0.0354	0.0390	0.0000	-0.3130	0.0230	0.0000	0.3051	0.0016
0.9000	1.6718	0.0824	0.0345	0.0300	0.0000	-0.3170	0.0180	0.0000	0.3135	0.0010
0.9000	1.7118	0.0824	0.0379	0.0230	0.0000	-0.2880	0.0000	0.0000	0.2955	0.0009
0.9000	1.7518	0.0824	0.0304	0.0200	0.0000	-0.2990	-0.0090	0.0000	0.2958	0.0008
0.9000	1.7918	0.0824	0.0370	0.0230	0.0000	-0.2770	-0.0280	0.0000	0.2854	0.0009
0.9000	1.8318	0.0824	0.0376	0.0220	0.0000	-0.2800	-0.0110	0.0000	0.2710	0.0009
0.9000	1.8718	0.0824	0.0424	0.0160	0.0000	-0.2400	0.0020	0.0000	0.2442	0.0010
0.9000	1.8918	0.0824	0.0509	0.0150	0.0000	-0.1800	0.0030	0.0000	0.2135	0.0011
0.9000	1.9068	0.0824	0.0509	0.0150	0.0000	-0.1800	0.0030	0.0000	0.2047	0.0011